MULTI-STRESS PROTEOMICS: THE GLOBAL PROTEIN RESPONSE TO MULTIPLE ENVIRONMENTAL STRESSORS IN THE PORCELAIN CRAB *PETROLISTHES CINCTIPES*

A Thesis

presented to

the Faculty of California Polytechnic State University

San Luis Obispo

In partial fulfilment

of the Requirements for the Degree

Master of Science in Biological Sciences

by

Michael A. Garland

August 2015

COMMITTEE MEMBERSHIP

TITLE: Multi-stress proteomics: The global protein response to multiple environmental stressors in the porcelain crab *Petrolisthes cinctipes*

AUTHOR: Michael A. Garland

DATE SUBMITTED: August 2015

COMMITTEE CHAIR: Lars Tomanek, Ph.D.
Associate Professor of Biological Sciences

COMMITTEE MEMBER: Nikki Adams, Ph.D.
Professor of Biological Sciences

COMMITTEE MEMBER: Kristin Hardy, Ph.D.
Assistant Professor of Biological Sciences

ABSTRACT

Multi-stress proteomics: The global protein response to multiple environmental stressors in the porcelain crab *Petrolisthes cinctipes*

Michael A. Garland

Global climate change is increasing the number of hot days along the California coast as well as increasing the incidence of off-shore upwelling events that lower the pH of intertidal seawater; thus, intertidal organisms are experiencing an increase in more than one stress simultaneously. This study seeks to characterize the global protein response of the eurythermal porcelain crab *Petrolisthes cinctipes* to changes in thermal, pH, and tidal regime treatments, either combined or individually. The first experiment examined temperature stress alone and sought to determine the effect of chronic temperature acclimation on the acute heat shock response. We compared the proteomic response of cheliped muscle tissue following a month-long acclimation to either (1) constant 10°C, (2) daily fluctuation from 10-20°C, or (3) daily fluctuation from 10-30°C, all followed by either a 30°C acute heat shock or 10°C control. We found that ATP supply via the phosphagen system, changes in glycolytic enzymes, muscle fiber restructuring, respiratory protein fragmentation, and immunity were primarily affected by acclimation and subsequent heat shock. Acclimation to the "extreme" regimes (10°C and 10-30°C) resulted in the greatest proteomic changes, while acclimation to the moderate regime (10-20°C) resulted in a more mild response to heat shock (i.e., fewer adjustments to relative protein abundance). The second experiment sought to determine the proteomic response of gill tissue following a 17 d acclimation to daily changes in pH (ambient pH 8.1 *vs* low pH 7.6), tidal regime (constant immersion *vs* 6 h emersion), and temperature (ambient 11°C *vs* 22-31°C heat shock during emersion). Low pH alone reduced expression of molecular chaperones of the endoplasmic reticulum, lectins, and serine proteases involved in activating the prophenoloxidase cascade. It also increased the abundance of Na^+/K^+-ATPase, nitrogen metabolism enzymes, and induced changes in tubulin expression, all suggesting an increase in ammonium excretion. Addition of emersion during low pH reduced the abundance of several metabolic proteins including those involved in the proposed ammonium excretion mechanism, suggesting a decrease in metabolic function in part to prevent toxic accumulation of ammonium in the branchial chambers. Combined pH, emersion, and thermal stress increased the abundance of proteins involved in cuticle binding and crosslinking. These results indicate that the responses to pH, tidal cycle, and temperature are highly dependent on one another and that changes in ER protein maturation, ion transport, immunity, and cuticle structure are the primary biochemical systems impacted by these environmental stressors in crustacean gill.

Keywords: proteomics, crustacean, gill, muscle, climate change, thermal stress, pH, hypercapnia, emersion, multi-stress, immunity, *Petrolisthes*

ACKNOWLEDGMENTS

I would like to thank Dr. Lars Tomanek for giving me an opportunity to grow as a scientist. His mentorship, encouragement, and support will not be forgotten. I would also like to thank my committee, Dr. Nikki Adams and Dr. Kristin Hardy, for their support and feedback, as well as Dr. Christina Vasquez for her thoughtful input into these manuscripts. A special thanks to Marcus Zuzow for his technical help throughout the years and for interesting conversations about philosophy and society.

I especially want to thank Holland Elder who shared in the ups and downs inherent in the endeavor of science (and academics in general). Thanks to all of my local friends and fellow lab members including Loredana Serafini, James Koman, Josh Mier, Hayley Chilton, Aubrie Fowler, Mark Hamer, Arlo White, Jessica Griffiths, Neha Patel, Alex Barbella, Michael Maples, Avery Cromwell, Molly Pendley, Kory Heiken, Christopher Sakoda, and all graduate students, faculty, and staff in the Biological Sciences department. My gratitude goes to the Stillman Lab for their invaluable collaboration as this research would not have been possible without them. I also want to thank my family for their support and encouragement throughout my years as a student.

This research was supported by National Science Foundation (NSF) grants MCB-1041225 and EF-1041227, and by the Council on Ocean Affairs, Science, and Technology (COAST).

TABLE OF CONTENTS

LIST OF TABLES

LIST OF FIGURES

1.0 INTRODUCTION

The biogeographic distribution of intertidal ectotherms is, aside from predation, determined largely by natural fluctuations in temperature and aerial exposure due to the tidal cycle (Pörtner, 2002; Tomanek, 2008, 2010; Finke et al., 2007). An organism's response to these stressors is impacted by other abiotic parameters including changes in pH and oxygen availability (Pörtner et al., 2005). Coastal ecosystems, from the intertidal to the edge of the continental shelf, are ecologically and economically critical environments that annually provide over US$14 trillion in ecosystem goods and services, which is nearly half the global contribution (Harley et al., 2006). As the global climate changes in response to anthropogenic CO_2 emissions, species can respond by either adapting genetically or through physiological plasticity, shifting their range distribution, or going extinct (Somero, 2010; Hofmann and Todgham, 2010). Some organisms, particularly ectotherms adapted to the mid- to high-intertidal, exhibit physiological plasticity that allow individuals to biochemically adapt to rapid temperature changes (Tomanek, 2010). This may possibly work as a first line of defense for mid-intertidal organisms adapted to moderately-variable temperature fluctuations (mesotherms), but recent studies suggest that high-intertidal organisms adapted to wide variations in temperature (eurytherms) are already pushed to their thermal limits on warm days (Tomanek, 2010). In order to predict the effects of climate change on intertidal ectotherms, we must first understand how they can acclimate to changing environmental conditions. Since multiple environmental

conditions are currently changing and will continue to change in the future, it is important to consider how the interaction of stressors affects the physiological response to stress.

1.1 Physical Science: Global climate change

The Earth's climate is driven by both natural forces and human activities. Since the industrial revolution of the 18th century, the anthropogenic output of greenhouse gases has contributed to climatic changes at rates that are unprecedented by millennia. These changes include an increase in global surface temperatures over land and ocean, decreased oceanic pH, less frequent but more intense precipitation events, reduction of the cryosphere (polar ice sheets), disruption in the balance of biogeochemical cycles, as well as other phenomena. While previous studies have warned of impending consequences of climate change, there is consensus in the scientific community that we are presently enduring human-driven shifts in climate and that these changes will continue indefinitely without mitigating action. The response to the threat of climate change requires an assessment of its effects on humans and the environment. It is therefore important to understand, in addition to the physical basis, the ecological and biological consequences of climate change (Cubasch et al., 2013).

Atmospheric and oceanic warming

The Earth's climate system is powered mostly by solar radiation. When this radiation reaches the earth, a certain amount is reflected back into space by the atmosphere. Radiation that is not reflected is absorbed by the Earth's surface and atmospheric constituents. To maintain the energy balance, the Earth emits the same Wattage of energy back into space in the form of longwave radiation

(LWR; Le Treut et al., 2007). Aerosols present in the atmosphere are capable of reflecting LWR back to the surface. This is known as the greenhouse effect, and gases with this reflective property are known as greenhouse gases (GHGs). The overall balance of the climate system can be altered in 3 major pathways: (1) altering the amount of radiation the Earth receives, (2) changing the fraction of radiation that is reflected by the atmosphere, and (3) changing the amount of LWR that is reflected back into space (Le Treut et al., 2007).

The third pathway is presently contributing a significant amount of change to the Earth's climate. Human industrial activities have increased the amount of GHGs in the atmosphere since the mid-18th century. GHG emissions are primarily attributed to fossil fuel burning, deforestation, and cement production (Cubasch et al., 2013). The anthropogenic emission of GHGs is largely responsible for the current increase in global temperatures over the past 2 centuries (Cubasch et al., 2013). In the past 100 years (1906 – 2005), the global mean surface temperature has increased by 0.74°C, with a 0.6°C increase occurring within the 20th century. The rate of increase is expected to multiply fivefold in the 21st century with a predicted rate of +3°C over 100 years; about 50% of this change over the next 20 years will be due to presently-committed climate change (Meehl et al., 2007). In addition to a steady increase in average temperature, GHG-induced climate change is predicted to increase the length, frequency, or intensity of weather events such as heat waves, extreme precipitation, and droughts, although there is regional variability in these parameters (Cubasch et al., 2013). Of all GHGs in the atmosphere, CO_2 is the

greatest anthropogenic contributor to changes in atmospheric chemistry (Hartmann et al., 2013). Through fossil fuel combustion and deforestation, atmospheric CO_2 levels have increased by about 40%, from the pre-industrial level of 280 ppm to approximately 384 ppm (Hartmann et al., 2013).

Atmospheric dynamics are influenced in part by the world's oceans due to their storage capacities for thermal energy and carbon. Of all the excess energy stored by the Earth over the past 50 years, approximately 93% has been stored in the oceans (Church et al., 2011; Levitus et al., 2012). Additionally, the oceans contain approximately 50 times more carbon than the atmosphere (ocean acidification is discussed in the next subsection) (Sabine et al., 2004). By absorbing about 30% of anthropogenic CO_2 emissions, and through their relatively large heat and carbon capacities, the oceans act as buffers that are slowing the effects of climate change (Mikaloff-Fletcher et al., 2006; Le Quéré et al., 2010). If the oceans were not taking up atmospheric carbon, the present concentration would be approximately 450 ppm rather than 384 ppm (Solomon et al., 2007; Sabine and Feely, 2007; Sabine et al., 2004; Feely et al., 2009).
The rate of increase in sea surface temperature (SST) is notably slower than that of the atmosphere due to water having a greater heat capacity than air (Sutton et al., 2007). Oceanic temperature varies on seasonal, interannual (e.g. phenomena such as the El Niño Southern Oscillation, or ENSO), decadal, and centennial timescales. Upper ocean temperature (UOT, depth ranging from 0 – 700 m) trends before 1971 are difficult to trace due to non-standardized instrumentation and sporadic sampling patterns (Boyer et al., 2009), although

estimates back to 1950 are available based on 5-year running means. The global sampling methodology was improved in 1971, and data since this time data has indicated a general increase in UOT over the past 40 years (1970-2010), primarily in the northern hemisphere (Levitus et al., 2009). Over this time period, average UOT is estimated to have increased by 0.09 – 0.13°C each decade for depth above 75 m. Between 0 – 200 m, temperature is estimated to have increased by 0.25°C over the past 40 years. Projections for temperature change in the top 100 m indicate an increase of 0.6°C or 2.0°C by 2100 according to climate scenarios RCP4.6 and 8.5, respectively (Rhein et al., 2013).

Ocean acidification

The oceans absorb about 30% of anthropogenic carbon emissions, thereby ameliorating the effects of fossil fuel combustion on atmospheric climate change (Mikaloff-Fletchet et al., 2006; Le Quéré et al., 2010). However, this comes at the cost of reducing the ocean's pH in a process known as ocean acidification (OA). The following subsection briefly describes the main chemical mechanisms of OA and then discusses observed impacts of OA on seawater chemistry.

In consideration of OA, there are 4 important chemical reactions that take place (denoted as Equations 1, 2, 4, and 5). The first reaction occurs when the Earth's atmosphere exchanges CO_2 with oceanic surface waters, with CO_2 changing from gaseous to aqueous form in the following reaction:

$$CO_{2(g)} \rightleftharpoons CO_{2(aq)}. \quad (1)$$

Starting at a given time, the concentrations of $CO_{2(g)}$ and $CO_{2(aq)}$ will equilibrate over approximately one year (Doney et al., 2009). As aqueous CO_2 concentration

increases, water and CO_2 react to become carbonic acid (H_2CO_3), which then goes through a series of carbonate chemistry reactions summarized in the following equation:

$$CO_2 + H_2O \rightleftharpoons H_2CO_3 \rightleftharpoons H^+ + HCO_3^- \rightleftharpoons 2H^+ + CO_3^{2-}. \quad (2)$$

The total inorganic carbon present in a system is described by the chemicals in this equation (dissolved CO_2, carbonic acid, bicarbonate, and carbonate) and the sum of their abundance is called dissolved inorganic carbon (DIC). This is defined as:

$$DIC = [CO_2] + [H_2CO_3] + [HCO_3^-] + [CO_3^{2-}]. \quad (3)$$

In a system with a pH of 8.1, the distribution of DIC is 90% bicarbonate, 9% carbonate, and 1% CO_2. As indicated in Equation 2, carbonic acid dissociates first into bicarbonate (HCO_3^-) and then into carbonate (CO_3^{2-}) ions, releasing a proton (H^+) in each reaction. An increase in proton concentration lowers the pH of the water as described by the following relationship:

$$pH = -\log_{10}[H^+]. \quad (4)$$

The pH and DIC of water can also be affected by biological reactions. The following equation demonstrates the relationship between photosynthesis and respiration/decomposition, which are both common reactions in the upper water column:

$$CO_2 + H_2O \rightleftharpoons CH_2O + O_2. \quad (5)$$

The photosynthetic process extracts CO_2 from the DIC pool to form organic carbon, whereas respiration and decomposition convert organic carbon into DIC. As CO_2 is produced from respiration and decomposition, it reacts with water as

described in Equation 2, thus forming bicarbonate ions and increasing the concentration of protons. As the proton concentration increases, the carbonate ion concentration subsequently decreases as the equilibrium shifts (Doney et al., 2009). This in turn decreases the concentration of calcium carbonate according to the following reaction:

$$Ca^{2+} + CO_3^{2-} \rightleftharpoons CaCO_3. \quad (6)$$

Calcium carbonate is used by marine organisms to excrete hard shells, develop skeletal structures, and balance internal pH levels. Thus, OA is expected to have a negative impact on marine organisms, particularly those that rely heavily on calcification for survival such as scleractinian corals (Doney et al., 2009). The ability to calcify depends heavily on the saturation state (Ω) of calcium carbonate:

$$\Omega = \frac{[Ca^{2+}][CO_3^{2-}]}{K'_{sp}}, \quad (7)$$

where K'_{sp}, the apparent solubility product, depends on temperature, pressure, and salinity. It also depends on the mineralization state of $CaCO_3$, which is usually in the form of calcite (most stable) or aragonite (less stable). Vaterite, the least stable form, will convert to calcite when exposed to water at ambient temperature without any kind of molecular chaperoning, and is usually not considered a biologically-relevant mineralization state except in a few rare cases (Plummer and Busenberg, 1982). The formation of $CaCO_3$ is favored when $\Omega > 1$ whereas dissolution is favored when $\Omega < 1$. Because K'_{sp} depends on mineral form, $\Omega_{calcite}$ and $\Omega_{aragonite}$ will have different values when all other parameters are equal.

The calculation of Ω requires knowing the concentration of carbonate ion, which itself may be derived using DIC and total alkalinity (TA, or sometimes A_T) data. TA is defined by Dickson (1981) as "the number of moles of hydrogen ion equivalent to the excess of proton acceptors over proton donors" as defined by their dissociation constants (K). It can be mathematically written as:

$$TA = X - Y, \tag{8}$$

where X and Y are the sums of the concentrations of chemical species as defined in Table 1. Proton acceptors must have $K \leq 10^{-4.5}$ at 25°C and zero ionic strength, and proton donors must have $K > 10^{-4.5}$. Other acids and bases that may be present are not typically present in significant concentrations in most seawater and can generally be ignored with no consequence. The determination of TA can be accomplished by using a Gran titration in a procedure detailed by the US Department of Energy (Dickson and Goyet, 1994).

Table 1. The sums of the concentration of proton acceptors and donators relevant for the calculation of total alkalinity. Proton acceptors (left column) must have K ≤ 10-4.5 at 25°C and zero ionic strength, whereas donators (right column) must have K > 10-4.5. Other acceptors and donators may exist in seawater but in most circumstances are negligible. Table based on data from OE (1994).

Expression of chemical species defined by ***X***	Expression of chemical species defined by ***Y***
$[HCO_3^-] + [CO_3^-] + [B(OH)_4^-] + [OH^-] + [HPO_4^{2-}] + 2[PO_4^{3-}] + [SiO(OH)_3^-] + [NH_3] + [HS^-]$	$[H^+]_F + [HSO_4^-] + [HF] + [H_3PO_4]$

Oceanic uptake of carbon has been estimated to be approximately 2 petagrams (Pg) yr^{-1} over the past several decades, warranting investigation of how the oceans will equilibrate with the ever-increasing carbon concentration of

the atmosphere (Takahashi et al., 2009). The Global Ocean Data Analysis Project (GLODAP) synthesized oceanographic data that was collected by scientific cruise expeditions during the 1990s. Based on information from this project, the current pH of surface waters in the open ocean ranges between 8.35 and 7.85, and on average is 8.11 (Key et al., 2004). The estimated average pH for pre-industrial oceans was 8.2, indicating approximately a 0.1 decrease in mean pH over the past two and a half centuries and representing a 26% increase in acidity (Doney et al., 2009; Royal Society, 2005).

In addition to cruise expeditions, key data collection for atmospheric and oceanic carbon trends has occurred in the North Pacific Ocean, particularly in and around Hawaii (Takahashi et al., 2009). The Mauna Loa and ALOHA stations have simultaneously recorded observational data of atmospheric CO_2, ocean surface pCO_2, and pH. These data illustrate the relationship between the three parameters (Fig. 1). While there are seasonal, geographic, and oceanographic variables to be considered, the general trend is that the rate of increase of ocean surface pCO_2 mirrors that of atmospheric CO_2 levels, increasing at 1.5 parts per million (ppm) per year. These data illustrate that, at least in the North Pacific, pCO2 in the open ocean is increasing concurrently with atmospheric CO_2 levels. The data from Hawaii correspond well with observations in the Atlantic from the Atlantic Time-Series Study and the European Station for Time-Series in the Ocean (Doney et al., 2009; Solomon et al., 2007). According to data from these stations, average ocean surface pH is decreasing at a rate of 0.02 units per decade (Solomon et al., 2007). At the present rate of CO_2

concentration increase, the ocean surface pH is expected to decrease by 0.2 - 0.4 pH units by the end of this century (Orr et al., 2005).

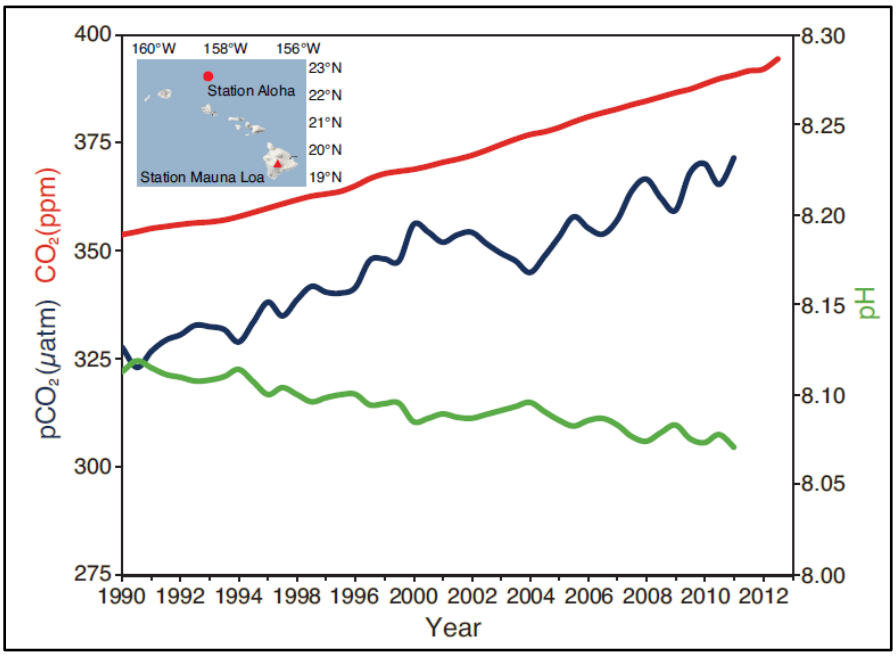

Figure 1. North Pacific time series data. Time series from 1990-2012 comparing atmospheric CO_2 (ppm) measured at Mauna Loa Observatory (red line) against ocean surface pCO_2 (blue line, µatm) and pH (green line) measured at Station ALOHA. Adapted from Hartmann et al., 2013 (after Doney et al., 2009; data from Dore et al., 2009).

Temperature and pH along the California coast

While studies of the open ocean convey the general trend of SST and OA, coastal areas are more variable and may exhibit different trends. Along the California coast, SST has been decreasing in contrast to average oceanic SST (Lima and Wethey, 2012). However, thermal limits are imposed on intertidal organisms while exposed to air rather than while underwater (Finke et al., 2007; Tomanek, 2008). With this in mind, average air temperature in California is expected to increase by 1-3°C in the mid-century, while increases of 3-5°C are expected by the end of the century (Cayan et al., 2009). This estimate is notably

higher than previous projections based on historical observations of California climate (Bonfills et al., 2008; Cayan et al., 2009). Decadal oscillations in temperature are accounted for in the models, and while they have some effect on temperature variability, they do not greatly detract from a linear trend of increasing temperature (Cayan et al., 2009). In addition to a steady annual increase in temperature, incidents of extreme heat (heatwaves) in California are expected to increase in both frequency and intensity, eventually spanning from June–September rather than predominantly in July and August (Hayhoe et al., 2004; Gershunov and Douville, 2008; Miller et al., 2008; Cayan et al., 2009).

Similar to SST, pH dynamics along coastal regions is quite different than those of the open ocean. Sources of biogeochemical drivers of water chemistry dynamics are both biotic and abiotic and include the atmosphere (e.g. airborne pollutants), adjacent landmass (e.g. runoff), benthic environment (e.g. ground-dwelling organisms), and oceanic influences (e.g. submarine volcanic eruptions and offshore upwelling) (Duarte et al., 2013). For example, the pH in tide pools can vary on a diel and seasonal cycle due to the respiration of organisms causing nocturnal decreases in pH followed by diurnal increase in pH due to the neutralizing effect photosynthesis; these pH variations can be as great as 0.5 units and depend in part on seasonal and regional productivity (Wootton et al., 2008; Duarte et al., 2013). Changes in land use (including agriculture and urbanization), eutrophication, mining, and other factors can all contribute to changes in coastal pH (Duarte et al., 2013).

The California coast experiences seasonal offshore upwelling and is considered to be global “hot spot” for acidification (Feely et al., 2008; Hauri et al., 2009; Gruber et al., 2012). This is particularly concerning because the California coast is one of the most productive coastlines in the world and is an important resource for seafood commerce (Gruber et al., 2012). Eastern boundary upwelling systems such as the California Current System (CCS) are driven by wind patterns that push surface seawater offshore, thereby pulling up deeper waters to the surface along the coast. These upwelled waters are more acidic (decreasing pH by approximately 0.3 units) and under-saturated with respect to aragonite (Hauri et al., 2009). Models have demonstrated that pH in the CCS has decreased by approximately 0.1 units and seasonal upwelling will likely reduce coastal pH to 7.8-7.6 (Fig. 2) (Gruber et al., 2012; Hauri et al., 2009). By 2050, it is projected under the high CO_2 emission (A2) scenario that the coast benthos will be under-saturated with aragonite almost year-round (Gruber et al., 2012).

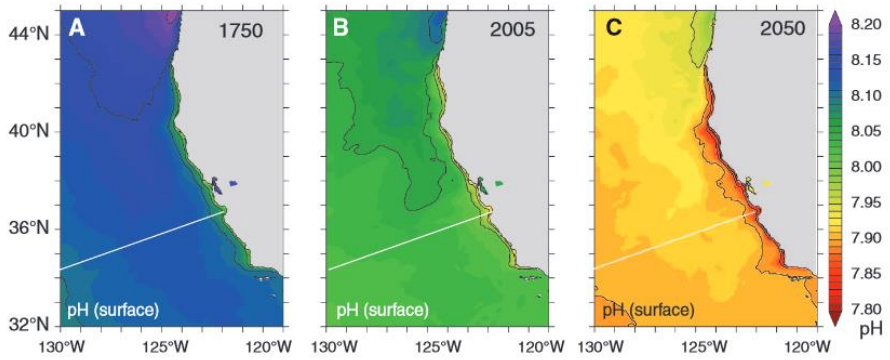

Figure 2. Acidification of the California Current System (CCS). Map illustrates decrease in surface pH of the CCS from (A) pre-industrial to (B) recent time, and (C) a subsequent decrease in surface pH by 2050 based on projections using a model based on high CO_2 emissions. Adapted from Gruber et al. (2012).

1.2 Biological Science: Physiological adaptation

Chronic and acute thermal stress

The ability of an organism to tolerate thermal stress plays a critical role in establishing its distribution limits in the rocky intertidal zone (Tomanek and Helmuth, 2002; Tomanek, 2002). The stress of high temperature is ubiquitous, affecting all levels of biological organization from molecules to behavioral ecology (Portner, 2006; Portner et al., 2010). Temperature is critical for optimal functionality and stability of biomolecules, particularly for lipids and proteins (Somero, 1969, Hochachka and Somero, 2002; Fields, 2001). The lipid membrane of cells separates the intracellular biological components from the outside and is important for signal transduction and solute transport. The membrane becomes more fluid and permeable as temperature increases, and is more viscous as temperature decreases (Singer and Nicolson, 1972; Spector and Yorek, 1985). The primary structure of proteins is held together through covalent peptide bonds, but the secondary, tertiary, and quaternary structures that impart catalytic function are held together by hydrogen bonds, salt bridges, disulfide bonds, and van der Waals interactions (Fields, 2001). Despite the large number of interactions, the net stabilization of these bonds for the entire protein is equivalent to the energy contained in a small number of hydrogen bonds (Jaenicke, 1991, 2000; Fields, 2001). Thus, energy input from environmental temperature, which affects protein flexibility and rigidity, is critical for maintaining the proper geometry during conformational changes throughout catalysis (Zaccai, 2000; Fields, 2001).

On a biochemical level, temperature is a measure of energy in the system. The higher the temperature, the more likely collisions between enzymes and substrates will occur due to increased kinetic energy. Thus, temperature has a generally positive effect on the rate of metabolism due to thermodynamics (expect in cases of metabolic depression) (Tattersall et al., 2012). One standard measure of changes in metabolic rate is the Q_{10} ratio, defined as

$$Q_{10} = \frac{k_{T+10}}{k_T} \tag{9}$$

where *k* is the reaction rate and *T* is the temperature. Thus, every increase in 10°C results in an increased reaction rate Q_{10}. For physiological processes, the general rule of thumb is that Q_{10} is approximately 2 or 3 (i.e., metabolic rate doubles or triples over an increase of 10°C) (Withers, 1992; Tatersall et al., 2012).

Organisms may maintain a variety of cellular mechanisms to cope with thermal stress and maintain homeostasis. Since temperature can affect metabolic rates, cells can undergo “metabolic temperature compensation” in order to maintain the appropriate rates of substrate turnover (Somero, 1969; Hochachka and Somero, 2002). Altering the enzyme-substrate (E-S) affinity is one such strategy that helps to restore metabolism to a normal rate. The E-S affinity can be measured as the inverse of the Michaelis-Menten constant (K_m), which at low substrate concentrations (such as found in cells) is used to determine the rate of catalysis (Alberty,1953; Somero 1969; Somero, 1978; Hochachka and Somero, 2002). To cope with changes in membrane fluidity, cells may compensate by increasing the proportion of saturated fatty acids to increase

viscosity, thereby keeping the cell intact and promoting proper function of the membrane (Singer and Nicolson, 1972; Spector and Yorek, 1985).

For sustained thermal insults, the heat-shock response (HSR) plays an important role in determining an organism's biogeographical distribution and is characterized by an increased synthesis of heat-shock proteins (HSPs), which are molecular chaperones that partake in a variety of functions that all relate to protein homeostasis (Tomanek, 2008; Feder and Hofmann, 1999). HSP70 is regarded as an important biomarker that indicates biochemical stress (Tomanek and Sanford, 2003). When temperature-sensitive proteins become denatured (unraveled) due to breakage of weak bonds, HSPs will bind to the hydrophobic side chains that are exposed, serving to stabilize the target protein's structure and prevent further denaturation. The HSPs will then assist the protein in re-folding itself to its proper conformation. If a protein becomes denatured to the point that it cannot be salvaged, the HSPs will direct the protein into the cell's protein degradation (proteolytic) cycle, thereby preventing it from conglomerating with other damaged proteins through hydrophobic interactions between exposed side chains (Tomanek, 2002). The HSR is thought to be controlled by a "cellular thermometer" in which HSPs are able to regulate their transcription levels through a negative feedback mechanism. In this model, there is equilibrium between HSPs and a factor called heat-shock transcription factor-1 (HSF1) where HSPs repress HSF1 by preferentially binding to it until thermal stress causes dissociation between the two proteins. (DiDomenico et al., 1982; Craig and Gross, 1991; Parsell and Lindquist, 1993; Morimoto, 1998).

The ability of an organism to cope with thermal stress depends largely on its evolutionary adaptation to the temperature variation in its environment. Stenothermal organisms, such as polar marine fishes, are adapted to live where temperature is generally static; thus, any drastic change in temperature is stressful and possibly lethal. A classic example of stenothermal adaptation is found in the Antarctic ice fishes of the suborder Notothenioidei, which are adapted to survive in a thermally stable, sub-freezing environment. Despite the unique evolution of anti-freeze proteins, ice fish have lost the ability to adapt to temperature fluctuations and produce an HSR. They constitutively synthesize HSPs only as chaperones; whether or not they will be able to adapt to climate change by re-evolving an HSR depends on the rate of ocean warming (Somero and DeVries, 1967; Petricorena and Somero, 2007; Hofmann et al., 2000).

Organisms that live on the warmer end of the temperature spectrum, such as those in the marine intertidal, are typically adapted to moderate or extreme fluctuations in temperature on a daily and/or seasonal basis. Those adapted to moderate and extreme fluctuations are respectively termed mesotherms and eurytherms (Tomanek, 2008). Cardiac performance and respirometry (oxygen consumption, proxy for metabolic rate) are two measures commonly employed to characterize an organism's physiological response to thermal stress (Pörtner, 2010). Thermal optima are usually near the pejus temperature (Tp; latin for "getting worse") and are influenced by oxygen availability, which is contingent on the rate of aerobic metabolism. Thus, there is a relationship between oxygen availability and thermotolerance (Pörtner, 2010).

Molecular and cellular studies on physiological stress have helped us to understand how organisms maintain homeostasis at the cellular level. Mesotherms often initiate an HSR (T_{on}, Fig. 3) when the environment reaches temperatures just outside the range normally encountered, but thermal limits are typically reached (HSP synthesis stops; T_{off}, Fig. 3) at a level that is still tolerable for sympatric eurytherms. In contrast with mesotherms, eurytherms must initiate an HSR in order to cope with temperature fluctuations that are normally encountered (Tomanek, 2008). Since eurytherms are already pressed to their thermal maxima on a normal basis (T_{peak}, Fig. 3), and stenotherms have no or limited ability to initiate an HSR, these two groups are at the greatest risk for increasing temperatures due to climate change (Tomanek, 2008).

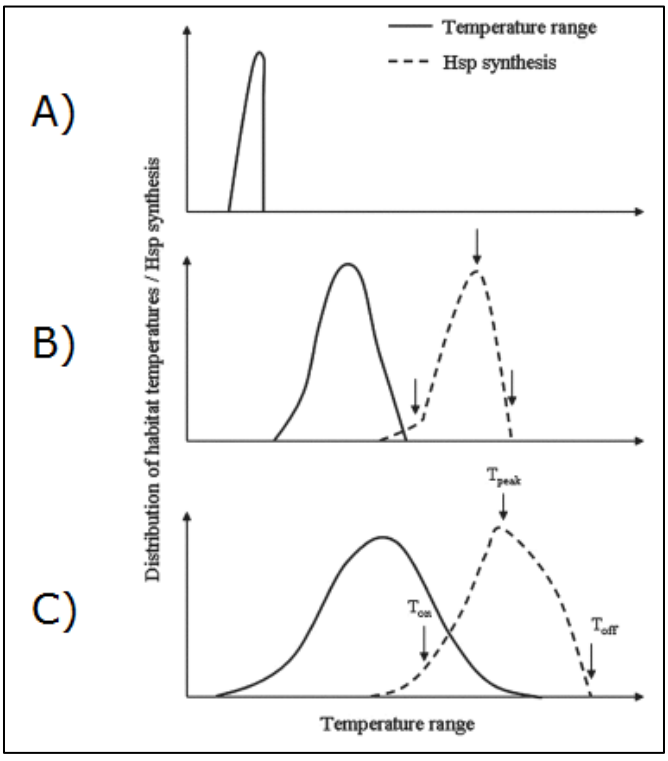

Figure 3. Acclimation capacity underlies thermal tolerance. Figure demonstrates the generalized relationship between acclimation capacity, temperature range, and heat shock response of (A) stenotherms found in thermally stable environments, (B) mesotherms found in environments of moderate thermal variability, and (C) eurytherms found in environments of extreme thermal variablility. Arrows point to general temperatures at which HSR is induced (T_{on}), HSP synthesis is maximized (T_{peak}), and where upper thermal limits are reached (T_{off}). Adapted from Tomanek (2008).

This model of environmental acclimatization has been demonstrated in a variety of organisms, especially intertidal invertebrates. Congeners of the sea snail genus *Tegula* (synonym: *Chlorostoma*) have been utilized as models to study thermal acclimation based on their latitudinal distribution, vertical distribution in the marine intertidal, and the thermal niche that each species occupies (Tomanek and Somero, 1999). One such study found that temperate subtidal congeners (*T. brunnea* and *T. montereyi*) initiated an HSR at temperatures below the HSR of a low-mid intertidal congener (*T. funebralis*), which in turn initiated an HSR below that of the tropical intertidal congener (*T. rugosa*) (Tomanek and Somero, 1999). Further research demonstrated that thermal acclimation of these snails at different temperatures could shift the temperatures for T_{on} and T_{peak}, but not for T_{off}. This suggests that thermal tolerance is plastic based on an individual's acclimation history, but this tolerance has an absolute limit based on that species' evolutionary history (Tomanek and Somero, 1999; Tomanek, 2002). This serves as a partial explanation for how thermal tolerance can dictate a species' biogeographical distribution across the intertidal and across latitudes (Tomanek, 2002).

How does natural selection operate on thermal stress limits? How did thermal niches come about? The answer lies partly in the molecular structure of proteins and the ability to synthesize appropriate molecular chaperones (e.g. HSPs and anti-freeze proteins). The ability of enzymes to catalyze reactions depends on their inherent flexibility, but increased flexibility is associated with increased thermal sensitivity (Fields, 2001). It is believed that stenothermal

organisms, such as the Notothenioid fish previously mentioned, have evolved flexible enzymes through amino acid substitutions that affect the secondary and tertiary structures; as a result, they can maintain the appropriate catalytic activity despite freezing temperatures. For organisms in extreme conditions, such as thermophilic bacteria in hot springs, amino acid substitutions have resulted in more rigid enzymes that impart thermostability (Kawamura et al., 1998; Fields, 2001). Thus, stenotherms of cold environments have traded the ability of thermal acclimatization for the ability to function optimally in cool, stable environments. Likewise, eurytherms can withstand hot temperatures but are not as efficient in cooler environments occupied by similar species that are optimally adapted to those conditions (Tomanek, 2008). A study on latitudinal distributions of the intertidal copepod *Tigriopus californicus* highlights the tradeoff of thermal adaptation. In this study, a heat-tolerant southern population was found to be less fit for competition in low to moderate temperatures compared to the cooler-adapted northern populations (Willett, 2010).

Additional note on molecular chaperones

It is important to note that onset of HSP synthesis may be induced (or possibly even repressed) by stresses other than temperature, and that HSPs are important in protein quality control outside of stressful conditions. There are different variants and families of HSPs that differ in molecular mass, cellular compartmentalization, degree of constitutive or inducible expression, and tissue specification (Feder and Hofmann, 1999). Of particular importance to this thesis are HSPs localized to the endoplasmic reticulum (ER), which are a prime

example of HSPs that regulate quality control in non-stressful conditions. Nascent proteins that are destined for secretion from the cell must enter the ER as unfolded polypeptides. In the ER they undergo glycosylation, formation of disulfide bridges, and oligomerization to become mature, folded proteins (Feige and Hendershot, 2013). The molecular chaperone called binding immunoglobulin protein (BiP), also known as 78 kDa glucose-regulated protein (GRP 78), is responsible for folding nascent proteins (Otero et al., 2010). It may also retrotranslocate irreversibly damaged proteins to the cytoplasm for proteolysis in a process called ER-associated degradation (ERAD) (Otero et al., 2010; Vembar and Brodsky, 2008). Another ER chaperone of note is endoplasmin, also called 94-kDa glucose-regulated protein (GRP 94), and represents the HSP90 family in the ER (Argon and Simen, 1999). In mammals, endoplasmin constitutes 5-10% of contents in the ER lumen with a concentration of 10 mg/mL (Koch et al., 1986). Similar to BiP, it folds nascent peptides and promotes ERAD of damaged proteins (Eletto et al., 2010; Marzec et al., 2012). It additionally binds calcium ions and is hypothesized to function in ER-associated calcium storage and release (Koch et al., 1986; Eletto et al., 2010; Marzec et al., 2012).

Hypercapnia

A decrease in oceanic pH can lead to waters that are corrosive to calcium carbonate ($CaCO_3$) skeletons and shells. A decrease in $CaCO_3$ saturation in acidified waters makes it difficult for calcifying organisms to repair their $CaCO_3$ skeletons or grow, and in extreme cases, decreased pH causes $CaCO_3$ skeletons to dissolve (Ries et al., 2009). For these reasons, most studies

investigating the biological effects of OA have been performed on what are perceived to be the most sensitive organisms: those that rely on the aragonite form of $CaCO_3$ for skeletogenesis, particularly cnidarians such as scleractinian corals (Whiteley, 2011). Echinoderms and molluscs (aside from cephalopods) have also been more intensely studied in the context of OA due to their poor iono-regulatory abilities. Studies have demonstrated that these taxa are limited in their ability to compensate for acid-base imbalances within their body compartments (Whiteley et al., 2011; Fabry et al., 2008). Results from these studies demonstrate that while some biological responses to OA can be explained (e.g., hemolymph pH is adjusted by $CaCO_3$ dissolution in mussels; Michaelidis et al., 2005), other responses (such as degradation of chitinous radular teeth of limpets; Marchant et al., 2010) are poorly understood and demonstrate that relatively little is known about the effects of OA compared to better-studied stressors such as temperature (Whiteley, 2011).

While the scientific community's focus on the effects of OA on sensitive species is far from a misguided endeavor, it has resulted in a lapse in knowledge about its effects on other taxa such as crustaceans (discussed below; Whiteley, 2011). However, within the last couple decades, an increased effort in understanding the biological impacts of OA have led to advances in our understanding of affected biological mechanisms. In teleosts, hypercapnia is thought to effect protein metabolism by decreasing protein production in the livers of Antarctic fishes (Langenbuch and Pörtner, 2003), reducing olfactory and homing abilities in larvae and adults of various species (Munday et al., 2009;

Dixson et al., 2010; Cripps et al., 2011), and decreasing auditory senses by affecting otolith formation (Simpson et al., 2011), all of which could potentially impact fish population management and sustainability in the face of overfishing (Munday et al., 2010). Effects of OA on protein metabolism have also been detected in the marine worm *Sipunculus nudus*, in which extreme hypercapnia causes a decrease in nitrogen excretion (correlating with decreased amino acid catabolism) (Langenbuch and Pörtner, 2002). In contrast, the polychaete *Nereis virens* was found to excrete more nitrogen in the form of ammonium (Widdicombe and Needham, 2007), suggesting that OA can have opposite effects on different organisms and emphasizing the need for caution in making extrapolations across taxa.

Crustaceans represent a neglected taxon in the scheme of OA studies (Whiteley, 2011). This is likely because crustaceans are considered good acid-base regulators and because they predominantly use calcite, a more stable form of $CaCO_3$ than aragonite, to mineralize their exoskeleton (Widdicombe and Spicer, 2008; Whiteley, 2011). However, crustaceans are ecologically important as primary and secondary consumers. They are also economically important as they account for millions of tons of biomass as pelagic zooplankton or as benthic adults. Most of the crustacean species (of which there are approximately 68,000 in existence) are marine species that will be affected by OW and OA (Whiteley, 2011).

Based on the potential impact made by this threat to crustaceans, it is critical to assess the future of crustaceans in the context of climate change and

physiological adaptation. In crustaceans, acid-base balance and ion regulation is maintained primarily through the gills, which also serve to take in oxygen gas from the water (Wheatly and Henry, 1992; Freire et al., 2008). Along the gill epithelia, active transport by Na^+/K^+ ATPase and V-type (vacuolar-type) proton ATPase create an ion gradient that allows for the electroneutral exchange of HCO_3^- for Cl^- and H^+ for Na^+ (Whiteley. 2011; Cameron and Iwama, 1987; Santos et al., 2007). Powering the Na^+/K^+ is an energetically-intensive process and can account for between 2.8-40% of total energy output of a single crustacean (Whiteley, 2011; Pannevis and Houlihan 1992; Leong and Manahan, 1997). Whiteley (2011) points out that although crustaceans are considered to be at reduced risk due to excellent compensatory mechanisms for acid-base balance, long term changes in pH could be energetically costly enough to impair fitness. For example, the tropical prawn *Macrobrachium rosenbergii* reduced protein biosynthesis during osmo- and iono-regulation when compared to controls in iso-osmotic salinities (Wang et al., 2004, Intanai et al., 2009), suggesting a trade-off in growth and health for long-term ion and acid-base balance (Whiteley, 2011).

Extracellular pH in crustaceans is also maintained in part by CO_2/HCO_3^- buffering in the hemolymph. CO_2 that is derived from metabolic ends contributes the most to extracellular acidification, but a steady-state equilibrium is reached between metabolic CO_2 production and excretion (Henry and Wheatly, 1992). Data suggest that CO_2 excretion is not modified to maintain the appropriate CO_2/HCO^{3-} ratio (Henry and Wheatly, 1992). Hemocyanin, the respiratory

pigment, may be affected by CO_2 or Cl^- concentration, but the affect varies between species and hemocyanin isoform (Magnum and Burnett, 1986).

The effects of OA on calcification in crustaceans are mixed and seem to depend on the duration of exposure as well as the degree of acidification in the environment. In review, Whiteley (2011) describes OA as affecting calcification rates in two ways. The first is by decreasing the pH of the exoskeletal compartment (Wood & Cameron 1985), and the second is by adversely affecting post-molt calcification through alteration of Ca^{2+}/HCO_3^- exchange across the gill epithelia (Neufield & Cameron 1992, Wheatly 1997).

Studies on calcification rates in crustaceans suggest that the effect of OA depends on duration and acidity of the exposure. Interestingly, $CaCO_3$ deposition in the exoskeleton is either increased or remains constant during a medium-term exposure to moderately-decreased pH in all crustacean species studied prior to the review by Whiteley, 2011. Increased calcium was first observed in the prawn *Penaeus monodon* followed by *Callinectes sapidus*, *Penaeus plebejus*, and *Homarus americanus* (Whiteley, 2011; Wickins,1984; Ries et al., 2009). The cuticle, which is an outer organic layer, may offer protection for moderate exposures to low pH (Whiteley, 2011). However, long-term exposure to lowered pH may induce morphological damage (shrimp), weaker wall plating (barnacle), and impaired growth due to metabolic compensation (barnacle), all of which could be detrimental to overall fitness (Whiteley, 2011; Kurihara et al., 2008; McDonald et al., 2009; Findlay et al., 2010).

1.3 The porcelain crab *Petrolisthes cinctipes*

Porcelain crabs (genus *Petrolisthes*) are marine decapod crustaceans that inhabit coastal regions throughout much of the world. They belong to the family Porcellanidae which is nested within the infraorder Anomura (Stillman, 2002). The Anomurans are a sister clade to Brachyurans, which are considered to be the “true crabs.” Anomuran body morphology is thought to have undergone the evolutionary process of carcinization, or becoming crab-like, independently of Brachyuran crabs (McLaughlin et al., 2004). This review will discuss the physiology and distribution, demography, and ecological behavior of the Anomuran *P. cinctipes* in the context of other Porcellanid species.

Eastern pacific *Petrolisthes* congeners

The genus *Petrolisthes* contains over 100 species and has a worldwide distribution. There are 46 species found along the coasts of the Eastern Pacific (Stillman, 2002). These species can be categorized latitudinally into four regional designations: north temperate (Alaska to California), gulf (northern Gulf of California), tropical (southern Gulf of California to Ecuador), and south temperate (Peru and Chile) (Fig. 4). These geographic bioregions discretely separate the presence of species groupings, with the exception of *P. armatus*, which is found in both gulf and tropical bioregions (Stillman, 2002). In addition to latitude, species are also discretely separated by vertical distribution along the intertidal.

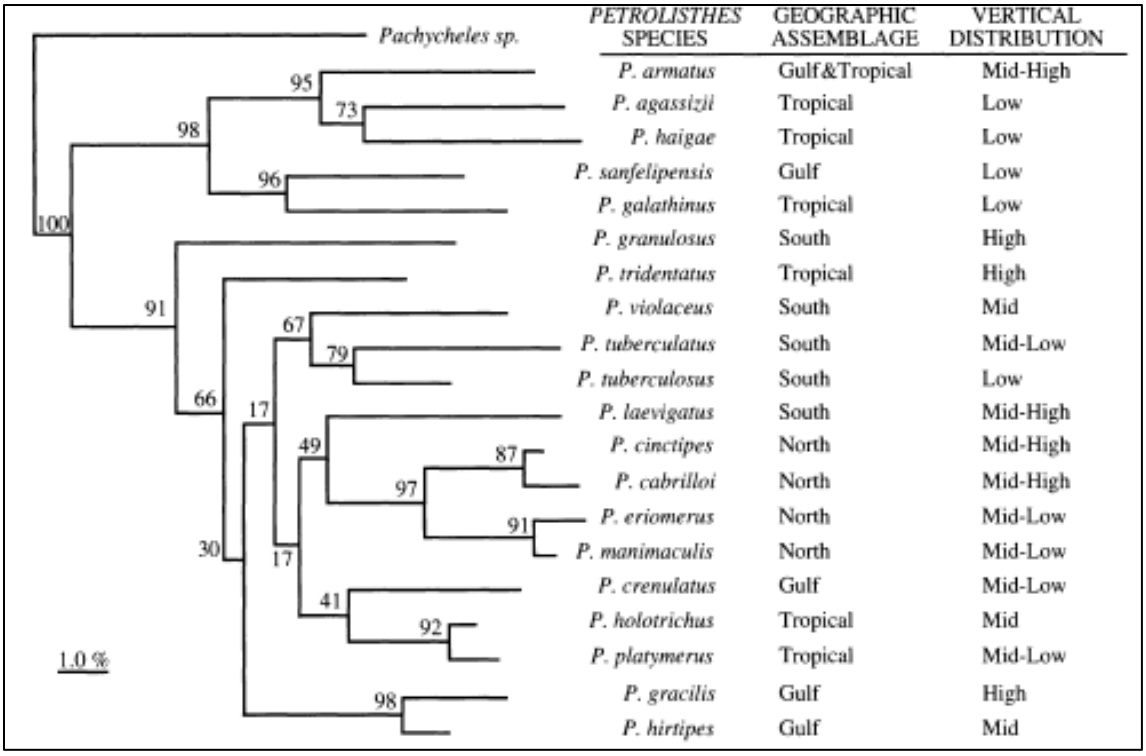

PETROLISTHES SPECIES	GEOGRAPHIC ASSEMBLAGE	VERTICAL DISTRIBUTION
P. armatus	Gulf&Tropical	Mid-High
P. agassizii	Tropical	Low
P. haigae	Tropical	Low
P. sanfelipensis	Gulf	Low
P. galathinus	Tropical	Low
P. granulosus	South	High
P. tridentatus	Tropical	High
P. violaceus	South	Mid
P. tuberculatus	South	Mid-Low
P. tuberculosus	South	Low
P. laevigatus	South	Mid-High
P. cinctipes	North	Mid-High
P. cabrilloi	North	Mid-High
P. eriomerus	North	Mid-Low
P. manimaculis	North	Mid-Low
P. crenulatus	Gulf	Mid-Low
P. holotrichus	Tropical	Mid
P. platymerus	Tropical	Mid-Low
P. gracilis	Gulf	High
P. hirtipes	Gulf	Mid

Figure 4. Phylogenetic tree of East Pacific *Petrolisthes* congeners illustrating respective latitudinal distribution and vertical zones. Phylogenetic relationship was constructed by comparing the 16sRNA gene. Legend: 1.0% indicates base pair length difference between species. Adapted from Stillman (2002).

These vertical zones are high (above the low high water mark), mid (mean water mark), and low (at or below the low low water mark). Additional intermediate vertical zones, such as mid high and mid low, are sometimes applied where there is clear spatial separation of different *Petrolisthes* congeners in these respective zones (Stillman, 2002).

Latitudinal zonation plays an important role in the physiology, and thus the distribution, of *Petrolisthes* congeners between bioregions, which form three distinct temperature classes. Both north and south temperate bioregions, together forming one temperature class, experience an annual average water temperature range of 8-18°C. Gulf *Petrolisthes* experience an annual average

water temperature range of 15-30°C, while tropical congeners are exposed to an annual average temperature of 20-30°C, with little variation in that temperature range. North and south temperate congeners nearest to the polar regions may experience a cooler temperature range between 8-11°C, and subtropical populations can sometimes experience temperatures as warm as the tropics during the summers (Stillman, 2002).

Vertical zonation is an equally important factor in spatial distribution of *Petrolisthes* congeners (Stillman, 2002). Species that spend most of their time in low, subtidal zones (usually stenotherms) are almost constantly underwater and thus experience little variation from water temperature. Species that are located in the mid- and high-intertidal zones (usually mesotherms and eurytherms) experience tidal sequences of ebb and flow; due to periodic exposure to water and air, they experience more highly variable differences in temperature (Stillman, 2002).

Physiology of *Petrolisthes cinctipes*

P. cinctipes inhabits the north temperature bioregion in the mid-high intertidal zone, ranging by most accounts from Porcher Island, British Columbia to Morro Bay, California (Stillman, 2002; Toonen, 2004). It is a rupestrine species, living under rocks and mussel beds (Stillman, 2002). It shares its latitudinal distribution with *P. eriomerus*, which typically lives in the mid-low intertidal zone. Other related porcellanids, *Pachycheles pubescens* and *Pa. rudens*, also live along the same bioregion.

Congeners living in the same latitude but in different vertical zones are ideal for comparing phenotypic plasticity between species. The mid-high zonation of *P. cinctipes* places it in conditions of high temperature variability and constant aerial exposure, whereas the lower zonation of *P. eriomerus* places it in conditions of lower temperatures and occasional emersion that occurs only during the lowest spring tides (Stillman and Somero, 1996). The temperatures under rocks in the mid-high intertidal zone can reach up to 31°C, 15°C higher than rocks in the low intertidal. The Arrhenius breaking temperature for *P. cinctipes* was found to be 31.5°C whereas for *P. eriomerus* it was 26.6°C (Stillman and Somero, 1996). This indicates that thermal stress is likely keeping the vertical distribution of *P. eriomerus* in check; however, it also suggests that *P. cinctipes* is likely near its thermal maximum during the most extreme heat events, and that it presently does not have the capacity to adjust to increasing temperatures brought about by global climate change (Stillman and Somero, 1996; Stillman and Somero, 2000).

An additional finding in the same study demonstrated that a leg membrane present on the ventral merus of each walking leg of *P. cinctipes* is involved in maintaining aerobic respiration during emersion. *P. eriomerus*, which lacks this membrane structure, switched to anaerobic respiration when maintained at 25°C for 5 h of emersion, whereas *P. cinctipes* did not under similar conditions (Stillman and Somero, 1996). Further investigation of the leg membrane amongst several *Petrolisthes* congeners found that it encompassed between 0-60% of the surface area of the meral segment depending on the species, and obscuring it

caused a 200-300% increase in lactate accumulation during emersion (Stillman, 2000). It is hypothesized that it is serves as a respiratory structure whose evolution has facilitated an increase in body size in some species of *Petrolisthes* (Stillman, 2000).

Demographics

A study on five Chilean porcelain crabs (*Petrolisthes granulosus*, *P. laevigatus*, *P. tuberculatus*, *P. violaceus*, and a closely related species, *Allopetrolisthes angulosus*) investigated how demographic factors, including relative abundance, sex ratio, maximum size, mature size, proportion of oviferous females, and presence of recruits varied between the center and boundaries of the populations of species (Rivadeneira et al., 2010). According to the abundant-center hypothesis (ACH), physiological constraints dictate that a particular species should be more abundant and more dense in the center of the distribution range, with abundance and density decreasing in the direction toward the boundaries of the population (Rivadeneira et al., 2010). In general, only two of the species corroborated the hypothesis in terms of relative abundance. Typically the female-to-male ratio was higher toward the center of the population, with fewer females and more males toward the boundaries. Maximum and mature sizes did not appear to match any trends in terms of relative location, nor did the proportion of oviferous females. However, recruits tended to be more abundant toward the equatorial direction, with absence of recruits toward the polar end of the population, suggesting that recruits survive better in lower latitiudes closer to the equator (Rivadeneira et al., 2010). The lack of recruits

toward the polar regions of *Petrolisthes* populations may be in part due to upwelling caused by offshore winds and equatorial flow. Upwelling fronts are usually high in nutrients that would support larvae (Mace and Morgan, 2006). This directional flow would disfavor the presence of planktonic larvae near the polar end in favor of the recruitment of juveniles toward the equatorial end of a population.

The distribution of larvae may also be due to ontogenic shifts in depth preference (Mace and Morgan, 2006). The larvae of *Petrolisthes cinctipes* are comprised of four apparent stages (see Fig. 5): prezoea, zoea I, zoea II, and megalopa (note that some authors consider the megalopa to be a postlarval stage, and thus would argue that *P. cinctipes* larvae are comprised of 3 stages; Gonor, 1970). Each stage may have a preference for depth, which in turn would affect its distribution amongst the currents, determining whether or not it is directed toward the coast for settlement or if it will remain in the ocean for further ontogenetic progress (Morgan and Mace, 2006). Presently, it is not clear how distant from the coast that larvae of *Petrolisthes* spp. are distributed, but several dynamics are likely involved, including geographic location, presence of bays or estuaries, freshwater flows from nearby rivers that affect salinity, among other factors (Morgan and Mace, 2006).

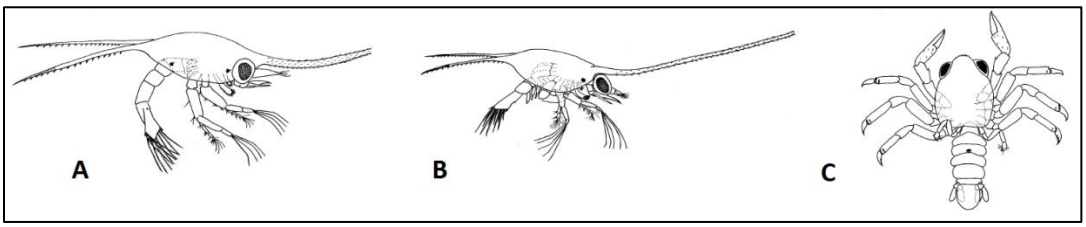

Figure 5. Drawings of *Petrolisthes cinctipes* larval and sub-adult stages. (A) Zoea I stage. (B) Zoea II stage. (C) Megalopa stage. Adapted from Gonor (1970).

Population genetics and evolution

Taxonomists regard porcelain crabs to be an interesting group of organisms for phylogenetic study, partly because it is a highly diversified taxon featuring variation in adult and larval morphology, color, and behavior (Hiller et al., 2006). Gonor's thesis on the larval morphology of *Petrolisthes* spp., including *P. cinctipes*, indicates that the location of a red chromatophore is species specific, and thus a good indicator for species identification (Gonor, 1970).

Early taxonomists relied on morphological features and color variation to set Porcellanid species apart from one another. Coloration has been a primary facet of decapod crustacean identification for decades, and the *Petrolisthes galathinus* complex contains species that are identified based on their coloration (Hiller et al., 2006). In 2001, Stillman and Reeb pioneered molecular techniques to distinguish evolutionary relationships between species of *Petrolisthes* by analyzing sequence divergence of the mitochondrial 16S rRNA gene. In this study, it was determined that *Petrolisthes* could be divided into two primary clades: spiny and smooth.

Stillman and Reeb (2001) questioned the validity of relying on color patterns to distinguish between the species of the *Petrolisthes galathinus* complex. Other researchers have followed up on this question by investigating how the molecular method of species identification matches up with color identification of species within the *P. galathinus* complex. Researchers measured the divergence of the 16S rRNA gene to distinguish between species in the complex. Additionally, they separately distinguished species based on the

following non-molecular parameters: discrete larval and adult morphometrics, sternal plate varation, and color (Hiller et al., 2006). The results indicates that color is in fact a reliable method of species determination within the *P. galathinus* complex. Additionally, this study compared the 16S rRNA gene of other Porcellanids as well as some Anomuran outgroups, such as hermit crabs, in order to test the monophyletic interpretation of Porcellanidae. The species *Petrocheles australiensis*, based on divergence of the 16S rRNA gene, was found to be placed outside of the Porcellanids. This brings into question whether porcelain crabs are monophyletic, as traditionally thought, or if they are actually a paraphyletic clade (Hiller et al., 2006).

Petrolisthes contains species that are free-living, partially-obligate, or fully-obligate symbiotes, establishing itself as a useful genus for applying a comparative approach to the study of the evolution of symbioses (Baeza, 2007). Congeners within *Petrolisthes* can be considered to exist within a continuum consisting of free-living and fully-obligate extremes. An example of a species placed somewhere in between the extremes is *P. armatus*, which exists symbiotically with other invertebrates only during certain benthic stages (Baeza, 2007).

The question arose as to the origins of symbiosis within *Petrolisthes;* it was hypothesized that high amounts of diversification, including adoption of a symbiotic lifestyle, was the consequence of high interspecific competition within the *Petrolisthes* genus (Baeza, 2007). To quantitatively determine the degree of symbiosis exhibited by a particular species, researchers developed a quotient of

symbiosis (QS), defined as “the number of sampling sites where specimens of a particular species were found associated with any type of living substratum (i.e. sponges, corals, sea anemones, sea urchins) divided by the total number of sampling sites from where crabs of the species in question were collected (Baeza, 2007).” Using this method, as well as phylogenetic data obtained from the 16S rRNA gene of various species, it was determined through maximum parsimony that symbiosis evolved at least twice within *Petrolisthes*, but interspecific competition did not play a significant role in its evolution (Baeza, 2007).

In addition to their evolution of symbiotic relationships, *Petrolisthes* congeners possess an unusual membrane structure on their walking appendages that offers significant evolutionary insight. The membrane is located on the meral leg segment in a decalcified area, and has been found to be involved in respiration (Stillman, 2000). The interspecific variation of the area of the membrane ranges between 0-60% of the area of the merus. Interestingly, aside from *Petrolisthes,* this membrane mode of respiration has only been found in Ocypodid ghost crabs (Brachyura) from Australia, offering interesting insight into convergent evolution between two relatively distant groups (Stillman, 2000).

Since *Petrolisthes* spp. are subject to segregation by vertical zonation, the presence or size of the membrane can be used to determine its importance based on the physiological and adaptational needs of certain *Petrolisthes* spp. For example, since crabs in the mid and high vertical zones are often exposed to air, their gills do not function in respiration as well as if they were submerged in

water. Therefore, the size of the membrane may correlate with the need for alternative modes of respiration (Stillman, 2000).

To investigate the evolutionary relationship between *Petrolisthes* congeners and the presence of the meral membrane, phylogeny was determined using the mitochondrial 16S rRNA gene (Stillman, 2000). Phylogenetically independent contrasts were used to determine the evolutionary relationship between membrane size and body size. The results indicated that the evolutionary origin of the membrane may not necessarily have been for respiration. The membrane was found to be contained completely within the "smooth" clade of Eastern Pacific *Petrolisthes* species, and it is speculated that membrane possession is the ancestral condition for this particular clade. It has been previously noted that in smaller *Petrolisthes* spp., the membrane does not play a large role in respiration. However, it appears to be an important part of respiration in larger species of *Petrolisthes* that are high in the intertidal zone since they have greater metabolic needs. In light of this, the respiratory nature of the membrane in larger species of *Petrolisthes* is an exaptation rather than an adaptation (Stillman, 2000).

Social Systems and Behavioral Ecology

The breeding of *Petrolisthes* spp. has been found to be highly dependent on seasonal factors. In Chile, oviferous females of *P. laevigatus* can be found in late winter (August), marking the start of the reproductive season (Lardies et al., 2010). Researchers have found that embryos take approximately two months to hatch into pre-zoea larvae. While the embryos conceived in August start to hatch

in October, *P. laevigatus* larvae continue hatching until late spring in December. This procession of hatching suggested that female crabs can undergo two spawns per breeding season (Lardies et al., 2010).

While the population size of male *P. laevigatus* remains relatively constant throughout the year, there is seasonal variation in the population size of females due to the reproductive season; therefore the sex ratio is highly variable (Lardies et al., 2010). Temperature is considered to be the primary factor of the seasons' influence on the population structure of *P. laevigatus*. Ovarian development is thought to be impacted by temperatures, therefore causing differential larval output during the breeding season by populations that inhabit different latitudinal zones (Lardies et al., 2010).

Seasonal variation in breeding is not as pronounced in all species of *Petrolisthes*. Oviferous *P. cinctipes* have been discovered in Monterey, California during all months except for October and November (Kerr and Duffus, 2005). Oviferous females are most abundant during May, August, and January through March, indicating that there is some predictable pattern in breeding. While it has been hypothesized that the release of *P. cinctipes* larvae is somehow related to tidal, lunar, or diurnal events, no such evidence has yet been found (Kerr and Duffus, 2005).

Oviferous females of *Petrolisthes* spp. are known to exhibit maternal behaviors that benefit the embryos in their brood. In the species *P. violaceus*, the fifth periopods are reduced and possess modified setae that are used to groom their brood (Förster and Baeza, 2001). Researchers observed that when foreign

debris was placed inside a brood of *P. violaceus*, the oviferous females did not make any active attempt at removing the debris. However, debris was incidentally removed through the passive grooming exhibited when oviferous females are not physically active and foraging (Förster and Baeza, 2001). In another experiment, oviferous females had their fifth periopods removed. The results showed that the removal of the grooming periopods significantly increased embryo mortality as well as the length of incubation until embryos hatched. Other species of *Petrolisthes* also have reduced fifth periopods, suggesting that other congeners potentially exhibit grooming behavior as well (Förster and Baeza, 2001)—this is likely to be the case for the *P. galathinus* complex, of which *P. violaceus* is a part of.

Courtship behavior of *Petrolisthes* spp. have been known for decades to be distinct between different species, and also varies within species (Molenock, 1975). In *P. cinctipes*, males establish territories and guard them; around 3-4 females may inhabit these territories. It has been noted that while larger males are guarding territories, smaller males are able to sneak around the large male and copulate with females in his territory. Once copulation is over, these females flee the male's territory. In addition to the females located in a male's territory, a male might also copulate with a female that passes nearby. Following copulation, males may immediately chase off the female, or he may stay with the female for two hours until the female starts to deposit eggs. At this point the male leaves while the female continues to deposit eggs (Molenock, 1975).

Both sexes of *Petrolisthes cinctipes* perform courtship behaviors; some of these behaviors are common between the sexes, while others are sex-specific (Molenock, 1975). Preliminary exchanges before copulation are not common, but they occur about 22% of the time (Förster and Baeza, 2001). Among most species of *Petrolisthes*, males and females may use their antennae to tap or lash each other, although this is not necessarily a courtship behavior. Females, in a rare event, may walk over males' chelae and carapace. Males appear to exhibit more courtship toward females than females do toward males. They may nudge the female with one claw, and then subsequently with the other claw. Shortly before copulation, males sometimes lift up their chelae and touch the female with the first pair of periopods. He then will touch the female with his first and second pair of periopods, and afterwards will begin copulation. *P. eriomerus* and *P. manimaculis* sometimes oscillate their third maxillipeds in the presence of females, only after making visual or tactile contact; other species of *Petrolisthes* have not exhibited maxilliped courtship behaviors (Molenock, 1975).

In porcelain crabs, maxillipeds are modified to have feathery structures which they use to filter feed in the water, catching detritus or small organisms such as *Artemia* (Gonor and Gonor, 1973). They extend and retract their maxillipeds in a feeding motion at the first sign that food is present; it is unknown whether or not the first sign of food is usually a visual or chemical cue. Depending on the situation, porcelain crabs will scrape rocks with their maxillipeds to remove detritus; other times they will pick up loose substrate and

gravel, catching the detritus as the gravel slips through the feathery structures (Molenock, 1975).

Maxillipeds are the only appendage used for the acquisition of food in porcelain crabs; the chelae are never used for feeding, and are apparently only used for intimidation and combat (Molenock, 1975; Rypien and Palmer, 2007). In the field, 40% of individuals in the *Petrolisthes cinctipes* population have puncture wounds on their chelae. While usually there is only one wound per individual, it provides evidence that there is aggressive intraspecific competition. While their chelae are large relative to their body size, they are not very robust and thus appear to be more for display rather than direct combat; however, combat does appear to take place (Rypien and Palmer, 2007).

P. cinctipes individuals live in conditions of high density, and therefore competition for food can be fierce. Observational studies show that there is a dominance hierarchy among groups of *P. cinctipes*, often with one male that controls territory with the water current that provides the best nutrition (Rypien and Palmer, 2007). Laboratory studies show that *P. cinctipes* indeed compete for foraging space using their chelae as weapons; it has also been demonstrated that males and females also compete for space, and chelae are not used for any sort of sexual aggression toward one another (Rypien and Palmer, 2007).

Size plays an important role for in terms of competition for foraging space (Donahue, 2004). Research indicates that as density increases, growth rate declines for all individuals, but it is particularly harsh for smaller individuals. In laboratory experiments that manipulated the nutritional level of the seawater,

smaller individuals were more sensitive to the effect of food level than larger individuals. Density-dependent agonistic interactions between individuals therefore lower feeding rate, and thus growth rate, particularly in smaller individuals (Donahue, 2004).

Donahue (2004) also notes that chelipeds are sometimes lost, particularly in smaller individuals. It was noted that when small individuals lost a cheliped, their carapace growth rate decreased (Donahue, 2004). This result was corroborated in a following study, where researchers speculated that the decrease in growth rate shifted the use of resources from growth to limb regeneration (Barria and Gonzales, 2008). However, Donahue (2004) also noted that while carapace width growth rate decreased, total biomass growth rate increased; additionally, the same study found that individual fecundity of *Petrolisthes cinctipes* is directly proportional to individual biomass (Fig. 6). This suggests that cheliped loss may convey a fitness advantage to smaller crabs when forced into a situation of suboptimal foraging by larger, more competitive crabs. To further investigate this behavior, studies should focus of determining the relationship between density, size, resource availability, and an individual crab's sex with respect to cheliped loss.

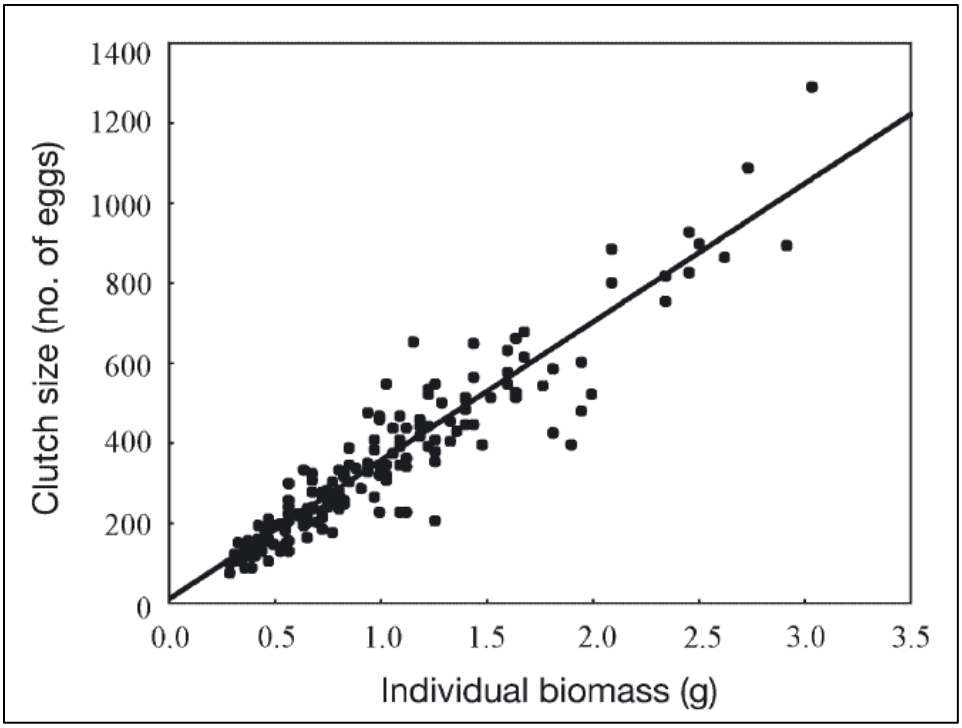

Figure 6. The fecundity of a *Petrolisthes cinctipes* female is directly proportional to her total individual biomass. Adapted from Donahue (2004).

2.0 THERMAL ACCLIMATION MANUSCRIPT

Adapted from:

Garland, M.A., Stillman, J.H., and Tomanek, L., 2015. The proteomic response of cheliped myofibril tissue in the eurythermal porcelain crab *Petrolisthes cinctipes* to heat shock following acclimation to daily temperature fluctuations. *Journal of Experimental Biology* 218, 388-403 doi:10.1242/jeb.112250

2.1 Abstract

The porcelain crab *Petrolisthes cinctipes* lives under rocks and in mussel beds in the mid-intertidal zone where it experiences immersion during high tide and saturating humid conditions in air during low tide, which can increase habitat temperature by up to 20°C. To identify the biochemical changes affected by increasing temperature fluctuations and subsequent heat shock (HS), we acclimated P. cinctipes for 30 days to one of three temperature regimes: 1) constant 10°C, 2) daily temperature fluctuations between 10-20°C (5 h up-ramp to 20°C, 1 h down-ramp to 10°C) and 3) 10-30°C (up-ramp to 30°C). After acclimation, animals were exposed to either 10°C or a 30°C HS to analyze the proteomic changes in claw muscle tissue. Following acclimation to 10-30°C (measured at 10°C), enolase and ATP-synthase increased in abundance. Following heat shock, isoforms of arginine kinase and glycolytic enzymes such as aldolase, triose phosphate isomerase and glyceraldehyde 3-phosphate dehydrogenase increased across all acclimation regimes. Full-length isoforms of hemocyanin increased abundance following acclimation to 10-30°C, but hemocyanin fragments increased after HS following constant 10°C and fluctuating 10-20°C, possibly playing a role as anti-microbial peptides. Following constant 10°C and fluctuating 10-20°C paramyosin and myosin heavy chain type-B increased in abundance, respectively, while myosin light and heavy chain decreased with HS. Actin-binding proteins, which stabilize actin filaments (filamin and tropomyosin), increased during HS following 10-30°C, however, actin

severing and depolymerization proteins (gelsolin and cofilin) increased during HS following 10-20°C, possibly promoting muscle fiber restructuring. RAF kinase inhibitor protein and prostaglandin reductase increased during HS following constant 10°C and fluctuating 10-20°C, possibly inhibiting an immune response during HS. The results suggest that ATP supply, muscle fiber restructuring and immune responses are all affected by temperature fluctuations and subsequent acute HS in muscle tissue. Furthermore, while HS after acclimation to constant 10°C and fluctuating 10-30°C showed the greatest effects on the proteome, moderately fluctuating temperatures (10-20°C) broadened the temperature range over which claw muscle was able to respond to an acute HS with limited changes in the muscle proteome.

2.2 Introduction

Environmental temperature has a ubiquitous effect on rates of biochemical reactions and cellular structures in ectothermic organisms, which have adapted their cellular processes and structures to cope with the specific thermal properties of their habitat (Somero, 2012; Tomanek, 2010). Organisms' ability to adjust biochemical processes to different body temperatures is in large part determined by the rate and amplitude of temperature change and their evolutionary history, e.g. the thermal environment they occupy, and recent thermal history, e.g. acclimatization. For example, intertidal organisms show different physiological responses to heat stress during emersion and immersion due to differing heating rates under each condition (Bjelde and Todgham, 2013; Tomanek and Somero, 2000) and closely related species occupying environments that vary greatly in thermal fluctuations along the physical gradient from the subtidal to the mid-intertidal zone differ in their ability to adjust cardiac thermal performance and heat-shock protein synthesis in response to temperature acclimation (Stillman, 2003; Tomanek and Somero, 1999). However, while we have a good understanding of the thermal range of organisms and their physiological plasticity in response to constant temperatures and acute heat stress, very little is known about how daily temperature fluctuations affect the physiology of organisms and determine the response to a subsequent acute heat stress.

Studies on the intertidal mussel *Mytilus* showed that acclimation to fluctuating temperatures broadened the range over which metabolic rate was

temperature-independent and that temperature range of filtration-feeding was expanded in comparison to animals acclimated to constant temperatures (Widdows, 1976). A study on the response of the water flea (*Daphnia pulex*) to various temperature fluctuations (15°C, 15-25°C and 15-30°C daily) showed that the greatest fluctuations reduced metabolic rates after six generations but increased temperature tolerance after over 15 generations (Chen and Stillman, 2012). Thus, greater fluctuations come with increased physiological costs but also increased stress tolerance, suggesting a trade-off between the two. The evolutionary adaptations to differences in temperature fluctuations are largely unknown, although a study on gammarid amphipods showed greater molecular diversity in myosin isoforms in congeners from thermally more variable environments (Rock et al., 2009). A study on the transcriptomic changes in liver tissue of annual killifish (*Austrofundulus limnaeus*) in response to constant and fluctuating daily temperatures showed that genes involved in cell growth and proliferation, molecular and chemical chaperones and maintenance of membrane integrity differ between these conditions, providing a framework for the cellular processes that might be affected by temperature fluctuations (Podrabsky and Somero, 2004). To our knowledge there has not been a study of the proteomic changes that might occur under fluctuating temperature regimes, especially not for intertidal organisms that are typically experiencing greatly fluctuating thermal conditions.

Proteomic analyses of non-model organisms have become possible recently due to the increasing number of completed genome sequences and

well-annotated expressed sequence tag (EST) libraries and have added to our understanding of the responses of marine organisms to temperature, osmotic, hypoxic and oxidative stress (Tomanek, 2011; Tomanek, 2014). Specifically, a number of recent proteomic analyses of gill tissue of several marine non-model organisms in response to acute heat and chronic warm temperature stress showed that temperature stress increases the abundance of oxidative stress proteins and molecular chaperones, presumably because of the effect of reactive oxygen species on the cytoskeleton (Dilly et al., 2012; Fields et al., 2012a; Fields et al., 2012b; Tomanek and Zuzow, 2010). However, how temperature fluctuations affect the proteomic response to heat stress is not known.

Species of the porcelain crab genus *Petrolisthes* are distributed from the shallow subtidal to mid-intertidal zone of rocky shores where they experience temperature fluctuations of up to 20°C during a tidal cycle under conditions that range from submersion to fully humid (Teranishi and Stillman, 2007). Furthermore, the trancriptome of several tissues of one species, *Petrolisthes cinctipes*, has been characterized in response to acute temperature stress (Tagmount et al., 2010; Teranishi and Stillman, 2007). *Petrolisthes cinctipes* occupies the mid- to high-intertidal zone and has one of the highest thermal tolerances of the temperate Petrolisthes congeners (Stillman and Somero, 2000). In addition, it shows limited adjustments in thermal limits, e.g. LT50, with increasing acclimation temperature, in contrast to its subtidal to low-intertidal temperate congeners (Stillman, 2003). Thus, given the thermal biology of P. cinctipes and with the transcriptomic database as a foundation for the

identification of proteins with mass spectrometry, we assessed how the proteome of claw muscle tissue changes during acclimation to three different ranges of temperature fluctuations and a subsequent heat stress. Our results suggest that different ranges of thermal fluctuations affect energy metabolism, oxygen delivery, actomyosin structures and dynamics and the immune response of claw muscle tissue during subsequent heat stress.

2.3 Materials and Methods

Animal collection, maintenance, and experimental design

Adult Petrolisthes cinctipes (Randall, 1839) were collected from the intertidal zone of Fort Ross, CA, USA (38°30’ 51″N, 123°14’ 34” W) in October 2008. The crabs were transported to the Romberg Tiburon Center for Environmental Studies (San Francisco State University, Tiburon, CA, USA), where they were maintained in a common garden acclimation under constant immersion at 10°C for 30 days. Following the common garden, crabs were randomly placed into three treatment groups (Fig. 7). Over 30 days, these groups experienced acclimation at either 10°C (“constant”) or daily heat ramps from 10-20°C (“moderate”) or 10-30°C (“extreme”). All thermal acclimations had temperature precision of at least ±0.5°C. In the two groups that experienced heat ramping, temperature was gradually increased over a 5 h period to the respective peak temperature, and then cooled to 10°C over 1 hour. After these temperature acclimations, crabs from each treatment were randomly placed in either a constant 10°C immersion or given a ramp-up to 30°C heat shock over 5 h. All individuals were given a 1 h recovery period at 10°C before being flash frozen in liquid nitrogen and stored at -80°C. Four claw segments (dactyl, propodus, carpus, and merus) were dissected and transported to the Environmental Proteomics Laboratory (Cal Poly, San Luis Obispo, CA, USA) on dry ice for proteomic analysis.

Homogenization

Claw tissue was lysed in ground glass homogenizers in a 1:4 ratio of homogenization buffer (7 mol L-1 urea, 2 mol L-1 thiourea, 1% ASB (amidosulfobetaine)-14, 40 mmol L-1 Tris-base, 40 mmol L-1 dithiotheitol, and 0.5% immobilized pH 4-7 gradient (IPG) buffer (GE Healthcare, Piscataway, NJ, USA)), solubilized at 20°C for 1 h, and then centrifuged at 16,100 g for 30 minutes at 20°C. Proteins were precipitated from the supernatant using a 1:4 ratio of ice-cold 10% trichloroacetic acid in acetone with an overnight incubation at -20°C. The samples were centrifuged at 18,000 g for 15 minutes at 4°C, after which the supernatant was discarded and the protein pellet washed with ice-cold acetone. Samples were again centrifuged according to the previous parameters and the supernatant was discarded. After briefly drying in air, the protein pellets were re-suspended in rehydration buffer (7 mol L-1 urea, 2 mol L-1 thiourea, 2% CHAPS (cholamidopropyldimethylammonio-propanesulfonic acid), 2% NP (nonyl phenoxylpolyethoxylethanol)-40), 0.002% bromophenol blue , 0.5% IPG (4-7) buffer, and 100 mmol L-1 dithioerythritol) and solubilized at 20°C for 1 hour. To determine the protein concentration in each sample, a concentration assay was performed using the 2D Quant Kit (GE Healthcare) according to the manufacturer's instructions.

Two-dimensional gel electrophoresis (2D-GE)

For first dimension electrophoresis, proteins were separated according to their isoelectric points (pI), using IPG gel strips (pH 4-7, 11 cm; GE Healthcare). Protein samples were diluted to a concentration of 2 µg µL-1 in rehydration

buffer, and 200 µL (400 µg) was loaded onto each IPG gel strip in one well of an isoelectric focusing cell (BioRad, Hercules, CA, USA). Protein solution was absorbed into each IPG gel strip over 5 h of passive rehydration followed by 12 h of active rehydration at 50 V. Separation and focusing of proteins was performed by running gel strips at 500 V for 1 h, 1000 V for 1 h, and then 8000 V for 2.5 h (maximum current 50 µA; all voltage changes occurred in rapid mode). After isoelectric focusing, gel strips were frozen at -80°C. After freezing for at least 1 h, gel strips were prepared for 2nd dimension SDS-PAGE by incubating them in equilibration buffer (6 mol L-1 urea, 375 mmol L-1 Trisbase, 30% glycerol, 2% SDS, 0.002% bromophenol blue) at 20°C for two 15 minute intervals, first with 65 mmol L-1 dithiothreitol and then with 135 mmol L-1 iodoacetamide. Gel strips were then placed over 11.8% polyacrylamide gels and electrophoresed (Criterion Dodeca; BioRad) for 55 minutes at 200 V. Following electrophoresis, gels were stained using colloidal Coomassie blue (G-250) overnight and then destained through repeated washing with milliQ water over 48 hours. Gels were then scanned with an Epson 1280 transparency scanner (Epson, Long Beach, CA, USA).

Gel image analysis

Digitized 2D gel images were analyzed using Delta 2D (version 3.6; Decodon, Greifswald, Germany) (Berth et al., 2007). To detect protein spots, gels from all treatments were multiplexed into a single fused image. The spot boundaries detected on the fused image were transferred back to the individual gels, establishing protein spot parameters for each gel. Following background

subtraction, the relative spot volume of each protein was quantified by normalization against the total spot volume of all proteins in the gel image.

Mass Spectrometry

Gel plugs were prepared for analysis using mass spectrometry (MS) according to previously published methods (Fields et al., 2012; Tomanek and Zuzow, 2010). Briefly, peptide mass fingerprints (PMFs) were obtained using a matrix-assisted laser desorption/ionization tandem time-of-flight (MALDI-ToF-ToF) mass spectrometer (UltraFlex II; Bruker Daltonics, Inc.; Billerica, MA, USA). To obtain b- and y-ion parameters, at least 6 peptides were selected for tandem MS. Spectral analysis of peptides followed previously published methods (Fields et al. 2012; Tomanek and Zuzow, 2010). FlexAnalysis (version 3.0; Bruker Daltonic, Inc.) was used to detect peptide peaks, using a signal-to-noise ratio of 6 for MS and 1.5 for MS/MS. Internal mass calibration was performed using porcine trypsin. Proteins were identified using Mascot (version 2.2; Matrix Science, Inc.; Boston, MA). PMFs and tandem mass spectra were combined and searched against the Porcelain Crab Array Database (PCAD), an EST library for P. cinctipes that contains 19,000 unique sequences (Tagmount et al 2010). Spectra that could not be identified with PCAD were searched against an EST library for the boreal spider crab, *Hyas araneus* (Harms et al., 2013). One missed cleavage was allowed during searches. For the MS/MS analysis, the precursor-ion mass tolerance was set at 0.6 Da (default Mascot value). Search results were deemed significant ($p \leq 0.05$) if their molecular weight search (MOWSE) score was

42 or higher for PCAD and 34 or higher for the H. araneus EST. For results with a significant MOWSE score, only positive identifications that included two matched peptide sequences were accepted.

Exploratory statistical analysis

We compared protein abundances between treatment groups via average linking of individual gels (Delta 2D) using a Pearson correlation metric. We performed a two-way ANOVA ($P \leq 0.02$) comparing thermal acclimation versus acute heat shock effects and grouped significantly changing proteins into hierarchical clusters. To better understand the importance of particular proteins in characterizing the proteomic response to different temperature treatments, we used principal component analysis (PCA; Delta 2D) based on proteins whose expression profiles significantly changed, regardless of whether they were identified with MS. Of the proteins that were identified with MS, we assigned component loading values which are quantifications of a protein's contribution to sample separation along a given component.

2.4 Results and discussion

We generated a fused image comprising gels from all temperature acclimation and acute heat shock (HS) treatments. In this fused gel image (Fig. 8), we detected 469 protein spots. Of these spots, 42% (197) changed abundance in response to temperature acclimation, acute HS, or their interaction; functional annotations were available for 73.6% (145) of these proteins (Table 2). Changes in protein abundance may be attributed to an increase or decrease in synthesis, degradation, or post-translational modifications (PTMs), including partial proteolysis. Thus, our interpretation is based on a subset of protein isoforms, which might not represent the full complement of isoforms of a particular protein and therefore might not represent the complete abundance of this protein. With these limitations in mind, our interpretations are meant to be hypotheses that generally require further validation.

To discuss the contribution of the cellular processes associated with the function of specific proteins, we grouped proteins into the following categories: ATP buffering, energy metabolism, respiratory, cytoskeletal and signaling proteins. Cytoskeletal proteins were separated into thin filament (actins), thick filament (myosins), and actin-binding proteins.

Principal component analysis

We conducted principal component analyses (PCAs) to assess the variation in protein abundance patterns based on statistical significance for acclimation, HS or interaction effects, based on a two-way permutation ANOVA ($p \leq 0.02$).

Principal components (PCs) that separated the treatments were analyzed further by identifying proteins that contributed the most to the separation, based on their loadings.

The first PCA (Fig. 9A) includes 83 proteins (65 identified) that were significant for an acclimation effect. The first component (PC1; 30.5%), separated both 10-30°C acclimation treatments (positive values on x-axis) from all other treatments. The second component (PC2; 16.4%) represented the effect of 10°C and 10-30°C acclimation regimes on a subsequent HS (negative values on y-axis). Heat shock following the 10-20°C acclimation only had a limited effect on shifting samples along PC2, suggesting that these temperature fluctuations induced a cellular response that prepared the animals for a 30°C HS requiring limited changes of the proteome. The 10°C and 10-30°C acclimation regimes did not do the same. Thus, moderate temperature fluctuations broadened the range over which the claw muscle could respond to heat stress.

Proteins representing ATP buffering (arginine kinase; AK), glycolysis (phosphoglycerate kinase and enolase), and thin (actin) filaments showed the most positive loadings (indicating greater abundances in the 10-30°C acclimation group; Table 3). ATP buffering and thin filament proteins also contributed highly negative loadings (lower abundances in the 10-30°C acclimation), suggesting that these functions changed the most with the most extreme daily temperature fluctuations. Interestingly, while some glycolytic proteins showed highly positive loadings (phosphoglycerate kinase and enolase), others showed highly negative loadings (fructose 1,6-bisphosphate aldolase or aldolase) for PC1, suggesting

differences between the preparatory and the pay-off phase of glycolysis. Similarly, while some full-length hemocyanins showed highly positive loadings (spots 58 and 59), others that are fragments of the full-length protein (spots 37 and 160) showed negative loadings, suggesting that full-length hemocyanin increased while fragments decreased in the 10-30°C acclimation (see below). PC2 separated the 10°C and 10-30°C HS treatments from all others. The pay-off phase of glycolysis and ATP buffering contributed the most to the positive loadings (Table 3), similar to PC1. ATP buffering (five AK isoforms) and actin-binding proteins (three filamin isoforms) contributed the most to the negative loadings (higher abundances at 10°C HS and 10-30°C HS). Additionally, a neurogenic notch homolog played a role during HS.

The PCA based on proteins that significantly changed with acute HS included 130 (90 identified) proteins (Fig. 9B). The HS treatments of all three acclimation regimes are separated along PC1 (23%; positive) and PC2 (15.8%; negative).

Glycolysis (glyceraldehyde 3-phosphate dehydrogenase or GAPDH), ATP-buffering, thin filaments and respiratory (or anti-microbial – see below) proteins (hemocyanins fragments) contributed highly positive loadings to PC1, with higher abundances following HS (Table 4). Four myosin heavy chain (three type B) isoforms contributed highly positive loadings. The negative loadings of respiratory proteins (full-length hemocyanins) and thick filaments (myosin non-type-B) along PC1 coincided with lower abundances during HS. The role of

prostaglandin reductase, which showed the second highest positive loading along PC1, might be to suppress inflammation during HS (see below).

Along PC2, positive loadings by four myosin regulatory light chain isoforms coincided with lower abundances during HS. Combined with the loadings for PC1, it seems that HS leads to higher abundances of myosin heavy chain (type B and non-type B) but lower abundances of different myosin regulatory heavy and light chain isoforms. Negative loadings of three filamins, an actin-binding protein that connects actin filaments (van der Flier and Sonnenberg, 2001), along PC2 were based on higher abundances during HS following the 10°C and 10-30°C acclimation regimes. Thus, HS leads to higher abundances of myosin heavy chain (but lower abundances of myosin regulatory light chain and distinct heavy chain isoforms), hemocyanin fragments (spots 12 and 138), filamins and arginine kinase isoforms.

Seventy-one proteins (55 identified) contributed significantly to the interaction effect (Fig.9C). PC1 (26.3%) separated the control (most positive) and the HS (most negative) treatments of the 10°C-30°C acclimation regime the most. PC2 (17.6%) separated the 10°C acclimation plus HS (most negative) from all other treatments. In contrast, 10°C-20°C acclimation control and 10°C-20°C acclimation control plus HS overlapped, again suggesting that moderate temperature fluctuations broaden the range over which claw muscle can respond to an acute heat stress.

More specifically, several thin filament and respiratory proteins (most positive loadings) increased with acclimation to 10-30°C, while ATP buffering and

thin and thick (myosin heavy chain) filament proteins (most negative loadings) increased with 10-30°C plus HS (Table 5). Also, full-length hemocyanins increased under the 10°C-30°C acclimation regime under control but not acute HS.

ATP buffering also contributed high negative loadings to PC2 by increasing abundances with HS following the 10°C acclimation. Thin and thick filaments contribute positive loadings, suggesting that some actins and myosin decreased abundance at 10°C acclimation plus HS. Two enolase isoforms showed positive loadings along PC2 (decreasing abundance with 10°C acclimation plus HS), while another glycolytic protein, GAPDH, showed highly negative loadings for PC2 (higher abundance with 10°C acclimation plus HS). This suggests that these glycolytic reactions are responding differently to HS following acclimation to 10°C: with a decrease and increase in abundance with HS for enolase and GAPDH, respectively. GAPDH also increases abundance with HS following the 10°C-30°C acclimation.

Energy metabolism

The majority of metabolic proteins identified are either involved in the transfer of phosphoryl groups, e.g., arginine kinase (AK), or in ATP production via glycolysis, e.g. GAPDH. We will first discuss them separately and then describe possible links.

Phosphotransfer proteins

Thirty arginine kinase (AK) isoforms changed abundance and were separated into four general groups: those with high abundance following the 10-30°C

acclimation (cluster I), high abundance following 10-20°C HS (and low abundance following 10-30°C; cluster II) and those with high abundance during HS following 10°C acclimation (and some isoforms following 10-30°C HS; cluster III) or all three acclimation treatments (cluster IV; Fig.10). These groupings are generally supported by the statistical results, indicating significance for acclimation (clusters I and II) or heat stress (cluster IV) alone or an interaction effect (cluster III). The number of AK isoforms varied from five (cluster I) to nine. The diversity of AK isoforms can in part be explained by the existence of four different AK transcripts in the *Petrolisthes* EST library (Tagmount et al., 2010). They may be separate isoforms for the cytosolic and mitochondrial compartment (Uda et al., 2006). Although no PTMs have been reported for AK, it is possible that AK has similar PTMs to its vertebrate functional-homolog, creatine kinase, which include nitrosylated or glutathionylated thiol groups that are related to oxidative stress and can affect creatine kinase activity (Reddy et al., 2000; Wolosker et al., 1996). Glutathionylation of one protein cysteine residue reduces the pI by 0.5 pH units (Ubuka et al., 1987). Interestingly, several AK isoforms that increase abundance with HS (clusters III and IV) show lower pIs that are about one pH unit lower than the majority of AK isoforms of cluster I, possibly indicating two glutathionylation sites (Fig. 10). Claw tissue includes four muscle subtypes (dactyl, propodus, carpus, and merus) but there is no evidence for muscle-specific AK isoforms. Another 2DGE analysis on the prawn *Marsupenaeus japonicas* showed three isoforms increasing abundance in

muscle tissue during recovery from hypoxic stress (Abe et al., 2007), suggesting that energetic stress causes changes in the abundance of multiple AK isoforms. Given that the temperature fluctuations applied in our experiment likely affected reaction rates and therefore caused high and fluctuating ATP consumption rates, we assume that AK's main function under these circumstances is the transfer of phosphoryl groups from arginine-phosphate to MgADP- to maintain ATP levels and thereby energy homeostasis (Ellington, 2001; Hochachka, 2003). However, AK also affects glycolytic rates through the release of inorganic phosphate, which serves as (i) a substrate for glycogen phosphorylase, leading to the breakdown of glycogen to glucose-1-phosphate, and (ii) a H+ buffer during glycogenolysis and glycolysis (Ellington, 2001; Griffiths, 1981). Support for a possible role of AK isoforms in regulating glycogenolysis comes from the identification of glycogen phosphorylase, which increased abundance with HS after acclimation to 10°C and 10-20°C (Fig. 11). Furthermore, glycogen phosphorylase is regulated by phosphorylation and, in addition, AMP levels (for an interesting historical account of this topic see Fischer, 2013), which are regulated in part by adenylate kinase, which catalyzes the conversion of two ADP into ATP and AMP and showed an interaction effect (Fig. 10). Together these findings suggest an important role for ATP-buffering and glycogenolysis during HS after acclimation to constant 10°C and moderately fluctuating temperatures, and a possible role for arginine and adenylate kinase in regulating these cellular pathways.

Glycolysis

Most of the metabolic proteins that changed during acclimation and acute HS are part of the glycolytic pathway (Fig. 11). Acclimation to different thermal conditions, followed by a 30°C HS, led to three major clusters of protein abundances: Cluster I showed increase abundances specifically during HS following the 10-30°C acclimation in nine protein isoforms. Six of the isoforms in this cluster were identified as GAPDH, one as triose phosphate isomerase (TPI), enolase and pyruvate dehydrogenase (PDH), respectively. Cluster II showed an increase in abundance of three enolase and one phosphoglycerate kinase isoforms during 10-30°C acclimation. Cluster III showed an increase in abundance by three enzymes, GAPDH (three isoforms), TPI and aldolase, during HS following acclimation to 10°C and 10-20°C. This cluster also includes glycogen phosphorylase. Thus, we have a cluster that is characterized by an increase in abundance with acclimation to 10-30°C (cluster II), and with HS following acclimation to 10-30°C (cluster I) and 10°C as well as 10-20°C (cluster III). Thus, the three reactions from fructose 1,6-bisphosphate to 1,3-bisphosphoglycerate, including aldolase, TPI and GAPDH, are potentially modified in response to acute HS (cluster III), possibly to support ATP production under acute stress conditions through glycolysis. Acclimation to constant daily fluctuations of 10-30°C led to an increase in three enolase isoforms, phosphoglycerate kinase and F1-ATP synthase β-subunit. The three isoforms of enolase differ mainly in pI but not mass, suggesting that they differ in PTMs. These changes also affected the response to acute HS following acclimation to

10-30°C, increasing the abundance of five additional GAPDH isoforms, TPI and enolase as well as PDH. Thus, the reactions of the triangle between aldolase, GAPDH and TPI characterize the response to acute HS following acclimation to constant (10°C) and moderate temperature fluctuations (10-20°C), but more extreme fluctuations require several additional enolase and GAPDH isoforms and phosphoglycerate kinase.

A possible explanation for the number of enolase and GAPDH isoforms are PTMs, e.g., glutathionylation, which is known to modify and affect the activity of GAPDH, TPI and aldolase (Dalle-Donne et al., 2009; Fratelli et al., 2003). In addition, enolase is modified by phosphorylation, acetylation and methylation (Zhou et al., 2010).

Energy metabolism - conclusion

The prominence of arginine kinase and glycolytic protein isoforms, e.g., GAPDH, in the proteomic responses to temperature acclimation and HS suggest an important role for phosphotransfer proteins and glycolysis in maintaining energy homeostasis in muscle tissue during temperature fluctuations. Creatine kinase (and by extension arginine kinase as well as adenylate kinase) and GAPDH (and phosphoglycerate kinase) are recognized as playing a role in providing an efficient intracellular network that couples ATP-consuming with ATP-producing processes based on near-equilibrium metabolic reactions, thereby improving the efficiency of the transfer of phosphoryl groups, specifically in cardiac muscle tissue (Dzeja and Terzic, 2003). The proteomic fingerprint we identified suggests that such a network exists in claw muscle and that it is modified during

temperature fluctuations and acute HS conditions that temporarily demand high ATP turnover. This further suggests that the energetics of temperature acclimation are dependent on the restructuring of the cellular architecture, specifically the microstructure of those networks that are able to maintain ATP concentrations despite greatly fluctuating rates of ATP consumption (Hochachka, 2003).

Hemocyanin

We identified eleven isoforms of hemocyanin, an oxygen-carrying protein of arthropods and molluscs (Burmester, 2001). In addition to its role as oxygen-carrier, hemocyanins have been shown to undergo a transition to function as phenoloxidases under certain in vivo conditions, and thus play a role in the sclerotization of the crustacean post-molt exoskeleton (Decker and Jaenicke, 2004). Hemocyanins also function as anti-microbial peptides after the C-terminal end of it is cleaved of during infection (Destoumieux-Garzon et al., 2001; Lee et al., 2003).

Hierarchical clustering of the abundances of hemocyanin isoforms suggests two major clusters (Fig. 12). Cluster I represents five isoforms that showed higher abundances with acclimation to 10-30°C, while cluster II has six isoforms that increased with HS following 10°C and 10-20°C, including one isoform that increased with HS following acclimation to 10-30°C. All hemocyanin isoforms in cluster I had masses equal or greater than 65kDa, representing the full-length sequence. In contrast, all six isoforms of cluster II had masses between 24-48kDa, and higher pIs than isoforms from cluster I. An almost

identical pattern of hemocyanin isoforms was observed in hemocytes of the Pacific white shrimp *Penaeus vannamei* upon virus infection (Chongsatja et al., 2007). Subsequent work showed that isoforms similar to those with low molecular mass in cluster II are peptides cleaved off the N-terminal hemocyanin sequence in white shrimp (Havanapan et al., 2009). Hemocyanin isoforms of intermediate mass (spots 62, 138, and 179) may represent peptides cleaved off the C-terminal end and may be phosphorylated by the ERK1/2 MAP kinase signaling pathway (see below for link to inflammation), explaining the relatively low pI of two of these isoforms (Havanapan et al., 2009). Only one of these three isoforms increased with HS after 10-30°C (spot 138).

Thus, the majority of cluster I represents full-length hemocyanin isoforms that were most likely increasing abundance in response to extreme daily temperature fluctuations, possibly to supply more oxygen. Cluster II most likely represents N- and C-terminal peptides cleaved off from full-length hemocyanins.

Cytoskeletal proteins

In myofibrillar tissue, cytoskeletal elements compose the sarcomeres that are involved in muscle contraction. We identified a number of cytoskeletal proteins changing in response to temperature fluctuations. We separated these proteins into three functional categories: thick filament (myosins), thin filament (actins), and actin-binding proteins.

Thick filament (myosins)

We identified 22 thick filament proteins, including isoforms of myosin heavy chain (MHC), myosin regulatory light chain (MLC), and paramyosin. While the N-

terminal of MHCs and MLCs make up the head of the thick filament that forms cross-bridges with actin, the C-terminal end of MHCs makes up the rod (Clark et al., 2002). Paramyosins are part of the core of the rod in invertebrates (Hooper et al., 2008; Squire, 2009).

The PCA showed that changes in thick filament proteins contribute greatly to variation in the HS effect (Table 4), and this is shown in their hierarchical clustering (Fig. 13). For example, proteins in cluster IV showed sharply decreasing abundances following acute HS, regardless of acclimation regime. This cluster contains five isoforms of the regulatory MLC with molecular masses between 20-24kDa (with one exception), as predicted, and five MHC isoforms, which suggests that acute thermal stress might negatively affect modulation of sarcomeric power output and stabilization of the MHC tail region (Tohtong et al., 1995; VanBuren et al., 1994). Several MHC isoforms from cluster IV showed increased abundances during acclimation, especially to 10-30°C, and range in mass from 75 to 108 kDa, below the predicted mass of 205 kDa (Mykles, 1997), a mass above the mass range of our 2D gels. Myosin fragments of this size have been identified to form during apoptosis, using 2D gel electrophoresis (Suarez-Huerta et al., 2000), and could be the result of a heat-activated increase in proteolytic activity of the proteasome (Mykles and Haire, 1991). However, the fact that these isoforms showed increased abundances with acclimation to greater temperature fluctuations and showed reduced abundances with HS, suggests that it is a chronic and not an acute temperature stress signal, leading to this fragmentation pattern. It seems unlikely that apoptosis was elevated at

10°C acclimation (relative to HS), but an increase with greater temperature fluctuations at control conditions (10°C) would be a reasonable hypothesis.

While cluster IV decreased in response to HS, abundances of proteins of clusters I, II, and III increased with HS in an acclimation-dependent manner. All HS-induced isoforms of MHC and paramyosin, which are known in decapod crustaceans to be indicative of fiber type (Medler et al., 2004), had masses below their predicted range. For some MHC (cluster I and II), these were even lower than for the 10-30°C acclimation induced MHC fragments (cluster IV), but they were also from a different MHC type, suggesting that they originated from a separate proteolytic target. Because these changes were HS-specific, it is possible that these changes are indicative of the beginning of increase in protein turnover for fiber type switching between fast twitch (F), slow twitch (S_1), and slow phasic (S_2) in response to HS. In support of this hypothesis, the 10-30°C acclimation plus HS increased slow-twitch tropomyosin (see Fig. 7), suggesting a shift to S_1 fiber type. Interestingly, gelsolin fragments, which are still able to sever actin filaments and represent an apoptotic signal (Kothakota et al., 1997), increased at 10-20°C acclimation plus HS (Fig. 7), possibly indicating that a 30°C HS following moderate temperature fluctuations causes a restructuring of the entire actomyosin complex.

Thin filament (actins)

Thin filaments are made of α- and β-actins and are the most abundant proteins in muscle tissue. We identified thirty different isoforms, with six cardiac-like muscle isoforms and 24 isoforms that are homologous to both α-actin of *Homarus*

americanus and β-actin of *Scylla paramamosain*. In histochemical studies that examine crustacean actin, isoform diversity stems in part from tissue- and cellular compartment-specific localization, including cardiac-, skeletal muscle-, and cytoplasm-specific variants (Varadaraj et al., 1996; Kim et al., 2009). *Artemia* have at least ten isoforms of actin, *Homerus americanus* has at least twelve, and eight have been found in *Gecarcinus lateralis* (Macias and Sastre, 1990; Ortega et al., 1992; Varadaraj et al., 1996; Kim et al., 2009). In the present study, we found 18 isoforms with a mass of at least 37 kDa, which is close to the predicted 42 kDa mass. The cytoskeleton is known to be involved in co-localization of energy metabolism enzymes, and a separate study has verified this to be the case in *P. cinctipes* claw tissue (Götz et al., 1999; Cayenne et al., 2011). Changes in abundance can be grouped into four clusters that showed a regular correlation with patterns of molecular mass.

Cluster I showed increased abundances of two actin isoforms with a molecular mass of 45 and 46kDa, close to the predicted 42kDa, following acclimation to 10°C and 10-30°C (Fig. 14). Cluster II showed three isoforms with masses below 28kDa with increased abundances after 10-30°C plus HS. Cluster III showed increased abundances following 10-20°C plus HS, with four cardiac muscle actins that ranged from 12 to 41kDa, and ten α/β-actins with masses from 17 to 57kDa, including five isoforms between 17-32kDa, a mass range that is unlikely to represent a full-length isoform. Cluster IV showed increased abundances of eleven actin isoforms (one a cardiac-like muscle actin) ranging from 50-58kDa after 10-30°C.

We can divide the clusters into acclimation- (I), HS- (III) and interaction clusters (II and IV). Clusters II and III, which showed increased abundance of actin fragments, indicate partial in vivo proteolysis during HS. The fact that gels from non-HS treatments didn't show partial proteolysis suggest that the occurrence of fragments is not an artifact of our sample preparation protocol but rather due to a low thermal stability intrinsic to actin, which depends on several actin-binding proteins and ATP levels, under in vivo conditions (Levitsky et al., 2008). Also, we observed a similar HS-induced pattern of partial proteolysis for actin isoforms in sea squirts of the genus *Ciona* (Serafini et al., 2011).

Actin-binding proteins

Actin-binding proteins (ABP) that regulate the dynamics of actin monomers and filaments also changed abundance. They can be categorized into four groups: actin filament stabilizing (tropomyosin, Tm; filamin and sarcomeric α-actinin), severing and capping (gelsolins), G-actin binding proteins that regulate F-actin filament length (profilin and cofilin), and regulatory proteins (troponin T, TnT) (Clark et al., 2002; Lee and Dominguez, 2010). The protein isoforms we identified as belonging to these categories grouped into four clusters (Fig. 15).

While 10°C acclimation plus HS led to an increase in most ABP (with cofilin and tropomyosin being the exceptions) across several clusters, cluster I was also characterized by increased abundances of cofilin (or actin depolymerization factor), the actin-severing protein gelsolin, the anchoring protein α-actinin and troponin T, which organizes the actin filament regulatory complex (Clark et al., 2002), following 10-20°C acclimation plus HS. Thus, we

hypothesize that chronic moderate temperature fluctuations plus HS sever and depolymerize actin filaments and thereby activate actin filament restructuring (Lee and Dominguez, 2010). Moderate temperature fluctuations may also strengthen anchoring of filaments to the Z-line through α-actinin. Interestingly, this cluster coincides with the increase in actin fragments (Fig. 14; cluster III).

Cluster II is the 10-30°C acclimation cluster with increased abundances of filamin, gelsolin and troponin (Fig. 15). The functions involve anchoring or bundling of actin filaments, severing and regulation of the tropomyosin/actin interaction, respectively. Cluster III showed an increase in two of the three proteins of the cluster, filamin and profilin, at 10°C acclimation plus HS, suggesting the need for anchoring or bundling actin filaments and binding of monomeric actin to control actin filament growth.

All three actin stabilizing proteins showed an increase in abundance following 10-30°C and HS in cluster IV. Tropomyosins stabilize filaments (Wegner, 1982), actinins anchor filaments to the Z-line in striated muscles (Clark et al., 2002), while filamins may anchor or bundle actin filaments (van der Flier and Sonnenberg, 2001). Interestingly, this cluster increased abundances in response to an acute HS but not the 10-30°C acclimation and thus represents a strategy to stabilize actin filaments during acute HS only. Actinin and filamins but not tropomyosin also increased in response to HS following the 10°C acclimation.

Overall, HS triggered increased abundances for ABP involved in stabilizing actin filaments following acclimation to 10°C and 10-30°C but not to 10-20°C, based on the abundance patterns of actinin (spot 127 only), several

filamins, and tropomyosin (10-30°C plus HS only). Our interpretation suggests that acclimation to 10-20°C plus HS caused actin filament severing and depolymerization, based on changes in gelsolin and cofilin, respectively, and therefore limited actin filament growth and length. Three different troponin T isoforms were abundant following acclimation to 10°C, 10-20°C and 10-30°C plus HS, respectively. Troponin T anchors tropomyosin to the troponin trimer complex, and in conjunction with actin is responsible for producing the "swivel" effect in muscles (Myers et al., 1996; Murakami et al., 2008). Thereby, troponin T is thought to organize the regulatory complex of actin filaments (Clark et al., 2002). Finally, there is only one 10-30°C acclimation cluster (II) with high abundances of filamin C, gelsolin and troponin T, suggesting that chronic temperature fluctuations require increased bundling of actin filaments, greater rates of severing and modifications of the regulatory complex of the actomyosin interactions.

Thin filaments and actin-binding proteins

Thin filaments (actins) showed a much greater number of fragments at 10-20°C plus HS than at 10-30°C plus HS (Fig. 14, cluster III versus cluster II), indicating a greater resistance to partial proteolysis during HS following acclimation to 10-30°C. This pattern corresponds with increased abundances of actinin, which anchors actin to the Z-line (Clark et al., 2002; Wegner, 1982), tropomyosin, which stabilizes actin filaments (Clark et al., 2002; Wegner, 1982) and filamin, an actin-anchoring or –bundling protein (van der Flier and Sonnenberg, 2001) (Fig. 15; cluster IV). Thus, all three of these ABP increased during HS following

acclimation to 10-30°C only and possibly stabilized actin filaments and thereby reduced fragmentation. Thus extreme but not moderate daily temperature fluctuations led to an increase in proteins that stabilize actin filaments and enhance their anchoring to the Z-line and thereby possibly reduce fragmentation during acute HS.

In a pattern that complements the pattern of actin stabilization, the greater fragmentation of actin during HS following acclimation to 10-20°C is accompanied by increased abundances of cofilin (actin depolymerization factor), gelsolin, actinin and tropomyosin (Fig. 15; cluster I). At least in the case of cofilin and gelsolin, it seems likely that greater filament depolymerization and severing may increase the susceptibility of actin to partial proteolysis during HS. This is consistent with the observation that filamentous actin is much more thermally stable and therefore resistant to partial proteolysis than globular actin (Levitsky et al., 2008).

We hypothesize that acclimation to extreme temperature fluctuations (10-30°C) induces resistance to actin filament depolymerization and severing during HS (no increase in cofilin and gelsolin), in part through the greater thermal stability of filamentous versus globular actin. We further hypothesize that acclimation to mild temperature fluctuations (10-20°C) induces an increase in actin filament depolymerization and severing proteins during HS (30°C) and therefore greater G-actin formation, which, because G-actin is thermally more labile and supposedly unfolds more readily during HS, increases access to proteases and therefore increases partial proteolysis. It is unclear if the putative

greater sensitivity for increased filament severing under the 10-20°C acclimation plus HS conditions reflects a more dynamic actomyosin complex under control conditions, and if greater filament stabilization following 10-30°C plus HS indicates a more rigid actomyosin complex under control conditions. We conjecture that actin filament dynamics may be undergoing adjustments, e.g. compensations, during temperature acclimation to maintain properties of the actomyosin complex similar to those known for enzyme activities and membrane fluidity (Hochachka and Somero, 2002).

Signaling proteins

Calcium ion regulation

Changes in Ca^{2+} concentration affect cellular processes ranging from transcriptional activity in the nucleus to changes in muscle contraction in myofibrillar tissues (Clapham, 2007). In crustaceans, Ca^{2+} regulation plays a key part in the molt cycle, depleting calcium from the CaCO3 cuticle during proecdysis (pre-molt) and restoring it during the post-molt sclerotization process (Ahearn et al., 2004).

Sarcoplasmic Ca^{2+}-binding proteins (SCPs) belong to the family of EF-hand calcium-binding proteins and are found only among invertebrates (White et al., 2011; Gao et al., 2006; Hermann and Cox, 1995). We identified two isoforms of SCPs with estimated masses of 22 kDa (#94) and 21 kDa (#95). One isoform (#95) showed a lower level with HS after acclimation to 10°C and 10-30°C, another one (#94) a decrease in abundance after acclimation to 10-20°C (Fig. 16). Spot 94 clusters with farnesoic acid O-methyltransferase and a notch

homolog, possibly suggesting a role in inhibiting developmental processes during HS following the 10°C acclimation.

Our MS/MS analysis identified the same three peptides for both SCP spots, and did not resolve why these SCPs have separate positions. Three SCP isoforms are possible splice variants in the freshwater crayfish *Procambrus clarkii* (White et al., 2011).

Although the exact function of SCPs is currently unknown (White et al., 2011), they are more highly expressed in fast twitch than slow tonic muscle tissue and serve as intracellular calcium ion buffers during contraction, similar to the function of parvalbumin. During the resting state, parvalbumin binds mostly Mg^{2+}, but during contraction it slowly releases Mg^{2+} to take up Ca^{2+}. Tropomyosin blocks actin binding to myosin until troponin C takes up Ca^{2+} (Clapham, 2007). Thus parvalbumin, and presumably SCP, limits competition with troponin C during contraction through slow Ca^{2+} uptake, which increases efficiency of the actomyosin contractile apparatus (White et al,. 2011; Berchtold et al., 2000; Wang and Metzger, 2008). Thus, it is possible that an increase in SCP leads to a sequestering of more Ca^{2+} and therefore a change in the interaction between actin and myosin. Regulation of cytosolic Mg^{2+} and Ca^{2+} could also be important mechanisms for dealing with temperature-related environmental stress, as a change in Mg^{2+} concentration is associated with cold shock in *P. clarkii* (White et al., 2011).

FK506-binding protein (FKBP), a prolyl isomerase, is characterized by the binding of the immune suppressant FK506, and stabilizes the closed state of two

calcium channels, ryanodine and IP_3 receptor (MacMillan, 2013). It's abundance increased, which might suggest that muscle contraction was inhibited, with HS following acclimation to 10°C and 10-20°C.

Sesquiterpenoid metabolism

Farnesoic acid O-methyltransferase (FaMeT) catalyzes the conversion from farnesoic acid (FA) to methyl farnesoate (MF), a sesquiterpendoid that is involved in crustacean morphogenesis, reproduction and molting (Kuballa et al., 2011; Nagaraju, 2011). Transcripts for FaMET have been detected in multiple crustacean tissues, including muscle (Nagaraju, 2011; Ruddell et al., 2003). The abundance of FaMeT increased with HS following acclimation to 10°C, decreased in response following 10-20°C, and increased again following 10-30°C (Fig. 16). Gill tissue showed changes in two FaMeT isoforms in response to pH and emersion stress (Garland et al., unpublished data). Both, temperature and salinity affected testicular development in a MF-dependent fashion in Carcinus maenas (Nagaraju and Borst, 2008). Together, these results suggest an important role for FaMeT in the response of crustaceans to acute environmental stress.

Inflammation

We identified five proteins of diverse functions that may be suppressing inflammation (Figs 16 and 17): RAF Kinase Inhibitor Protein or (RKIP; also known as phosphatidylethanolamine-binding protein or PEBP) (Granovsky and Rosner, 2008), NADP-dependent leukotriene B_4 hydroxydehydrogenase (LTB_4DH) also known as prostaglandin reductase, a protein directly involved in

the inactivation of the inflammatory mediator leukotriene B_4 (LTB_4), phosphohistidine phosphatase (PHP)-like janus protein, 14-3-3ζ and FKBP (see above). The four proteins possibly inhibiting inflammation fall into two clusters that show increasing abundances with HS following acclimation to 10-20°C (II: PGR and PHP) and 10°C (III: RKIP and 14-3-3). We hypothesize that HS suppresses inflammation after acclimation to 10°C and 10-20°C but not 10-30°C.

RKIP possibly represents a central node in a hypothetical network of signaling pathways that regulate inflammation (Fig. 17). RKIP inhibits the MEK-ERK1/2 MAP kinase module (Yeung et al., 2000; Yeung et al., 1999) and thereby the phosphorylation of phospholipase A_2, directly inhibiting the synthesis of pro-inflammatory prostanoids from arachidonic acid, including prostaglandin E_2 (PGE), via cyclooxygenase (COX), and leukotrienes, like leukotriene B_4 (LTB4), via lipooxygenase (LOX). Further downstream, prostaglandin reductase (PGR), which also functions as LTB_4-hydroxdehydrogenase (LTB_4-DH), catabolizes PGE and LTB_4 into inactive metabolites, thereby suppressing an immune reaction and hemocyte recruitment (Marks et al., 2009; Tai, 2011). In addition to being inhibited by RKIP, RAF kinase, as part of the ERK1/2 MAP kinase module, can be inhibited if it gets phosphorylated by protein kinase A (PKA) and subsequently sequestered from the membrane by 14-3-3 (Dumaz and Marais, 2003). RKIP also interferes with the activation of the pro-inflammatory transcription factor nuclear kappa B (NFκB) by inhibiting the phosphorylation of the inhibitor protein IκB through IκB kinase, which in turn inhibits the disassociation of NFκB-IκB to an active form of NFκB (Yeung et al., 2001). Finally, phosphorylated RKIP binds to

G-protein-coupled receptor kinase (GPCR kinase or GRK), leading to the dissociation of a G-protein-GPCR complex and prolonged G-protein signaling (Keller et al., 2004; Lorenz et al., 2003). Interestingly, it is a GPCR that activates the ERK1/2 module. Furthermore, it is possible that a β-subunit of the G-protein is a substrate of phosphohistidine phosphatase (PHP) (Lorenz et al., 2003).

Notch is a transmembrane receptor protein that is activated by ligands from other cells during development, triggering the proteolytic cleavage of the intracellular domain of notch, which activates gene expression by the NFκB-like transcription factor CSL (Marks et al., 2009). Also, there is evidence for a synergistic interaction between notch and NFκB (Barbarulo et al., 2011). Furthermore, notch seems to modulate cellular metabolism, specifically glucose uptake and glycolysis (Ciofani and Zuniga-Pflucker, 2005; Graziani et al., 2008; Landor et al., 2011), and thus might be involved in regulating some of the changes in abundance of glycolytic enzymes with HS following acclimation to 10°C.

2.5 Conclusion

PCAs based on the significantly changing proteins showed that the response to HS is greater following acclimation to 10°C and 10-30°C in comparison to 10-20°C (Fig. 9). Thus, the 10-30°C acclimation regime was severe enough that porcelain crabs did not acclimate to a daily occurrence of a 30°C HS. The fact that the response to HS following acclimation to 10-20°C was limited, suggests that the proteomic changes that occurred during acclimation increased resistance to a subsequent 30°C HS. However, there are few changes accompanying the 10-20°C acclimation regime *per se*. Increasing levels of actin fragments and actin-binding proteins cofilin, gelsolin and actinin with HS following acclimation to 10-20°C suggest that organisms are instead primed to deal with HS by changing actin filament structure and possible dynamics while changing other cellular processes only to a limited extent. In this context it is worth noting that we did not detect any molecular chaperones in any of the treatments, with the exception of FKBP, most likely because they are less abundant than the proteins we detected (Carberry et al., 2014).

HS following acclimation to 10°C is presumably the most stressful of our treatments, as indicated by PCA (Fig. 9C). HS caused a strong increase in ATP-buffering (Fig. 10, cluster III), glycolysis (one GAPDH), actomyosin restructuring (two paramyosin and MHC isoforms), a number of ABP and signaling proteins that might suppress an immune response. HS after acclimation to 10-30°C was similarly stressful, based on our PCAs (Fig. 9A and 9B). Acclimation to daily 10-30°C (measured at 10°C) increased ATP-buffering, metabolic (enolase,

phosphoglycerate kinase and ATP synthase), respiratory (hemocyanin) and filament (MHC and actin) proteins. A subsequent 30°C HS increased ATP-buffering, different metabolic (TPI, GAPDH, enolase and PDH), one respiratory (hemocyanin) and several filament (MHC and actin) proteins as well as actin-binding proteins that stabilize actin filaments (filamin, actinin and tropomyosin).

Thus, temperature fluctuations always require ATP-buffering, and greater fluctuations require modifications of glycolytic proteins and ATP synthase as well as an increase in hemocyanins. Chronic temperature fluctuations require modifications in thick and thin filaments. Most importantly, moderate temperature fluctuations are characterized by proteins that depolymerize and sever actin filaments, possibly to restructure actomyosin fibers to modify ATP-turnover rates, while extreme temperature fluctuations increase the proteins that stabilize actin filaments. It is possible that both changes cause actomyosin fibers to modify their functional properties. Finally, at least acute HS inhibits inflammation, possibly making crustaceans more susceptible to pathogens.

The proteome of claw muscle adjusted to temperature fluctuations by modifying proteins involved in ATP production, oxygen transport, the structure and dynamics of the actomyosin complex and inflammation. Acute HS is always the dominant driver of these changes. Acclimation to 10°C caused the greatest proteomic changes, acclimation to 10-20°C required few additional proteomic modifications and acclimation to 10-30°C required intermediate proteomic changes in response to a subsequent acute 30°C HS. The daily occurrence of an acute 30°C HS is thus above the threshold at which *P. cinctipes* is able to fully

acclimate. Our results suggest that while intertidal crustaceans are already experiencing great temperature fluctuations, which are preparing the animals for a subsequent greater HS, more extreme fluctuations will be physiologically costly due to the daily and broad modifications of the proteome associated with such shifts in temperature ranges.

3.0 MULTI-STRESS MANUSCRIPT

Adapated from:

Garland, M.A., Paganini, A., Vasquez, M.C., Stillman, J.H., Tomanek, L. (in preparation). Multi-stressor synergies: the proteomic response of gill to low pH depends on daily emersion and heat stress in the intertidal porcelain crab *Petrolisthes cinctipes*.

3.1 Abstract

The effect of low pH on organisms inhabiting the rocky intertidal zone has to be assessed in the context of a fluctuating environment (emersion) and additional physical factors (heat stress). Here we acclimated the intertidal porcelain crab *Petrolisthes cinctipes* to different regimes of aerial exposure (immersion or 6 h of emersion, 11°C seawater) and temperature stress (constant ambient 11°C or 31°C during emersion) under either constant pH 8.1 or nighttime low pH 7.6 over a 17 d period to assess the effect of these treatments on the proteome of gill tissue. Low pH reduced the abundance of a number of chaperones of the endoplasmic reticulum (ER) that are involved in the maturation of secretory proteins during immersion but not under emersion. Low pH reduced the abundance of glyco-binding lectins and serine proteases involved in the activation cascade of phenoloxidases (PO) leading to the synthesis of quinones. Mild heat shock (HS; during emersion) more than emersion alone modified the response to low pH of several glyco-binding proteins, serine proteases, peritrophins and transglutaminase, all proteins involved in binding chitin and connecting chitin fibers as well as cross-linking chitin binding proteins. Low pH both increased and decreased the abundance of different full-length hemocyanin isoforms, depending on emersion; emersion alone did so as well, but HS increased the abundance of a number of N- and C-terminal fragments, which might have PO and anti-microbial activity, respectively. Low pH (emersion-dependent on emersion condition), emersion and HS alone affected a number of

cuticle binding proteins in a similar way. Emersion alone, more than low pH, decreased the abundance of proteins representing ATP-buffering (arginine kinase), glycolysis, TCA cycle and oxidative phosphorylation (F1-ATP synthase). However, HS increased several arginine kinase and F1-ATP synthase isoforms, possibly to facilitate greater ATP turnover and to dissipate the proton gradient across the inner mitochondrial membrane to limit the production of reactive oxygen species. Low pH increased the abundance of Na^+-K^+ ATPase while levels of V-type H^+-ATPase and several tubulin isoforms were elevated as well, in agreement with a proposed model of ammonium (NH_4^+) excretion across the crustacean gill as a mechanism to excrete H^+ through the transport of acidified vesicles towards the apical membrane. Together, our results suggests emersion- and HS-dependent responses to low pH that affect protein maturation in the ER, active ion transport and cuticle structure and thereby possibly passive ion permeability.

3.2 Introduction

Climate change due to increasing levels of atmospheric CO_2 is affecting marine communities worldwide (Doney et al., 2011; Hoegh-Guldberg and Bruno, 2010). Up to 25% of the CO_2 emitted by human activities is absorbed by the world's oceans (Le Quéré et al., 2009). Once dissolved in seawater, CO_2 forms carbonic acid, which dissociates into bicarbonate ions and protons, leading to a decrease in oceanic pH (ocean acidification) (Doney et al., 2009). While the oceanic pH has already fallen by 0.1 units, average oceanic pH is expected to drop by 0.4 units by the year 2100 and 0.8 by the year 2300 (Caldeira and Wickett, 2003). Furthermore, coastal upwelling along the California coast brings CO_2-enriched waters to the surface and is expected to intensify as ocean acidification continues, making it a world "hot spot" of decreased pH (Gruber et al., 2012). The physiological effects of the predicted changes in oceanic pH on marine organisms will depend in part on interactions with other environmental factors and how much they will change e.g. temperature, salinity, oxygen and food availability (Whiteley, 2011; Wittmann and Pörtner, 2013). In addition, current levels of environmental fluctuations have to be taken into account when considering the effects of such co-stressors on modifying the response to low pH.

The rocky intertidal is probably the most dynamic coastal environment where organisms experience large fluctuations in emersion (aerial exposure), oxygen, temperature, food availability and pH (Helmuth et al., 2006; Hofmann et al., 2014). Two of these seem of particular relevance for modifying the response to low pH: emersion and temperature. For example, crustacean species

accumulate CO_2 and HCO_3^- in residual branchial water during emersion, which affects their ability to compensate for respiratory acidosis and regulate ionic composition (Burnett and McMahon, 1987). Species that due to their environment or behavioral activity differ in the duration of emersion they experience, also vary in their strategy of dealing with increasing levels of P_{CO2} in their hemolymph during emersion (Burnett and McMahon, 1987). Thus, the association of environmentally-induced acidosis during emersion is likely affecting the cellular responses of intertidal organisms to low pH, but little is known about this interaction. Furthermore, intertidal organisms also frequently experience acute heat stress during emersion (Stillman and Somero, 1996; Tomanek and Somero, 1999). The response to heat stress is not only dependent on a species' temperature range and recent thermal history (Tomanek, 2008; Tomanek, 2010), but also depends on tidal (immersion *versus* emersion) conditions (Bjelde and Todgham, 2013; Tomanek and Somero, 2000). Importantly, as increasing temperatures decrease hemolymph pH and thus challenge the acid-base balance (Hochachka and Somero, 2002), it is likely that acclimation to frequent sublethal heat stress modifies the response to low pH as well. Thus, investigating the effect of low pH in combination with emersion and heat stress provides a more natural perspective of how intertidal organisms respond to low pH.

While the majority of studies investigating the effect of ocean acidification focused on performance measures at the level of the organism, i.e growth, reproduction and respiration rates, far fewer have focused at global changes in

subcellular processes, i.e. transcriptomic level (Evans et al., 2013; Fehsenfeld et al., 2011; Padilla-Gamiño et al., 2013; Todgham and Hofmann, 2009), with even fewer studies focusing on the proteome. A major advantage of omic studies is their ability to discover the involvement of cellular processes in the response to low pH that were hitherto not considered.

Increasing genomic information, mainly in the form of extensive expressed sequence tag (EST) libraries, have made proteomic studies on non-model organisms more feasible (Tomanek, 2011; Tomanek, 2014). For example, recent studies have investigated the proteomic response of marine invertebrates to temperature (Fields et al., 2012a; Fields et al., 2012b; Garland et al., 2015; Serafini et al., 2011; Tomanek and Zuzow, 2010), salinity (Tomanek et al., 2012), hypoxia (Fields et al., 2014), oxidative stress (McDonagh and Sheehan, 2006; McDonagh and Sheehan, 2007; Tomanek, 2015), UV radiation (Campanale et al., 2011) and pollutants (Apraiz et al., 2006). However, few studies have focused on the response to low pH at the level of the proteome. One study on larvae of the barnacle *Balanus amphitrite* showed changes in the abundance of proteins involved in energy metabolism, respiration and protein homeostasis in response to elevated P_{CO2} (Wong et al., 2011). Studies on larvae of the Pacific oyster, *Crassostrea gigas*, and the commercial oyster, *C. hongkongensis*, showed reduced abundances of several proteins involved in energy metabolism and calcification as well as the overall level of protein phosphorylation in response to high P_{CO2} (Dineshram et al., 2013; Dineshram et al., 2012). A study on the Eastern oyster, *C. virginica*, showed elevated levels of several oxidative

stress proteins in mantle tissue in response to a two-week acclimation to high P_{CO2} (~3,520 μatm or pH7.5), a level oysters experience in their estuarine habitats during summer (Tomanek et al., 2011).

Because crustaceans possess an exoskeleton made of the more stable calcite, which might make them less sensitive to low pH, they have only recently become the focus of a number of ocean acidification studies (Whiteley, 2011). Their susceptibility to low pH is dependent on a number of factors, including life stage, activity level, salinity, oxygen availability and ultimately the ability to regulate ionic composition (Dissanyake, 2014; Whiteley, 2011). Here we focus on the intertidal porcelain crab species *Petrolisthes cinctipes*, which experiences temperature fluctuations of up to 20°C during emersion in its mid-intertidal habitat (Teranishi and Stillman, 2007). Also, the transcriptomic response of this species to acute heat stress has been characterized and thus provides a foundation for the identification of proteins by mass spectrometry (Tagmount et al., 2010; Teranishi and Stillman, 2007). Importantly, *P. cinctipes* is an osmo-conformer and thus likely to be less capable of responding to ionic shifts due to low pH than freshwater or estuarine crustaceans, which are generally good ion-regulators (Hunter, 1986).

Following a two-week acclimation period, we found that gill tissue of *P. cinctipes* changed abundance of proteins involved in protein homeostasis, ion transport and the phenoloxidase-activation cascade in response to low pH during immersion, but that the response was modified by both emersion and heat

stress. We discuss which cellular processes might be affected by these changes and how they might modify the ion transport properties of gill.

3.3 Materials and Methods

Note: Materials and methods (up until sample processing) closely follow those of Paganini et al. (2014).

Animal collection and maintenance

Adult *Petrolisthes cinctipes* (Randall, 1839) were collected from the intertidal zone of Fort Ross, CA, USA (38.5143° N, 123.2438° W) during a morning low tide on March 13, 2012. Only males were collected in order to control for sex-related physiological differences. Collected crabs were placed in coolers with aerated local seawater and transported back to the Romberg Tiburon Center for Environmental Studies (approximate 90 minute trip to Tiburon, CA, USA). Crabs were placed into recirculating artificial seawater (Instant Ocean, Spectrum Brands, Inc.; 12 ± 0.5°C, salinity 33.3 ± 0.2, ambient pH 8.09 ± 0.08) for approximately 24 h, without feeding, before being placed in acclimation treatments. Recirculating water was filtered with 20 μm and 100 μm mechanical filters, activated carbon, UV sterilization, and foam fractionation using a protein skimmer. On each morning during the acclimation experiment, crabs were individually fed identical amounts of Shellfish Diet® (Reed Mariculture, Inc., http://www.reedmariculture.com; 30% *Isochrysis* sp., 30% *Tetraselmis* sp., 20% *Pavlov* sp., 20% *Thallosiosira weissflogii*).

Experimental design

Crabs were randomly and individually placed in acrylic cylinders for the duration of the acclimation experiment. The experimental design consisted of

three lidded, insulated acrylic tanks (Aqua Logic, USA) that each experienced different acclimation conditions. Each tank contained 40 acrylic cylinders (7 cm diameter by 15 cm height) arranged in a 5 x 8 cylinder pattern on top of a raised, porous platform. At the base of each cylinder was reticulated foam filter (5.3 cm thick; Aquatic Ecosystems, PF7) that allowed for the manipulation of water chemistry in each individual cylinder while still allowing for circulation with surrounding water when necessary. Each tank possessed standpipes that kept crabs submerged at a constant depth of 5 cm during full immersion, with water kept at a constant temperature of 11 ± 0.5°C. The three tanks were designed to manipulate the following parameters: pH, air exposure, and temperature (methods described below). Crabs were exposed to changes in these parameters for 17 days before being flash frozen in liquid nitrogen and stored at -80°C.

Nocturnal pH manipulation

All three tanks were designed such that during the night, half of the crabs experienced an ambient pH (8.12 ± 0.12) while the other half experienced a lower pH (7.60 ± 0.04). Vinyl tubing (6.35 mm) equipped with 0.94 L hr^{-1} irrigation drippers (Netafim 71) was threaded through the tank lid and suspended over each cylinder, with magnetic drive pumps (Iwaki MD 40) delivering water at a controlled rate from either an ambient pH reservoir or a CO_2-acidified low pH reservoir. Water was delivered from each reservoir for 5 h during the night, from 03:00 to 8:00. The reticulated filter base in each cylinder insulated the water, preventing pH mixing between treatments while water was being pumped. At

08:00, pumping stopped and water in each cylinder equilibrated to ambient pH (approximately pH 8.12) across all treatments within 2 hours. Acidified water was recirculated through the system and equilibrated to an ambient pH through aeration by air pumps (Whitewater) and protein skimmers (EuroReef). The pH was monitored every minute in a random acrylic cylinder with a pH electrode (Omega) connected to a pH data logger (pH/H-SD1, Omega). The pH electrode was moved to a different cylinder each day to detect spatial variation in pH, and was calibrated every 5 days with NBS buffers 4, 7, and 10 (Fisher; SB101, SB110, SB 115). Monitoring was supplemented with spectrophotometric determination of pH at different time points.

Daily emersion and temperature ramping cycles

While crabs in Tank 1 were constantly immersed throughout the experiment, crabs in Tanks 2 and 3 experienced afternoon emersion events (Fig. 18). Secondary lower standpipes in Tanks 2 and 3 were each connected to separate solenoid valves (Hayward PVC/CPVC) that activated and began draining the tanks at 12:00 each afternoon (by 12:30, the cylinders experienced total emersion). During emersion, temperature in Tank 2 was regulated through vigorous bubbling by air pumps, equilibrating the air temperature with that of the water (approximately 11°C). In Tank 3, air temperature was controlled by a thermoregulator (Love 16A3, Dwyer Instruments) that ramped temperature up during the simulated low tide from 12:00 to 17:00. Temperature ramped to four different maxima over the course of the experiment: 22.5°C at an average rate of 2.9°C h^{-1} on days 1-3; 27°C at an average rate of 4°C h^{-1} on days 4-6, 28°C at an

average rate of 4.3°C on days 7-15; and 31°C at an average rate of 5°C h^{-1} on days 16-17. Thermoregulation stopped at 17:00 and the solenoid valves closed at 17:30 on each day, fully immersing the crabs in 11°C water by 18:00.

Water chemistry

Seawater samples for pH and total alkalinity were simultaneously collected bi-weekly between 07:45-08:00 h while ambient and acidified water was being pumped into the respective cylinders. The pH was measured spectrophotometrically measured using m-Cresol Purple sodium dye (PharmaSpec UV-1700, Shimazdu, Columbia, MD, USA; Sigma-Aldrich no. 211761, St. Louis, MO, USA) following the modified protocol of DOE (DOE, 1994). Total alkalinity by mass (μmol kg^{-1} seawater) was determined with a linear Gram procedure using a dosimat 765 pH-meter (Metrohm Herisau Switzerland) (Gran, 1952). Nitrate, nitrite, and ammonium levels were measured with colorimetric assays (Salifert, American Pharmaceuticals) and were consistently undetectable above 0 mg^{-1}.Additional parameters of seawater carbonate chemistry ($[HCO^{3-}]$, $[CO_3^{2-}]$, P_{CO2}, $\Omega_{calcite}$, and $\Omega_{aragonite}$, where Ω is the saturate state) were calculated in the statistical computing program R (version 3.1.1) using the SeaCarb package (version 3.0.6) (R Development Team, 2014; Lavigne et al., 2011). Seawater salinity, temperature, pH, and alkalinity were used as the input parameters (flag 8) using the total pH scale (pH_T). Total phosphate and total silicate were assumed to be 0 mol kg^{-1}. Statistical differences between pH treatments were determined using Welch's *t*-test (Table 13).

Homogenization

Gill tissue was dissected from frozen crabs in a 4°C cold room and then rinsed in ice-cold filtered seawater. Gill samples were lysed using ground glass pestles in a 1:12 ratio of homogenization buffer [7 mol L^{-1} urea, 2 mol L^{-1} thiourea, 1% ASB (amidosulfobetaine)-14, 40 mmol L^{-1} Tris-base, 40 mmol L^{-1} dithiotheitol, 0.5% immobilized pH 4-7 gradient (IPG) buffer (GE Healthcare, Piscataway, NJ, USA), and cOmplete ULTRA Mini protease inhibitor cocktail (1 tablet per 10 mL of buffer; Roche Applied Science Corporation, Indianapolis, IN, USA)], solubilized at 20°C for 1 hour, and then centrifuged at 16,100 *g* for 30 minutes at 20°C. Proteins were precipitated from the supernatant using a 1:4 ratio of ice-cold 10% trichloroacetic acid in acetone with an overnight incubation at -20°C. The samples were centrifuged at 18,000 *g* for 15 minutes at 4°C, after which the supernatant was discarded and the protein pellet washed in ice-cold acetone with vortexing. Samples were again centrifuged according to the previous parameters and the supernatant was discarded. After briefly drying in the air, the protein pellets were re-suspended in a 1:8 ratio of rehydration buffer [7 mol L^{-1} urea, 2 mol L^{-1} thiourea, 2% CHAPS (cholamidopropyl-dimethylammonio-propanesulfonic acid), 2% NP (nonyl phenoxylpolyethoxylethanol)-40), 0.002% bromophenol blue , 0.5% IPG (4-7) buffer, and 100 mmol L^{-1} dithioerythritol] through repeated vortexing and solubilizing at 20°C for 1 hour. To determine the protein concentration in each sample, a concentration assay was performed using the 2D Quant Kit (GE Healthcare) according to the manufacturer's instructions.

Two-dimensional gel electrophoresis (2DGE)

For 1st dimension electrophoresis, proteins were separated according to their respective isoelectric points (pI) using IPG gel strips (pH 4-7, 11 cm; GE Healthcare). Protein samples were diluted to a 2 µg μL^{-1} ratio in rehydration buffer, and 200 µL (400 µg) was loaded onto each IPG gel strip in the wells of an isoelectric focusing cell (BioRad, Hercules, CA, USA). Protein solution was absorbed into each IPG gel strip over 5 hours of passive rehydration followed by 12 hours of active rehydration at 50 V. Separation and focusing of proteins was performed by subjecting gel strips to 500 V for 1 hour, 1000 V for 1 hour, and then 8000 V for 2.5 hours (maximum current 50 µA; all voltage changes occurred in rapid mode). After isoelectric focusing, gel strips were frozen at -80°C.

After freezing for at least 1 hour, gel strips were prepared for 2nd dimension SDS-PAGE by incubating them in equilibration buffer (6 mol L^{-1} urea, 375 mmol L^{-1} Tris-base, 30% glycerol, 2% SDS, 0.002% bromophenol blue) at 20°C for two 15 minute intervals, first with 65 mmol L^{-1} dithiothreitol and then with 135 mmol L^{-1} iodoacetamide. Gel strips were then placed over 11.8% polyacrylamide gels and electrophoresed (Criterion Dodeca; BioRad) for 55 minutes at 200 V. Following electrophoresis, gels were stained overnight using colloidal Coomassie blue (G-250) and then destained through repeated washing with milliQ water over 48 hours. Gels were then scanned with an Epson 1280 transparency scanner (Epson, Long Beach, CA, USA).

Gel image analysis

Digitized 2D gel images were analyzed using Delta 2D (version 3.6; Decodon, Greifswald, Germany; Berth et al., 2007). To detect protein spots, gels from all treatments were multiplexed into a single fused image. The spot boundaries detected on the fused image were transferred back to the individual gels, establishing protein spot parameters for each gel. Following background subtraction, the relative spot volume of each protein was quantified by normalization against the total spot volume of all proteins in the gel image.

Mass Spectrometry

Proteins spots that significantly changed in abundance according to pH, tidal, and thermal acclimation were manually excised using a tissue puncher. Gel plugs were prepared for analysis using mass spectroscopy (MS) according to previously published methods (Fields et al., 2012; Tomanek and Zuzow, 2010).

Peptide mass fingerprints (PMFs) were obtained using a matrix-assisted laser desorption/ionization tandem time-of-flight (MALDI-ToF-ToF) mass spectrometer (UltraFlex II; Bruker Daltonics, Inc.; Billerica, MA, USA). To obtain b- and y-ion parameters, at least 6 peptides were selected for analysis.

Spectral analysis of peptides followed previously published methods (Fields et al. 2012; Tomanek and Zuzow, 2010). FlexAnalysis (version 3.0; Bruker Daltonic, Inc.) was used to detect peptide peaks, using a signal-to-noise ratio of 6 for MS and 1.5 for tandem MS (MS/MS). Internal mass calibration was performed using porcine trypsin.

Proteins were identified using Mascot (version 2.2; Matrix Science, Inc.; Boston, MA). PMFs and tandem mass spectra were combined and searched against the Porcelain Crab Array Database (PCAD), an EST library for *P. cinctipes* that contains approximately 19,000 unique sequences. A secondary database containing a *Hyas araneus* EST library was utilized when no matches for a protein sample were found using PCAD. One missed cleavage was allowed during searches. For the MS/MS analysis, the precursor-ion mass tolerance was set at 0.6 Da (default Mascot value). Search results were deemed significant ($p \leq 0.05$) if their molecular weight search (MOWSE) score was 42 or higher using PCAD and 34 or higher using the *H. araneus* library.().

Exploratory statistical analysis

Protein abundances between treatment groups were compared via average linking of gels (Delta2D) using a Pearson correlation metric. To compensate for unbalanced nesting, a two-way ANOVA ($P \leq 0.05$) was used to compare pH *versus* tidal treatments (Tanks 1 and 2), and another two-way ANOVA ($P \leq 0.05$) was used to compare pH *versus* temperature treatments (Tanks 2 and 3). Significantly changing proteins in each analysis were grouped into hierarchical clusters organized by functional category. To better understand the importance of particular proteins in characterizing the proteomic response to different temperature treatments, we used PCA (Delta 2D) based on proteins whose expression profiles significantly changed, regardless of whether they were identified with MS. Of the proteins that were identified with MS, we assigned

component loading values which are quantifications of a protein's contribution to sample separation along a given component.

3.4 Results and discussion

Experimental design and data analysis

We first investigated the effect of low pH (pH 8.1 *versus* 7.6) under constant immersion (Fig. 18A). Animals experienced low pH conditions between 3:00 – 8:00 every morning for 17 days. Simultaneously we investigated the effect of pH fluctuations during acclimation to conditions simulating a daily low tide (emersion) in the afternoon (12:00 to 18:00) at an air temperature of 11°C (Fig. 18B). Finally, we simultaneously evaluated the additional effect of a daily 31°C heat shock (*versus* no HS) during emersion to assess its effect on the response to low pH (Fig. 18C). Animals were collected at 10:00 on the last day of acclimation for all three experiments. Based on gill samples from all treatments, we generated a proteome map to detect 835 and identify 234 proteins (Fig. 19 and Table 6).

To investigate the interaction effects between tidal regime x pH (no comparison with the HS treatments; Fig. 18A and B only) and temperature x pH (no comparison with the immersion treatments; Fig. 18B and C only), we conducted two separate two-way permutation ANOVAs ($p \leq 0.05$), because the experimental design was not balanced and thus did not allow to analyze all three experiments together. Thus, reference to a tidal regime (or E for emersion) main effect is based on a comparison between the two immersion and the two emersion treatments (pH 8.1 and 7.6) and does not include an implicit comparison with the emersion-HS-pH treatments (Fig. 18C). The same is true when we refer to a temperature (T) effect, which compares the four emersion

treatments at different pH values without and with a daily HS only. The designation of main (E, T or P) or interaction (I) effects are indicated in the tables accompanying each heat map and are given for each ANOVA separately. Based on the permutation ANOVAs, we conducted different principal component analyses (PCAs) to assess the role of both pH and tidal regime (emersion) main effects and their interaction and pH and temperature (HS) main effects and their interaction. We also conducted post-hoc Tukey pairwise comparisons for a subset of the proteins (indicated in graphs depicting changes in their abundance). Because the ANOVA results are based on the entire set of proteins, but the pairwise comparisons are based on using a general linear model to the abundance changes of a single protein, not all proteins showing significance for a main or interaction effect (ANOVA), also showed a significant difference in pairwise comparisons.

Importantly, changes in protein abundance can be attributed to an increase or decrease in synthesis, degradation, post-translational modifications (PTMs) and partial proteolysis. Furthermore, because our analysis may not represent all the isoforms of a protein, they may not represent the complete abundance of this protein. Thus, while our interpretations are based on as many isoforms or proteins as possible representing a single protein or a cellular process, they are still hypotheses that require further validation.

Principal component analyses – tidal regime x pH

The first set of PCAs included proteins that are significant for either a tidal regime (immersion/emersion) or pH main (Figs 20A-B and Tables 7-8) or an interaction

effect (Fig. 20C and Table 9). Principal component 1 (PC1) separated the immersion-pH 7.6 treatment (positive section of x-axis) from all other treatments and explained 34.6% of the variation in protein abundance. PC2 mainly separated the low (positive section of the y-axis) from the high pH treatments and explained 12.2%, with some exceptions due to some overlap between emersion-pH 7.6 and immersion-pH 8.1.

Proteins putatively involved in vesicle transport (tubulins), gill cuticle structure (cuticle proteins), urea cycle (argininosuccinate synthetase), ion regulation (Na^+-K^+-ATPase) and oxygen transport (full-length hemocyanin) contributed positively to PC1 (Table 9A) and generally showed greater protein abundances under immersion-pH 7.6 (below). Proteins involved in oxygen transport and possibly catechol oxidase and antimicrobial activity (several full-length, low and high molecular mass fragments of hemocyanins, respectively), cuticle structure (DD5 cuticle proteins), energy metabolism (arginine kinase or AK) and chaperoning of glycoproteins within the endoplasmic reticulum (calreticulin) contributed negative loadings (Table 9B), with generally lower abundances under immersion-pH 7.6. These results suggest that low pH increased abundance of proteins involved in ion regulation, urea cycle, vesicle transport, cuticle structure and oxygen transport, but only in response to constant immersion not when experiencing daily emersion. Daily emersion actually canceled the low pH effect observed under constant immersion (partial overlap of emersion-pH 7.6 and immersion-pH 8.1). Conversely, low pH canceled the effect of emersion (emersion-pH 8.1 *versus* emersion-pH 7.6).

Similar to PC1, proteins involved in vesicle transport, ion regulation, cuticle structure and oxygen transport contributed positive loadings to PC2 and were generally associated with greater protein abundances during low pH treatments (Table 9C). Proteins involved in vesicle transport and cuticle structure contributed negative loadings to PC2 (Table 9D). Proteins with additional functions, like immune function or cross-linking of chitin-binding proteins (C-type lectin and peritrophin; see below), energy metabolism (pyruvate dehydrogenase or PDH) and chaperoning (calreticulin) also contributed negative loadings and showed lower abundances at pH 7.6.

To summarize, proteins putatively involved in ion regulation, urea cycle, vesicle transport and cuticle structure as well as full-length and fragments of hemocyanins contributed the most to PC 1 and 2, although PC1 was more heavily affected by hemocyanin isoforms than PC2. Despite the overlap in functions represented by proteins with high loadings for PC1 and PC2, only two hemocyanins, one calreticulin and Na^+-K^+-ATPase isoform contributed to both, possibly indicating shifts in isoforms based on PTMs.

Principal component analyses – temperature x pH

The second set of PCAs included proteins that were significant for either a temperature (no or a 31ºC heat shock - HS) or pH main (Figs 21A-B and Tables 10-11) or an interaction effect (Fig. 21C and Table 12) – all during acclimation to daily emersion from 12:00 – 18:00. The latter separated the HS-pH 8.1 and no-HS-pH 7.6 (here “mild” stress) treatments (negative section of x-axis) from the HS-pH 7.6 and no-HS-pH 8.1 (here “extreme” - most and least - stressful)

treatments (positive section) along PC1, explaining 32.5% of the variation. PC2 mainly separated the HS (positive section of y-axis) from the no-HS treatments, explaining 23.1%. These results illustrate a strong interaction effect between HS and pH treatment. In other words, at pH 8.1, HS shifted protein abundance patterns towards the emersion-pH 7.6 treatments, but at pH 7.6, HS shifted abundance patterns towards emersion-pH 8.1. Thus, depending on the pH at which HS occurred, the shift HS caused was in opposite directions along PC1.

Among the proteins contributing the most positive loadings to PC1, associated with higher abundances at extreme (HS-pH 7.6 and no-HS-pH 8.1) treatments, were two full-length hemocyanin isoforms, a CLIP-domain serine protease 2 (also described as a pro-phenoloxidase - proPO - activating factor or PPAF), fibrillin-2, an extracellular matrix glycoprotein that contributes to the maintenance of microfibrils in the cuticle (Giraud-Guille, 1984; Zhang et al., 1994), actin and five metabolic proteins representing glycolysis (glyceraldehyde 3-phosphate dehydrogenase or GAPDH), tricarboxylic acid (TCA) cycle (mitochondrial malate dehydrogenase or mMDH and PDH) and the urea cycle (glutamate dehydrogenase and argininosuccinate synthetase 1) (Table 12A). Proteins contributing negative loadings, with generally lower abundances under extreme treatments, were seven cuticle proteins, two full-length hemocyanins and a F1-ATP synthase β-subunit (Table 12B). Thus, extreme treatments caused an increase in proteins representing metabolism (NADH-producing reactions), the urea cycle, a shift in proteins involved in oxygen transport and a decrease in cuticle proteins.

Proteins contributing to the effect of HS regardless of pH (positive loadings to PC2), by increasing abundance during HS, are a serine protease (testisin-like), lectin E and three cuticle protein isoforms (all of which may affect the sclerotization of gill cuticle – see below), two tubulin and three F1-ATP synthase isoforms (Table 12C). The negative loadings to PC2 were contributed by four full-length hemocyanins, several metabolic proteins, which overlap with positive loadings for PC1, fibrillin-2 and two cuticle proteins (Table 12D). During HS, lectin E, serine protease and cuticle proteins may be involved in the proPO activation cascade and thus the sclerotization and restructuring of the cuticle (see below for details). HS also increased ATP synthase and decreased full-length hemocyanin isoforms.

While daily emersion at pH 7.6 effectively canceled the proteomic changes of pH 7.6 during acclimation to constant immersion (Fig. 20C), the effect of daily emersion plus daily HS in turn depends on pH, with a daily HS shifting protein abundance patterns towards the emersion (no HS)-pH 7.6 treatment when animals were acclimated to pH 8.1 (Fig. 21C).

<u>Protein homeostasis: protein maturation in the endoplasmic reticulum (ER) and protein degradation</u>

Molecular chaperones and proteases, which regulate protein homeostasis, responded either due to daily HS (cluster I), pH (III) or showed mainly an interaction effect (II; Fig. 22 – significance for main or interaction effects for each protein are based on two separate permutation ANOVAs, $p \leq 0.05$). More specifically, low pH, more so under immersion than emersion, decreased the

abundance of several chaperones, including endoplasmin (homolog of glucose-regulated protein94 or GRP94), calreticulin and protein disulfide isomerase (PDI), involved in protein maturation of excretory proteins in the endoplasmic reticulum (Fig. 23) (Braakman and Hebert, 2013; Bulleid, 2013). Isoforms of another ER chaperone involved in protein maturation, BiP (homolog of GRP78) decreased abundance at low pH under emersion only (spot#286) and increased abundance in response to temperature (spot#251) (Fig. 23). We interpret these results as indicating that pH 7.6 lowers the rate of protein maturation in the ER, but that emersion and daily HS either cancel this effect or increase one particular ER chaperone, BiP (GRP78), respectively. The only inducible heat-shock protein 70 (HSP70) we identified showed an interaction effect between tidal regime x pH but no differences in the pairwise comparison of treatments and no change with acclimation to daily HS (Figs. 22 and 23).

We identified several proteins belonging to the ubiquitin-proteasome and the lysosomal (autophagy) protein degradation pathways (Wong and Cuervo, 2012). A proteasome α-type 6 subunit showed reduced levels with low pH under both tidal regimes (pH main effect) and a significant response when emersed daily (Figs. 22, cluster III, and 23). The lysosomal aspartic proteases cathepsin D showed lower levels with emersion and cathepsin B showed lower levels at immersion-pH 7.6 and emersion-pH 8.1 in comparison to immersion-pH 8.1 (Figs. 22 and 23). Cathepsin B also showed a pH main effect, with higher levels at pH 7.6 in response to emersion (Fig. 22). Both pathways are involved in the degradation of proteins and the recycling of amino acids. Together with the

lower levels of three ER chaperones at immersion-pH 7.6, lower levels of the proteasome subunit and cathepsin B strongly support the hypothesis that immersion-pH 7.6 reduced protein maturation in the ER and simultaneously down-regulated protein degradation via the ubiquitin-proteasome and lysosomal (autophagy) protein degradation pathways. This response to low pH is less significant in response to emersion-pH 7.6. While cathepsins B and D are both considered to be the major proteases in the turnover of cell organelles, i.e. autophagy (Muller et al., 2012), they responded in opposite directions to immersion-pH 7.6. Both cathepsins also responded in the same opposite ways in lysosomes of HeLa cells treated with hydrogen peroxide (Yoon et al., 2011). In this context it is interesting that the hydrogen peroxide scavenging peroxiredoxin was elevated with immersion-pH 7.6 and was only marginally insignificant in comparison to immersion-pH 8.1 (P=0.065; see below). The possibility of low pH increasing levels of antioxidant proteins, including peroxiredoxins, has been shown for the Easter oyster *C. virginica* (Tomanek et al., 2011) and ER protein maturation, which generates hydrogen peroxide (Tomanek, 2015), might be reduced to limit a further increase in levels of reactive oxygen species (ROS).

Serine proteases and lectins

Two masquerade-like serine proteases (MSP; spot#14 and 19) with homology to CLIP-domain serine proteases (CLIP-SP) and pro-phenoloxidase (proPO) activating factor (PPAF), decreased abundance in response to low pH under immersion (Figs 22, cluster III, and 6C). In contrast, another MSP (spot#31)

showed abundances that were higher at low pH under immersion relative to both emersion treatments (Figs 22, II, and 23B). Crustacean MSPs have been shown to bind microbial pathogens and exhibit anti-microbial activity, in part through the proPO activation cascade, which leads to the formation of quinones and melanin to facilitate the phagocytosis of pathogens (Jitvaropas et al., 2009). Other SP isoforms (spot#221 and 455), also with homologies to CLIP-SP or PPAF, showed an increase in abundance at low pH with emersion plus daily HS but not emersion without HS (Figs 22 and 23A). Two SP isoforms (spot#231 and 477) showed a temperature main effect due to higher levels with daily HS (Fig. 22). An additional SP (spot# 392) was lower at pH 8.1 during emersion with HS but not without HS (Fig. 23B).

CLIP-SP are activated through the lectin-complement pathway, including C-type lectin and β-1,3-D-glucan-binding proteins (Fig. 23), which recognize bacterial and fungal cell wall components, such as β-1,3-glucans, peptidoglycans and lipopolysaccharides (Soderhall and Cerenius, 1998). An isoform of lectin E showed an increase in abundance with low pH during emersion plus HS, similar to two of the CLIP-SP, but because it showed reduced but non-significant abundances with low pH during immersion treatment, it clustered with two MSP (Figs. 22 and 23C). In contrast, a C-type lectin increased in abundance at high pH in response to emersion (Figs 22 and 23C). The β-1,3-D-glucan-binding protein showed a temperature main effect, with higher levels in response to HS and clustered with four serine proteases (Fig. 22, I).

The results suggest that pH 7.6 lowers abundances of several CLIP-SP (e.g. MSPs) and lectin isoforms during immersion, while one MSP isoform increased, suggesting a shift between PTMs. HS during emersion, however, affected another set of CLIP-SP, more so at low pH. These results suggest that the proPO activation pathway is up-regulated at immersion-pH 7.6 and emersion-HS at both pH 8.1 and 7.6 (Fig. 23). Besides its importance in the immune response of crustaceans, the proPO activation cascade also affects cuticle sclerotization (hardening) and coloration.

Chitin-binding proteins: peritrophins and cuticle proteins

Of the four isoforms of peritrophin A, two showed a pH effect, but opposite changes in abundance during emersion-no HS (spot#543 and 573) and one (spot#608) a temperature effect with higher levels with daily HS (Figs 22, cluster I, and 23A). All three are clustering with four serine proteases and a β-1,3D-glucan-binding protein. A fourth one (spot#453) showed an interaction effect between pH and tidal regime (Figs 22 and 23B). None of the pairwise comparisons were significant (Fig. 23). Peritrophins consists of registers of cysteine residues linked by disulfide bonds, which interact with chitin, representing so-called chitin-binding domains or CBD (Hegedus et al., 2009). Chitin is a polymer of N-acetyl glucosamine and a major component of the arthropod cuticle. Furthermore, the disulfide bridges are likely formed in the ER by PDI. By binding to chitin through the CBD, it is possible that peritrophins organize chitin microfibrils (Hegedus et al., 2009).

Transglutaminase showed a temperature main effect, with higher abundances with HS (Figs 22 and 23A). It is involved in the cross-linking of cuticle proteins in horseshoe crabs (Matsuda et al., 2007) and C-type lectins are among its substrate (Shibata et al., 2010). Finally, fibrillin showed a temperature x pH interaction effect (Figs 22 and 23B). It is an extracellular glycoprotein involved in modifying fibers of connective tissue in the cuticle (Giraud-Guille, 1984; Zhang et al., 1994).

While immersion-pH 7.6 reduced the abundance of a lectin and several MSPs, suggesting a decrease in the activity of the proPO activation pathway (Fig. 22, III), one MSP and a SP isoform were higher during immersion-pH 7.6 (II). Emersion modified the response to low pH of these latter SP isoforms (II). Acclimation to daily emersion-HS increased abundances of a glucan-binding protein, SP, peritrophins and transglutaminase, all proteins involved in binding to chitin and connecting chitin fibers as well as cross-linking chitin-binding proteins (I). These modifications suggest that chitin-related structures of the gill cuticle are constantly undergoing changes, possibly to maintain the integrity of its structure during immersion-pH 8.1, but that low pH inhibits (modified by emersion) and daily HS activates the proPO activation and its downstream pathways (Fig. 24).

Cuticle proteins

Cuticle protein isoforms responded to pH, emersion and daily HS in five main clusters (Fig. 25). DD5 cuticle proteins were lower with emersion but simultaneously showed an interaction effect when acclimated to daily HS, with

higher abundances at pH 8.1-HS (Fig. 25; cluster I). Mainly DD5, but also an RR2-cuticle protein and a tentative cuticle protein isoforms showed higher abundances at pH 7.6 during immersion but not emersion and thus were significant for an interaction effect between tidal regime x pH (II). Twelve DD5 and two arthrodial cuticle proteins (AMP16.3) isoforms either showed lower abundances at low pH (pH main effect), or showed higher abundance in response to pH 8.1 during emersion but not immersion and thus an interaction effect (III). Nineteen DD5 isoforms showed a temperature main effect, with higher abundances with daily HS (IV). Most of these isoforms had a mass of ~50 kDa, five of ~90 kDa. Finally, DD5, DD9A and AMP16.3 showed higher levels during emersion or showed an interaction effect (V).

Cuticle proteins are part of the organic matrix of the cuticle, and are characterized by the Rebers-Riddiford (R-R) consensus sequence motif, which has been shown to bind to chitin, possibly playing a role in the cross-linking of chitin fibers (Rebers and Riddiford, 1988; Rebers and Willis, 2001). Specifically, DD5 cuticle proteins isolated from epidermal cells underlying the exoskeleton of the penaeid prawn *Penaeus japonicas* have been shown to contain repeated R-R sequence motifs (Ikeya et al., 2001). We also identified several small arthrodial cuticle proteins (<12kDa) that are known to be part of uncalcified cuticles that allow for ion and gas exchange (Andersen, 1998; Andersen, 1999; Faircloth and Shafer, 2007).

Thus, both cuticle proteins and peritrophins bind chitin and possibly organize chitin fibers. Transglutaminase might be directly involved in the cross-

linking of these chitin-binding proteins (Matsuda et al., 2007). All three together suggest that the chitin-fiber mesh of the gill cuticle is undergoing structural modifications, possibly affecting ion permeabilities through change in abundance of chitin-binding proteins (CBP) and proteins that cross-link these CBP in response to different pH, immersion-emersion and temperature acclimation conditions. Furthermore, an increase in the production of quinones through the proPO activation pathway could facilitate the cross-linking of CBP (Fig. 24).

Hemocyanin

Overall we identified forty-five hemocyanin isoforms, which differed in mass and pI (Fig. 26). With the mass of full-length hemocyanin being 75 kDa and our highest mass being 81 kDa, we set a cut-off at 75±6 kDa for the full-length protein. There was also a noticeable drop in mass between 37 and 31 kDa, suggesting that some of the spots represented higher and lower molecular mass fragments. Thus, seventeen spots represented full- (~69-81 kDa), seventeen high- (~37-67 kDa; HMMF) and eleven low-molecular mass fragments (~19-31 kDa; LMMF). Using this classification, levels of full-length isoforms were lower with daily HS (Fig. 26, cluster I), increased with emersion (II), shifted from lower to higher abundance at pH 7.6 with acclimation shifting from immersion to emersion (III), were lower with emersion and daily HS (IV and V) and shifted from being lower at low pH during immersion and emersion to higher at low pH with daily emersion-HS (VI). Interestingly, full-length fragments of cluster I that decreased in response to daily HS regardless of pH had much lower pIs than those of cluster VI, which increased in response to pH 7.6-HS, suggesting a role

for PTMs. Levels of HMMF showed higher levels at low pH during emersion but not immersion (III), lower levels with emersion (IV), and higher levels with emersion-HS (VII and VIII). LMMF showed an increase at low pH during emersion-HS (VII), similar to HMMF, but the majority increased with HS regardless of pH (mainly VIII). Importantly, LMMF clustered only with HMMF (VII and VIII). Furthermore, analysis of the pI values showed that LMMF have a more basic pI (pI 6.23) than HMMF and full-length (pI 5.57 and 5.59, respectively) isoforms.

Thus, changes in pH affected the abundance of full-length hemocyanin isoforms mainly when accompanied by changes in tidal regime or temperature acclimation, but some were lower in response to daily HS regardless of pH (Fig. 26, I and IV). HMMF showed an emersion (IV), temperature (HS) (VIII) and tidal regime x pH (III) effect and LMMF showed either a temperature (VIII) or tidal regime x pH (V and VII) effect.

A similar pattern of hemocyanin fragment formation was described for the Pacific white shrimp *Penaeus vannamei* in response to virus infection (Chongsatja et al., 2007). Subsequent work showed that the acidic and basic fragments represented the C- and N-terminal ends of hemocyanin, respectively (Havanapan et al., 2009). Applied to our study, LMMF would represent the N-terminal and HMMF isoforms the C-terminal end.

Full-length hemocyanins function mainly as oxygen-carrying and H^+-buffering proteins in arthropods and molluscs (Burmester, 2002). Acclimation to higher temperatures has shown to increase the percentage of hemocyanin

hexamers *versus* di-hexamers, with parallel shifts in linker-subunits connecting the hexamers (Decker and Foll, 2000; Decker et al., 2007), although it is unclear if similar shifts occur due to acclimation to daily HS. Furthermore, low pH enhances the effect of temperature in decreasing oxygen affinity of crustacean hemocyanin (Weber et al., 2008), suggesting that the changes in abundance of full-length isoforms are in part due to adjusting hemocyanin conformation and abundance to maintain both its oxygen binding and buffering capacity.

Due to the lack of water flow and exchange, emersion can lead to an increase in hemolymph P_{CO2} and bicarbonate and thus to the acidification of branchial reserve waters in gill (Burnett and McMahon, 1987). Emersion regardless of pH increased the abundance of one full-length isoforms and one HMMF (Fig. 26, II). In contrast, several full-length isoforms showed a decrease with emersion (V). Emersion-pH 7.6 would most likely further acidify the branchial waters and hemolymph. When compared to immersion-pH 7.6, emersion-pH 7.6 increased the abundance of several full-length isoforms and HMMF (III), suggesting that both play a role in H^+-buffering. Finally, acclimation to daily HS will further decrease hemolymph pH (Hochachka and Somero, 2002). These conditions, increased the abundance of a number of HMM and LMM fragments (VII and VIII), possibly further increasing the H^+-buffering capacity of the hemolymph. Given these results, in addition to full-length isoforms, HMMF and LMMF may add to the H^+-buffering capacity of the hemolymph during emersion-pH 7.6 and emersion-HS.

In addition to playing a potential role in H^+-buffering, C-terminal (here HMM) and N-terminal (here LMM) fragments of hemocyanins also function as anti-microbial peptides and catechol oxidases, respectively (Decker et al., 2007; Destoumieux-Garzon et al., 2001; Lee et al., 2003; Terwilliger, 1999). The HMM fragments changed with emersion, emersion-pH 7.6 and HS (Fig. 26). Similarly to the present results, acute HS also increased the formation of hemocyanin fragments in a mass range similar to the one reported here for the HMMF in cheliped muscle of *P. cinctipes* (Garland et al., 2015). Thus, HS seems to be activating *in vivo* proteolysis of hemocyanins and generating C-terminal fragments, possibly to enhance anti-microbial defenses.

Simultaneously (at least during HS), cleavage of hemocyanin may also activate the catechol oxidase activity (conversion of *o*-diphenols to *o*-quinones) of the N-terminal (here LMM) fragment, similar to the activation of pro-phenoloxidases to phenoloxidases by serine proteases with homologies to CLIP-SP and PPAF (Jaenicke and Decker, 2004; Kawabata et al., 1995; Lee et al., 2004). Importantly, in contrast to phenoloxidases, which catalyze both the oxidation of monophenol (tyrosine) to *O*-diphenol (tyrosinase activity) and of *o*-diphenols to *o*-quinone (catechol oxidase or COX), LMMF only show COX activity (Fig. 24) (Terwilliger, 1999).

The conversion of tyrosine to quinones (and further to melanin) by phenoloxidases and COXs has been shown to play a role in (i) the primary immune response, as melanin is used to encapsulate invading pathogens, with their membrane glycoproteins activating the lectin complement and the proPO

activation pathway able to induce the COX activity of hemocyanins, (ii) the sclerotization (hardening) of the cuticle and (iii) coloration of crustaceans (Jaenicke and Decker, 2004; Terwilliger and Ryan, 2006; Wang et al., 2001). Adding to the possibility that our treatments affected the synthesis of quinones is the observation that a key enzyme of tyrosine catabolism, fumarylacetoacetate, decreased in abundance with emersion-low pH and during acclimation to daily HS, possibly shifting tyrosine catabolism towards quinone synthesis (see below).

Thus, the pattern of hemocyanin proteolysis, in addition to the activation of the lectin complement, involving CLIP-serine proteases, provides further evidence for the induction of the proPO activation pathway, suggesting that tyrosine catabolism may be diverted to the synthesis of quinones and melanin (Fig. 24). Furthermore, quinones may in turn be used to cross-link cuticle proteins and peritrophins, cuticle binding proteins, possibly by transglutaminase. While the proPO activation pathway is the hallmark of the crustacean immune response (Amparyup et al., 2013), together, the proteomic changes we observed suggest cuticle sclerotization as the main process being most likely inhibited by low pH during immersion, but activated with acclimation to daily HS regardless of pH.

Energy and nitrogen metabolism

We identified proteins involved in ATP buffering (arginine kinase [AK]), glycolysis (GAPDH and enolase), pentose-phosphate pathway (PPP; 6-phosphoglucono lactonase), TCA cycle (PDH, citrate synthase [CS], dihydrolipoyl dehydrogenase [DHLDH] and MDH]), oxidative phosphorylation (F1 ATP synthase β) and urea

cycle (glutamate dehydrogenase) as responding to the different acclimation regimes (Fig. 27).

Results from the permutation ANOVA showed that metabolic proteins changed abundance predominantly in response to pH (cluster I), daily HS (II, some in IV), emersion (III and IV) or showed an interaction effect between tidal regime x pH and temperature x pH (III and V).

Cluster I, showed lower abundances of two key metabolic enzymes, AK and F1-ATP synthase (spot#669 and 184), in response to immersion-pH 7.6 only, indicating a possible decrease in energy metabolism and thus ATP supply (Figs 27 and 28A). In addition, argininosuccinate synthetase (spot#457), a urea cycle enzyme that is responsible for the incorporation of the second nitrogen ammonium into the urea molecule (Chandel, 2015), clustered with these metabolic enzymes and showed an interaction effect between temperature x pH. It showed a significant decrease in response to emersion-pH 8.1-HS, possibly indicating a decrease in nitrogen metabolism and breakdown of amino acids (Fig. 28). Another argininosuccinate synthetase isoform (spot#458) showed higher abundance with immersion- but not emersion-pH 7.6 (cluster III), suggesting that low pH increased nitrogen metabolism in gill, but that HS as well as emersion overall decreased urea production (Figs 27 and 28).

Proteins in cluster II generally showed increasing abundances with daily HS (Figs 27 and 28). One of two AK isoforms (spot#641) of this cluster increased with daily HS (temperature effect) and might buffer ATP fluctuations due to temperature-induced changes in reaction rates during HS in accordance with the

results from another proteomic analysis of cheliped muscle tissue, which showed that daily extreme temperature fluctuations induced higher abundances of several AK isoforms in *P. cinctipes* (Garland et al., 2015). Another AK isoform (spot#621) showed higher abundances with emersion.

AK catalyzes the transfer of phosphoryl groups from phosphoarginine to ADP and is therefore able to maintain high ATPase activities (Wallimann et al., 2007). However, the reverse is true as well: By catalyzing the formation of phosphoarginine in the intermembrane space of mitochondria, AK is able to recycle ADP to maintain high ATP production rates (Dzeja and Terzic, 2003; Guzun et al., 2012). Thus, depending on the cellular location of AK isoforms (mitochondria *versus* cytosolic), higher levels may facilitate higher ATP production or consumption rates or both. As we will see, we observed increased abundances of both ATP synthase and ATPase isoforms (see below).

Cluster II also included six F1-ATP synthase β isoforms. One showed lower abundances with emersion (spot#510), three higher abundances in response to daily HS (spots#463, 601 and 611), and three with higher levels in response to emersion-pH 7.6-HS only (Figs 27 and 28B). The fact that the majority of F1-ATP synthase β isoforms showed elevated levels with emersion-HS or emersion-pH 7.6-HS suggests that acute shifts towards lower pH level require higher ATP synthase activity, most likely to dissipate (uncouple) the proton gradient that a temporary increase in body temperature might cause due to higher reaction rates along the ETC (Mailloux et al., 2013). In contrast to the ß

subunit, the only ATP synthase α subunit (spot#522) decreased in response to daily HS (Figs 27, cluster IV, and 28D).

Cluster III included proteins with reduced abundances in response to emersion or with an interaction effect between tidal regime x pH. The discussion of these abundance changes is included in separate sections, i.e. ion regulation and signaling (see below).

Cluster IV included proteins that either showed lower abundances in response to emersion or daily HS. One AK isoform (spot#561) showed lower levels with emersion-HS, another one (spot#557) lower levels with emersion-pH 7.6 (Fig. 27 and 28D). Two glycolytic enzymes were either lower with emersion (one GAPDH and two enolase isoforms) or with daily HS (one GAPDH-spot#). One TCA cycle enzyme, citrate synthase, was lower with emersion, another one, DLDH, which represents α-ketoglutarate dehydrogenase subunit E_3 either showed lower levels with emersion or a temperature (spots#568 and 506, respectively). Finally, a F1-ATP synthase α subunit isoforms decreased with daily HS and a β subunit decreased with emersion. Together, these patterns suggest a slowdown of NADH and ATP, first with emersion in comparison to immersion and then further with emersion-HS.

Fumarylacetoacetase (spot#268) is an enzyme of tyrosine catabolism and showed an interaction effect between tidal regime x pH, with (non-significantly) lower levels with emersion-pH 7.6. Levels were also low with emersion-HS (Fig. 28D). The reason this is a noticeable, is that two additional enzymes of this pathway, 4-hydroxylphenolpyruvate oxidase and homogentisate 1,2-

dioxygenase, also changed in response to lowering pH and increasing acclimation temperature in gill tissue of the spider crab *Hyas araneus* (Harms et al., submitted), suggesting that tyrosine metabolism generally shifts in response to pH and temperature changes. Low levels of fumarylacetoacetase with emersion-HS would favor tyrosine metabolism to be diverted to the synthesis of quinones and in agreement with the induction of the proPO activation pathway and higher abundances of cuticle binding proteins and transglutaminase (Fig. 24).

A mitochondrial (spot#514) and an additional (spot#131) isoform of NADP-dependent malic enzyme with unknown cellular location showed lower levels with emersion (Figs 27 and 28D). The main role of the mitochondrial isoform is to produce NADPH during the conversion of malate to pyruvate. The role of the cytosolic isoform, in conjunction with ATP citrate lyase and cytosolic MDH, is to facilitate the transfer of acetyl-CoA from mitochondria to the cytosol for the synthesis of fatty acids (Chandel, 2015). Thus, emersion lowered abundances of malic enzyme, parallel to the overall reduction in the abundance of metabolic enzymes. However, the abundance of the mitochondrial isoform was higher with immersion-pH 7.6 in comparison to emersion-pH 7.6 (Fig. 28D), possibly to increase the production of NADPH as reducing equivalents and to increase the scavenging of reactive oxygen species (Tomanek, 2015). Interestingly, an isoform of mitochondrial MDH decreased under the same conditions and would therefore not compete with malic enzyme for malate as a substrate (Figs 27 and 28).

In summary, immersion-pH 7.6 lowered the abundance of AK and F1-ATP synthase, while emersion lowered the abundance of other isoforms of both of these enzymes as well as glycolytic and TCA cycle enzymes regardless of pH. Surprisingly few metabolic enzymes showed an interaction effect between tidal regime x pH. In addition, a number of the enzymes that lowered abundance with emersion also showed lower abundance with emersion-HS. Thus, emersion, based on protein abundances, established a new metabolic state, overall lowering metabolic activities of glycolysis, TCA and urea cycle. Deviating from this pattern are enzymes from cluster II, which include AK, F1-ATP synthase and 6-phosphogluconolactonase from the PPP. The increase in abundance of AK (similar to creatine kinase) and F1-ATP synthase together facilitates their role as protonophores by maintaining high ATP turnover rates to dissipate the proton gradient across the inner mitochondrial membrane and thereby control the production of ROS during HS (Mailloux et al., 2013). The cytosolic isoform of 6-phosphogluconolactonase might simultaneously provide reducing equivalents in form of NADPH to the two ROS scavenging systems, the glutathione and the thioredoxin-peroxiredoxin system (Murphy, 2012; Tomanek, 2015). At odds with this were the abundance patterns of two oxidative stress proteins, the peroxisomal catalase and peroxiredoxin (Fig. 27; clusters III and IV). Both are following more closely the general trend of a depression of energy metabolism in response to emersion regardless of a daily HS.

Hormone metabolism

We identified two spots as farnesoic acid O-methyltransferase (FaMet). The first isoform (spot#417) decreased in abundance with low pH (pH main effect), while the second (spot#436) decreased with emersion (Fig. 27 and 28). They differed in pI, which suggests a small PTM, e.g. phosphorylation (Holford et al., 2004). Farnesoic acid O-methyltransferase converts farnesoic acid (FA) into the juvenile hormone-like methyl farnesoate (MF), which is involved in the regulation of several aspects of arthropod physiology, including development, reproduction, and molting (Kuballa et al., 2011; Nagaraju, 2007; Nagaraju, 2011).

Hemolymph levels of MF increased in response to hyposaline conditions and showed an interaction with temperature in the green crab *Carcinus maenas* (Lovett et al., 2006; Lovett et al., 2001; Nagaraju and Borst, 2008). Both low pH and emersion, especially when associated with enough water loss and accumulation of protons and bicarbonate, are likely to affect ion regulation of gill tissue in *P. cinctipes* (see below) and it is possible that FaMet plays an important yet unspecified role in this response.

It is likely that the activities of FaMet and FA/MF are mediated through the retionoid X receptor (RXR) as the RXR of *Daphnia magna* forms a heterodimer with the ecdysteroid receptor (EcR) and, in conjunction with MF and related compounds, promotes transcription (Wang and LeBlanc, 2009). Supporting this assumption, we also observed changes in three isoforms of the aldehyde dehydrogenase 8 family member A1 (ALDH8A1). This isoform converts 9-cis-retinal to 9-cis-retinoic acid, which is a high-affinity ligand of RXR (Heyman et al.,

1992; Levin et al., 1992). Two of three isoforms of ALDH8A1 were lower with emersion, with one isoform (spot#137) clustering with FaMet (spot#436). One (spot#531, Figs 27 and 28B) responded to pH 7.6 during immersion with lower abundances in comparison to pH 8.1, suggesting a role in responding to low pH. Thus, FaMet and ALDH8A1 may provide fewer ligands for the RXR:EcD complex during immersion-pH 7.6 and during emersion in general, conditions that are associated with lower abundances of proPO activation pathway and metabolic proteins, respectively.

Ion regulation

We also identified changes in proteins directly involved in ion regulation. The Na^+-K^+-ATPase β2 isoform increased abundance in response to immersion-pH 7.6 relative to all other treatments (Figs 27 and 28C). The V-type H^+-ATPase showed a higher abundance with immersion, with non-significantly elevated levels at immersion-pH 7.6 (Figs 27 and 28D). In addition, an extracellular GPI-linked carbonic anhydrase (CA) showed higher levels at pH 7.6 (pH main effect) in emersed animals regardless if they experienced HS or not (Figs 27 and 28B). Glycosylphosphatidylinositol (GPI)-linked proteins are localized to the membrane of the ER from where they can be transported in vesicles towards the cell membrane where they are excreted (Gilmour and Perry, 2009).

The Na^+-K^+-ATPase of crustacean gill is localized within the basolateral membrane and has been shown to transport ammonium (NH_4^+), which has the same ionic radius as K^+ (Henry et al., 2012). A possible mechanism of the route of excretion of NH_4^+ across the apical membrane of the crustacean gill involves

acidified vesicles and microtubules (Weihrauch et al., 2004; Weihrauch et al., 2002). More specifically, following import by the Na^+-K^+-ATPase, NH_4^+ is proposed to dissociate into ammonia (NH_3) and H^+ within the cytosol. Ammonia crosses membranes more easily and diffuses into vesicles acidified by the V-type H^+-ATPase, which are subsequently transported towards the apical membrane by a microtubular network (Weihrauch et al., 2002). In this context it is important to recall that one argininosuccinate synthetase 1 isoform showed higher abundances with immersion-pH 7.6 (Figs 27 and 28C), which may be directly linked to the transport or turnover of ammonium. Of further relevance in this context is that interaction effect of glutamate dehydrogenase (GDH), with its highest abundance with immersion-pH 7.6 (Fig. 27 and 28E). GDH can generate another ammonium molecule that is incorporated into urea via the urea cycle (Chandel, 2015). Thus, both proteins suggest that the urea cycle is more active at low than at high pH during immersion, suggesting another pathway contributing to the excretion or turnover of ammonium ions and their role in responding to acidification.

Furthermore, emersion canceled the response to low pH of Na^+-K^+-ATPase, argininosuccinate synthetase, FaMet and ALDH8A1, suggesting a greater tolerance towards low pH with aerial emersion (Fig. 27). Also, the transport of acidified vesicles depends on the cell's microtubule network, which showed accompanying changes in tubulin isoforms (Fig. 29; cluster I). Since levels of Na^+-K^+-ATPase, V-type H^+-ATPase and tubulin isoforms were high at immersion-pH 7.6, our results support the hypothesis that crustacean eliminate

proton equivalents through the excretion of ammonium across the gill (Weihrauch et al., 2004). Possibly adding to this mechanism is a higher turnover rate of the urea cycle. As FaMet is known to play a role in the response of crustaceans to osmotic stress, it, together with ALDH8A1, may be involved the regulation of the response to low pH.

Cytoskeletal proteins

A number of actin and tubulin isoforms changed in response to emersion or HS (Fig. 29; clusters I, II, and IV). Six (10%) isoforms of these two proteins showed a significant pH effect and five showed a HS main effect; however, eight demonstrated an interaction effect, suggesting that pH stress impacts how the cytoskeleton is rearranged in response to emersion and HS. In general, low pH increased levels of cytoskeletal proteins when crabs were constantly immersed (I), whereas emersion and HS increased abundance of other isoforms in a complementary pattern (II). The majority of cytoskeletal proteins were abundant when crabs were acclimated to daily HS (IV), and proteins of this cluster were not abundant in other treatments, suggesting HS-specific roles for these specific isoforms. Surprisingly, in the temperature x pH analysis, all but three proteins were significant for a pH main effect, emphasizing the greater role HS has on affecting the cytoskeleton.

The identified cytoskeletal proteins either belonged to the microtubule (α- and β-tubulin isoforms) or microfilament (mostly α- and β-actin isoforms) networks. Tubulin and actin isoforms are fairly evenly spread throughout the clusters, but their abundance patterns may be mechanistically unrelated. We will

discuss microtubule and microfilament proteins separately as these networks are biochemically and functionally distinct.

Microtubules are made up by heterodimers of α- and β-tubulin, which in eukaryotes are often transcribed by multiple genes, thus allowing for a diversity of α/β dimers. In addition, tubulins are characterized by a number of PTMs, which affect a number of cellular processes (Garnham and Roll-Mecak, 2012). We identified 38 α and β isoforms as changing abundance. The microtubule network regulates a number of cellular processed by forming dynamic supramolecular structures (Janke and Bulinski, 2011). In crab gill tissue, the ammonia excretion mechanism hypothesized by Weihrauch et al. proposed that the microtubule network facilitates the transport of acidified vesicles containing ammonium toward the cell membrane for exocytosis (Weihrauch et al., 2002). In cluster I (Fig. 29), three tubulin isoforms increased abundance during immersion-only, but four showed an interaction effect between tidal regime x pH. These changes correlate with elevated Na^+/K^+ ATPase levels in response to low pH, supporting the hypothesis that microtubules are involved in ammonium excretion in the gill of *P. cinctipes*.

Ammonium excretion during emersion may result in the accumulation of bicarbonate and protons in branchial water stores, possibly modifying the ammonium excretion process (Burnett and McMahon, 1987). The shift from immersion to emersion affected a number of tubulin isoforms in opposite patterns (I and II), likely representing shifts in PTMs. HS during emersion exerted an

effect on a greater number of isoforms, possibly because of greater acute changes in reaction rates with HS due to Q_{10} effects (IV).

We identified twenty-three (mostly α and β) actin isoforms of which fourteen were significant for a temperature main effect. Four isoforms decreased in abundance in response to emersion (Fig. 29; I); low pH stress contributed to this decrease, although not significantly. HS decreased two isoforms, another one increased due to emersion (II). The pattern of cluster III, containing four actins, is rather inconspicuous. Cluster IV, in which proteins are abundant during HS, contained eleven actin isoforms, which overall increased in abundance.

Changes in actin abundances may be influenced by Rho-GDP dissociation inhibitor (Rho-GDI, Fig. 27), which sequesters Rho, a major regulator of the actin cytoskeleton, from membranes to the cytosol (Marks et al., 2009). Low pH repressed Rho-GDI abundance when crabs are constantly immersed, whereas the opposite effect is seen with emersion. Thus, in addition to other cellular functions, Rho-GDI may be altering isoform abundance patterns in the microfilament network.

3.5 Conclusion

The proteomic response of *P. cinctipes* gill tissue to low pH revealed interactions with both tidal regime (immersion *versus* emersion) and temperature stress (no *versus* daily HS). Emersion, possibly leading to the accumulation of P_{CO2} and bicarbonate as well as to acidification of branchial reserve water (Burnett and McMahon, 1987), canceled a number of proteomic changes to low pH occurring during immersion, leading to a partial overlap of the immersion pH 8.1 and emersion pH 7.6 treatments (Fig. 20C). This shift occurred in regards to the activation of PO activitation cascade (Fig. 22, II), oxygen transport (Fig. 26, III and V), cuticle structure (Fig. 22, II, and Fig. 25, II), ion transport and urea cycle (Fig. 27, III), energy metabolism (Fig. 27, V) and tubulin isoform abundance (Fig. 29, I and II). Emersion, in contrast to immersion, might cause acidification of branchial reserve water in crustaceans, and thus might activate the homeostatic response to effectively compensate for low pH conditions by changing these cellular processes.

A 31°C heat shock during emersion in animals that were acclimated to pH 8.1 caused a proteomic response similar to animals experiencing emersion without HS at pH 7.6 (Fig. 21C). Thus, animals acclimated to emersion showed a similar response during low pH and HS at 8.1. Given that hemolymph pH decreases with increasing temperature by approximately -0.019 pH units per °C (Hochachka and Somero, 2002), it is likely that HS (from 11 to 31°C) caused a temporary decrease in pH of approximately 0.38 units or to pH 7.77, causing low

pH conditions similar to the low pH treatment at least during part of the day. However, while the time of low pH (morning) and HS (afternoon emersion) was decoupled, the finding that the HS-pH 7.6 canceled the effect of pH 7.6 with emersion but no HS and be similar to the proteomic response to emersion and pH 8.1 treatment, represents a synergistic effect than we have not seen being described before. Since samples of the HS-pH 7.6 treatment are almost entirely in the positive section of PC2 (Fig. 21C), proteins contributing to PC2 might provide insight into the cellular changes associated with this synergistically compensatory outcome (Table 12).

Several proteins with positive loadings for PC2 showed higher abundances in response to HS – pH 7.6 in a pairwise comparison to no HS-pH 8.1 (e.g. testisin-like serine protease, two F1-ATP synthase ß isoforms and lectin E). Three DD5 cuticle proteins also contributed positive loadings. As almost all other samples are in the negative section of the y-axis, few proteins with negative loadings show a consistent pattern in how abundances differ between these two treatments. Thus, higher abundances of elements of the PO activation cascade (lectins and serine proteases), cuticle proteins and ATP synthase might contribute to this interaction between HS and low pH. It is unclear if the higher abundance of ATP synthase is equated with higher rates of metabolism, possibly indicating higher metabolic costs.

REFERENCES

Abe, H., Hirai, S. and Okada, S. (2007). Metabolic responses and arginine kinase expression under hypoxic stress of the kuruma prawn *Marsupenaeus japonicus*. *Comp Biochem Phys A* 146, 40-6.

Ahearn, G.A., Mandal, P.K., and Mandal, A. (2004). Calcium regulation in crustaceans during the molt cycle: a review and update. *Comp Biochem Physl A* 137, 247-57.

Alberty, R.A. (1953). The relationship between Michaelis constants, maximum velocities and the equilibrium constant for an enzyme-catalyzed reaction. *Journal of the American Chemical Society* 75, 1928-32.

Amparyup, P., Charoensapsri, W. and Tassanakajon, A. (2013). Propehnoloxidase system and its role in shrimp immune responses against major pathogens. *Fish & Shellfish Immunology* 34, 990-1001.

Andersen, S. O. (1998). Characterization of proteins from arthrodial membranes of the lobster, Homarus americanus. *Comp Biochem Physiol A Mol Integr Physiol* 121, 375-83.

Andersen, S. O. (1999). Exoskeletal proteins from the crab, Cancer pagurus. *Comp Biochem Physiol A Mol Integr Physiol* 123, 203-11.

Apraiz, I., Mi, J. and Cristobal, S. (2006). Identification of proteomic signatures of exposure to marine pollutants in mussels (Mytilus edulis). *Mol Cell Proteomics* 5, 1274-85.

Argon, Y. and Simen, B.B. (1999). GRP94, an ER chaperone with protein and peptide binding properties. *Seminars in Cell and Developmental Biology* 10, 495-505.

Baeza, J.A., 2007. The origins of symbiosis as a lifestyle in marine crabs (genus *Petrolisthes*) from the eastern Pacific: Does interspecific competition play a role? *Revista de BiologíaMarina y Oceanografía* 42, 7-21.

Barbarulo, A., Grazioli, P., Campese, A. F., Bellavia, D., Di Mario, G., Pelullo, M., Ciuffetta, A., Colantoni, S., Vacca, A., Frati, L. et al. (2011). Notch3 and canonical NF-kappaB signaling pathways cooperatively regulate Foxp3 transcription. *J Immunol* 186, 6199-206.

Barria, E.M., and Gonzales, M.I. (2008). The effect of autotomy and regeneration of the chelipeds on growth and development in *Petrolisthes laevigatus*. *Crustaceana* 81, 641-52.

Berchtold, M.W., Brinkmeier, H., and Müntener, M. (2000). Calcium ion in skeletal muscle: Its crucial role for muscle function, plasticity, and disease. *Physiol Rev* 80, 1215-65.

Bjelde, B. E. and Todgham, A. E. (2013). Thermal physiology of the fingered limpet *Lottia digitalis* under emersion and immersion. *J Exp Biol* 216, 2858-69.

Bonfills, C., Santer, B.D., Pierce, D.W. (2008). Detection and attribution of temperature changes in the mountainous western United States. *Journal of Climate* 21, 6404-24.

Boyer, T. P., Antonov, J. I., Baranova, O. K., Garcia, H. E., Johnson, D. R., Locarnini, R. A., Mishonov, A. V., O'Brien, T. D., Seidov, D., Smolyar, I. V., Zweng, M. M. (2009). World Ocean Database 2009, edited by: Levitus, S., NOAA Atlas NESDIS 66, US Gov. Printing Office, Wash., DC, 216 pp., DVDs.

Braakman, I. and Hebert, D. N. (2013). Protein folding in the Endoplasmic Reticulum. In *The Endoplasmic Reticulum.*, eds. S. Ferro-Novick, T. A. Rapoport and R. Schekman), pp. 63-79. Cold Spring Harbor: Cold Spring Harbor Press.

Bulleid, N. J. (2013). Disulfide bond formation in the mammalian endoplasmic reticulum. In *The Endoplasmic Reticulum.*, eds. S. Ferro-Novick T. A. Rapoport and R. Schekman), pp. 81-92. Cold Spring Harbor: Cold Spring Harbor Press.

Burmester, T. (2001). Molecular evolution of the arthropod hemocyanin superfamily. *Mol Biol Evol* 18, 184-95.

Burmester, T. (2002). Origin and evolution of arthropod hemocyanins and related proteins. *J Comp Physiol B* 172, 95-107.

Burnett, L. E. and McMahon, B. R. (1987). Gas exchange, hemolymph acid-base status, and the role of branchial water stores during air exposure in three litoral crab species. *Physiological Zoology* 60, 27-36.

Caldeira, K. and Wickett, M. E. (2003). Oceanography: anthropogenic carbon and ocean pH. *Nature* 425, 365.

Cameron, J.N., Iwama, G.K. (1987). Compensation of progressive hypercapnia in channel catfish and blue crabs. *J Exp Biol* 133, 183–97.

Campanale, J. J., Tomanek, L. and Adams, N. (2011). Exposure to ultraviolet radiation causes proteomic changes in embryos of the purple sea urchin, *Strongylocentrotus purpuratus. Journal of Experimental Marine Biology and Ecology* 397, 106-120.

Carberry, S., Zweyer, M., Swandulla, D. and Ohlendieck, K. (2014). Comparative proteomic analysis of the contractile-protein-depleted fraction from normal versus dystrophic skeletal muscle. *Anal Biochem* 446, 108-15.

Cayan, D., Tyree, M., Dettinger, M., et al. (2009). Climate change scenarios and sea level rise estimates for the California 2008 Climate Change Scenarios Assessment. *California Climate Change Center* CEC-500-2009-014-D.

Cayenne, A.P., Gabert, B., and Stillman, J.H. (2011). Identification of proteins interacting with lactate dehydrogenase in claw muscle of the porcelain crab *Petrolisthes cinctipes*. *Comp Biochem Phys D* 6, 393-8.

Chandel, N. S. (2015). Navigating Metabolism. Cold Spring Harbor: Cold Spring Harbor Press.

Chen, X. and Stillman, J. H. (2012). Multigenerational analysis of temperature and salinity variability affects on metabolic rate, generation time and actue thermal and salinity tolerance in *Daphnia pulex. J Therm Biol* 37, 185-194.

Chongsatja, P. O., Bourchookarn, A., Lo, C. F., Thongboonkerd, V. and Krittanai, C. (2007). Proteomic analysis of differentially expressed proteins in Penaeus vannamei hemocytes upon Taura syndrome virus infection. *Proteomics* 7, 3592-601.

Church, J.A., White, N.J., Konikow, L.F., Domingues, C.M., Cogley, J.G., Rignot, E., Gregory, J.M., van den Broeke, M.R., Monaghan, A.J., Velicogna, I. (2011). Revisiting the Earth's sea-level and energy budgets from 1961 to 2008. *Geophysical Research Letters* 38, doi:10.1029/2011GL048794.

Ciofani, M. and Zuniga-Pflucker, J. C. (2005). Notch promotes survival of pre-T cells at the beta-selection checkpoint by regulating cellular metabolism. *Nat Immunol* 6, 881-8.

Clapham, D.E. (2007). Calcium signaling. *Cell* 131, 1047-58

Clark, K. A., McElhinny, A. S., Beckerle, M. C. and Gregorio, C. C. (2002). Striated muscle cytoarchitecture: an intricate web of form and function. *Annu Rev Cell Dev Biol* 18, 637-706.

Craig, E.A. and Gross, C.A. (1991). Is hsp70 the cellular thermometer? *Trends in Biochemical Sciences* 16, 135-40.

Cripps, I.L., Munday, P.L., McCormick, M.I. (2011). Ocean acidification affects prey detection by a predatory reef fish. *Plos one* 6, e22736.

Cubasch, U., D. Wuebbles, D. Chen, M.C. Facchini, D. Frame, N. Mahowald, Winther, J.-G. (2013). Introduction. In: Climate Change 2013: The Physical Science Basis. Contribution of Working Group I to the Fifth Assessment Report of the Intergovernmental Panel on Climate Change [Stocker, T.F., D. Qin, G.-K. Plattner, M. Tignor, S.K. Allen, J. Boschung, A. Nauels, Y. Xia, V. Bex and P.M. Midgley (eds.)]. Cambridge University Press, Cambridge, United Kingdom and New York, NY, USA. Dalle-Donne, I., Rossi, R., Colombo, G., Giustarini, D. and Milzani, A. (2009). Protein S-glutathionylation: a regulatory device from bacteria to humans. *Trends Biochem Sci* 34, 85-96.

Decker, H. and Foll, R. (2000). Temperature adaptation influences the aggregation state of hemocyanin from Astacus leptodactylus. *Comp Biochem Physiol A Mol Integr Physiol* 127, 147-54.

Decker, H. and Jaenicke, E. (2004). Recent findings on phenoloxidase activity and antimicrobial activity of hemocyanins. *Dev Comp Immunol* 28, 673-87.

Decker, H., Hellmann, N., Jaenicke, E., Lieb, B., Meissner, U. and Markl, J. (2007). Minireview: Recent progress in hemocyanin research. *Integr Comp Biol* 47, 631-44.

Destoumieux-Garzon, D., Saulnier, D., Garnier, J., Jouffrey, C., Bulet, P. and Bachere, E. (2001). Crustacean immunity. Antifungal peptides are generated from the C terminus of shrimp hemocyanin in response to microbial challenge. *J Biol Chem* 276, 47070-7.

Dickson, A.G. (1981). An exact definition of total alkalinity and a procedure for the estimation of alkalinity and total inorganic carbon from titration data. *Deep Sea Research Part A: Oceanographic Research Papers* 28, 609-23.

Dickson, A.G., and Goyet, C. (1994). Handbook of methods for the analysis of the various parameters of the carbon dioxide system in sea water. Version 2. (No. ORNL/CDIAC--74). Oak Ridge National Lab., TN (United States).

DiDomenico, B.J., Bugalsky, G.E., and Lindquist, S. (1982). The heat shock response is self-regulated at both the transcriptional and posttranscriptional levels. *Cell* 31, 593-603.

Dilly, G. F., Young, C. R., Lane, W. S., Pangilinan, J. and Girguis, P. R. (2012). Exploring the limit of metazoan thermal tolerance via comparative proteomics: thermally induced changes in protein abundance by two hydrothermal vent polychaetes. *Proc Royal Soc B* 279, 3347-56.

Dineshram, R., Wong, K. K., Xiao, S., Yu, Z., Qian, P. Y. and Thiyagarajan, V. (2012). Analysis of Pacific oyster larval proteome and its response to high-CO2. *Mar Pollut Bull* 64, 2160-7.

Dineshram, R., Thiyagarajan, V., Lane, A., Ziniu, Y., Xiao, S. and Leung, P. T. Y. (2013). Elevated CO_2 alters larval proteome and its phosphorylation status in the commercial oyster, *Crassostrea hongkongensis. Marine Biology* 160, 2189-2205.

Dissanyake, A. (2014). Ocean acidification and warming effects on Crustacea: Possible future scenarios. In *The Mediterranean Sea: Its history and present challenges.*, eds. S. Goffredo and Z. Dubinsky), pp. 363-372. Dordrecht: Springer Science+Business Media.

Dixson, D.L., Munday, P.L., Jones, G.P. (2010). Ocean acidification disrupts the innate ability of fish to detect predator olfactory cues. *Ecology Letters* 13, 68-75.

Donahue, M.J. (2004). Size-dependent competition in a gregarious porcelain crab *Petrolisthes cinctipes* (Anomura: Porcellanidae). *Marine Ecology Progress Series* 267, 219-31.

Doney, S. C., Fabry, V. J., Feely, R. A. and Kleypas, J. A. (2009). Ocean acidification: The other CO_2 problem. *Annual Review of Marine Science* 1, 169-192.

Doney, S. C., Ruckelshaus, M., Duffy, J. E., Barry, J. P., Chan, F., English, C. A., Galindo, H. M., Grebmeier, J. M., Hollowed, A. B., Knowlton, N. et al. (2011). Climate change impacts on marine ecosystems. *Annu Review of Marine Science* 4, 11-37.

Duarte, C.M., Hendriks, I.E., Moore, T.S., Olsen, Y.S., Steckbauer, A., Ramajo, L., Carstensen, J., Trotter, J.A., McCulloch, M. (2013). Is ocean acidification an open-ocean syndrome? Understanding anthropogenic impacts on seawater pH. *Estuaries and Coasts* 36, 221–36.

Dumaz, N. and Marais, R. (2003). Protein kinase A blocks Raf-1 activity by stimulating 14-3-3 binding and blocking Raf-1 interaction with Ras. *J Biol Chem* 278, 29819-23.

Dzeja, P. P. and Terzic, A. (2003). Phosphotransfer networks and cellular energetics. *J Exp Biol* 206, 2039-47.

Eletto, D., Dersh, D., Argon, Y. (2010). GRP94 in ER quality control and stress responses. *Seminars in Cell and Developmental Biology* 21, 479-85.

Ellington, W. R. (2001). Evolution and physiological roles of phosphagen systems. *Annu Rev Physiol* 63, 289-325.

Evans, T. G., Chan, F., Menge, B. A. and Hofmann, G. E. (2013). Transcriptomic responses to ocean acidification in larval sea urchins from a naturally variable pH environment. *Mol Ecol* 22, 1609-25.

Fabry, V.J., Seibel, B.A., Feely, R.A., Orr, J.C. (2008). Impacts of ocean acidification on marine fauna and ecosystem processes. *ICES Journal of Marine Science* 65, 414-32.

Faircloth, L. M. and Shafer, T. H. (2007). Differential expression of eight transcripts and their roles in the cuticle of the blue crab, Callinectes sapidus. *Comp Biochem Physiol B Biochem Mol Biol* 146, 370-83.

Feder, M.E. and Hofmann, G.E. (1999). Heat-shock proteins, molecular chaperones and the stress response: Evolutionary and ecological physiology. *Annu. Rev. Physiol*. 61, 243-82.

Feely R.A., Sabine, C.L., Hernandez-Ayon, J.M., Ianson, D., Hales, B. (2008). Evidence for upwelling of corrosive “acidified” water onto the continental shelf. *Science* 320, 1490–2.

Feely, R.A., Doney, S.C., Cooley, S.R. (2009). Ocean acidification : present conditions and future changes in a high-CO2 world. Oceanography 22, 36-47.

Fehsenfeld, S., Kiko, R., Appelhans, Y., Towle, D. W., Zimmer, M. and Melzner, F. (2011). Effects of elevated seawater pCO(2) on gene expression patterns in the gills of the green crab, Carcinus maenas. *BMC Genomics* 12, 488.

Feige, M.J. and Hendershot, L.M. (2013). Quality control of integral membrane proteins by assembly-dependent membrane integration. *Molecular Cell* 51, 297-309.

Fields, P.A. (2001). Review: Protein function at thermal extremes: balancing stability and flexibility. *Comparative Biochemistry and Physiology Part A* 129, 417-31.

Fields, P. A., Cox, K. M. and Karch, K. R. (2012a). Latitudinal variation in protein expression after heat stress in the salt marsh mussel *Geukensia demissa*. *Integr Comp Biol* 52, 636-47.

Fields, P. A., Zuzow, M. J. and Tomanek, L. (2012b). Comparative proteomics of blue mussel (*Mytilus*) congeners to temperature acclimation. *J Exp Biol* 215, 1106-1116.

Fields, P. A., Eurich, C., Gao, W. L. and Cela, B. (2014). Changes in protein expression in the salt marsh mussel Geukensia demissa: evidence for a shift from anaerobic to aerobic metabolism during prolonged aerial exposure. *J Exp Biol* 217, 1601-12.

Findlay, H.S., Kendall, M.A., Spicer, J.I., Widdicombe, S. (2010). Post-larval development of two intertidal barnacles at elevated CO_2 and temperature. *Mar Biol* 157, 725-35.

Finke, G., Navarrete, S., Bozinovic, F. (2007) Tidal regimes of temperate coasts and their influences on aerial exposure for intertidal organisms. *Marine Ecology Progress Series* 343, 57–62

Fischer, E. H. (2013). Cellular regulation by protein phosphorylation. *Biochem Biophys Res Commun* 430, 865-7.

Förster, C. and Baeza, J.A. (2001). Active brood care in the anomuran crab *Petrolisthes violaceus* (Decapoda: Anomura: Porcillanidae): Grooming of brooded embryos by the fifth pereiopeds. *Journal of Crustacean Biology* 2, 606-15.

Fratelli, M., Demol, H., Puype, M., Casagrande, S., Villa, P., Eberini, I., Vandekerckhove, J., Gianazza, E. and Ghezzi, P. (2003). Identification of proteins undergoing glutathionylation in oxidatively stressed hepatocytes and hepatoma cells. *Proteomics* 3, 1154-61.

Freire, C.A., Onken, H., McNamara, J.C. (2008). A structure–function analysis of ion transport in crustacean gills and excretory organs. *Comp Biochem Physiol A* 151, 272–304.

Gao, Y., Gillen, C.M., Wheatly, M.G. (2006). Molecular characterization of the sarcoplasmic calcium-binding protein (SCP) from crayfish *Procambarus clarkii*. *Comp Biochem Phys B* 144, 478-87.

Garland, M. A., Stillman, J. H. and Tomanek, L. (2015). The proteomic response of cheliped myofibril tissue in the eurythermal porcelain crab, *Petrolisthes cinctipes*, to heat shock following acclimation to daily temperature fluctuations. *Journal of Experimental Biology* 218, 388-403.

Garnham, C. P. and Roll-Mecak, A. (2012). The chemical complexity of cellular microtubules: tubulin post-translational modification enzymes and their roles in tuning microtubule functions. *Cytoskeleton (Hoboken)* 69, 442-63.

Gilmour, K. M. and Perry, S. F. (2009). Carbonic anhydrase and acid-base regulation in fish. *Journal of Experimental Biology* 212, 1647-61.

Giraud-Guille, M. M. (1984). Fine structure of the chitin-protein system in the crab cuticle. *Tissue Cell* 16, 75-92.

Gonor, S.L. (1970). The larval histories of four Porcellanid Anomurans (Crustacea, Decapoda) from Oregon. Master's Thesis, Oregon State University.

Götz, R., Schlüter, E., Shoham, G., and Zimmermann, F.K. (1999). A potential role of the cytoskeleton of *Saccharomyces cerevisiae* in a functional organization of glycolytic enzymes. *Yeast* 15, 1619-29.

Granovsky, A. E. and Rosner, M. R. (2008). Raf kinase inhibitory protein: a signal transduction modulator and metastasis suppressor. *Cell Res* 18, 452-7.

Graziani, I., Eliasz, S., De Marco, M. A., Chen, Y., Pass, H. I., De May, R. M., Strack, P. R., Miele, L. and Bocchetta, M. (2008). Opposite effects of Notch-1 and Notch-2 on mesothelioma cell survival under hypoxia are exerted through the Akt pathway. *Cancer Res* 68, 9678-85.

Griffiths, J. R. (1981). A fresh look at glycogenolysis in skeletal muscle. *Biosci Reports* 1, 595-610.

Gruber, N., Hauri, C., Lachkar, Z., Loher, D., Frolicher, T. L. and Plattner, G. K. (2012). Rapid progression of ocean acidification in the California Current System. *Science* 337, 220-3.

Gurshenov, A. and Douville, H. (2008). Extensive summer hot and cold extremes under current and possible future climatic conditions: Europe and North America. *Climate Extremes and Society* 74-98.

Guzun, R., Gonzalez-Granillo, M., Karu-Varikmaa, M., Grichine, A., Usson, Y., Kaambre, T., Guerrero-Roesch, K., Kuznetsov, A., Schlattner, U. and Saks, V. (2012). Regulation of respiration in muscle cells in vivo by VDAC through interaction with the cytoskeleton and MtCK within Mitochondrial Interactosome. *Biochim Biophys Acta* 1818, 1545-54.

Harley, C.D.G., Hughes, A.R., Hultgren, K.M., Miner, B.G., Sorte, C.J.B., Thornber, C.S., Rodriguez, L.F., Tomanek, L., Williams, S.L. (2006). The impacts of climate change in coastal marine systems. *Ecology Letters* 9, 228-41.

Harms, L., Lucassen, M., Schiffer, M., Mark, F. C., Storch, D., Pörtner, H.-O., Zuzow, M. J. and Tomanek, L. (submitted). Population-specific proteomic responses of gill tissue of the spider crab *Hyas araneus* to simultaneously elevated PCO_2 and temperature. *Journal of Experimental Biology*.

Hartmann, D.L., A.M.G. Klein Tank, M. Rusticucci, L.V. Alexander, S. Brönnimann, Y. Charabi, F.J. Dentener, E.J. Dlugokencky, D.R. Easterling, A. Kaplan, B.J. Soden, P.W. Thorne, M. Wild, Zhai, P.M. (2013) Observations: Atmosphere and Surface. In: Climate Change 2013: The Physical Science Basis. Contribution of Working Group I to the Fifth Assessment Report of the Intergovernmental Panel on Climate Change [Stocker, T.F., D. Qin, G.-K. Plattner, M. Tignor, S.K. Allen, J. Boschung, A. Nauels, Y. Xia, V. Bex and P.M. Midgley (eds.)]. Cambridge University Press, Cambridge, United Kingdom and New York, NY, USA.

Hauri, C., Gruber, N., Plattner, G.-K., Alin, S., Feely, R.A., Hales, B., Wheeler, P.A. (2009). Ocean acidification in the California current system. *Oceanography* 22, 60-71.

Havanapan, P. O., Kanlaya, R., Bourchookarn, A., Krittanai, C. and Thongboonkerd, V. (2009). C-terminal hemocyanin from hemocytes of *Penaeus vannamei* interacts with ERK1/2 and undergoes serine phosphorylation. *J Proteome Res* 8, 2476-83.

Hegedus, D., Erlandson, M., Gillott, C. and Toprak, U. (2009). New insights into peritrophic matrix synthesis, architecture, and function. *Annu Rev Entomol* 54, 285-302.

Helmuth, B., Mieszkowska, N., Moore, P. and Hawkins, S. J. (2006). Living on the edge of two changing worlds: forecasting the responses of rocky intertidal ecosystems to climate change. *Annual Review of Ecology, Evolution and Systematics* 37, 373-404.

Henry, R. P., Lucu, C., Onken, H. and Weihrauch, D. (2012). Multiple functions of the crustacean gill: osmotic/ionic regulation, acid-base balance, ammonia excretion, and bioaccumulation of toxic metals. *Front Physiol* 3, 431.

Hermann, A. and Cox, J.A. (1995). Sarcoplasmic calcium-binding protein. *Comp Biochem Phys B* 111, 337-45.

Heyhoe, K., Cayan, D., Field, C.B., et al. (2004). Emissions pathways, climate change, and impacts on California. *Proceedings of the National Academy of Sciences of the United States of America* 101, 12422-7.

Heyman, R. A., Mangelsdorf, D. J., Dyck, J. A., Stein, R. B., Eichele, G., Evans, R. M. and Thaller, C. (1992). 9-cis retinoic acid is a high affinity ligand for the retinoid X receptor. *Cell* 68, 397-406.

Hiller, A., Kraus, H., Almon, M., Werding, B., (2006). The *Petrolisthes galathinus* complex: Species boundaries basedon color pattern, morphology and molecules, and evolutionary interrelationships between this complex and other Porcellanidae (Crustacea: Decapoda: Anomura). *Molecular Phylogenetics and Evolution* 40, 547-69.

Hochachka, P. W. and Somero, G. N. (2002). Biochemical adaptation: Mechanism and process in physiological evolution. Oxford: Oxford University Press.

Hochachka, P. W. (2003). Intracellular convection, homeostasis and metabolic regulation. *J Exp Biol* 206, 2001-9.

Hoegh-Guldberg, O. and Bruno, J. F. (2010). The impact of climate change on the world's marine ecosystems. *Science* 328, 1523-8.

Hofmann, G.E., Buckley, B.A., Airaksinen, S., Keen, J.E., Somero, G.N. (2000). Heat-shock protein expression is absent in the antarctic fish Trematomus bernacchii (family Nototheniidae). *Journal of Experimental Biology* 203, 2331-9.

Hofmann, G.E. and Todgham, A.E. (2010). Living in the now: physiological mechanisms to tolerate a rapidly changing environment. *Annual Review of Physiology* 72, 127–45.

Hofmann, G. E., Evans, T. G., Kelly, M. W., Padilla-Gamiño, J. L., Blanchette, C., Washburn, L., Chan, F., McManus, M. A., Menge, B. A., Gaylord, B. et al. (2014). Exploring local adaptation and the ocean acidification seascape - studies in the California Current Large Marine Ecosystem. *Biogeosciences* 11, 1053-1064.

Holford, K. C., Edwards, K. A., Bendena, W. G., Tobe, S. S., Wang, Z. and Borst, D. W. (2004). Purification and characterization of a mandibular organ protein from the American lobster, Homarus americanus: a putative farnesoic acid O-methyltransferase. *Insect Biochem Mol Biol* 34, 785-98.

Hooper, S.L., Hobbs, K.H., and Thuma, J.B. (2008). Invertebrate muscles: Thin and thick filament structure; molecular basis of contraction and its regulation, catch and asynchronous muscle. *Prog Neurobiol.* 86, 72-127.

Keller, E. T., Fu, Z. and Brennan, M. (2004). The role of Raf kinase inhibitor protein (RKIP) in health and disease. *Biochem Pharmacol* 68, 1049-53.

Ikeya, T., Persson, P., Kono, M. and Watanabe, T. (2001). The DD5 gene of the decapod crustacean Penaeus japonicus encodes a putative exoskeletal protein with a novel tandem repeat structure. *Comp Biochem Physiol B Biochem Mol Biol* 128, 379-88.

Intanai, I., Taylor, E.W., Whiteley, N.M. (2009). Effects of salinity on rates of protein synthesis and oxygen uptake in the postlarvae and juveniles of the tropical prawn *Macrobrachium rosenbergii* (de Man). *Comp Biochem Physiol A* 152, 372–8.

Jaenicke, R. (1991). Protein stability and molecular adaptation to extreme conditions. *Eur. J. Biochem.* 202, 715-28.

Jaenicke, R. (2000). Stability and stabilization of globular proteins in solution. *J. Biotechnol.* 79, 193-203.

Jaenicke, E. and Decker, H. (2004). Functional changes in the family of type 3 copper proteins during evolution. *Chembiochem* 5, 163-9.

Janke, C. and Bulinski, J. C. (2011). Post-translational regulation of the microtubule cytoskeleton: mechanisms and functions. *Nat Rev Mol Cell Biol* 12, 773-86.

Jitvaropas, R., Amparyup, P., Gross, P. S. and Tassanakajon, A. (2009). Functional characterization of a masquerade-like serine proteinase homologue from the black tiger shrimp Penaeus monodon. *Comp Biochem Physiol B Biochem Mol Biol* 153, 236-43.

Kawabata, T., Yasuhara, Y., Ochiai, M., Matsuura, S. and Ashida, M. (1995). Molecular cloning of insect pro-phenol oxidase: a copper-containing protein homologous to arthropod hemocyanin. *Proc Natl Acad Sci U S A* 92, 7774-8.

Kawamura, S., Abe, Y., Ueda, T. et al., 1998. Investigation of the structural basis for thermostability of DNA-binding protein HU from Bacillus stearothermophilus. *J. Biol. Chem.* 273, 19982-7.

Kerr, K.A. and Duffus, D.A. (2005). Timing of larval release in the porcelain crab, *Petrolisthes cinctipes* (Decapoda: Anomura), in Clayoquot Sound, British Columbia. *Crustaceana* 78, 1041-51.

Key, R.M., Kozyr, A., Sabine, C.L., et al. (2004). A global ocean carbon climatology: Results from Global Data Analysis Project (GLODAP). *Global Biogeochemical Cycles* 18, doi:10.1029/2004GB002247.

Kim, B.K., Kim, K.S., Oh, C-W., Mykles, D.L., Lee, S.G., Kim, H.J., and Kim, H-W. (2009). Twelve actin-encoding cDNAs from the American lobster, Homarus americanus: Cloning and tissue expression of eight skeletal muscle, one heart, and three cytoplasmic isoforms. *Comp Biochem Phys B* 153, 178-84.

Koch, G., Smith, M., Macer, D., Webster, P., Mortara, R. (1986). Endoplasmic reticulum contains a common, abundant calcium-binding glycoprotein, endoplasmin. *Journal of Cell Science* 86, 217-32.

Kothakota, S., Azuma, T., Reinhard, C., Klippel, A., Tang, J., Chu, K., McGarry, T. J., Kirschner, M. W., Koths, K., Kwiatkowski, D. J. et al. (1997). Caspase-3-generated fragment of gelsolin: effector of morphological change in apoptosis. *Science* 278, 294-8.

Kuballa, A. V., Holton, T. A., Paterson, B. and Elizur, A. (2011). Moult cycle specific differential gene expression profiling of the crab *Portunus pelagicus*. *BMC Genomics* 12, 147.

Kurihara, H., Matsui, M., Furukawa, H., Hayashi, M., Ishimatsu, A. (2008). Long-term effects of predicted future seawater CO_2 conditions on the survival and growth of the marine shrimp *Palaemon pacificus*. *J Exp Mar Biol Ecol* 367, 41-6.

Landor, S. K., Mutvei, A. P., Mamaeva, V., Jin, S., Busk, M., Borra, R., Gronroos, T. J., Kronqvist, P., Lendahl, U. and Sahlgren, C. M. (2011). Hypo- and hyperactivated Notch signaling induce a glycolytic switch through distinct mechanisms. *Proc Natl Acad Sci USA* 108, 18814-9.

Langenbuch, M. and Pörtner, H.-O. (2003). Energy budget of hepatocytes from Antarctic fish (*Pachycara brachycephalum* and *Lepidonotothen kempi*) as a function of ambient CO_2: pH-dependent limitations of cellular protein biosynthesis? *Journal of Experimental Biology* 206, 3895-3903.

Lardies, M.A., Rojas, J.M., Werhtmann, I.S. (2010). Breeding biology and population structure of the intertidal crab *Petrolisthes laevigatus* (Anomura: Porcellanidae) in central-southern Chile. *Journal of Natural History* 38, 375-88.

Le Treut, H., Somerville, R., Cubasch, U., Ding, Y., Mauritzen, C., Mokssit, A., Peterson, T., Prather, M. (2007). hapter 1: Historical Overview of Climate Change in Climate Change 2007: The Physical Science Basis. Contribution of Working Group I to the Fourth Assessment Report of the Intergovernmental Panel on Climate Change.

Le Quéré, C., Raupach, M. R., Canadell, J. G., Marland, G. and al., e. (2009). Trends in the sources and sinks of carbon dioxide. Nature Geoscience 2, 831-836.

Le Quéré, C., Takahashi, T., Buitenhuis, E.T., Rödenbeck, C., Sutherland, S.C. (2010). mpact of climate change and variability on the global oceanic sink of CO_2. *Global Biogeochemical Cycles* 24, doi:10.1029/2009GB003599.

Lee, S. H. and Dominguez, R. (2010). Regulation of actin cytoskeleton dynamics in cells. *Mol Cells* 29, 311-25.

Lee, S. Y., Lee, B. L. and Soderhall, K. (2003). Processing of an antibacterial peptide from hemocyanin of the freshwater crayfish *Pacifastacus leniusculus*. *J Biol Chem* 278, 7927-33.

Lee, S. Y., Lee, B. L. and Soderhall, K. (2004). Processing of crayfish hemocyanin subunits into phenoloxidase. *Biochem Biophys Res Commun* 322, 490-6.

Leong, P., Manahan, D.T. (1997). Metabolic importance of Na^+/K^+-ATPase activity during sea urchin development. *J Exp Biol* 200, 2881–92.

Levin, A. A., Sturzenbecker, L. J., Kazmer, S., Bosakowski, T., Huselton, C., Allenby, G., Speck, J., Kratzeisen, C., Rosenberger, M., Lovey, A. et al. (1992). 9-cis retinoic acid stereoisomer binds and activates the nuclear receptor RXR alpha. *Nature* 355, 359-61.

Levitsky, D. I., Pivovarova, A. V., Mikhailova, V. V. and Nikolaeva, O. P. (2008). Thermal unfolding and aggregation of actin. *Febs J* 275, 4280-95.

Levitus, S., Antonov, J.I., Boyer, T.P., Locarnini, R.A.,Garcia, H.E., Mishonov, A.V. (2009). Global ocean heat content 1955–2008 in light of recently revealed instrumentation problems. *Geophysical Research Letters* 36, doi:10.1029/2008GL037155.

Levitus, S., Antonov, J.I., Boyer, T.P., Baranova, O.K., Garcia, H.E., Locarnini, R.A., Mishinov, A.V., Reagan, J.R., Seidov, D., Yarosh, E.S., Zweng, M.M. (2012). World ocean heat content and thermosteric sea level change (0–2000 m), 1955–2010. *Geophysical Research Letters* 39, doi: 10.1029/2012GL051106.

Lima, F.P. and Wethey, D.S. (2012). Three decades of high-resolution coastal sea surface temperatures reveal more than warming. *Nature Communications* 3, 704.

Lorenz, K., Lohse, M. J. and Quitterer, U. (2003). Protein kinase C switches the Raf kinase inhibitor from Raf-1 to GRK-2. *Nature* 426, 574-9.

Lovett, D. L., Verzi, M. P., Clifford, P. D. and Borst, D. W. (2001). Hemolymph levels of methyl farnesoate increase in response to osmotic stress in the green crab, Carcinus maenas. *Comp Biochem Physiol A Mol Integr Physiol* 128, 299-306.

Lovett, D. L., Tanner, C. A., Glomski, K., Ricart, T. M. and Borst, D. W. (2006). The effect of seawater composition and osmolality on hemolymph levels of methyl farnesoate in the green crab Carcinus maenas. *Comp Biochem Physiol A Mol Integr Physiol* 143, 67-77.

Mace, A.J., Morgan, S.G., (2006) Biological and physical coupling in the lee of a small headland: Contrasting transport mechanisms for crab larvae in an upwelling region. *Marine Ecology Progress Series* 324, 185-96.

Macias, M.T. and Sastre, L. (1990). Molecular cloning and expression of four actin isoforms during *Artemia* development. *Nucleic Acids Res* 18, 5219-25.

MacMillan, D. (2013). FK506 binding proteins: cellular regulators of intracellular Ca^{2+} signaling. *Eur J Pharmacol* 700, 181-93.

Magnum, C.P. and Burnett, L.E. (1986). The CO_2 sensitivity of the hemocyanins and its relationship to Cl^- sensitivity. *Biological Bulletin* 171, 248-63.

Mailloux, R. J., McBride, S. L. and Harper, M. E. (2013). Unearthing the secrets of mitochondrial ROS and glutathione in bioenergetics. *Trends Biochem Sci* 38, 592-602.

Marchant, H.K., Calosi, P., Spicer, J.I. (2010). Short-term exposure to hypercapnia does not compromise feeding, acid–base balance or respiration of *Patella vulgata* but surprisingly is accompanied by radula damage. *Journal of the Marine Biological Association of the United Kingdom* 90, 1379-84.

Marks, F., Klingmüller, U. and Müller-Decker, K. (2009). Cellular signal processing: An introduction to the molecular mechanisms of signal tr ansduction. New York: Garland Science, Taylor and Francis Group

Marzec, M., Eletto, D., Argon, Y. (2012). GRP94: An HSP90-like protein specialized for protein folding and quality control in the endoplasmic reticulum. *Biochimica et Biophysica Acta-Molecular Cell Research* 1823, 774-87.

Matsuda, Y., Koshiba, T., Osaki, T., Suyama, H., Arisaka, F., Toh, Y. and Kawabata, S. (2007). An arthropod cuticular chitin-binding protein endows injured sites with transglutaminase-dependent mesh. *J Biol Chem* 282, 37316-24.

McDonagh, B. and Sheehan, D. (2006). Redox proteomics in the blue mussel *Mytilus edulis*: carbonylation is not a pre-requisite for ubiquitination in acute free radical-mediated oxidative stress. *Aquat Toxicol* 79, 325-33.

McDonagh, B. and Sheehan, D. (2007). Effect of oxidative stress on protein thiols in the blue mussel Mytilus edulis: proteomic identification of target proteins. *Proteomics* 7, 3395-403.

McDonald, M.R., McClintock, J.B., Amsler, C.D., Rittschof, D., Angus, R.A., Orihuela, B., Lutostanski, K. (2009). Effects of ocean acidification over the life history of the barnacle *Amphibalanus amphitrite*. *Mar Ecol Prog Ser* 385,179-87.

McLaughlin, P.A., Lemaitre, R., Tudge, C.C. (2004). Carcinization in the Anomura – fact or fiction? II. Evidence from larval, megalopal and early juvenile morphology. *Contributions to Zoology* 73, 165-205.

Medler, S., Lilley, T. and Mykles, D. L. (2004). Fiber polymorphism in skeletal muscles of the American lobster, *Homarus americanu*s: continuum between slow-twitch (S1) and slow-tonic (S2) fibers. *J Exp Biol* 207, 2755-67.

Meehl, G. A., J. M. Arblaster, Tebaldi, C. (2007). Contributions of natural and anthropogenic forcing to changes in temperature extremes over the U.S. *Geophys. Res. Lett.* 34, L19709 doi:10.1029/2007GL030948.

Michaelidis, B., Ouzounis, C., Paleras, A., Pörtner, H.-O. (2005). Effects of long-term moderate hypercapnia on acid – base balance and growth rate in marine mussels *Mytilus galloprovincialis*. *Marine Ecology Progress Series* 293, 109–18

Mikaloff Fletcher, S.E., Gruber, N., Jacobson, A.R., et al. (2006). Inverse estimates of anthropogenic CO2 uptake, transport, and storage by the ocean. *Global Biogeochemical Cycles* 20, doi: 10.1029/2005GB002530.

Miller, N.L., Heyhoe, K., Jin, J., Auffhammer, M. (2008). Climate, extreme heat, and electricity demand in California. *Journal of Applied Meteorology and Climatology* 47, 1834-44.

Molenock, J. (1975). Evolutionary aspects of communication in the courtship behavior of four species of Anomuran crabs (*Petrolisthes*). *Behavior* 53, 1-30.

Morimoto, R.I. (1998). Regulation of the heat shock transcriptional response: cross talk between a family of heat shock factors, molecular chaperones, and negative regulators. *Genes and Development* 12, 3788-96.

Muller, S., Dennemarker, J. and Reinheckel, T. (2012). Specific functions of lysosomal proteases in endocytic and autophagic pathways. *Biochim Biophys Acta* 1824, 34-43.

Munday, M.L., Dixson, D.L., Donelson, J.M., Jones, G.P., Pratchett, M.S., Devitsina, G.V., Døving, K.B. (2009). Ocean acidification impairs olfactory discrimination and homing ability of a marine fish. *Proceedings of the National Academy of Sciences* 106, 1848-52.

Murakami, K., Stewart, M., Nozawa, K., Tomii, K., Tomii, N., Igarashi, N., Shirakihara, Y., Wakatsuki, S., Yasunaga, T., Wakabayashi, T. (2008). Structural basis for tropomyosin overlap in thin (actin) filaments and the generation of a molecular swivel by troponin-T. *Proc Natl Acad Sci USA* 105, 7200-5.

Murphy, M. P. (2012). Mitochondrial thiols in antioxidant protection and redox signaling: distinct roles for glutathionylation and other thiol modifications. *Antioxid Redox Signal* 16, 476-95.

Myers, C.D., Goh, P.Y., Allen, T.S., Bucher, E.A., Bogeart, T. (1996). Developmental genetic analysis of Troponin T mutations in striated and nonstriated muscle cells of *Caenorhabditis elegans*. *J Cell Biol* 132, 1061-77.

Mykles, D. L. (1997). Crustacean muscle plasticity: molecular mechanisms determining mass and contractile properties. *Comp Biochem Phys B* 117, 367-78.

Mykles, D. L. and Haire, M. F. (1991). Sodium dodecyl sulfate and heat induce two distinct forms of lobster muscle multicatalytic proteinase: the heat-activated form degrades myofibrillar proteins. *Arch Biochem Biophys* 288, 543-51.

Nagaraju, G. P. (2007). Is methyl farnesoate a crustacean hormone? *Aquaculture* 272, 39-54.

Nagaraju, G. P. and Borst, D. W. (2008). Methyl farnesoate couples environmental changes to testicular development in the crab *Carcinus maenas*. *J Exp Biol* 211, 2773-8.

Nagaraju, G. P. (2011). Reproductive regulators in decapod crustaceans: an overview. *J Exp Biol* 214, 3-16.

Neufield, D.S. and Cameron, J.N. (1992). Postmoult uptake of calcium by the blue crab (*Callinectes sapidus*) in water of low salinity. *J Exp Biol* 171, 283-99.

Orr, J.C., Fabry, V.J., Aumont Olivier, et al. (2005). Anthropogenic ocean acidification over the twenty-first century and its impact on calcifying organisms. *Nature* 437, 681-6.

Ortega, M.A., Macias, M.T., Martinez, J.L., Palmero, I., and Sastre, L. (1992). Expression of actin isoforms in *Artemia*. *Sym Soc Exp Biol* 46, 131-7.

Otero, J.H., Lizák, B., Hendershot, L.M. (2010). Life and death of a BiP substrate. *Seminars in Cell and Developmental Biology* 21, 472-8.

Padilla-Gamiño, J. L., Kelly, M. W., Evans, T. G. and Hofmann, G. E. (2013). Temperature and CO2 additively regulate physiology, morphology and genomics responses of larval sea urchins, *Strongylocentrotus purpuratus*. *Proceedings of the Royal Society B* 280.

Paganini, A.W., Miller, N.A., Stillman, J.H. (2014). Temperature and acidification variability reduce physiological performance in the intertidal zone porcelain crab *Petrolisthes cinctipes*. *Journal of Experimental Biology* 217, 3974-80.

Pannevis, M.C. and Houlihan, D.F. (1992). The energetic cost of protein synthesis in isolated hepatocytes of rainbow trout (*Oncorhynchus mykiss*). *J Comp Physiol B* 162, 393–400.

Parsell, D.A. and Lindquist, S. (1993). The function of heat-shock proteins in stress tolerance: degradation and reactivation of damaged proteins. *Annual Review of Genetics* 27, 437-96.

Petricorena, Z.L.C. and Somero, G.N. (2007). Biochemical adaptations of notothenioid fishes: Comparisons between cold temperate South American and New Zealand species and Antarctic species. *Comparative Biochemistry and Physiology Part A: Molecular & Integrative Physiology* 147, 799-807.

Plummer, L. N., and Busenberg, E. (1982). The solubilities of calcite, aragonite and vaterite in CO_2-H_2O solutions between 0 and 90°C, and an evaluation of the aqueous model for the system $CaCO_3$-CO_2-H_2O. *Geochimica et Cosmochimica Acta* 46, 1011-40.

Podrabsky, J. E. and Somero, G. N. (2004). Changes in gene expression associated with acclimation to constant temperatures and fluctuating daily temperatures in an annual killifish *Austrofundulus limnaeus*. *J Exp Biol* 207, 2237-54.

Pörtner, H.-O. (2002). Climate variations and the physiological basis of temperature dependent biogeography: systemic to molecular hierarchy of thermal tolerance in animals. *Comparative Biochemistry and Physiology Part A: Molecular and Integrative Physiology* 132, 739–61

Pörtner, H.-O., Langenbuch, M., and Michaelidis, B. (2005). Synergistic effects of temperature extremes, hypoxia, and increases in CO_2 on marine animals: From Earth history to global change. *Journal of Geophysical Research* 110, doi:10.1029/2004JC002561.

Pörtner, H.-O. (2006). Physiological limits to biogeography and biodiversity? A climate change perspective. Peter Hochachka Memorial Lecture, University of British Columbia, Vancouver.

Pörtner, H.-O., Bennett, A.F., Bozinovic, F., et al. (2010). Trade-offs in thermal adaptation: The need for a molecular to ecological integration. *Physiological and Biochemical Zoology* 79, 295-313.

Rebers, J. E. and Willis, J. H. (2001). A conserved domain in arthropod cuticular proteins binds chitin. *Insect Biochem Mol Biol* 31, 1083-1093.

Rebers, J. E. and Riddiford, L. M. (1988). Structure and expression of a *Manduca sexta* larval cuticle gene homologous to Drosophila cuticle genes. *J Mol Biol* 203, 411-23.

Reddy, S., Jones, A. D., Cross, C. E., Wong, P. S. and Van Der Vliet, A. (2000). Inactivation of creatine kinase by S-glutathionylation of the active-site cysteine residue. *Biochem J* 347, 821-7.

Rhein, M., S.R. Rintoul, S. Aoki, E. Campos, D. Chambers, R.A. Feely, S. Gulev, G.C. Johnson, S.A. Josey, A. Kostianoy, C. Mauritzen, D. Roemmich, Talley, L.D. Wang, F. (2013) Observations: Ocean. In: Climate Change 2013: The Physical Science Basis. Contribution of Working Group I to the Fifth Assessment Report of the Intergovernmental Panel on Climate Change [Stocker, T.F., D. Qin, G.-K. Plattner, M. Tignor, S.K. Allen, J. Boschung, A. Nauels, Y. Xia, V. Bex and P.M. Midgley (eds.)]. Cambridge University Press, Cambridge, United Kingdom and New York, NY, USA.

Ries, J., Cohen, A., McCorkle, D. (2009). Marine calcifiers exhibit mixed responses to CO_2-induced ocean acidification. *Geology* 37, 1131–4

Rivadeneira, M.M., Hernéaz, P., Baeza, J.A., Boltaña, S., Cifuentes, M., et al. (2010). Testing the abundant-centre hypothesis using intertidal porcelain crabs along the Chilean coast: linking abundance and life-history variation. *Journal of Biogeography* 37, 486-98.

Rock, J., Magnay, J. L., Beech, S., El Haj, A. J., Goldspink, G., Lunt, D. H. and Whiteley, N. M. (2009). Linking functional molecular variation with environmental gradients: myosin gene diversity in a crustacean broadly distributed across variable thermal environments. *Gene* 437, 60-70.

Royal Society. The Royal Society. London (2005). Ocean acidification due to increasing atmospheric carbon dioxide. Policy Document 12/05, 60.

Ruddell, C. J., Wainwright, G., Geffen, A., White, M. R., Webster, S. G. and Rees, H. H. (2003). Cloning, characterization, and developmental expression of a putative farnesoic acid O-methyl transferase in the female edible crab *Cancer pagurus*. *Biol Bull* 205, 308-18.

Rypien, K.L. and Palmer, A.R. (2007). The effect of sex, size, and habitat on the incidence of puncture wounds in the claws of the porcelain crab *Petrolisthes cinctipes* (Anomura: Porcellanidae). *Journal of Crustacean Biology* 27, 59-64.

Sabine, C.L., Feely, R.A., Gruber, N., et al. (2004). The ocean sink for anthropogenic CO_2. *Science* 16, 367-71.

Sabine, C. L. and Feely, R. A. (2007). 3. The oceanic sink for carbon dioxide. *Greenhouse Gas Sinks* 31.

Serafini, L., Hann, J. B., Kültz, D. and Tomanek, L. (2011). The proteomic response of sea squirts (genus *Ciona*) to acute heat stress: A global perspective on the thermal stability of proteins. *Comp Biochem Phys D* 6, 322-334.

Shibata, T., Ariki, S., Shinzawa, N., Miyaji, R., Suyama, H., Sako, M., Inomata, N., Koshiba, T., Kanuka, H. and Kawabata, S. (2010). Protein crosslinking by transglutaminase controls cuticle morphogenesis in Drosophila. *PLoS One* 5, e13477.

Simpson, S.D., Munday, P.L., Wittenrich, M.L. (2011). Ocean acidification erodes crucial auditory behaviour in a marine fish. *Biology Letters* 7, 917-20.

Singer S.J., and Nicolson, G.L. (1972). The fluid mosaic model of the structure of cell membranes. *Science* 175, 720-31.

Soderhall, K. and Cerenius, L. (1998). Role of the prophenoloxidase-activating system in invertebrate immunity. *Curr Opin Immunol* 10, 23-8.

Santos, L.C.F., Belli, N.M., Augusto, A., Masui, D.C., Leone, F.A., McNamara, J.C., Furriel, R.P.M. (2007). Gill (Na+, K+)-ATPase in diadromous, freshwater palaemonid shrimps: species-specific kinetic characteristics and alpha-subunit expression. *Comp Biochem Physiol A* 148, 178–88

Somero, G.N. and DeVries, A.L. (1967). Temperature tolerance of some antarctic fishes. *Science* 156, 257-8.

Somero, G.N. (1969). Enzymic mechanisms of temperature compensation: Immediate and evolutionary effects of temperature on enzymes of aquatic poikilotherms. *The American Naturalist* 103, 517-530.

Somero, G.N. (1978). Temperature adaptation of enzymes: Biological optimization through structure-function compromises. *Annual Review of Ecology and Systematics* 9, 1-29.

Somero, G.N. (2012). The physiology of climate change: how potentials for acclimatization and genetic adaptation will determine ‘winners’ and ‘losers’. *Journal of Experimental Biology* 213, 912-20.

Somero, G. N. (2012). The physiology of global change: linking patterns to mechanisms. *Annu Rev Mar Sci* 4, 39-61.

Spector A.A., and Yorek, M.A. (1985). Membrane lipid composition and cellular function. *Journal of Lipid Research* 26, 1015-35.

Squire, J.M. (2009). Muscle myosin filaments: cores, crowns, and couplings. *Biophys Rev* 1, 149-60.

Stillman, J. and Somero, G. (1996). Adaptation to temperature stress and aerial exposure in congeneric species of intertidal porcelain crabs (genus *Petrolisthes*): correlation of physiology, biochemistry and morphology with vertical distribution. *J Exp Biol* 199, 1845-55.

Stillman, J.H., 2000. Evolutionary history and adaptive significance of respiratory structures on the legs of intertidal porcelain crabs, genus *Petrolisthes*. *Physiological and Biochemical Zoology* 73, 86-96.

Stillman, J. H. and Somero, G. N. (2000). A comparative analysis of the upper thermal tolerance limits of eastern Pacific porcelain crabs, genus *Petrolisthes*: influences of latitude, vertical zonation, acclimation, and phylogeny. *Physiol Biochem Zool* 73, 200-208.

Stillman, J.H. and Reeb, C.A. (2001). Molecular phylogeny of Eastern Pacific porcelain crabs, genera *Petrolisthes* and *Pachycheles*, based on the mtDNA 16S rDNA sequence: Phylogeographic and systematic implications. *Molecular Phylogenetics and Evolution* 19, 236-45.

Stillman, J.H. (2002). Causes and consequences of thermal tolerance limits in rocky intertidal porcelain crabs, genus *Petrolisthes*. *Integrative and Comparative Biology* 42, 790-6.

Stillman, J. H. (2003). Acclimation capacity underlies susceptibility to climate change. *Science* 301, 65.

Suarez-Huerta, N., Lecocq, R., Mosselmans, R., Galand, P., Dumont, J. E. and Robaye, B. (2000). Myosin heavy chain degradation during apoptosis in endothelial cells. *Cell Prolif* 33, 101-14.

Sutton, R.T., Dong, B., Gregory, J.M. (2007). Land/sea warming ratio in response to climate change: IPCC AR4 model results and comparison with observations. *Geophysical Research Letters* 34, doi:10.1029/2006GL028164.

Tagmount, A., Wang, M., Lindquist, E., Tanaka, Y., Teranishi, K. S., Sunagawa, S., Wong, M. and Stillman, J. H. (2010). The porcelain crab transcriptome and PCAD, the porcelain crab microarray and sequence database. *PLoS One* 5, e9327.

Tai, H. H. (2011). Prostaglandin catabolic enzymes as tumor suppressors. *Cancer Metastasis Rev* 30, 409-17.

Takahashi, T., Sutherland, S.C., Wanninkhof, R., et al. (2009). Climatological mean and decadal change in surface ocean pCO_2, and net sea–air CO_2 flux over the global oceans. *Deep Sea Research Part II: Topical Studies in Oceanography* 56, 554-77.

Tattersall, G.J., Sinclair, B.J., Withers, P.C., et al. (2012). Coping with thermal challenges: physiological adaptations to environmental temperatures. *Comprehensive Physiology* 2, 2151-202.

Teranishi, K. S. and Stillman, J. H. (2007). A cDNA microarray analysis of the response to heat stress in hepatopancreas tissue of the porcelain crab *Petrolisthes cinctipes*. *Comparative Biochemistry and Physiology, Part D* 2, 53-62.

Terwilliger, N. B. (1999). Hemolymph proteins and molting in crustaceans and insects. *American Zoologist* 39, 589-599.

Terwilliger, N. B. and Ryan, M. C. (2006). Functional and phylogenetic analyses of phenoloxidases from brachyuran (*Cancer magister*) and branchiopod (*Artemia franciscana*, *Triops longicaudatus*) crustaceans. *Biological Bulletin* 210, 38-50.

Todgham, A. E. and Hofmann, G. E. (2009). Transcriptomic response of sea urchin larvae Strongylocentrotus purpuratus to CO2-driven seawater acidification. *Journal of Experimental Biology* 212, 2579-94.

Tohtong, R., Yamashita, H., Graham, M., Haeberle, J., Simcox, A., and Maughan, D. (1995). Impairment of muscle function caused by mutations and phosphorylation sites in myosin regulatory light chain. *Nature* 374, 650-3.

Tomanek, L. and Somero, G. N. (1999). Evolutionary and acclimation-induced variation in the heat-shock responses of congeneric marine snails (genus *Tegula*) from different thermal habitats: Implications for limits of thermotolerance and biogeography. *J Exp Biol* 202, 2925-2936.

Tomanek, L. and Somero, G. N. (2000). Time course and magnitude of synthesis of heat-shock proteins in congeneric marine snails (genus *Tegula*) from different tidal heights. *Physiol Biochem Zool* 73, 249-256.

Tomanek, L. (2002). The heat-shock response: Its variation, regulation and ecological importance in intertidal gastropods (genus *Tegula*). *Integrative and Comparative Biology* 42, 797-807.

Tomanek, L. and Helmuth, B. (2002). Physiological ecology of rocky intertidal organisms: A synergy of concepts. *Integrative and Comparative Biology* 42, 771-5.

Tomanek, L. and Sanford, E. (2003). Heat-shock protein 70 (Hsp70) as a biochemical stress indicator: An experimental field test in two congeneric intertidal gastropods (genus: *Tegula*). *Biol. Bull.* 205, 276–84.

Tomanek, L. (2008). The importance of physiological limits in determining biogeographical range shifts due to global climate change: The heat-shock response *Physiological and Biochemical Zoology* 81, 709-717.

Tomanek, L. (2010). Variation in the heat shock response and its implication for predicting the effect of global climate change on species' bioegographic distribution ranges and metabolic costs. *J Exp Biol* 213, 971-979.

Tomanek, L. and Zuzow, M. J. (2010). The proteomic response of the mussel congeners *Mytilus galloprovincialis* and *M. trossulus* to acute heat stress: implications for thermal tolerance and metabolic costs of thermal stress. *Journal of Experimental Biology* 213, 3559-3574.

Tomanek, L. (2011). Environmental proteomics: Changes in the proteome of marine organisms in response to environmental stress, pollutants, infection, symbiosis and development. *Annu Rev Mar Sci* 3, 373-399.

Tomanek, L., Zuzow, M. J., Ivanina, A. V., Beniash, E. and Sokolova, I. M. (2011). Proteomic response to elevated P_{CO2} level in eastern oyster, *Crassostrea virginica*: evidence for oxidative stress. *Journal of Experimental Biology* 214, 1836-1844.

Tomanek, L., Zuzow, M. J., Hitt, L. R., Serafini, L. and Valenzuela, J. J. (2012). Proteomics of hyposaline stress in blue mussel congeners (genus *Mytilus*): implications for biogeographic range limits in response to climate change. *Journal of Experimental Biology* 215, 3905-3916.

Tomanek, L. (2014). Proteomics to study adaptations in marine organisms to environmental stress. *J Proteomics* 105, 92-106.

Tomanek, L. (2015). Proteomic responses to environmentally induced oxidative stress. *Journal of Experimental Biology*.

Toonen, R.J. (2004). Genetic evidence of multiple paternity of broods in the intertidal crab *Petrolisthes cinctipes*. *Marine Ecology Progress Series* 270, 259-63.

Ubuka, T., Masuoka, N., Yoshida, S. and Ishino, K. (1987). Determination of isoelectric point value of 3-mercaptopyruvate sulfurtransferase by isoelectric focusing using ribonuclease A-glutathione mixed disulfides as standards. *Anal Biochem* 167, 284-9.

Uda, K., Fujimoto, N., Akiyama, Y., Mizuta, K., Tanaka, K., Ellington, W. R. and Suzuki, T. (2006). Evolution of the arginine kinase gene family. *Comp Biochem Phys D* 1, 209-18.

VanBuren, P., Waller, G.S., Harris, D.E., Trybus, K.M., Warshaw, D.M., and Lowey, S. (1994). The essential light chain is required for full force production by skeletal muscle myosin. *Proc Natl Acad Sci USA* 91, 12403-7.

van der Flier, A. and Sonnenberg, A. (2001). Structural and functional aspects of filamins. *Biochim Biophys Acta* 1538, 99-117.

Varadaraj, K., Kumari, S.S., and Skinner, D.M. (1996). Actin-encoding cDNAs and gene expression during the intermolt cycle of the Bermuda land crab *Gecarcinus lateralis*. *Gene* 171, 177-84.

Vembar, S.S. and Brodsky, J.L. (2008). One step at a time: endoplasmic reticulum-associated degradation. *Nature Reviews Molecular Cell Biology* 9, 944-57.

Wallimann, T., Tokarska-Schlattner, M., Neumann, D., Epand, R. M., Epand, R. F., Andres, R. H., Widmer, H. R., Hornemann, T., Saks, V., Agarkova, I. et al. (2007). The phosphocreatine circuit: molecular and cellular physiolgy of creatine kinases, sensitivity to free radicals, and enhancement by creatine supplementation. In *Molecular System Bioenergetics: Energy for Life*, (ed. V. Saks), pp. 195-264. Weinheim: WILEY-VCH Verlag GmbH & Co. KGaA.

Wang, R., Lee, S. Y., Cerenius, L. and Soderhall, K. (2001). Properties of the prophenoloxidase activating enzyme of the freshwater crayfish, *Pacifastacus leniusculus*. *Eur J Biochem* 268, 895-902.

Wang, W. and Metzger, J.M. (2008). Parvalbumin isoforms for enhancing cardiac diastolic function. *Cell Biochem Biophys* 51, 1-8.

Wang, W.N., Wang, A.L., Bao, L., Wang, J.P., Liu, Y., Sun, R.Y. (2004). Changes of protein-bound and free amino acids in the muscle of the freshwater prawn *Macrobrachium nipponense* in different salinities. *Aquaculture* 233, 561–71.

Wang, Y. H. and LeBlanc, G. A. (2009). Interactions of methyl farnesoate and related compounds with a crustacean retinoid X receptor. *Mol Cell Endocrinol* 309, 109-16.

Weber, R. E., Behrens, J. W., Malte, H. and Fago, A. (2008). Thermodynamics of oxygenation-linked proton and lactate binding govern the temperature sensitivity of O2 binding in crustacean (Carcinus maenas) hemocyanin. *J Exp Biol* 211, 1057-62.

Wegner, A. (1982). Kinetic analysis of actin assembly suggests that tropomyosin inhibits spontaneous fragmentation of actin filaments. *J Mol Biol* 161, 217-27.

Weihrauch, D., Ziegler, A., Siebers, D. and Towle, D. W. (2002). Active ammonia excretion across the gills of the green shore crab Carcinus maenas: participation of Na(+)/K(+)-ATPase, V-type H(+)-ATPase and functional microtubules. *Journal of Experimental Biology* 205, 2765-75.

Weihrauch, D., Morris, S. and Towle, D. W. (2004). Ammonia excretion in aquatic and terrestrial crabs. *J Exp Biol* 207, 4491-504.

Wheatly, M.G., Henry, R.P. (1992). Extracellular and intracellular acid–base regulation in crustaceans. *J Exp Zool* 263, 127–42

White, A.J., Northcutt, M.J., Rohrback, S.E., Carpenter, R.O., Niehaus-Sauter, M.M., Gao, Y., Wheatly, M.G., and Gillen, C.M. (2011). Characterization of sarcoplasmic calcium binding protein (SCP) variants from freshwater crayfish *Procambarus clarkii*. *Comp Biochem Phys B* 160, 8-14.

Whiteley NM (1999) Acid–base regulation in aquatic crustaceans: role of bicarbonate ions. In: Egginton S, Taylor EW, Raven JA (eds) Regulation of acid–base status in animals and plants. SEB Seminar Series 68, Cambridge University Press, Cambridge, 233-55.

Whiteley, N. M. (2011). Physiological and ecological responses of crustaceans to ocean acification. *Marine Ecology Progress Series* 430, 257-271.

Wickins, J.F. (1984). The effect of hypercapnic seawater on growth and mineralization in penaeid prawns. *Aquaculture* 41, 37-48.

Widdicombe, S. and Needham, H.R. (2007). Impact of CO_2-induced seawater acidification on the burrowing activity of *Nereis virens* and sediment nutrient flux. *Marine Ecology Progress Series* 341, 111-22.

Widdicombe, S., Spicer, J.I. (2008). Predicting the impact of ocean acidification on benthic biodiversity: What can animal physiology tell us? *J Exp Mar Biol Ecol* 366, 187–97.

Widdows, J. (1976). Physiological adaptation of *Mytilus edulis* to cyclic temperatures. *J Comp Physiol* 105, 115-128.

Willett, C.S. (2010). Potential fitness trade-offs for thermal tolerance in the intertidal copepod *Tigriopus californicus*. *Evolution* 64, 2521-34.

Withers, P.C. (1992). Comparative animal physiology. 949. Fort Worth, TX: Saunders College.

Wittmann, A. C. and Pörtner, H.-O. (2013). Sensitivities of extant animal taxa to ocean acidification. *Nature Climate Change*.

Wolosker, H., Panizzutti, R. and Engelender, S. (1996). Inhibition of creatine kinase by S-nitrosoglutathione. *FEBS Lett* 392, 274-6.

Wong, E. and Cuervo, A. M. (2012). Integration of clearance mechanisms: the proteasome and autophagy. In *Protein Homeostasis*, eds. R. I. Morimoto D. J. Selkoe and J. W. Kelley), pp. 47-65. New York: Cold Spring Harbor Press.

Wong, K. K., Lane, A. C., Leung, P. T. and Thiyagarajan, V. (2011). Response of larval barnacle proteome to CO(2)-driven seawater acidification. *Comp Biochem Physiol Part D Genomics Proteomics* 6, 310-21.

Wood, C.M., Cameron, J.N. (1985). Temperature and the physiology of intracellular and extracellular acid–base regulation in the blue crab *Callinectes sapidus*. *J Exp Biol* 114, 151–79.

Wootton, J.T., Pfister, C.A., Forester, J.D. (2008). Dynamic patterns and ecological impacts of declining ocean pH in a high-resolution multi-year dataset. *Proceedings of the National Academy of Sciences of the United States of America* 105, 18848–53

Yeung, K., Seitz, T., Li, S., Janosch, P., McFerran, B., Kaiser, C., Fee, F., Katsanakis, K. D., Rose, D. W., Mischak, H. et al. (1999). Suppression of Raf-1 kinase activity and MAP kinase signalling by RKIP. *Nature* 401, 173-7.

Yeung, K., Janosch, P., McFerran, B., Rose, D. W., Mischak, H., Sedivy, J. M. and Kolch, W. (2000). Mechanism of suppression of the Raf/MEK/extracellular signal-regulated kinase pathway by the raf kinase inhibitor protein. *Mol Cell Biol* 20, 3079-85.

Yeung, K. C., Rose, D. W., Dhillon, A. S., Yaros, D., Gustafsson, M., Chatterjee, D., McFerran, B., Wyche, J., Kolch, W. and Sedivy, J. M. (2001). Raf kinase inhibitor protein interacts with NF-kappaB-inducing kinase and TAK1 and inhibits NF-kappaB activation. *Mol Cell Biol* 21, 7207-17.

Yoon, J., Bang, S. H., Park, J. S., Chang, S. T., Kim, Y. H. and Min, J. (2011). Increased in vitro lysosomal function in oxidative stress-induced cell lines. *Appl Biochem Biotechnol* 163, 1002-11.

Zaccai, G. (2000). How soft is a protein? A protein dynamics force constant measured by neutron scattering. *Science* 288, 1604-7.

Zhang, H., Apfelroth, S. D., Hu, W., Davis, E. C., Sanguineti, C., Bonadio, J., Mecham, R. P. and Ramirez, F. (1994). Structure and expression of fibrillin-2, a novel microfibrillar component preferentially located in elastic matrices. *J Cell Biol* 124, 855-63.

Zhou, W., Capello, M., Fredolini, C., Piemonti, L., Liotta, L. A., Novelli, F. and Petricoin, E. F. (2010). Mass spectrometry analysis of the post-translational modifications of alpha-enolase from pancreatic ductal adenocarcinoma cells. *J Proteome Res* 9, 2929-36.

Table 2. Proteins identified in the acclimation manuscript. Table includes estimated and predicted molecular mass (kDa), isoelectric point (pI), gene band identifier, MASCOT score, number of peptides matched, sequence coverage, and putative functional category.

3	Paramyosin (long form)		✓		69	6.40	103.02	5.46	isotig00035	77	3	1%	Thick filament
4	Arginine kinase		✓		35	5.93	39.96	6.05	gi|170186144	170	5	20%	Phosphotransfer
5	Arginine kinase	✓	✓		31	6.47	39.96	6.05	gi|170187671	391	8	42%	Phosphotransfer
6	Cardiac-like muscle actin		✓		31	6.03	41.65	5.23	gi|170182268	167	3	14%	Thin filament
7	Arginine kinase		✓	✓	28	6.58	39.96	6.05	gi|170186144	294	7	29%	Phosphotransfer
8	Glyceraldehyde-3-phosphate dehydrogenase		✓		28	6.24	18.66	5.58	gi|170197231	86	3	21%	Energy metabolism
9	Phosphatidylethanolamine-binding protein		✓		28	6.00	20.36	6.07	gi|170189936	127	3	11%	Signaling
10	Hemocyanin		✓	✓	27	6.94	76.32	5.83	gi|170187274	201	5	17%	Respiratory
11	Peroxiredoxin 5 isoform B	✓	✓		25	6.78	19.88	8.88	gi|170265337	205	3	28%	Signaling
12	Hemocyanin	✓	✓		25	6.76	76.32	5.83	gi|170187274	275	6	26%	Respiratory
13	α/β-Actin		✓		23	5.78	41.91	5.16	gi|170182624	321	5	24%	Thin filament
17	Gelsolin		✓		18	5.67	81.77	4.79	gi|170227754	273	3	20%	Actin-binding
18	Gelsolin	✓			18	5.38	81.77	4.79	gi|170227754	358	4	25%	Actin-binding
21	FK506-binding protein	✓	✓	✓	12	6.76	11.69	7.87	gi|170246946	102	1	23%	Signaling
22	Profilin	✓		✓	9	6.76	13.89	6.27	gi|170182510	279	4	34%	Actin-binding
23	Arginine kinase	✓			46	6.66	39.96	6.05	gi|170186144	385	9	35%	Phosphotransfer
25	Paramyosin		✓		16	5.94	103.02	5.46	isotig00035	38	2	0%	Thick filament
26	Myosin heavy chain type B		✓		14	6.09	218.87	6.00	gi|170270277	158	3	13%	Thick filament
27	Myosin heavy chain type B			✓	13	6.08	218.87	6.00	gi|170270277	100	2	5%	Thick filament
29	Cardiac-like muscle actin	✓			12	6.27	41.65	5.23	gi|170182268	172	2	11%	Thin filament
30	Prostaglandin reductase		✓		19	5.84	36.49	8.31	gi|170218863	68	2	7%	Signaling
32	Phosphohistidine phosphatase 1	✓	✓		11	6.39	13.82	5.34	gi|170217426	155	2	13%	Signaling
33	Cofilin	✓	✓	✓	19	6.45	19.34	8.50	isotig01165	201	5	11%	Actin-binding
34	α/β-Actin	✓	✓		17	6.27	41.91	5.16	gi|170182624	184	4	20%	Thin filament
35	α/β-Actin	✓	✓		17	6.29	41.91	5.16	gi|170182624	193	3	16%	Thin filament
36	Glyceraldehyde-3-phosphate dehydrogenase		✓		15	6.44	18.66	5.58	gi|170197231	336	5	29%	Energy metabolism
37	Hemocyanin	✓			24	6.30	75.27	5.52	gi|170187274	109	2	9%	Respiratory
38	Myosin heavy chain type B		✓		16	6.10	218.87	6.00	gi|170270277	99	2	5%	Thick filament
39	α/β-Actin	✓	✓	✓	14	6.26	41.91	5.16	gi|170182624	270	3	16%	Thin filament
40	Cardiac-like muscle actin		✓		21	6.22	41.65	5.23	gi|170182268	96	2	8%	Thin filament
42	Cardiac-like muscle actin	✓	✓	✓	13	6.31	41.65	5.23	gi|170182268	191	2	11%	Thin filament
46	Filamin-A	✓	✓	✓	68	6.87	267.69	5.81	isotig02107	54	2	3%	Actin-binding
49	Filamin-C			✓	63	6.68	262.65	5.90	gi|170202097	98	2	8%	Actin-binding
50	Enolase	✓		✓	55	6.68	39.85	5.45	gi|170254092	181	3	16%	Energy metabolism
51	Enolase	✓		✓	54	6.79	47.24	6.18	gi|170237664	202	3	14%	Energy metabolism
52	α/β-Actin		✓		36	5.76	41.91	5.16	gi|170182624	390	6	27%	Thin filament

Table 2 continued.

53	Myosin regulatory light chain		✓		24	4.19	22.58	4.70	gi|170184074	281	5	11%	Thick filament
57	Hemocyanin		✓	✓	79	6.01	75.27	5.52	gi|170278434	153	3	15%	Respiratory
58	Hemocyanin	✓	✓	✓	78	6.06	77.54	5.37	gi|170185161	122	3	14%	Respiratory
59	Hemocyanin	✓	✓	✓	79	6.10	75.27	5.52	gi|170278434	128	2	10%	Respiratory
62	Pseudohemocyanin-1			✓	56	5.27	79.57	5.69	gi|170189674	60	2	9%	Respiratory
67	Proteasome β-subunit type-6-like		✓		24	6.71	25.10	5.41	gi|170204742	46	2	6%	Signaling
70	Glyceraldehyde-3-phosphate dehydrogenase	✓	✓		15	6.79	35.54	6.54	gi|170198680	147	3	15%	Energy metabolism
71	Myosin heavy chain type B	✓	✓		13	6.68	218.87	6.00	gi|170270277	82	2	5%	Thick filament
73	Glyceraldehyde-3-phosphate dehydrogenase	✓	✓	✓	17	6.52	18.66	5.58	gi|170197231	318	5	29%	Energy metabolism
74	Glyceraldehyde-3-phosphate dehydrogenase	✓	✓	✓	16	6.45	18.66	5.58	gi|170197231	48	2	15%	Energy metabolism
75	Glyceraldehyde-3-phosphate dehydrogenase		✓		23	6.56	18.66	5.58	gi|170197231	253	3	18%	Energy metabolism
78	α/β-Actin		✓	✓	57	4.62	41.91	5.16	gi|170190957	77	2	5%	Thin filament
79	α/β-Actin			✓	51	5.28	41.91	5.16	gi|170190957	390	7	21%	Thin filament
80	α/β-Actin			✓	53	5.12	41.91	5.16	gi|170190957	172	4	12%	Thin filament
81	α/β-Actin	✓		✓	45	4.97	41.91	5.16	gi|170190957	439	7	21%	Thin filament
82	α/β-Actin	✓			54	6.64	41.91	5.16	gi|170190957	419	6	18%	Thin filament
83	Farnesoic acid O-methyltranferase	✓			43	4.56	31.45	4.56	gi|170188611	178	3	14%	Signaling
84	α/β-Actin	✓			39	4.85	41.91	5.16	gi|170190957	132	2	9%	Thin filament
85	α/β-Actin	✓	✓	✓	37	4.84	41.91	5.16	gi|170190957	400	6	21%	Thin filament
86	Sarcomeric α-actinin	✓			35	4.84	97.75	6.04	gi|170222152	132	6	30%	Actin-binding
87	Glycogen phosphorylase		✓		33	5.46	97.96	6.82	gi|170202348	147	5	17%	Energy metabolism
88	α/β-Actin		✓		32	5.56	41.91	5.16	gi|170182624	210	4	20%	Thin filament
89	Arginine kinase		✓	✓	31	5.71	40.34	6.34	gi|170183164	258	5	18%	Phosphotransfer
90	Arginine kinase		✓		29	5.45	40.34	6.34	gi|170183164	221	5	18%	Phosphotransfer
91	Arginine kinase		✓		29	5.42	40.34	6.34	gi|170183164	81	2	6%	Phosphotransfer
92	α/β-Actin	✓		✓	28	5.43	41.91	5.16	gi|170182624	198	4	18%	Thin filament
94	Sarcoplasmic calcium-binding protein	✓			22	4.68	21.93	4.60	gi|170182977	168	3	14%	Signaling
95	Sarcoplasmic calcium-binding protein		✓	✓	21	4.70	21.93	4.60	gi|170182977	161	3	14%	Signaling
96	Myosin regulatory light chain		✓		46	6.86	22.58	4.70	gi|170184074	273	5	11%	Thick filament
99	α/β-Actin		✓		46	5.22	41.91	5.16	gi|170190957	257	4	9%	Thin filament
100	Arginine kinase	✓			17	5.23	46.00	4.90	gi|170183164	283	5	23%	Phosphotransfer
101	Arginine kinase		✓		22	5.39	46.00	4.90	gi|170183164	202	4	15%	Phosphotransfer
102	Arginine kinase	✓	✓	✓	19	5.48	46.00	4.90	gi|170183164	135	3	11%	Phosphotransfer
103	14-3-3 ζ			✓	36	4.66	27.96	4.65	gi|170194925	42	3	15%	Signaling
105	Myosin regulatory light chain		✓		21	4.20	22.58	4.70	gi|170184074	206	3	8%	Thick filament
106	Glyceraldehyde-3-phosphate dehydrogenase	✓	✓	✓	40	6.88	18.66	5.58	gi|170197231	344	3	24%	Energy metabolism

Table 2 continued.

107	Arginine kinase	✓	✓	✓	38	6.86	46.00	4.90	gi|170186144	263	7	30%	Phosphotransfer
108	Arginine kinase	✓			35	6.64	46.00	4.90	gi|170186144	457	9	30%	Phosphotransfer
109	Arginine kinase	✓	✓	✓	35	6.80	46.00	4.90	gi|170186144	241	6	29%	Phosphotransfer
110	Arginine kinase		✓		35	6.66	46.00	4.90	gi|170186144	386	9	30%	Phosphotransfer
111	Arginine kinase		✓		35	6.84	46.00	4.90	gi|170186144	153	4	19%	Phosphotransfer
112	Triose-phosphate isomerase			✓	34	6.87	28.99	5.83	gi|170207221	119	3	16%	Energy metabolism
113	Arginine kinase	✓	✓	✓	33	6.79	46.00	4.90	gi|170186144	341	8	34%	Phosphotransfer
114	Arginine kinase	✓	✓	✓	33	6.63	46.00	4.90	gi|170186144	298	8	30%	Phosphotransfer
115	Arginine kinase	✓	✓	✓	31	6.63	46.00	4.90	gi|170186144	277	7	29%	Phosphotransfer
116	Arginine kinase	✓	✓	✓	40	6.81	46.00	4.90	gi|170186144	382	9	30%	Phosphotransfer
118	Paramyosin			✓	44	6.68	103.69	5.55	gi|170186119	142	3	18%	Thick filament
119	Muscle myosin heavy chain		✓		95	5.53	135.52	5.49	gi|170208087	113	3	21%	Thick filament
120	Muscle myosin heavy chain	✓	✓	✓	95	5.49	135.52	5.49	gi|170208087	70	2	10%	Thick filament
123	Myosin heavy chain type 1		✓		75	5.50	219.58	5.76	gi|170219699	65	2	10%	Thick filament
125	Gelsolin-like isoform 1			✓	90	5.03	44.36	7.68	gi|170227754	44	2	12%	Actin-binding
126	Muscle myosin heavy chain		✓		20	5.36	135.52	5.49	gi|170208087	110	3	15%	Thick filament
127	Sarcomeric α-actinin	✓			63	5.21	97.75	6.04	gi|170222152	295	6	30%	Actin-binding
128	α/β-Actin			✓	50	6.09	41.91	5.16	gi|170190957	374	6	18%	Thin filament
129	Enolase		✓		43	6.30	47.24	6.18	gi|170237664	321	7	38%	Energy metabolism
130	Glyceraldehyde-3-phosphate dehydrogenase	✓		✓	40	6.56	18.66	5.58	gi|170197231	348	4	24%	Energy metabolism
131	Fast myosin heavy chain		✓		41	6.40	47.85	5.24	gi|170220415	146	2	26%	Thick filament
132	α/β-Actin		✓		53	6.11	41.91	5.16	gi|170190957	400	7	21%	Thin filament
133	Troponin T		✓		53	6.15	45.88	4.97	gi|170228768	120	2	15%	Thin filament
134	Arginine kinase	✓			37	6.63	46.00	4.90	gi|170186144	366	9	30%	Phosphotransfer
135	α/β-Actin			✓	50	6.27	41.91	5.16	gi|170190957	226	5	12%	Thin filament
136	α/β-Actin			✓	50	6.19	41.91	5.16	gi|170190957	388	6	18%	Thin filament
137	Pyruvate dehydrogenase E1 α-subunit	✓	✓	✓	45	6.23	43.20	7.58	gi|170183821	49	2	10%	Energy metabolism
138	Hemocyanin		✓		45	6.28	75.27	5.52	gi|170187274	209	4	18%	Respiratory
139	Notch-type protein	✓	✓	✓	67	6.62	44.88	7.22	gi|170248782	130	6	28%	Signaling
141	Filamin-C	✓	✓	✓	66	6.53	249.86	6.12	gi|170202097	80	2	9%	Actin-binding
142	Filamin-A	✓	✓		61	6.65	287.86	6.61	gi|170203114	76	2	8%	Actin-binding
143	Phosphoglycerate kinase-like		✓		54	6.61	53.54	9.17	gi|170203088	229	6	27%	Energy metabolism
145	Arginine kinase	✓			46	6.57	46.00	4.90	gi|170186144	151	4	16%	Phosphotransfer
146	Filamin	✓			83	6.82	249.86	6.12	gi|170220786	86	2	11%	Actin-binding
148	Cardiac-like muscle actin		✓		53	6.21	41.65	5.23	gi|170182268	169	2	11%	Thin filament
149	Enolase	✓			53	6.72	39.85	5.45	gi|170254092	161	4	19%	Energy metabolism

Table 2 continued.

149	Enolase	✓			53	6.72	39.85	5.45	gi|170254092	161	4	19%	Energy metabolism
150	Cardiac-like muscle actin		✓		41	5.75	41.65	5.23	gi|170182268	162	3	14%	Thin filament
153	Arginine kinase	✓			31	5.93	46.00	4.90	gi|170186144	264	7	33%	Phosphotransfer
154	Arginine kinase	✓			32	6.86	46.00	4.90	gi|170200859	391	8	29%	Phosphotransfer
155	Triose-phopshate isomerase		✓		31	6.85	26.98	5.87	gi|170254610	233	4	26%	Energy metabolism
156	Arginine kinase		✓		29	6.17	46.00	4.90	gi|170186144	88	3	14%	Phosphotransfer
157	Troponin T		✓		28	5.82	45.58	4.97	gi|170228768	96	2	11%	Thin filament
158	Adendylate kinase			✓	28	6.65	29.30	8.05	gi|170218197	502	8	27%	Phosphotransfer
159	Arginine kinase	✓			28	5.65	46.00	4.90	gi|170183164	137	3	9%	Phosphotransfer
160	Hemocyanin subunit 1	✓			27	6.15	25.41	5.99	gi|170195414	168	4	17%	Respiratory
161	α/β-Actin		✓		25	5.77	41.91	5.16	gi|170182624	217	4	20%	Thin filament
162	Arginine kinase		✓		22	5.60	46.00	4.90	gi|170183164	206	4	9%	Phosphotransfer
163	Arginine kinase	✓			21	5.57	46.00	4.90	gi|170183164	353	5	21%	Phosphotransfer
164	Myosin regulatory light chain		✓		21	4.14	22.58	4.70	gi|170184074	176	3	8%	Thick filament
165	Arginine kinase		✓		20	5.21	46.00	4.90	gi|170183164	62	2	6%	Phosphotransfer
167	Glyceraldehyde-3-phosphate dehydrogenase	✓			20	6.55	18.66	5.58	gi|170197231	172	3	21%	Energy metabolism
168	Troponin T			✓	52	6.80	45.88	4.97	gi|170228768	45	2	8%	Thin filament
178	Slow muscle myosin S1 heavy chain			✓	66	5.51	58.53	5.22	gi|170194515	148	4	14%	Thick filament
179	Hemocyanin subunit 4		✓		65	5.47	77.04	5.30	gi|170214816	96	3	13%	Respiratory
180	α/β-Actin			✓	53	4.91	41.91	5.16	gi|170190957	223	6	18%	Thin filament
183	Arginine kinase		✓		29	5.69	46.00	4.90	gi|170183164	373	5	22%	Phosphotransfer
184	Arginine kinase		✓		23	5.17	46.00	4.90	gi|170183164	90	3	10%	Phosphotransfer
185	α/β-Actin		✓		20	5.10	41.91	5.16	gi|170190957	151	4	6%	Thin filament
187	Hemocyanin		✓		24	6.75	75.27	5.52	gi|170187274	215	5	17%	Respiratory
189	Paramyosin (long form)	✓			67	6.19	103.02	5.83	isotig00035	62	2	0%	Thick filament
192	Tropomyosin (slow muscle isoform)	✓	✓	✓	47	4.48	32.89	4.74	gi|170187278	348	7	26%	Thin filament
193	F1-ATP synthase β-subunit	✓			68	6.13	55.80	5.31	gi|170221081	361	7	33%	Energy metabolism
194	Myosin heavy chain type 1			✓	81	5.55	219.58	5.76	gi|170219699	64	2	10%	Thick filament
198	Myosin regulatory light chain		✓		20	4.12	22.58	4.70	gi|170184074	311	6	14%	Thick filament
200	Myosin heavy chain type 1		✓		95	5.63	219.58	5.76	gi|170219699	100	2	9%	Thick filament
203	α/β-Actin			✓	50	5.90	41.91	5.16	gi|170190957	380	6	18%	Thin filament
204	Tropomyosin (slow muscle isoform)	✓	✓	✓	47	4.51	32.89	4.74	gi|170187278	407	8	27%	Thin filament
320	Fructose 1,6-bisphosphate aldolase	✓			15	5.44	25.64	5.47	gi|170216091	287	5	31%	Energy metabolism
387	α/β-Actin			✓	58	5.28	41.91	5.16	gi|170190957	193	6	15%	Thin filament
439	Myosin heavy chain type B	✓			108	6.10	218.87	6.00	gi|170211824	42	2	8%	Thick filament

Table 3. Loading values for principal components associated with an acclimation effect. The positive and negative loadings values are given for proteins that significantly changed in abundance in response to acclimation treatment. Only the top 10 contributing proteins identified using MS/MS are indicated.

Component loading rank	Principal component 1		Principal component 2	
	Protein (spot ID)	Loading value	Protein (spot ID)	Loading value
Positive loadings for acclimation effect				
1	Gelsolin (18)	1.3186	Enolase (50)	1.4194
2	Hemocyanin (37)	1.2507	Phosphoglycerate kinase (143)	1.3506
3	Arginine kinase (5)	1.2112	Enolase (149)	1.2628
4	Fructose 1,6-bisphosphate aldolase (320)	1.2073	Arginine kinase (23)	1.2576
5	Cardiac-like muscle actin (29)	1.2030	Muscle myosin heavy chain (120)	1.2374
6	Myosin heavy chain type B (71)	1.1539	Enolase (51)	1.2247
7	Hemocyanin subunit 1 (160)	1.1395	Hemocyanin (58)	1.0674
8	α/β-Actin (84)	1.0984	α/β-Actin (82)	1.0664
9	Arginine kinase (100)	1.0963	Hemocyanin (59)	1.0536
10	α/β-Actin (85)	1.0526	Arginine kinase (145)	0.9337
Negative loadings for acclimation effect				
1	Gelsolin (18)	–1.6349	Arginine kinase (109)	–2.1154
2	Hemocyanin (37)	–1.5935	Arginine kinase (102)	–2.0273
3	Arginine kinase (5)	–1.5332	Notch-type protein (139)	–1.9344
4	Fructose 1,6-bisphosphate aldolase (320)	–1.5319	Filamin-C (141)	–1.9090
5	Cardiac-like muscle actin (29)	–1.5179	Filamin-A (142)	–1.8065
6	Myosin heavy chain type B (71)	–1.5089	Arginine kinase (116)	–1.7500
7	Hemocyanin subunit 1 (160)	–1.4944	Filamin-A (46)	–1.7448
8	α/β-Actin (84)	–1.4927	α/β-Actin (39)	–1.6239
9	Arginine kinase (100)	–1.4520	Arginine kinase (107)	–1.6090
10	α/β-Actin (85)	–1.4032	Arginine kinase (114)	–1.4448

Table 4. Loading values for principal components associated with a heat shock effect. The positive and negative loadings values are given for proteins that significantly changed in abundance in response to heat shock treatment. Only the top 10 contributing proteins identified using MS/MS are indicated.

Component loading rank	Principal component 1		Principal component 2	
	Protein (spot ID)	Loading value	Protein (spot ID)	Loading value
Positive loadings for heat shock effect				
1	GAP dehydrogenase (8)	1.9067	Sarcoplasmic Ca^{2+}-binding protein (95)	1.7940
2	Prostaglandin reductase (30)	1.8708	Myosin regulatory light chain (105)	1.4420
3	Arginine kinase (4)	1.8526	α/β-Actin (85)	1.3084
4	α/β-Actin (185)	1.8511	Myosin regulatory light chain (53)	1.2316
5	Myosin heavy chain type B (71)	1.8142	Myosin regulatory light chain (164)	1.0045
6	Muscle myosin heavy chain (126)	1.7344	Myosin regulatory light chain (198)	0.8680
7	Hemocyanin (12)	1.7327	Arginine kinase (7)	0.8186
8	Myosin heavy chain type B (26)	1.7262	α/β-Actin (78)	0.8182
9	Peroxiredoxin 5 isoform B (11)	1.7057	Myosin heavy chain type B (38)	0.7772
10	Myosin heavy chain type B (38)	1.6357	Arginine kinase (110)	0.7329
Negative loadings for heat shock effect				
1	Hemocyanin (58)	–1.6951	Filamin-C (141)	–2.2402
2	Hemocyanin (57)	–1.6464	Filamin-A (142)	–2.1902
3	Troponin T (133)	–1.6351	Notch-type protein (139)	–2.1898
4	Muscle myosin heavy chain (119)	–1.6135	Filamin-A (46)	–2.0921
5	Myosin heavy chain type 1 (200)	–1.6073	Arginine kinase (109)	–2.0472
6	Myosin regulatory light chain (96)	–1.6019	Arginine kinase (102)	–2.0086
7	α/β-Actin (132)	–1.5946	Arginine kinase (111)	–2.0012
8	Arginine kinase (110)	–1.5669	Hemocyanin (138)	–1.9705
9	Hemocyanin (59)	–1.5660	Paramyosin (3)	–1.8089
10	Cardiac-like muscle actin (148)	–1.5277	Arginine kinase (116)	–1.7964

Table 5. Loading values for principal components associated with an acclimation x heat shock interaction. The positive and negative loadings values are given for proteins that significantly changed in abundance in response to an interaction between acclimation and heat shock treatments. Only the top 10 contributing proteins identified using MS/MS are indicated.

Component loading rank	Principal component 1		Principal component 2	
	Protein (spot ID)	Loading value	Protein (spot ID)	Loading value
Positive loadings for interaction effect				
1	α/β-Actin (128)	1.7323	α/β-Actin (85)	1.5237
2	α/β-Actin (136)	1.7158	Sarcoplasmic Ca^{2+}-binding protein (95)	1.4294
3	Hemocyanin (58)	1.6991	α/β-Actin (78)	0.9058
4	α/β-Actin (79)	1.6647	Enolase (51)	0.9041
5	Hemocyanin (59)	1.6032	Cofilin (33)	0.8396
6	α/β-Actin (135)	1.4906	Slow muscle myosin S1 heavy chain (178)	0.8298
7	Hemocyanin (57)	1.4780	Arginine kinase (7)	0.7623
8	Cardiac-like muscle actin (122)	1.4513	Arginine kinase (113)	0.7188
9	Phosphoglycerate kinase (143)	1.2923	Enolase (50)	0.6708
10	Hemocyanin subunit 2 precursor (62)	1.2545	Muscle myosin heavy chain (120)	0.5270
Negative loadings for interaction effect				
1	Arginine kinase (89)	–1.7986	Arginine kinase (116)	–2.1995
2	Cardiac-like muscle actin (42)	–1.4293	GAP dehydrogenase (106)	–2.1973
3	α/β-Actin (39)	–1.3576	Arginine kinase (107)	–2.1907
4	Myosin heavy chain type B(27)	–1.3297	Notch-type protein (139)	–2.0801
5	GAP dehydrogenase (73)	–1.2943	Arginine kinase (109)	–1.8695
6	Filamin-C (141)	–1.2213	Filamin-A (46)	–1.8568
7	α/β-Actin (92)	–1.1390	Paramyosin (118)	–1.7689
8	Slow muscle myosin S1 heavy chain (178)	–1.0188	Troponin T (168)	–1.7318
9	Arginine kinase (102)	–0.9598	α/β-Actin (121)	–1.6839
10	Arginine kinase (109)	–0.7862	Arginine kinase (102)	–1.6388

B. Figures for acclimation manuscript

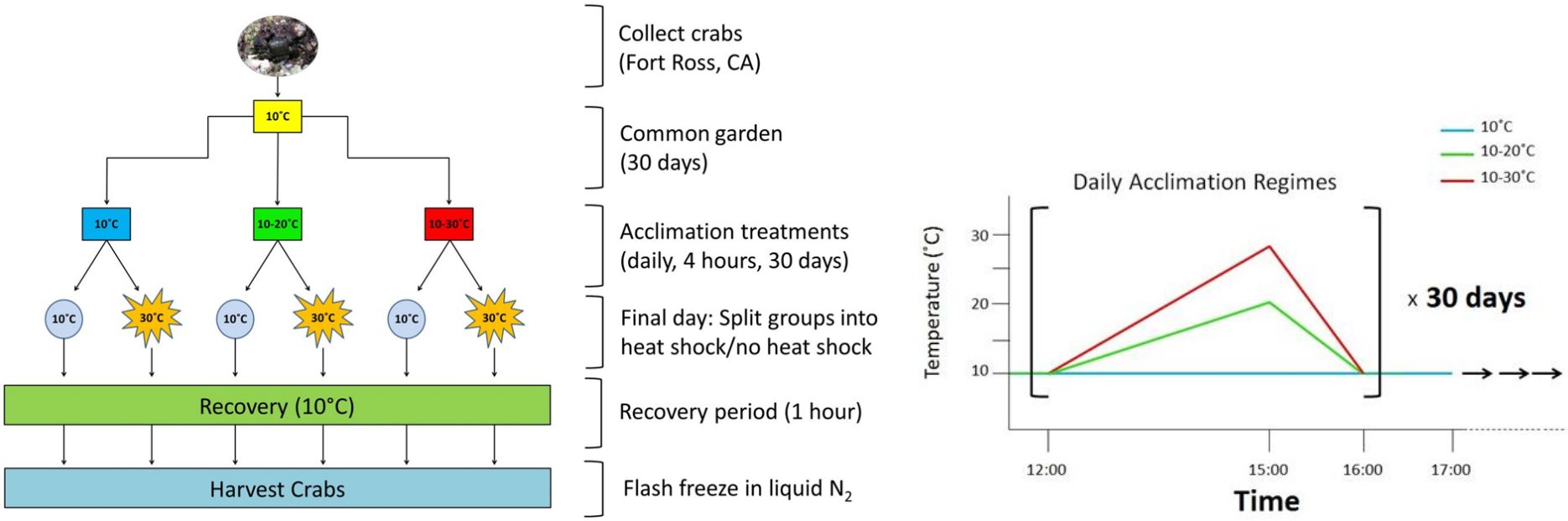

Figure 7. Experimental design of the thermal acclimation experiment. (Left) Flow chart of experiment from specimen collection to post-experimental harvesting. (Right) Graph of daily acclimation regimes over the course of one day.

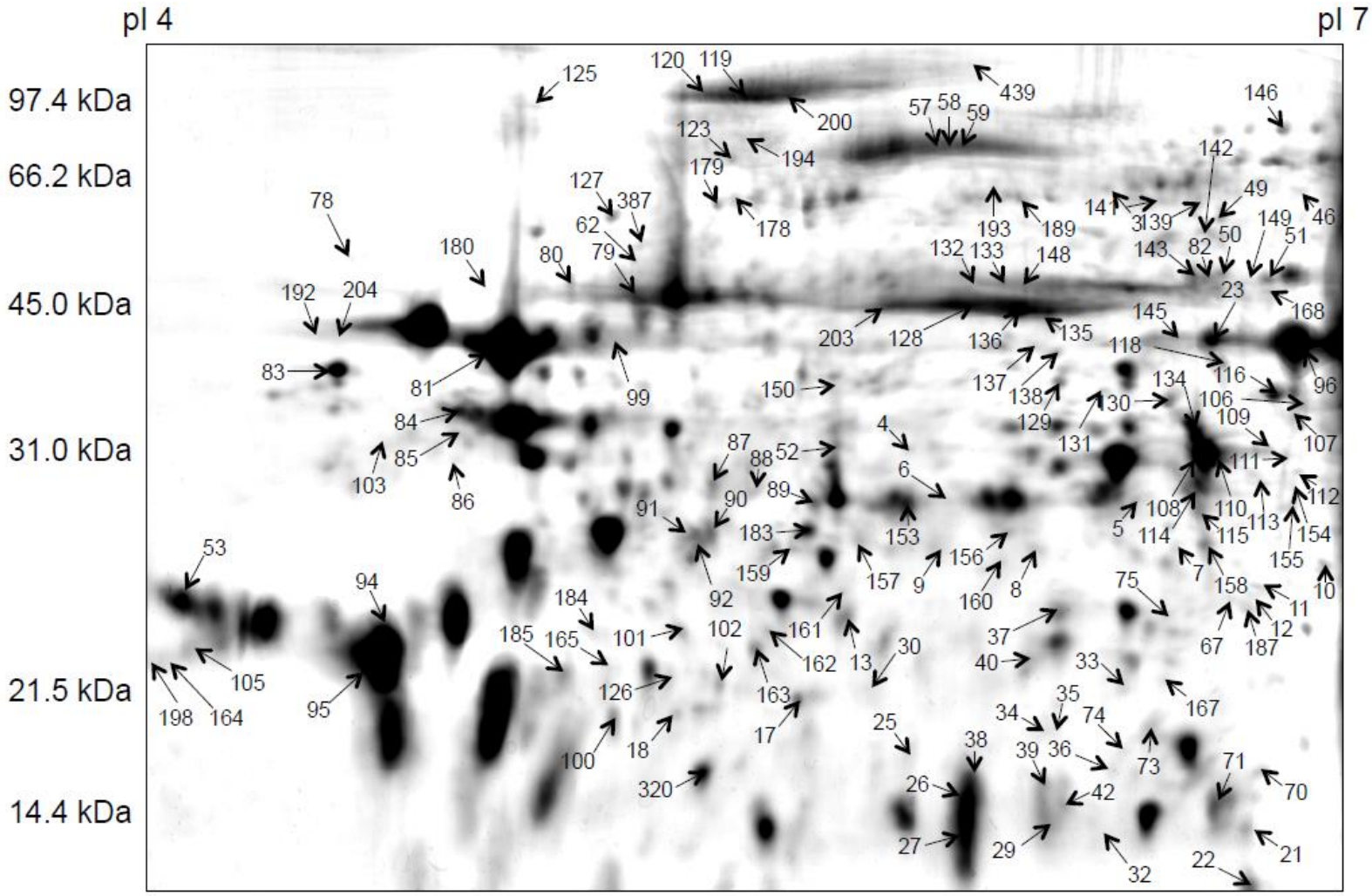

Figure 8. Proteome map of gels from all six treatments depicting 469 protein spots from claw muscle tissue of the intertidal porcelain crab *Petrolisthes cinctipes*. The proteome map represents average pixel volumes for each protein spot. Numbered spots are those that changed abundance in response to acclimation and heat stress treatments (two-way permutation ANOVA; P≤0.02) and were identified using tandem mass spectrometry (for identification, see Table 2).

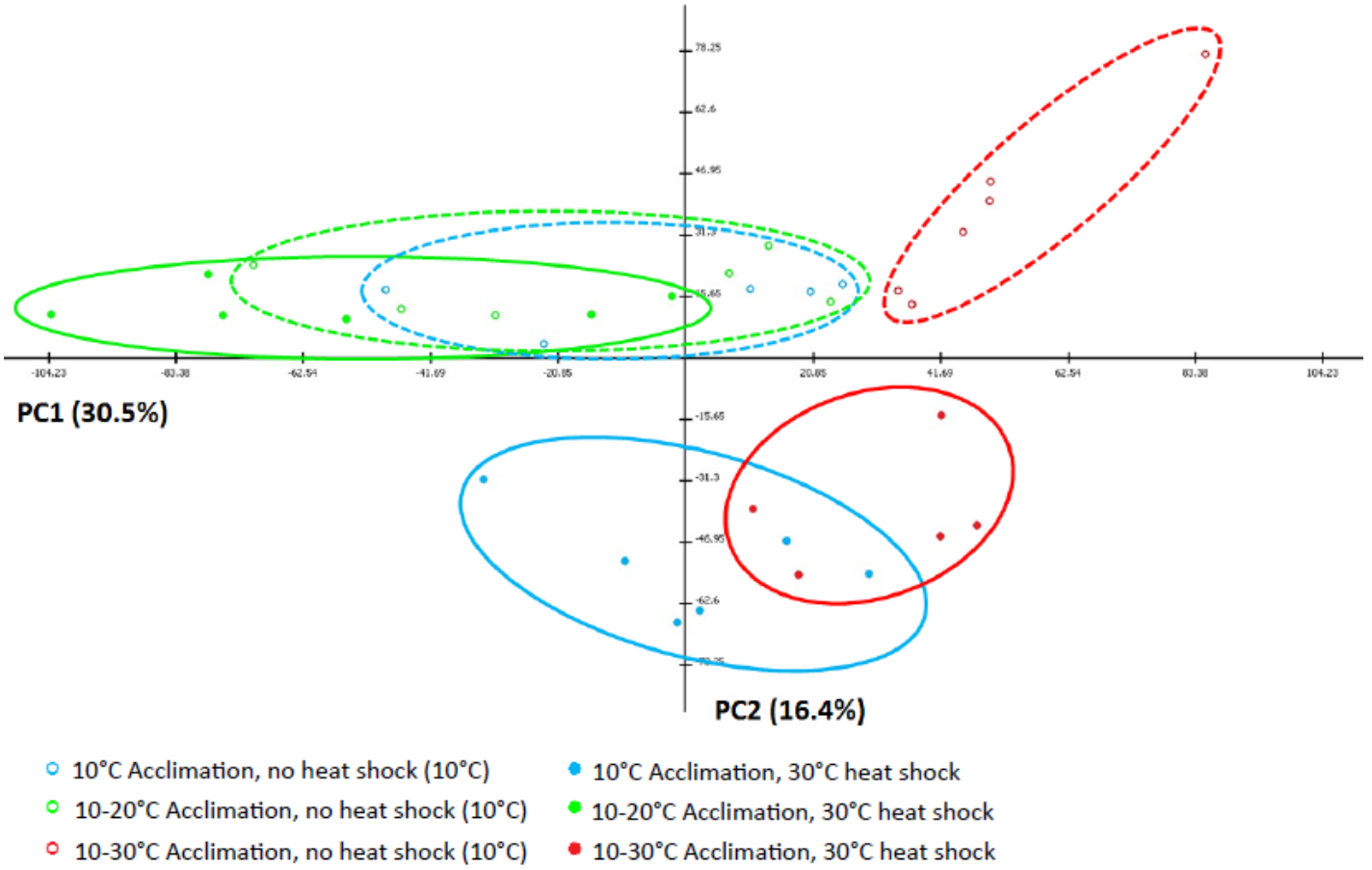

Figure 9A. Principal component analysis (PCA) of all proteins that changed in abundance in response to acclimation variation. Analysis is based on a two-way permutation ANOVA, P≤0.02. Each symbol represents a crab acclimated to 10°C (blue), 10–20°C (green) and 10–30°C (red) and either subsequently exposed to 10°C (striated) or a 5 h up-ramp to a 30°C heat shock plus a 1 h down-ramp 10°C recovery (solid line) (samples collected after recovery at 10°C). Principal components 1 and 2 (PC1 and PC2) and the percentage of the total variation of the selected (significant protein) data set they explain are shown.

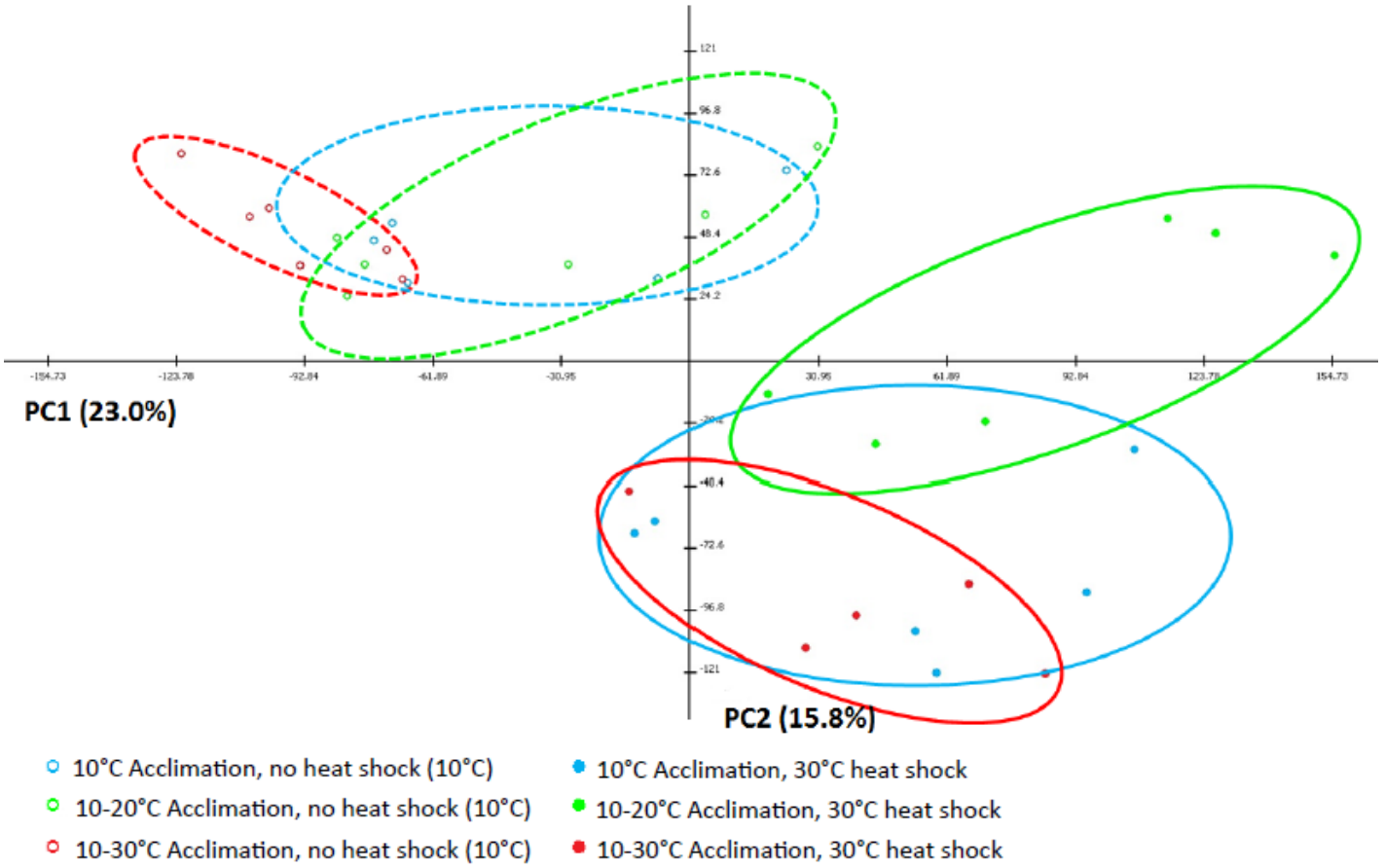

Figure 9B. Principal component analysis (PCA) of all proteins that changed in abundance in response to heat shock variation. Analysis is based on a two-way permutation ANOVA, P≤0.02. Each symbol represents a crab acclimated to 10°C (blue), 10–20°C (green) and 10–30°C (red) and either subsequently exposed to 10°C (striated) or a 5 h up-ramp to a 30°C heat shock plus a 1 h down-ramp 10°C recovery (solid line) (samples collected after recovery at 10°C). Principal components 1 and 2 (PC1 and PC2) and the percentage of the total variation of the selected (significant protein) data set they explain are shown.

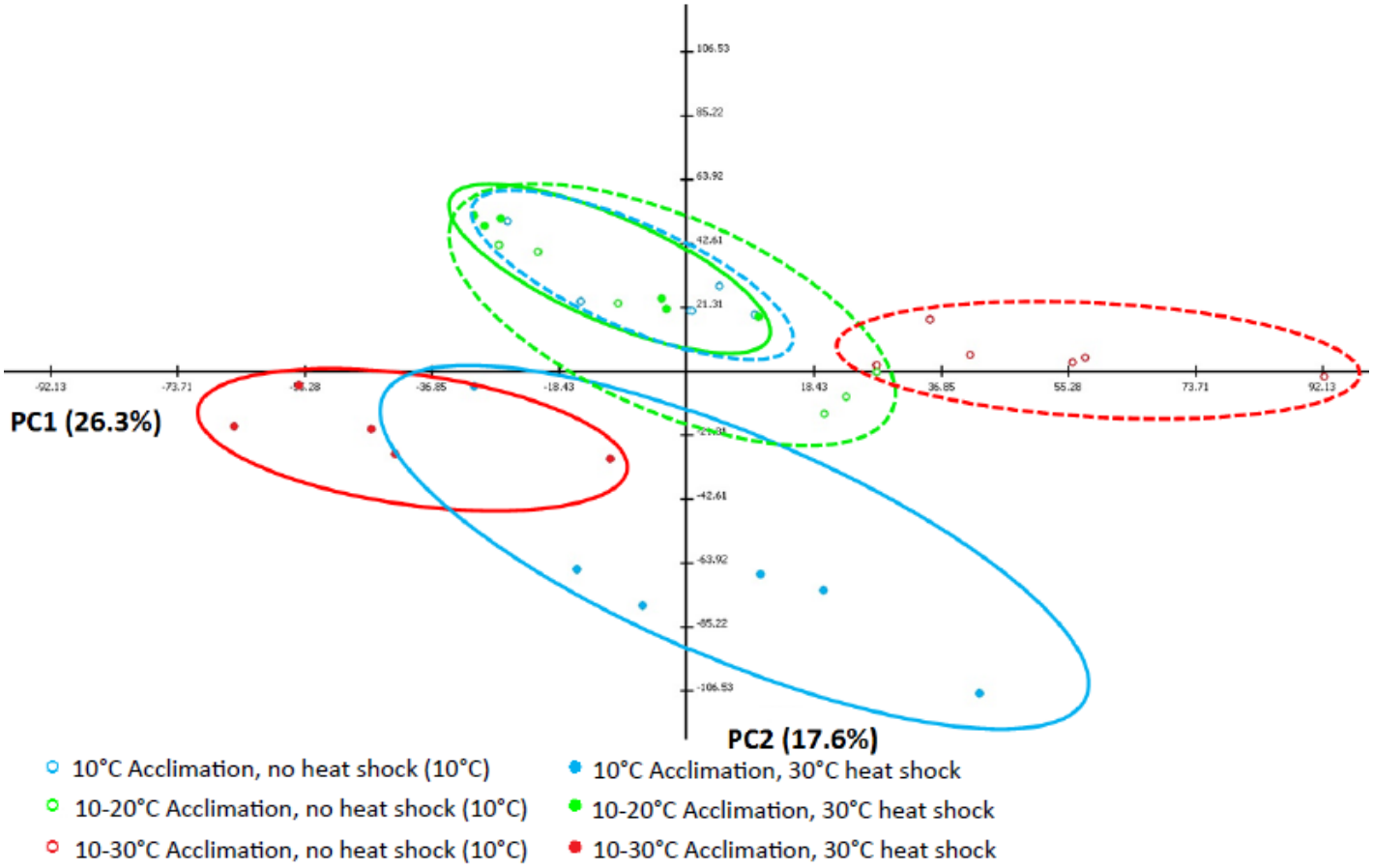

Figure 9C. Principal component analysis (PCA) of all proteins that changed in abundance in response to an interaction of acclimation and heat shock variation. Analysis is based on a two-way permutation ANOVA, P≤0.02. Each symbol represents a crab acclimated to 10°C (blue), 10–20°C (green) and 10–30°C (red) and either subsequently exposed to 10°C (striated) or a 5 h up-ramp to a 30°C heat shock plus a 1 h down-ramp 10°C recovery (solid line) (samples collected after recovery at 10°C). Principal components 1 and 2 (PC1 and PC2) and the percentage of the total variation of the selected (significant protein) data set they explain are shown.

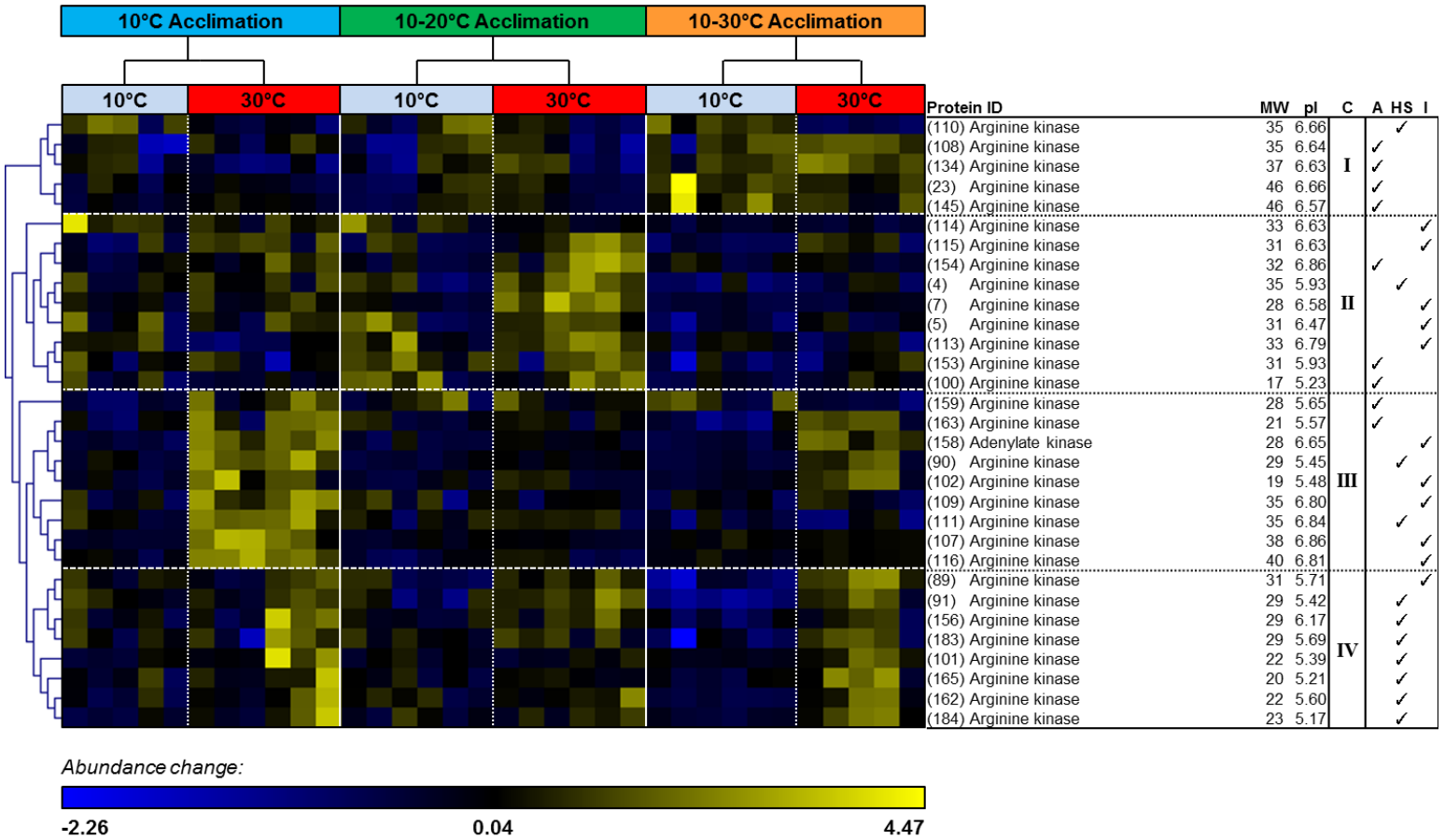

Protein ID	MW	pI	C	A	HS	I
(110) Arginine kinase	35	6.66			✓	
(108) Arginine kinase	35	6.64		✓		
(134) Arginine kinase	37	6.63	I	✓		
(23) Arginine kinase	46	6.66		✓		
(145) Arginine kinase	46	6.57		✓		
(114) Arginine kinase	33	6.63				✓
(115) Arginine kinase	31	6.63				✓
(154) Arginine kinase	32	6.86		✓		
(4) Arginine kinase	35	5.93			✓	
(7) Arginine kinase	28	6.58	II			✓
(5) Arginine kinase	31	6.47				✓
(113) Arginine kinase	33	6.79				✓
(153) Arginine kinase	31	5.93		✓		
(100) Arginine kinase	17	5.23		✓		
(159) Arginine kinase	28	5.65		✓		
(163) Arginine kinase	21	5.57		✓		
(158) Adenylate kinase	28	6.65				✓
(90) Arginine kinase	29	5.45			✓	
(102) Arginine kinase	19	5.48	III			✓
(109) Arginine kinase	35	6.80				✓
(111) Arginine kinase	35	6.84			✓	
(107) Arginine kinase	38	6.86				✓
(116) Arginine kinase	40	6.81				✓
(89) Arginine kinase	31	5.71				✓
(91) Arginine kinase	29	5.42			✓	
(156) Arginine kinase	29	6.17			✓	
(183) Arginine kinase	29	5.69			✓	
(101) Arginine kinase	22	5.39	IV		✓	
(165) Arginine kinase	20	5.21			✓	
(162) Arginine kinase	22	5.60			✓	
(184) Arginine kinase	23	5.17			✓	

Figure 10. Hierarchical clustering of changes in abundance of phosphotransfer proteins. Pearson's correlation, in response to acclimation to daily temperature fluctuations and subsequent control (10°C) and heat shock (30°C) exposures from claw muscle tissue of the porcelain crab *Petrolisthes cinctipes*. Blue coloring represents a lower than average protein abundance (standardized values, normalized volumes), whereas yellow represents greater than average protein abundance. Each column represents an individual muscle, grouped by treatment (N=5-6 for each treatment). The rows represent the standardized abundances of proteins, organized by clusters of similar abundance changes (C), that are identified to the right and whose molecular mass (MW) and isoelectric point (pI) is listed. Significances for an acclimation (A), heat shock (HS) or interaction (I) effect are ticked based on a two-way permutation ANOVA (P≤0.02).

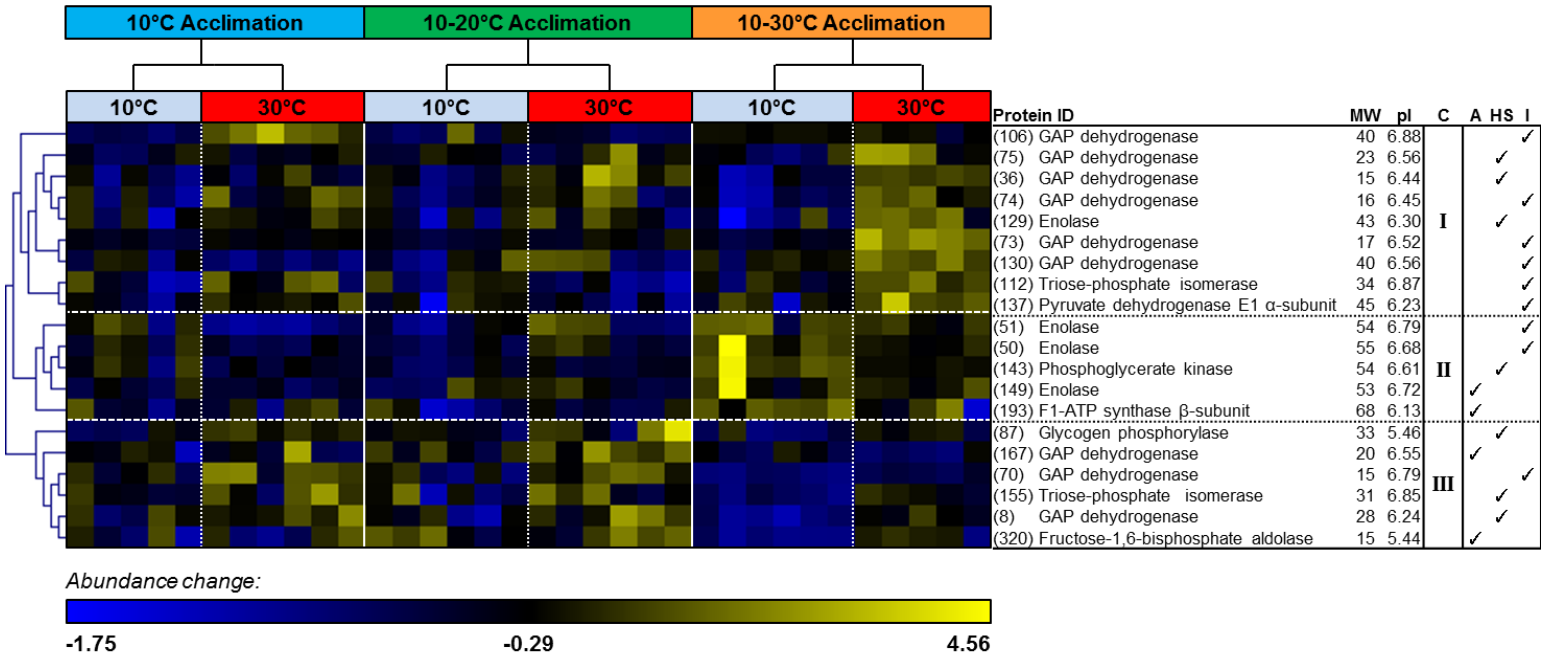

Protein ID	MW	pI	C	A	HS	I
(106) GAP dehydrogenase	40	6.88				✓
(75) GAP dehydrogenase	23	6.56			✓	
(36) GAP dehydrogenase	15	6.44			✓	
(74) GAP dehydrogenase	16	6.45				✓
(129) Enolase	43	6.30	I		✓	
(73) GAP dehydrogenase	17	6.52				✓
(130) GAP dehydrogenase	40	6.56				✓
(112) Triose-phosphate isomerase	34	6.87				✓
(137) Pyruvate dehydrogenase E1 α-subunit	45	6.23				✓
(51) Enolase	54	6.79				✓
(50) Enolase	55	6.68				✓
(143) Phosphoglycerate kinase	54	6.61	II		✓	
(149) Enolase	53	6.72		✓		
(193) F1-ATP synthase β-subunit	68	6.13		✓		
(87) Glycogen phosphorylase	33	5.46			✓	
(167) GAP dehydrogenase	20	6.55		✓		
(70) GAP dehydrogenase	15	6.79				✓
(155) Triose-phosphate isomerase	31	6.85	III		✓	
(8) GAP dehydrogenase	28	6.24			✓	
(320) Fructose-1,6-bisphosphate aldolase	15	5.44		✓		

Figure 11. Hierarchical clustering of changes in abundance of energy metabolism proteins. Pearson's correlation, in response to acclimation to daily temperature fluctuations and subsequent control (10°C) and heat shock (30°C) exposures from claw muscle tissue of the porcelain crab *Petrolisthes cinctipes*. Blue coloring represents a lower than average protein abundance (standardized values, normalized volumes), whereas yellow represents greater than average protein abundance. Each column represents an individual muscle, grouped by treatment (N=5-6 for each treatment). The rows represent the standardized abundances of proteins, organized by clusters of similar abundance changes (C), that are identified to the right and whose molecular mass (MW) and isoelectric point (pI) is listed. Significances for an acclimation (A), heat shock (HS) or interaction (I) effect are ticked based on a two-way permutation ANOVA (P≤0.02).

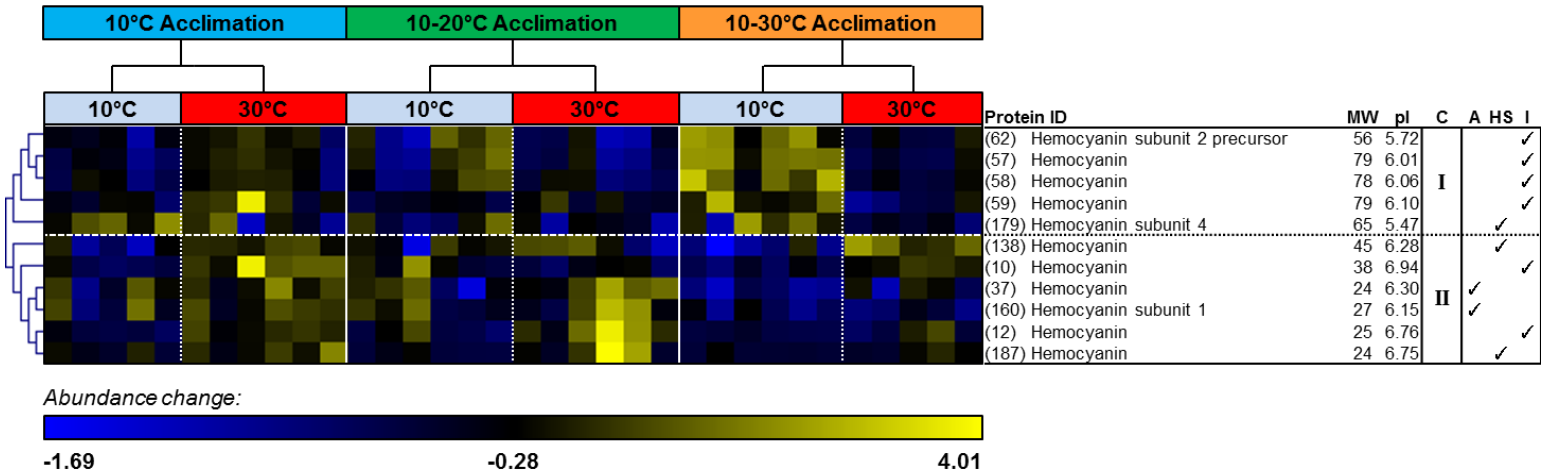

Figure 12. Hierarchical clustering of changes in abundance of hemocyanins. Pearson's correlation, in response to acclimation to daily temperature fluctuations and subsequent control (10°C) and heat shock (30°C) exposures from claw muscle tissue of the porcelain crab *Petrolisthes cinctipes*. Blue coloring represents a lower than average protein abundance (standardized values, normalized volumes), whereas yellow represents greater than average protein abundance. Each column represents an individual muscle, grouped by treatment (N=5-6 for each treatment). The rows represent the standardized abundances of proteins, organized by clusters of similar abundance changes (C), that are identified to the right and whose molecular mass (MW) and isoelectric point (pI) is listed. Significances for an acclimation (A), heat shock (HS) or interaction (I) effect are ticked based on a two-way permutation ANOVA (P≤0.02).

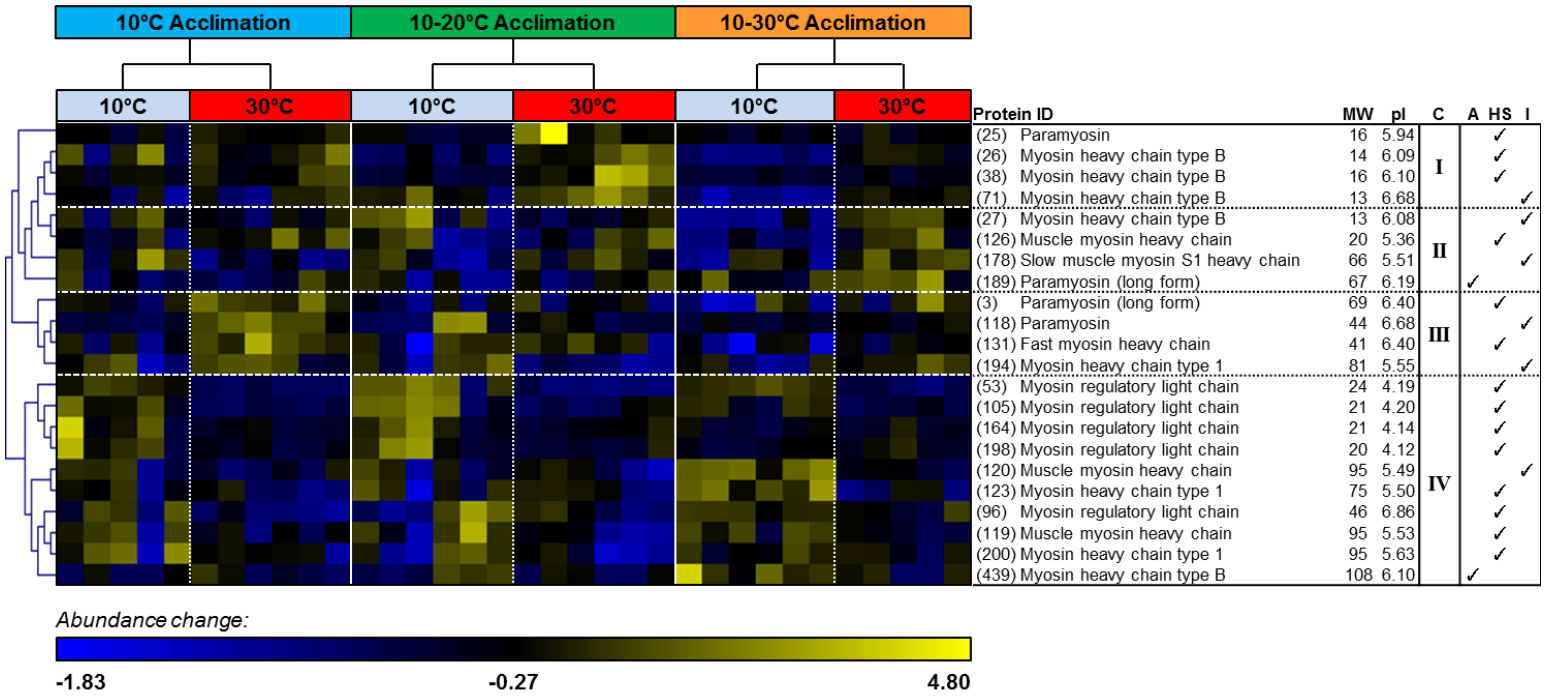

Protein ID	MW	pI	C	A	HS	I
(25) Paramyosin	16	5.94	I		✓	
(26) Myosin heavy chain type B	14	6.09			✓	
(38) Myosin heavy chain type B	16	6.10			✓	
(71) Myosin heavy chain type B	13	6.68				✓
(27) Myosin heavy chain type B	13	6.08	II			✓
(126) Muscle myosin heavy chain	20	5.36			✓	
(178) Slow muscle myosin S1 heavy chain	66	5.51				✓
(189) Paramyosin (long form)	67	6.19		✓		
(3) Paramyosin (long form)	69	6.40	III		✓	
(118) Paramyosin	44	6.68				✓
(131) Fast myosin heavy chain	41	6.40			✓	
(194) Myosin heavy chain type 1	81	5.55				✓
(53) Myosin regulatory light chain	24	4.19	IV		✓	
(105) Myosin regulatory light chain	21	4.20			✓	
(164) Myosin regulatory light chain	21	4.14			✓	
(198) Myosin regulatory light chain	20	4.12			✓	
(120) Muscle myosin heavy chain	95	5.49				✓
(123) Myosin heavy chain type 1	75	5.50			✓	
(96) Myosin regulatory light chain	46	6.86			✓	
(119) Muscle myosin heavy chain	95	5.53			✓	
(200) Myosin heavy chain type 1	95	5.63			✓	
(439) Myosin heavy chain type B	108	6.10		✓		

Figure 13. Hierarchical clustering of changes in abundance of thick filament proteins. Pearson's correlation, in response to acclimation to daily temperature fluctuations and subsequent control (10°C) and heat shock (30°C) exposures from claw muscle tissue of the porcelain crab *Petrolisthes cinctipes*. Blue coloring represents a lower than average protein abundance (standardized values, normalized volumes), whereas yellow represents greater than average protein abundance. Each column represents an individual muscle, grouped by treatment (N=5-6 for each treatment). The rows represent the standardized abundances of proteins, organized by clusters of similar abundance changes (C), that are identified to the right and whose molecular mass (MW) and isoelectric point (pI) is listed. Significances for an acclimation (A), heat shock (HS) or interaction (I) effect are ticked based on a two-way permutation ANOVA (P≤0.02).

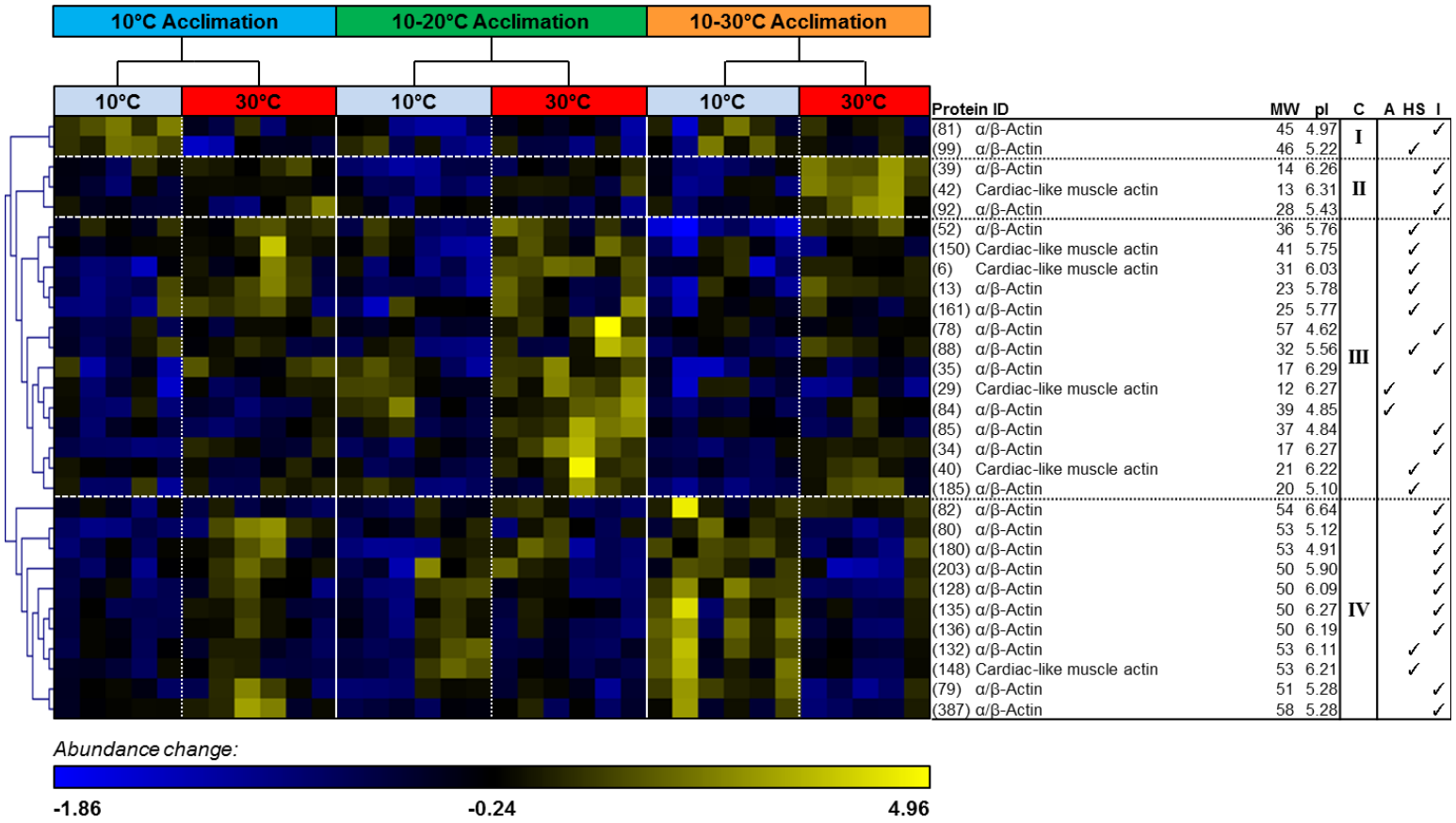

Protein ID	MW	pI	C	A	HS	I
(81) α/β-Actin	45	4.97	I			✓
(99) α/β-Actin	46	5.22			✓	
(39) α/β-Actin	14	6.26	II			✓
(42) Cardiac-like muscle actin	13	6.31				✓
(92) α/β-Actin	28	5.43				✓
(52) α/β-Actin	36	5.76	III		✓	
(150) Cardiac-like muscle actin	41	5.75			✓	
(6) Cardiac-like muscle actin	31	6.03			✓	
(13) α/β-Actin	23	5.78			✓	
(161) α/β-Actin	25	5.77			✓	
(78) α/β-Actin	57	4.62				✓
(88) α/β-Actin	32	5.56			✓	
(35) α/β-Actin	17	6.29				✓
(29) Cardiac-like muscle actin	12	6.27		✓		
(84) α/β-Actin	39	4.85		✓		
(85) α/β-Actin	37	4.84				✓
(34) α/β-Actin	17	6.27				✓
(40) Cardiac-like muscle actin	21	6.22			✓	
(185) α/β-Actin	20	5.10			✓	
(82) α/β-Actin	54	6.64	IV			✓
(80) α/β-Actin	53	5.12				✓
(180) α/β-Actin	53	4.91				✓
(203) α/β-Actin	50	5.90				✓
(128) α/β-Actin	50	6.09				✓
(135) α/β-Actin	50	6.27				✓
(136) α/β-Actin	50	6.19				✓
(132) α/β-Actin	53	6.11			✓	
(148) Cardiac-like muscle actin	53	6.21			✓	
(79) α/β-Actin	51	5.28				✓
(387) α/β-Actin	58	5.28				✓

Figure 14. Hierarchical clustering of changes in abundance of thin filament proteins. Pearson's correlation, in response to acclimation to daily temperature fluctuations and subsequent control (10°C) and heat shock (30°C) exposures from claw muscle tissue of the porcelain crab *Petrolisthes cinctipes*. Blue coloring represents a lower than average protein abundance (standardized values, normalized volumes), whereas yellow represents greater than average protein abundance. Each column represents an individual muscle, grouped by treatment (N=5-6 for each treatment). The rows represent the standardized abundances of proteins, organized by clusters of similar abundance changes (C), that are identified to the right and whose molecular mass (MW) and isoelectric point (pI) is listed. Significances for an acclimation (A), heat shock (HS) or interaction (I) effect are ticked based on a two-way permutation ANOVA (P≤0.02).

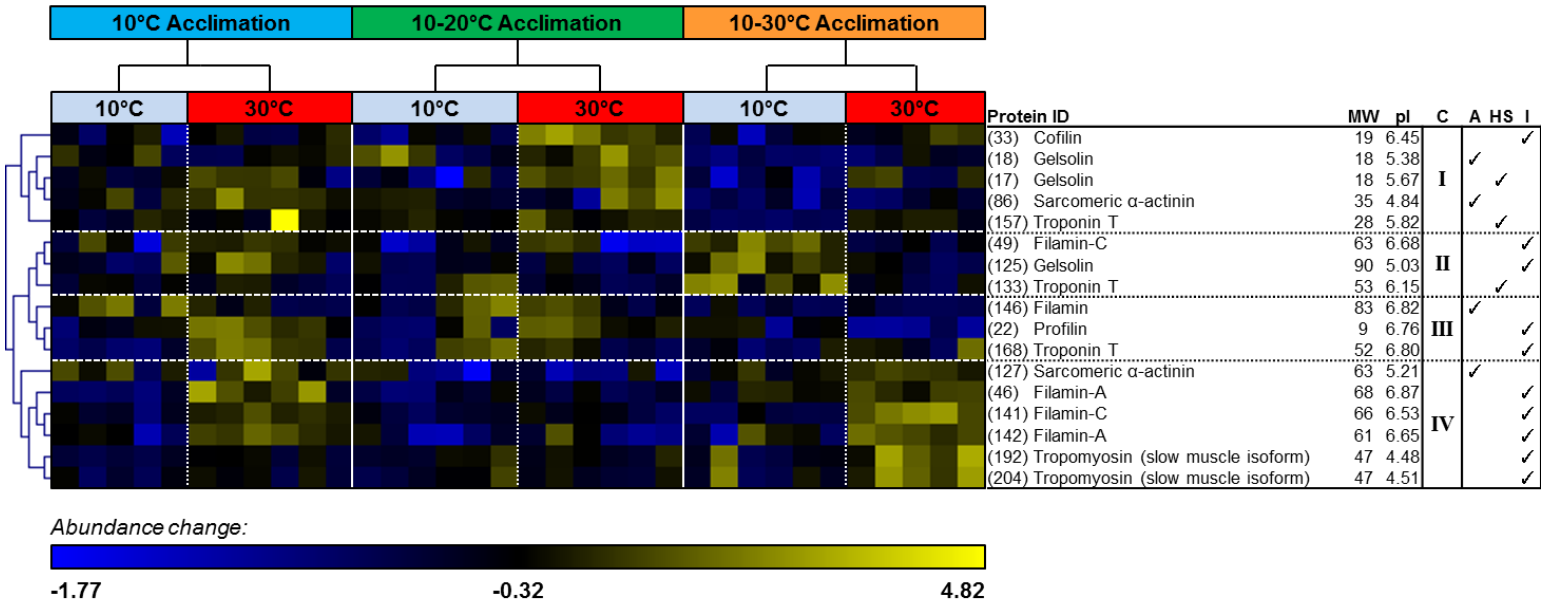

Protein ID	MW	pI	C	A	HS	I
(33) Cofilin	19	6.45				✓
(18) Gelsolin	18	5.38		✓		
(17) Gelsolin	18	5.67	I		✓	
(86) Sarcomeric α-actinin	35	4.84		✓		
(157) Troponin T	28	5.82			✓	
(49) Filamin-C	63	6.68				✓
(125) Gelsolin	90	5.03	II			✓
(133) Troponin T	53	6.15			✓	
(146) Filamin	83	6.82		✓		
(22) Profilin	9	6.76	III			✓
(168) Troponin T	52	6.80				✓
(127) Sarcomeric α-actinin	63	5.21		✓		
(46) Filamin-A	68	6.87				✓
(141) Filamin-C	66	6.53	IV			✓
(142) Filamin-A	61	6.65				✓
(192) Tropomyosin (slow muscle isoform)	47	4.48				✓
(204) Tropomyosin (slow muscle isoform)	47	4.51				✓

Figure 15. Hierarchical clustering of changes in abundance of actin-binding proteins. Pearson's correlation, in response to acclimation to daily temperature fluctuations and subsequent control (10°C) and heat shock (30°C) exposures from claw muscle tissue of the porcelain crab *Petrolisthes cinctipes*. Blue coloring represents a lower than average protein abundance (standardized values, normalized volumes), whereas yellow represents greater than average protein abundance. Each column represents an individual muscle, grouped by treatment (N=5-6 for each treatment). The rows represent the standardized abundances of proteins, organized by clusters of similar abundance changes (C), that are identified to the right and whose molecular mass (MW) and isoelectric point (pI) is listed. Significances for an acclimation (A), heat shock (HS) or interaction (I) effect are ticked based on a two-way permutation ANOVA (P≤0.02).

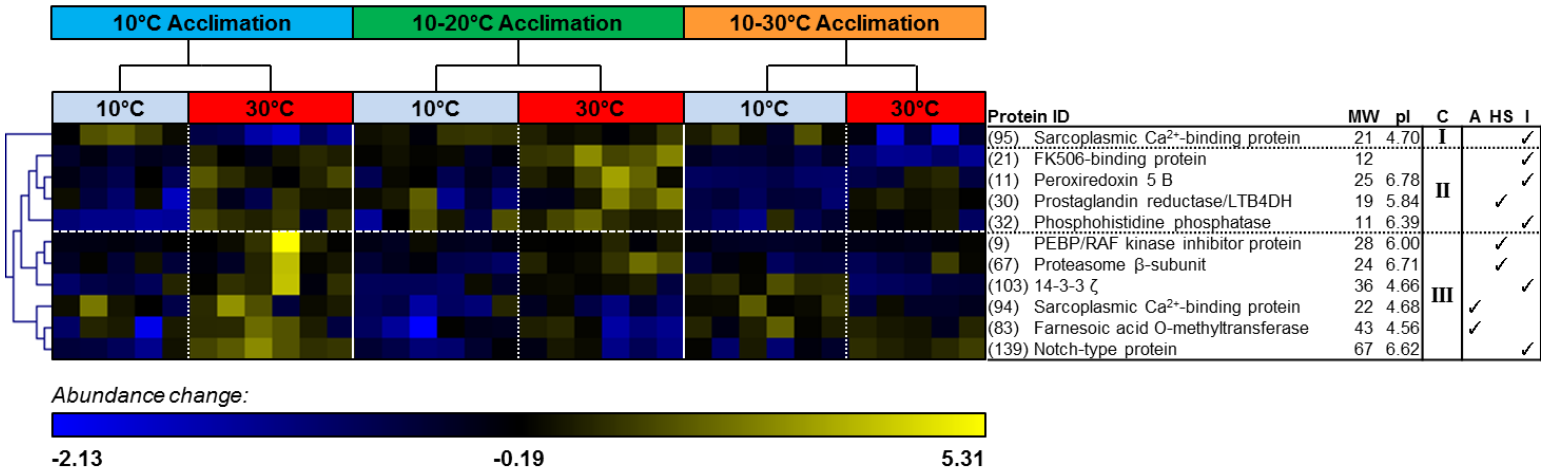

Protein ID	MW	pI	C	A	HS	I
(95) Sarcoplasmic Ca^{2+}-binding protein	21	4.70	I			✓
(21) FK506-binding protein	12		II			✓
(11) Peroxiredoxin 5 B	25	6.78				✓
(30) Prostaglandin reductase/LTB4DH	19	5.84			✓	
(32) Phosphohistidine phosphatase	11	6.39				✓
(9) PEBP/RAF kinase inhibitor protein	28	6.00	III		✓	
(67) Proteasome β-subunit	24	6.71			✓	
(103) 14-3-3 ζ	36	4.66				✓
(94) Sarcoplasmic Ca^{2+}-binding protein	22	4.68		✓		
(83) Farnesoic acid O-methyltransferase	43	4.56		✓		
(139) Notch-type protein	67	6.62				✓

Figure 16. Hierarchical clustering of changes in abundance of signaling proteins. Pearson's correlation, in response to acclimation to daily temperature fluctuations and subsequent control (10°C) and heat shock (30°C) exposures from claw muscle tissue of the porcelain crab *Petrolisthes cinctipes*. Blue coloring represents a lower than average protein abundance (standardized values, normalized volumes), whereas yellow represents greater than average protein abundance. Each column represents an individual muscle, grouped by treatment (N=5-6 for each treatment). The rows represent the standardized abundances of proteins, organized by clusters of similar abundance changes (C), that are identified to the right and whose molecular mass (MW) and isoelectric point (pI) is listed. Significances for an acclimation (A), heat shock (HS) or interaction (I) effect are ticked based on a two-way permutation ANOVA (P≤0.02).

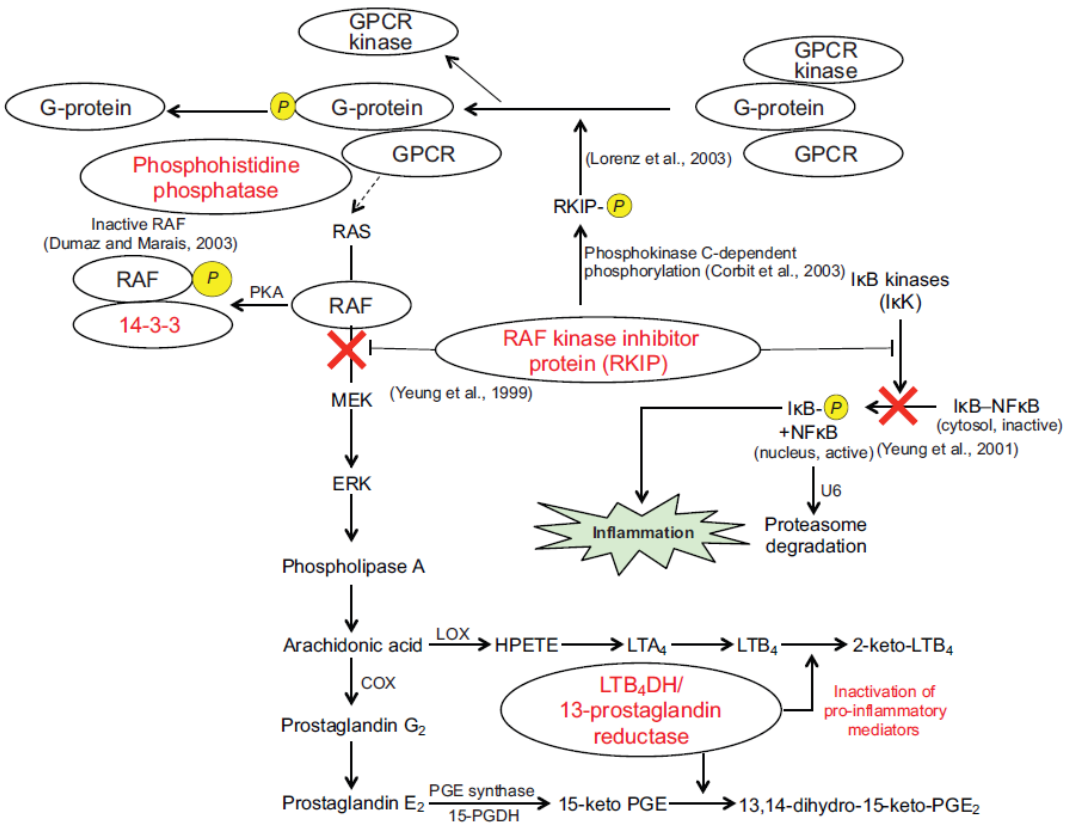

Figure 17. A schematic showing hypothetical pathways and cellular processes affected by changes in abundance of several signaling proteins that might inhibit an innate immune response. Putative protein phosphorylation is indicated with yellow circles. Red text indicates signaling proteins; red crosses represent immune response. For details, see text. COX, cyclooxygenase; ERK, extracellular signal-regulated kinase; GPCR, G-protein coupled receptor; HPETE, arachidonic acid 5-hydroperoxide; IκB, inhibitor of kappa B; LOX, lipooxygenase; LTA4, leukotriene A4; LTB4, leukotriene B4; LTB4DH, leukotriene B4 hydroxydehydrogenase; MEK, mitogen-activated protein kinase kinase; NFκB, nuclear factor kappa B; PGDH, prostaglandin dehydrogenase; PGE, prostaglandin E; PKA, protein kinase A; RAF, rapidly accelerated fibrosarcoma.

C. Tables for multi-stress manuscript

Table 6. Proteins identified in the multi-stress manuscript. Table includes estimated and predicted molecular mass (kDa), isoelectric point (pI), gene band identifier, MASCOT score, number of peptides matched, sequence coverage, and putative functional category. E = emersion/immersion (or tidal) treatment, T = temperature treatment, P = pH treatment,I = interaction of two treatments respective to the analysis. A checkmark indicates significant change in abundance of a particular protein in response to the indicated treatment.

Spot ID	Protein ID	E	P	I	T	P	I	Functional Category	MW (kDa) Estimated	pI Estimated	MW (kDa) Predicted	pI Predicted	Database ID	Mascot Score	Peptide Matches	Sequence Coverage (%)
2	Hemocyanin				✓			Respiratory	21	6.77	75	5.52	gi|170187274	67	2	9
9	DD5 cuticle protein		✓					Cuticle	113	4.73	138	5.43	gi|170216257	69	2	12
12	DD5 cuticle protein		✓					Cuticle	113	4.76	138	5.43	gi|170211011	70	2	7
13	DD5 cuticle protein	✓					✓	Cuticle	107	4.47	138	5.43	gi|170223047	103	3	22
14	Masquerade-like serine protease		✓					Protein homeostasis	103	4.29	99	5.21	gi|170196719	105	3	10
16	Hemocyanin α-subunit				✓			Respiratory	80	5.92	77	5.37	gi|170206072	60	2	9
17	DD5 cuticle protein			✓				Cuticle	106	4.56	138	5.43	gi|170223047	65	2	12
18	DD5 cuticle protein			✓				Cuticle	105	4.60	138	5.43	gi|170223047	74	2	12
19	Masquerade-like serine protease		✓					Protein homeostasis	102	4.33	99	5.21	gi|170196719	113	3	10
20	DD5 cuticle protein			✓				Cuticle	102	4.61	138	5.43	gi|170223047	82	2	12
21	DD5 cuticle protein	✓						Cuticle	97	4.65	138	5.43	gi|170223047	74	2	12
22	DD5 cuticle protein						✓	Cuticle	100	4.55	138	5.43	gi|170223047	82	2	12
23	DD5 cuticle protein			✓				Cuticle	101	4.56	138	5.43	gi|170211011	81	3	16
24	DD5 cuticle protein			✓			✓	Cuticle	98	4.67	138	5.43	gi|170223047	78	3	22
25	DD5 cuticle protein	✓					✓	Cuticle	101	4.53	138	5.43	gi|170223047	101	2	12
26	DD5 cuticle protein			✓				Cuticle	100	4.42	138	5.43	gi|170223047	77	2	12
27	DD5 cuticle protein	✓					✓	Cuticle	102	4.48	138	5.43	gi|170223047	96	2	12
28	DD5 cuticle protein			✓			✓	Cuticle	101	4.50	138	5.43	gi|170211011	78	2	7
29	DD5 cuticle protein			✓				Cuticle	100	4.48	138	5.43	gi|170223047	93	3	22
30	DD5 cuticle protein			✓			✓	Cuticle	98	4.70	138	5.43	gi|170211011	82	2	7
31	Masquerade-like serine protease	✓						Protein homeostasis	98	4.28	99	5.21	gi|170196719	106	3	10
33	DD5 cuticle protein		✓				✓	Cuticle	98	4.74	138	5.43	gi|170211011	71	3	16
35	DD5 cuticle protein			✓	✓			Cuticle	91	4.43	138	5.43	gi|170223047	116	3	22
40	DD5 cuticle protein		✓		✓			Cuticle	91	4.48	138	5.43	gi|170223047	125	3	22
41	DD5 cuticle protein			✓	✓			Cuticle	91	4.50	138	5.43	gi|170211011	126	3	16
42	DD5 cuticle protein		✓		✓			Cuticle	91	4.52	138	5.43	gi|170211011	120	3	16
43	DD5 cuticle protein			✓			✓	Cuticle	90	4.55	138	5.43	gi|170211011	121	3	16
44	DD5 cuticle protein		✓					Cuticle	90	4.68	138	5.43	gi|170211011	112	3	16
45	DD5 cuticle protein			✓	✓			Cuticle	90	4.58	138	5.43	gi|170223047	103	3	22

Table 6 continued.

46	DD5 cuticle protein			✓			Cuticle	91	4.63	138	5.43	gi|170211011	124	3	16
47	Hemocyanin			✓			Respiratory	81	4.86	78	5.37	gi|170185161	114	4	20
50	α-Actin	✓				✓	Cytoskeletal	80	5.51	42	5.16	gi|170192696	78	2	9
60	Fibrillin-2					✓	Protein homeostasis	74	6.59	1304	5.16	gi|170231876	102	3	15
63	Hemocyanin				✓		Respiratory	77	6.26	78	5.37	gi|170211405	70	2	11
68	Hemocyanin	✓					Respiratory	77	5.61	77	5.44	gi|170189674	59	2	9
69	Hemocyanin		✓			✓	Respiratory	76	6.40	75	5.52	gi|170278434	72	2	10
71	DD5 cuticle protein	✓					Cuticle	76	4.44	138	5.43	gi|170216257	78	2	12
73	DD5 cuticle protein			✓			Cuticle	76	4.63	138	5.43	gi|170216257	115	3	16
74	Hemocyanin subunit 3			✓			Respiratory	76	4.83	77	5.20	gi|57901143	61	2	3
75	β-Actin	✓			✓		Cytoskeletal	77	5.51	33	5.01	isotig02875	50	3	12
76	Hemocyanin		✓				Respiratory	76	5.61	77	5.44	gi|170189674	69	2	9
77	β-Actin	✓					Cytoskeletal	74	5.52	42	5.30	gi|1703103	136	4	12
78	Hemocyanin		✓		✓		Respiratory	74	5.48	75	5.52	gi|170278434	91	2	10
79	Hemocyanin	✓					Respiratory	74	5.61	77	5.59	gi|170183126	91	4	15
81	Hemocyanin	✓					Respiratory	73	6.07	75	5.52	gi|170278434	117	2	10
84	Hemocyanin		✓			✓	Respiratory	72	6.33	75	5.52	gi|170278434	102	2	10
90	Hemocyanin	✓					Respiratory	72	5.59	78	5.37	gi|170211405	113	2	11
94	Hemocyanin			✓			Respiratory	71	5.19	78	5.37	gi|170185161	100	3	14
95	Hemocyanin			✓		✓	Respiratory	70	6.04	75	5.52	gi|170278434	115	2	10
98	Hemocyanin			✓			Respiratory	69	5.02	78	5.37	gi|170185161	108	3	14
107	Hemocyanin					✓	Respiratory	67	5.65	78	5.37	gi|170185161	144	4	20
112	Hemocyanin			✓			Respiratory	70	5.85	78	5.37	gi|170185161	123	4	20
113	Hemocyanin			✓			Respiratory	67	5.58	78	5.37	gi|170185161	138	4	20
114	Hemocyanin			✓			Respiratory	69	4.40	78	5.37	gi|170185161	80	3	14
120	DD5 cuticle protein			✓		✓	Cuticle	69	4.48	138	5.43	gi|170216257	67	2	12
130	Hemocyanin			✓		✓	Respiratory	67	6.01	75	5.52	gi|170278434	104	2	10
131	NADP-dependent malic enzyme	✓					Energy metabolism	66	6.39	131	8.01	gi|170221448	74	2	12
132	Calreticulin			✓			Protein homeostasis	65	4.35	47	4.36	isotig01258	70	2	4
134	DD5 cuticle protein			✓			Cuticle	66	4.66	138	5.43	gi|170211011	65	2	13

Table 6 continued.

137	Aldehyde dehydrogenase	✓						Energy metabolism	64	4.62	53	5.78	gi|170242662	125	3	16
142	Hemocyanin			✓			✓	Respiratory	66	5.85	78	5.37	gi|170211405	49	2	11
143	DD5 cuticle protein		✓					Cuticle	64	4.74	138	5.43	gi|170211011	120	3	3
149	α-Tubulin				✓			Cytoskeletal	63	5.09	50	5.00	gi|170244245	170	5	25
153	α-Tubulin	✓						Cytoskeletal	62	5.16	50	5.00	gi|170244245	283	6	29
154	DD5 cuticle protein			✓				Cuticle	64	4.51	138	5.43	gi|170223047	69	2	12
155	F1-ATP synthase β-subunit	✓						Energy metabolism	61	5.19	56	5.03	gi|170245256	273	7	40
156	α-Tubulin	✓						Cytoskeletal	61	5.23	50	5.00	gi|170244245	288	6	32
157	Hemocyanin subunit 4	✓			✓			Respiratory	63	5.37	77	5.30	gi|170214816	152	6	27
158	Aldehyde dehydrogenase	✓						Energy metabolism	63	6.47	58	8.49	gi|170242661	89	2	10
162	Protein disulfide isomerase		✓			✓		Protein homeostasis	64	4.70	55	4.64	gi|170251897	187	5	29
163	Hemocyanin subunit 4	✓						Respiratory	62	5.31	77	5.30	gi|170214816	152	5	25
164	Hemocyanin			✓				Respiratory	64	5.88	78	5.37	gi|170185161	47	2	8
177	DD5 cuticle protein	✓						Cuticle	62	4.80	138	5.43	gi|170211011	97	2	7
179	Hemocyanin subunit 4						✓	Respiratory	63	5.70	77	5.30	gi|170214816	68	2	9
181	Endoplasmin (GRP 94)			✓				Protein homeostasis	61	4.72	91	4.87	isotig00944	170	5	11
183	α-Tubulin			✓				Cytoskeletal	61	5.26	50	5.00	isotig00591	84	3	8
184	F1-ATP synthase β-subunit			✓				Energy metabolism	61	4.75	56	5.31	gi|170221081	374	7	39
198	Glutamate dehydrogenase			✓			✓	Energy metabolism	61	6.79	62	7.00	gi|170195052	46	2	9
199	Hemocyanin				✓			Respiratory	58	5.42	78	5.49	gi|170214319	150	4	19
209	F1-ATP synthase β-subunit		✓					Energy metabolism	59	4.87	56	5.03	gi|170245256	153	5	28
210	Endoplasmin (GRP 94)		✓					Protein homeostasis	60	4.67	91	4.87	isotig00944	101	3	5
211	Hemocyanin				✓			Respiratory	59	5.36	78	5.37	gi|170211405	90	2	11
214	Phosphopyruvate hydratase	✓						Energy metabolism	56	6.82	47	6.18	isotig01921	117	4	12
221	Serine protease				✓			Protein homeostasis	56	4.58	56	5.11	gi|170259685	123	3	19
226	DD5 cuticle protein				✓			Cuticle	56	4.55	138	5.43	gi|170223047	133	3	22
228	β-Actin	✓						Cytoskeletal	54	5.52	42	5.30	isotig02875	272	6	24
231	Serine protease				✓			Protein homeostasis	56	4.64	44	5.07	gi|170236702	102	3	18
234	DD5 cuticle protein				✓			Cuticle	54	4.69	138	5.43	gi|170223047	139	3	22
245	Phosphopyruvate hydratase	✓						Energy metabolism	56	6.76	47	6.18	isotig01921	70	4	12

Table 6 continued.

249	DD5 cuticle protein	✓					Cuticle	55	4.41	138	5.43	gi|170223047	90	3	22
250	DD5 cuticle protein			✓			Cuticle	54	4.47	138	5.43	gi|170223047	112	3	22
251	BiP (GRP 78)			✓			Protein homeostasis	53	4.74	73	4.98	gi|170205314	257	7	24
254	DD5 cuticle protein			✓			Cuticle	54	4.61	138	5.43	gi|170223047	176	3	22
257	DD5 cuticle protein		✓				Cuticle	54	4.81	138	5.43	gi|170216257	59	2	12
258	Citrate synthase	✓					Energy metabolism	54	6.43	52	7.22	gi|170184486	52	3	15
264	Catalase			✓			Energy metabolism	53	6.51	59	6.58	gi|170216595	71	3	15
265	DD5 cuticle protein			✓			Cuticle	53	4.56	138	5.43	gi|170223047	162	3	22
268	Fumarylacetoacetase		✓				Energy metabolism	54	6.83	46	6.74	gi|170201843	110	4	19
271	Hemocyanin subunit 2	✓					Respiratory	51	5.51	76	5.51	gi|170225916	138	5	27
272	Hemocyanin α-subunit	✓		✓			Respiratory	54	5.66	77	5.37	gi|170206072	61	2	9
278	DD5 cuticle protein			✓			Cuticle	53	4.53	138	5.43	gi|170223047	191	3	22
280	β-Actin			✓			Cytoskeletal	53	5.63	42	5.30	gi|170198993	121	4	19
286	BiP (GRP 78)		✓			✓	Protein homeostasis	52	4.81	73	4.98	gi|170205314	166	3	12
287	α-Tubulin	✓		✓			Cytoskeletal	52	6.04	50	5.00	gi|170244245	270	7	36
292	DD5 cuticle protein			✓			Cuticle	51	4.63	138	5.43	gi|170223047	113	3	22
293	DD5 cuticle protein			✓			Cuticle	52	4.69	138	5.43	gi|170211011	48	2	13
295	DD5 cuticle protein			✓			Cuticle	52	4.59	138	5.43	gi|170211011	74	2	7
296	Hemocyanin subunit 6		✓				Respiratory	50	6.11	78	5.21	gi|170234586	91	3	19
300	F1-ATP synthase β-subunit					✓	Energy metabolism	51	5.34	56	5.31	gi|170221081	286	8	44
314	β-Actin			✓			Cytoskeletal	49	6.01	42	5.30	gi|170198993	89	4	19
316	α-Tubulin		✓				Cytoskeletal	50	5.71	50	5.00	gi|170244245	117	4	21
327	Arthrodial cuticle protein AMP16.3			✓			Cuticle	48	5.12	18	6.74	gi|170202504	312	8	36
328	Glyceraldehyde-3-phosphate dehydrogenase	✓					Energy metabolism	49	6.82	19	5.58	gi|170197231	73	3	21
329	DD5 cuticle protein		✓		✓		Cuticle	50	4.59	138	5.43	gi|170211011	54	2	13
335	Hemocyanin			✓			Respiratory	49	5.29	78	5.37	gi|170185161	109	5	29
336	Cathepsin D	✓					Protein homeostasis	48	5.91	42	6.00	gi|170218525	98	4	16
337	Glyceraldehyde-3-phosphate dehydrogenase			✓			Energy metabolism	49	6.64	19	5.58	gi|170197231	180	5	29
339	DD5 cuticle protein			✓			Cuticle	49	4.69	138	5.43	gi|170211011	90	3	16
344	DD5 cuticle protein			✓			Cuticle	48	4.42	138	5.43	gi|170211011	59	2	13

Table 6 continued.

347	β-Actin				✓			Cytoskeletal	48	5.35	42	5.30	gi|170188410	195	5	23
349	Arthrodial cuticle protein AMP16.3						✓	Cuticle	48	5.54	18	6.74	gi|170202504	230	7	30
350	DD5 cuticle protein			✓				Cuticle	47	4.47	138	5.43	gi|170211011	70	2	13
358	V-type proton ATPase subunit A	✓						Energy metabolism	47	5.79	71	5.20	gi|170210033	43	2	8
366	Pyruvate dehydrogenase E1 α-subunit			✓				Energy metabolism	47	6.10	43	8.59	gi|170246380	76	2	9
380	Pyruvate dehydrogenase E1 α-subunit			✓			✓	Energy metabolism	45	6.38	43	7.58	gi|170183821	73	2	10
391	α-Tubulin				✓			Cytoskeletal	45	5.54	50	5.00	gi|170244245	216	6	32
392	Serine protease						✓	Protein homeostasis	45	6.49	43	5.16	gi|170244245	72	2	7
393	β-Actin				✓			Cytoskeletal	44	5.12	42	5.30	gi|170188410	215	7	26
398	α-Tubulin				✓			Cytoskeletal	44	6.23	50	5.00	gi|170244245	182	5	24
401	β-Tubulin		✓					Cytoskeletal	45	6.44	43	5.76	gi|170189060	198	5	24
402	β-Actin						✓	Cytoskeletal	45	5.01	42	5.30	gi|170188410	185	6	26
403	β-Actin	✓						Cytoskeletal	45	4.95	42	5.30	gi|170185032	212	4	24
404	α-Tubulin				✓			Cytoskeletal	44	5.29	50	5.00	gi|170244245	179	4	21
405	Na/K ATPase β2-subunit			✓				Energy metabolism	44	5.81	38	6.01	gi|170279013	56	3	15
406	Hemocyanin subunit 4				✓			Respiratory	44	5.39	77	5.30	gi|170214816	77	3	13
407	β-Tubulin			✓				Cytoskeletal	44	6.01	51	4.88	gi|170189060	209	5	24
411	α-Tubulin				✓			Cytoskeletal	43	5.43	50	5.00	gi|170244245	237	6	32
412	α-Tubulin				✓			Cytoskeletal	44	5.57	50	5.00	gi|170244245	352	7	36
414	Transglutaminase				✓			Protein homeostasis	43	5.01	86	5.64	gi|170247915	46	3	11
415	β-Tubulin			✓			✓	Cytoskeletal	43	6.18	51	4.88	gi|170189060	192	6	24
417	Farnesoic acid O-methyltransferase		✓					Energy metabolism	41	4.42	31	4.64	gi|170186165	101	2	12
421	β-Tubulin			✓				Cytoskeletal	41	6.25	51	4.88	gi|170189060	226	8	31
427	α-Tubulin				✓			Cytoskeletal	42	5.40	50	5.00	gi|170244245	308	7	36
428	β-Tubulin	✓						Cytoskeletal	42	5.83	51	4.88	gi|170189060	113	5	13
430	β-Actin				✓			Cytoskeletal	42	5.75	42	5.30	gi|170185032	116	3	19
436	Farnesoic acid O-methyltransferase	✓						Energy metabolism	41	4.59	31	4.64	gi|170186165	87	2	12
440	β-Tubulin				✓			Cytoskeletal	42	5.04	51	4.88	gi|170186360	58	2	9
444	Neurogenic notch-like	✓						Energy metabolism	41	4.18	1364	5.17	gi|170197496	47	2	9
448	Hemocyanin				✓			Respiratory	41	4.92	78	5.37	gi|170185161	77	3	14

Table 6 continued.

449	β-Tubulin				✓			Cytoskeletal	41	5.68	51	4.88	gi|170189060	194	4	19
451	α-Tubulin				✓			Cytoskeletal	41	5.37	50	5.00	gi|170244245	197	5	25
452	β-Tubulin			✓				Cytoskeletal	40	5.96	51	4.88	gi|170189060	190	6	19
453	Peritrophin A			✓				Protein homeostasis	41	4.12	25	5.88	gi|170213195	55	2	7
455	Testisin-like serine protease						✓	Protein homeostasis	41	4.87	32	9.33	gi|170227739	121	4	15
456	β-Tubulin	✓					✓	Cytoskeletal	41	6.33	51	4.88	gi|170189060	65	2	7
457	Argininosuccinate synthetase 1						✓	Energy metabolism	40	6.66	47	6.07	gi|170239511	50	2	7
458	Argininosuccinate synthetase 1			✓				Energy metabolism	40	6.77	47	6.07	gi|170239511	66	3	12
459	β-Tubulin				✓			Cytoskeletal	41	5.76	51	4.88	gi|170192063	102	4	18
460	β-Tubulin			✓				Cytoskeletal	41	6.30	51	4.88	gi|170189060	136	5	19
463	F1F0-ATP synthase β-subunit				✓			Energy metabolism	40	5.24	56	4.98	gi|170205333	57	3	19
467	β-actin				✓			Cytoskeletal	39	4.98	42	5.38	gi|170185032	129	3	19
470	β-Tubulin						✓	Cytoskeletal	40	5.93	51	4.88	gi|170189060	109	3	14
477	Serine protease				✓			Protein homeostasis	39	4.81	31	4.71	gi|170234166	81	4	21
490	F1-ATP synthase β-subunit						✓	Energy metabolism	37	5.27	56	5.31	gi|170221081	371	9	48
494	β-Tubulin				✓			Cytoskeletal	38	5.36	51	4.88	gi|170192063	278	6	23
495	β-Tubulin	✓						Cytoskeletal	38	5.51	51	4.88	gi|170192063	230	5	23
498	β-Tubulin		✓				✓	Cytoskeletal	37	5.30	51	4.88	gi|170192063	125	4	17
502	β-actin				✓			Cytoskeletal	37	5.06	42	5.30	gi|170188410	231	6	26
506	Dihydrolipoyl dehydrogenase				✓			Energy metabolism	37	6.44	54	7.17	gi|170262454	63	2	8
510	F1-ATP synthase β-subunit	✓					✓	Energy metabolism	38	4.85	56	5.03	gi|170245256	189	5	29
513	Hemocyanin				✓			Respiratory	37	5.72	75	5.52	gi|170278434	52	2	10
514	NADP-dependent malic enzyme	✓						Energy metabolism	36	6.33	131	8.01	gi|170221448	107	4	25
521	Cathepsin B			✓		✓		Protein homeostasis	35	5.93	37	7.53	gi|170204440	113	4	13
522	ATP synthase α-subunit				✓			Energy metabolism	36	6.68	59	9.01	isotig00596	42	2	4
525	β-actin	✓						Cytoskeletal	36	5.01	42	5.30	gi|170185032	122	3	19
531	Aldehyde dehydrogenase		✓					Energy metabolism	35	6.04	53	6.25	gi|170242662	118	4	20
536	α-Tubulin				✓			Cytoskeletal	35	5.33	50	5.00	gi|170244245	196	5	23
538	β-actin	✓			✓			Cytoskeletal	35	5.70	42	5.30	gi|170186899	126	3	16
542	β-1,3-D-glucan binding protein				✓			Protein homeostasis	34	5.27	152	6.00	gi|170249859	74	4	22

Table 6 continued.

543	Peritrophin A		✓					Protein homeostasis	35	4.39	25	5.88	gi|170213195	50	2	7
547	RR-2 cuticle protein			✓	✓			Cuticle	35	6.46	22	7.75	gi|170222048	70	3	14
548	DD5 cuticle protein	✓				✓		Cuticle	34	4.57	138	5.43	gi|170223047	65	2	12
550	β-Tubulin				✓			Cytoskeletal	34	5.11	51	4.88	gi|170189060	162	3	14
556	β-Tubulin				✓			Cytoskeletal	34	4.99	51	4.88	gi|170192063	100	4	17
557	Arginine kinase		✓					Energy metabolism	34	6.41	40	6.34	gi|170200859	179	7	24
560	Proteasome α-subunit type 6		✓					Protein homeostasis	34	6.36	28	7.58	gi|170187668	70	2	9
561	Arginine kinase				✓			Energy metabolism	34	6.64	40	6.19	gi|170186144	198	7	31
564	Tentative cuticle protein			✓				Cuticle	34	6.47	13	8.51	gi|170205039	65	2	10
568	Dihydrolipoyl dehydrogenase	✓						Energy metabolism	34	5.82	54	7.17	gi|170262454	60	3	13
569	Glyceraldehyde-3-phosphate dehydrogenase						✓	Energy metabolism	34	6.74	19	5.58	gi|170197231	85	3	18
573	Peritrophin A		✓			✓		Protein homeostasis	33	4.40	25	5.88	gi|170213195	128	4	19
574	α-Tubulin				✓			Cytoskeletal	34	5.33	50	5.00	gi|170211387	87	2	12
577	β-Actin					✓		Cytoskeletal	34	5.71	42	5.30	gi|170186899	143	3	16
582	α-Tubulin				✓			Cytoskeletal	33	5.49	50	5.00	gi|170244245	190	5	23
594	Hemocyanin				✓			Respiratory	32	5.45	78	5.37	gi|170185161	74	3	14
596	β-Tubulin	✓						Cytoskeletal	32	4.79	51	4.88	isotig00502	35	3	7
597	β-Tubulin				✓			Cytoskeletal	31	4.86	51	4.88	gi|170186360	275	6	27
601	F1-ATP synthase β-subunit				✓			Energy metabolism	32	5.41	56	5.31	gi|170221081	328	8	41
602	HSP 70			✓				Protein homeostasis	32	6.74	71	5.37	gi|170220788	106	4	21
608	Peritrophin A				✓			Protein homeostasis	31	4.56	25	5.88	gi|170213195	63	2	7
611	F1-ATP synthase β-subunit				✓			Energy metabolism	31	5.22	56	5.31	gi|170198456	173	6	30
613	6-phosphogluconolactonase	✓			✓			Energy metabolism	31	6.01	27	6.83	gi|170206777	89	4	17
621	Arginine kinase	✓						Energy metabolism	31	5.85	40	6.19	gi|170187671	74	4	20
622	Hemocyanin			✓				Respiratory	31	6.31	78	5.37	gi|170185161	77	5	29
641	Arginine kinase			✓	✓			Energy metabolism	30	6.03	40	6.05	gi|170187671	53	4	17
667	GPI-linked carbonic anhydrase					✓		Energy metabolism	28	6.37	34	7.13	gi|170245757	49	2	8
669	Arginine kinase		✓					Energy metabolism	27	5.20	40	6.19	gi|585342	60	2	6
679	β-Actin				✓			Cytoskeletal	26	5.01	42	5.30	gi|170185032	112	3	14
686	Rho GDP-dissociation inhibitor			✓				Energy metabolism	26	4.97	23	5.14	gi|170196449	50	3	15

Table 6 continued.

690	β-Actin				✓			Cytoskeletal	26	5.20	42	5.30	gi|10304437	64	2	6
695	Peroxiredoxin				✓			Energy metabolism	26	5.50	22	5.48	gi|170196483	45	2	7
700	Malate dehydrogenase		✓				✓	Energy metabolism	25	6.52	35	9.42	gi|170204397	43	2	9
701	β-Actin		✓					Cytoskeletal	25	4.96	42	5.30	gi|170185032	92	3	14
715	Hemocyanin				✓			Respiratory	20	6.23	75	5.52	gi|170187274	103	4	17
716	α-Tubulin					✓		Cytoskeletal	23	5.55	50	5.00	gi|170211387	137	3	17
717	Hemocyanin				✓			Respiratory	22	6.42	75	5.52	gi|170187274	161	5	17
737	Hemocyanin			✓				Respiratory	21	6.41	75	5.52	gi|170187274	180	5	17
740	Cuticle protein 6	✓						Cuticle	20	5.66	22	4.89	gi|170220180	114	2	10
752	β-Tubulin	✓						Cytoskeletal	19	4.60	51	4.88	gi|170191148	46	2	8
754	Hemocyanin				✓			Respiratory	19	6.28	75	5.52	gi|170187274	87	4	13
756	β-Tubulin	✓						Cytoskeletal	19	4.64	51	4.88	gi|170191148	60	5	26
758	Hemocyanin			✓				Respiratory	19	6.22	75	5.52	gi|170187274	102	4	13
780	Lectin E		✓				✓	Protein homeostasis	16	5.80	18	5.74	gi|170195268	106	4	26
783	Actin E				✓			Cytoskeletal	15	5.25	26	5.07	gi|170188410	127	3	15
785	DD9A cuticle protein	✓						Cuticle	13	4.07	14	4.09	gi|170191353	107	3	14
799	C-type lectin			✓				Protein homeostasis	13	6.56	32	4.51	gi|170197799	43	2	7
802	β-Actin				✓			Cytoskeletal	14	4.89	42	5.30	gi|170185032	54	2	11
803	Hemocyanin			✓	✓			Respiratory	14	5.86	78	5.37	gi|170185161	102	6	35
807	Actin E				✓			Cytoskeletal	14	5.25	26	5.07	gi|170188410	111	3	15
811	Arthrodial cuticle protein AMP16.3			✓		✓		Cuticle	10	4.16	18	6.74	gi|170191641	111	3	23
819	Arthrodial cuticle protein AMP16.3			✓	✓			Cuticle	8	4.42	18	6.74	gi|170211697	69	3	20
823	Hemocyanin γ subunit 1	✓						Respiratory	10	5.91	77	5.55	gi|170183126	42	3	16
828	Arthrodial cuticle protein AMP16.3	✓						Cuticle	9	5.34	18	6.74	gi|170213139	56	3	11
834	Hemocyanin				✓			Respiratory	21	6.72	75	5.52	gi|170187274	96	5	22

Table 7. Loading values for principal components associated with a tidal (emersion) effect. The positive and negative loadings values are given for proteins that significantly changed in abundance in response to tidal treatment. Only the top 10 contributing proteins identified using MS/MS are indicated.

	Principle Component 1		Principle Component 2	
Component Loading Rank	Protein (Spot ID)	Loading Value	Protein (Spot ID)	Loading Value
	Positive Loadings for Emersion Effect			
	(a)		(c)	
1	Cathepsin D (336)	1.4580	DD5 cuticle protein (41)	2.1472
2	Argininosuccinate synthetase 1 (458)	1.3349	DD5 cuticle protein (35)	1.9192
3	Hemocyanin (79)	1.3255	DD5 cuticle protein (13)	1.5624
4	β-Actin (77)	1.3166	DD5 cuticle protein (29)	1.5594
5	Hemocyanin (76)	1.2902	DD5 cuticle protein (120)	1.4615
6	β-Actin (75)	1.2842	β-Actin (538)	1.3697
7	Na^+/K^+ ATPase β2-subunit (405)	1.2836	Na^+/K^+ ATPase β2-subunit (405)	1.2927
8	α-Tubulin (183)	1.2515	DD5 cuticle protein (134)	1.2631
9	DD5 cuticle protein (26)	1.2386	β-Tubulin (460)	1.1485
10	α-Tubulin (156)	1.2345	Arthrodial cuticle protein AMP16.3 (828)	1.1149
	Negative Loadings for Emersion Effect			
	(b)		(d)	
1	DD5 cuticle protein (249)	-1.3745	Fumarylacetoacetase (268)	-2.6209
2	DD5 cuticle protein (20)	-1.2296	β-Tubulin (415)	-2.1301
3	Arthrodial cuticle protein AMP16.3 (811)	-1.2198	Aldehyde dehydrogenase (158)	-1.7833
4	Hemocyanin (622)	-1.2114	β-Actin (228)	-1.6988
5	Hemocyanin γ-subunit (823)	-1.1769	NADP-dependent malic enzyme (131)	-1.6481
6	β-Actin (403)	-1.1443	DD5 cuticle protein (18)	-1.5673
7	β-Tubulin (596)	-1.1383	β-Actin (525)	-1.5456
8	β-Tubulin (752)	-1.1374	F1-ATP synthase β-subunit (510)	-1.5268
9	β-Tubulin (756)	-1.1230	Glyceraldehyde-3-phosphate dehydrogenase (328)	-1.5008
10	β-Tubulin (428)	-1.1067	α-Tubulin (316)	-1.4718

Table 8. Loading values for principal components associated with a pH effect. The positive and negative loadings values are given for proteins that significantly changed in abundance in response to pH treatment. Only the top 10 contributing proteins identified using MS/MS are indicated.

	Principle Component 1		Principle Component 2	
Component Loading Rank	Protein (Spot ID)	Loading Value	Protein (Spot ID)	Loading Value
	Positive Loadings for pH Effect			
	(a)		(c)	
1	Na^+/K^+ ATPase β2-subunit (405)	1.5937	DD5 cuticle protein (120)	2.0735
2	DD5 cuticle protein (35)	1.5470	DD5 cuticle protein (42)	1.4541
3	β-Tubulin (460)	1.5081	Arthrodial cuticle protein AMP16.3 (819)	1.4187
4	DD5 cuticle protein (41)	1.4569	β-Actin (701)	1.0814
5	Tentative cuticle protein (564)	1.4209	DD5 cuticle protein (23)	1.0208
6	DD5 cuticle protein (134)	1.4111	DD5 cuticle protein (24)	0.9260
7	β-Tubulin (421)	1.3708	Peritrophin A (573)	0.8330
8	DD5 cuticle protein (29)	1.3489	DD5 cuticle protein (20)	0.7764
9	Argininosuccinate synthetase 1 (458)	1.3487	DD5 cuticle protein (40)	0.6843
10	DD5 cuticle protein (40)	1.3415	Hemocyanin (622)	0.6754
	Negative Loadings for pH Effect			
	(b)		(d)	
1	Calreticulin (132)	-1.4568	Fumarylacetoacetase (268)	-2.4983
2	Arginine kinase (669)	-1.2539	BiP (GRP 78) (286)	-2.2790
3	Arthrodial cuticle protein AMP16.3 (819)	-1.2394	Proteasome α-subunit type 6 (560)	-1.9081
4	DD5 cuticle protein (18)	-1.2261	Hemocyanin (69)	-1.4756
5	DD5 cuticle protein (20)	-1.2227	Protein disulfide isomerase (162)	-1.3866
6	Hemocyanin (622)	-1.1979	Hemocyanin (84)	-1.3648
7	Arthrodial cuticle protein AMP16.3 (811)	-1.1937	Argininosuccinate synthetase 1 (458)	-1.3255
8	β-Tubulin (452)	-1.1539	Lectin E (780)	-1.1234
9	Serine protease masquerade-like (14)	-1.1128	Malate dehydrogenase (700)	-1.1117
10	DD5 cuticle protein (24)	-1.0874	Serine protease masquerade-like (14)	-1.0659

Table 9. Loading values for principal components associated with a tidal (emersion) x pH interaction. The positive and negative loadings values are given for proteins that significantly changed in abundance in response to a tidal x pH interaction effect. Only the top 10 contributing proteins identified using MS/MS are indicated.

	Principle Component 1		Principle Component 2	
Component Loading Rank	Protein (Spot ID)	Loading Value	Protein (Spot ID)	Loading Value
	Positive Loadings for Emersion x pH Interaction Effect			
	(a)		(c)	
1	β-Tubulin (460)	1.4308	β-Tubulin (407)	1.9372
2	Tentative cuticle protein (564)	1.3915	DD5 cuticle protein (43)	1.8249
3	Argininosuccinate synthetase 1 (458)	1.3828	DD5 cuticle protein (41)	1.7278
4	Na^+/K^+ ATPase β2-subunit (405)	1.3341	DD5 cuticle protein (29)	1.6323
5	α-Tubulin (183)	1.3247	Hemocyanin (112)	1.4786
6	β-Tubulin (421)	1.2838	Na^+/K^+ ATPase β2-subunit (405)	1.4690
7	DD5 cuticle protein (134)	1.2599	DD5 cuticle protein (26)	1.4129
8	DD5 cuticle protein (26)	1.2567	Hemocyanin subunit 6 (296)	1.2996
9	Hemocyanin (78)	1.1790	Hemocyanin (737)	1.2802
10	DD5 cuticle protein (154)	1.1691	β-Tubulin (421)	1.1966
	Negative Loadings for Emersion x pH Interaction Effect			
	(b)		(d)	
1	Hemocyanin (758)	-1.2667	α-Tubulin (316)	-2.3994
2	Hemocyanin (737)	-1.2221	C-type lectin (799)	-1.3521
3	DD5 cuticle protein (45)	-1.2071	β-Tubulin (452)	-1.2672
4	Arginine kinase (641)	-1.1977	Pyruvate dehydrogenase E1 α-subunit (380)	-1.1600
5	DD5 cuticle protein (23)	-1.1190	Calreticulin (132)	-1.1589
6	Hemocyanin (130)	-1.0904	DD5 cuticle protein (350)	-0.9087
7	Calreticulin (132)	-1.0229	RR-2 cuticle protein (547)	-0.6861
8	Hemocyanin subunit 6 (296)	-1.0059	DD5 cuticle protein (548)	-0.6362
9	Hemocyanin (142)	-1.0011	Peritrophin A (453)	-0.5181
10	Hemocyanin (164)	-0.9628	DD5 cuticle protein (17)	-0.4635

Table 10. Loading values for principal components associated with a temperature effect. The positive and negative loadings values are given for proteins that significantly changed in abundance in response to temperature treatment. Only the top 10 contributing proteins identified using MS/MS are indicated.

	Principle Component 1		Principle Component 2	
Component Loading Rank	Protein (Spot ID)	Loading Value	Protein (Spot ID)	Loading Value
	Positive Loadings for Temperature Effect			
	(a)		(c)	
1	Glyceraldehyde-3-phosphate dehydrogenase (337)	1.4132	6-Phosphogluconolactonase (613)	1.5566
2	Arginine kinase (561)	1.3977	Peritrophin A (608)	1.4153
3	Hemocyanin α-subunit (16)	1.3645	Hemocyanin subunit 4 (406)	1.4122
4	Hemocyanin subunit 3 (74)	1.3516	Arthrodial cuticle protein AMP16.3 (819)	1.4039
5	α-Tubulin (398)	1.3052	BiP (GRP 78) (251)	1.3890
6	β-Actin (280)	1.2952	Serine protease (231)	1.3835
7	Hemocyanin α-subunit (272)	1.2751	DD5 cuticle protein (43)	1.3071
8	ATP synthase α-subunit (522)	1.2721	DD5 cuticle protein (27)	1.2949
9	Hemocyanin (47)	1.2531	F1-ATP synthase β-subunit (300)	1.2423
10	DD5 cuticle protein (73)	1.2472	DD5 cuticle protein (35)	1.1890
	Negative Loadings for Temperature Effect			
	(b)		(d)	
1	β-Actin (679)	-1.5747	Hemocyanin subunit 4 (179)	-2.4196
2	β-Tubulin (459)	-1.5744	Hemocyanin (107)	-2.3864
3	β-Tubulin (597)	-1.5591	Arthrodial cuticle protein AMP16.3 (349)	-2.2616
4	Hemocyanin (594)	-1.5529	Hemocyanin (84)	-2.2452
5	α-Tubulin (451)	-1.5520	β-Tubulin (470)	-2.1512
6	DD5 cuticle protein (227)	-1.5492	β-Tubulin (456)	-2.0459
7	Hemocyanin (513)	-1.5475	β-Tubulin (498)	-1.9783
8	DD5 cuticle protein (292)	-1.5436	β-Actin (502)	-1.9119
9	DD5 cuticle protein (265)	-1.5400	α-Tubulin (391)	-1.8033
10	Actin E (783)	-1.5306	β-Tubulin (449)	-1.8030

Table 11. Loading values for principal components associated with a pH effect. The positive and negative loadings values are given for proteins that significantly changed in abundance in response to pH treatment. Only the top 10 contributing proteins identified using MS/MS are indicated.

	Principle Component 1		Principle Component 2	
Component Loading Rank	Protein (Spot ID)	Loading Value	Protein (Spot ID)	Loading Value
	Positive Loadings for pH Effect			
	(a)		(c)	
1	α-Tubulin (419)	1.2699	β-Actin (577)	1.7761
2	DD5 cuticle protein (548)	1.2439	DD5 cuticle protein (25)	1.1959
3	Peritrophin A (573)	1.2421	Peritrophin A (573)	1.1956
4	GPI-linked carbonic anhydrase (667)	1.2125	Serine protease testisin-like (455)	1.1110
5	Arthrodial cuticle protein AMP16.3 (349)	1.2095	Arthrodial cuticle protein AMP16.3 (811)	1.0829
6	Hemocyanin subunit 4 (179)	1.1866	α-Tubulin (419)	1.0099
7	Serine protease testisin-like (455)	1.1777	BiP (GRP 78) (286)	0.6823
8	Hemocyanin (107)	1.1632	β-Tubulin (456)	0.5850
9	β-Tubulin (470)	1.1625	α-Tubulin (716)	0.5482
10	β-Tubulin (456)	1.1509	Hemocyanin (142)	0.5079
	Negative Loadings for pH Effect			
	(b)		(d)	
1	Hemocyanin (78)	-1.2453	β-Actin (75)	-1.3885
2	β-Tubulin (415)	-1.1118	β-Tubulin (415)	-1.3333
3	Protein disulfide isomerase (162)	-1.0980	Pyruvate dehydrogenase E1 α-subunit (390)	-0.9020
4	Pyruvate dehydrogenase E1 α-subunit (380)	-1.0965	Cathepsin B (521)	-0.8607
5	β-Actin (75)	-1.0084	Protein disulfide isomerase (162)	-0.7673
6	α-Tubulin (716)	-0.9399	Hemocyanin (78)	-0.7043
7	Arthrodial cuticle protein AMP16.3 (811)	-0.8565	DD5 cuticle protein (548)	-0.5629
8	Hemocyanin (63)	-0.7928	Hemocyanin subunit 4 (179)	-0.3430
9	β-Actin (577)	-0.7054	Arthrodial cuticle protein AMP16.3 (349)	-0.0944
10	DD5 cuticle protein (25)	-0.6959	Hemocyanin (63)	-0.0757

Table 12. Loading values for principal components associated with a temperature x pH interaction. The positive and negative loadings values are given for proteins that significantly changed in abundance in response to a temperature x pH interaction effect. Only the top 10 contributing proteins identified using MS/MS are indicated.

	Principle Component 1		Principle Component 2	
Component Loading Rank	Protein (Spot ID)	Loading Value	Protein (Spot ID)	Loading Value
	Positive Loadings for Temperature x pH Interaction Effect			
	(a)		(c)	
1	Hemocyanin (69)	1.5148	Serine protease testisin-like (455)	2.0293
2	Serine protease (392)	1.4988	DD5 cuticle protein (30)	1.8019
3	Fibrillin-2 (60)	1.3478	F1-ATP synthase β-subunit (510)	1.7548
4	Glyceraldehyde-3-phosphate dehydrogenase (569)	1.2158	F1-ATP synthase β-subunit (490)	1.6724
5	Glutamate dehydrogenase (198)	1.2135	β-Tubulin (498)	1.5406
6	Argininosuccinate synthetase 1 (457)	1.2098	Lectin E (780)	1.4410
7	Malate dehydrogenase (700)	1.2019	DD5 cuticle protein (33)	1.4401
8	Hemocyanin (84)	0.9813	DD5 cuticle protein (24)	1.3870
9	Pyruvate dehydrogenase E1 α-subunit (380)	0.9523	β-Tubulin (470)	1.3844
10	β-Actin (402)	0.8636	F1-ATP synthase β-subunit (300)	1.2452
	Negative Loadings for Temperature x pH Interaction Effect			
	(b)		(d)	
1	DD5 cuticle protein (28)	-1.6269	Hemocyanin (95)	-1.5839
2	DD5 cuticle protein (25)	-1.5444	Hemocyanin (130)	-1.4269
3	DD5 cuticle protein (13)	-1.4477	Argininosuccinate synthetase 1 (457)	-0.6452
4	DD5 cuticle protein (27)	-1.4259	Glyceraldehyde-3-phosphate dehydrogenase (569)	-0.5603
5	DD5 cuticle protein (43)	-1.3571	Hemocyanin (142)	-0.4784
6	DD5 cuticle protein (22)	-1.3440	Glutamate dehydrogenase (198)	-0.3900
7	Hemocyanin (142)	-1.3371	Fibrillin-2 (60)	-0.3198
8	F1-ATP synthase β-subunit (300)	-1.2717	DD5 cuticle protein (25)	-0.3194
9	DD5 cuticle protein (120)	-0.9623	DD5 cuticle protein (28)	-0.2759
10	Hemocyanin (130)	-0.9085	Hemocyanin (69)	-0.1386

Table 13. Water chemistry parameters in the multi-stress experiment. Parameters were calculated in R (v 3.1.1) using SeaCarb (v 3.0.6). For the relevant parameters, significance (indicated by *) between ambient and low pH treatments was evaluated using Welch's t-test.

Parameter	Ambient pH (pH 8.1)	Low pH (pH 7.6)	d.f.	T-statistic	P
Salinity	33.75 ± 0.28	33.48 ± 0.38			
Temperature (ºC)	22.50 ± 0.50	21.50 ± 0.50			
pH_T	8.12 ± 0.02	7.61 ± 0.03	5.05	-15.24	< 0.001*
DIC	2451.81 ± 119.49	2679.16 ± 177.51	5.26	1.06	0.33
TA (µequiv kg-1)	2814.85 ± 130.14	2761.12 ± 188.22	5.34	-0.23	0.82
pCO_2 (µatm)	404.45 ± 34.17	1532.60 ± 53.39	5.10	17.80	< 0.001*
$[HCO_3^-]$ (µmol kg^{-1})	2164.83 ± 107.28	2536.14 ± 166.54	5.12	1.87	0.12
$[CO_3^{2-}]$ (µmol kg^{-1})	274.72 ± 13.13	95.03 ± 11.46	5.89	-10.31	< 0.001*
Ω_{cal}	4.35 ± 0.21	1.50 ± 0.18	5.90	-10.29	< 0.001*
Ω_{ara}	6.66 ± 0.32	2.30 ± 0.28	5.85	-10.17	< 0.001*

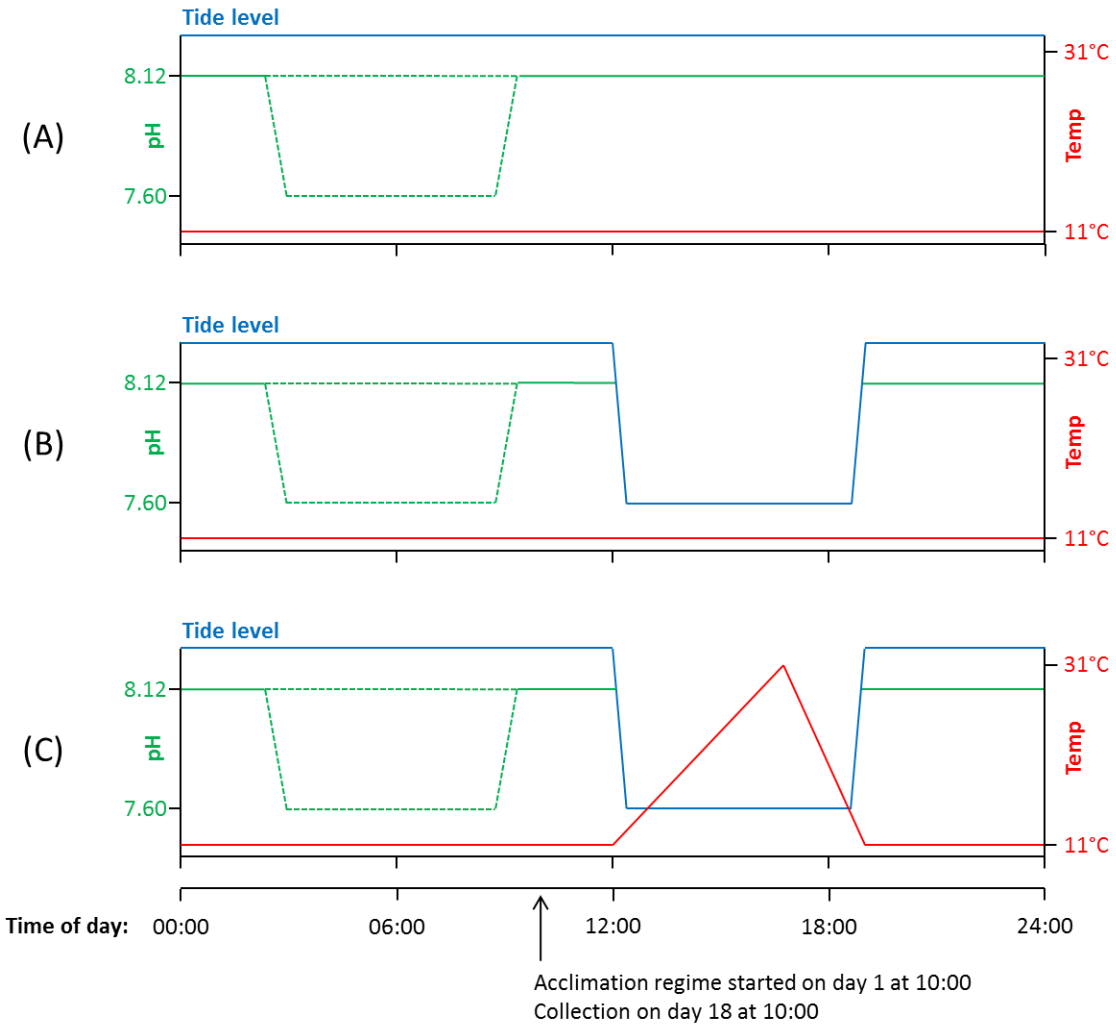

Figure 18. Representation of the experimental design illustrating the 24-hour acclimation cycles of each tank. (A) Crabs in Tank 1 experienced constant emersion at 11°C, but pH varied nocturnally for one half of the individual subjects (ambient pH 8.1 versus pH 7.6) from 03:00 to 8:00. (B) Crabs in Tank 2 experienced a similar cycle except for a 6-hour emersion event between 12:00 and 18:00. (C) Crabs in Tank 3 experienced an acclimation cycle identical to those in Tank 2 except for a thermal stress event concurrent with emersion where temperature ramped up to a maximum ranging from 22-31°C, depending on the day of the experiment (see Materials and Methods). Solid lines indicate all crabs experienced the denoted condition. Dotted lines indicate one half of the crabs received the denoted treatment (applies to pH treatment only).

Figure 19. Fused gel image (proteome map) of all gels depicting 835 protein spots from gill tissue of the intertidal porcelain crab *Petrolisthes cinctipes*. The proteome map represents average pixel volumes for each protein spot. Numbered spots were those that changed abundance in response to pH, tidal (immersion/emersion), and temperature treatments (two-way permutation ANOVA; P≤0.05) and were identified using tandem mass spectrometry (for identifications see Table 6).

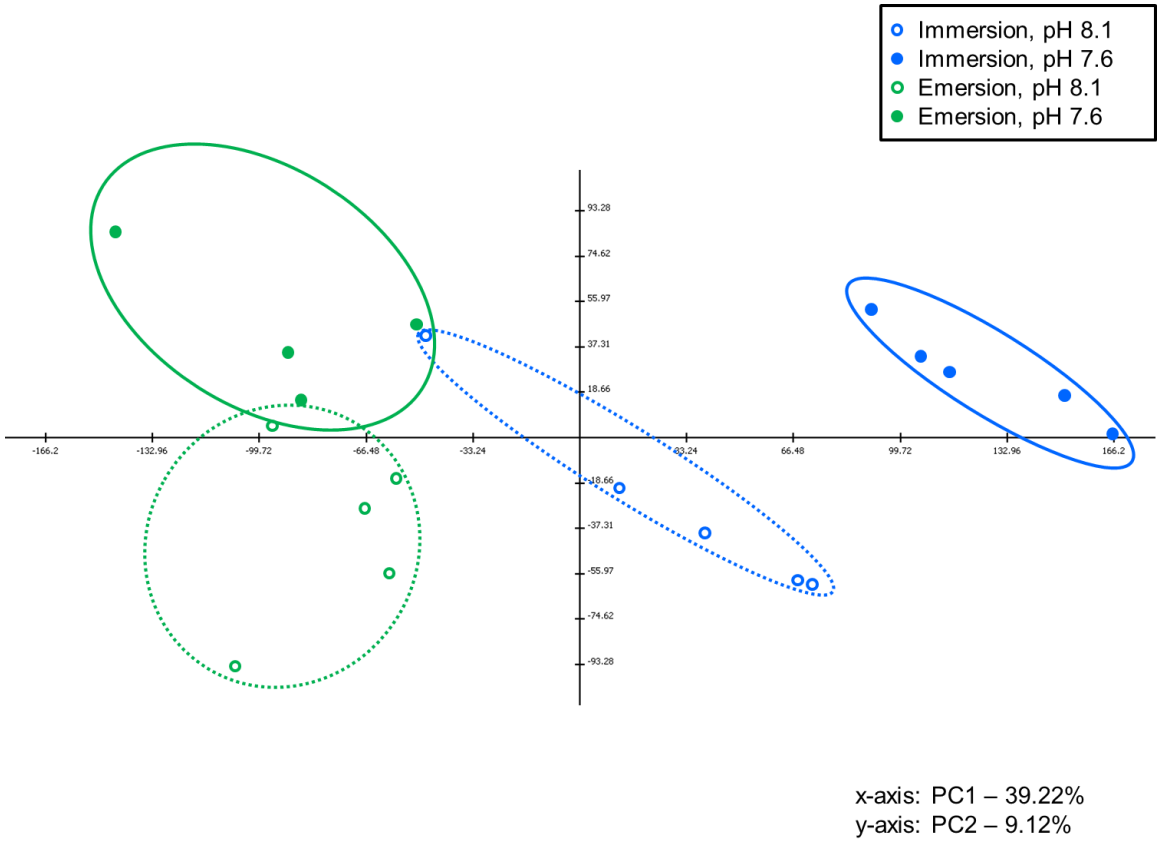

Figure 20A. Principal component analysis (PCA) of all proteins that changed in abundance in response to tidal (emersion) variation. Analysis is based on a 2-way ANOVA, $p \leq 0.05$, 1000 permutations. Each treatment is represented by color for tidal regime (blue = constant immersion, green = 6 h emersion) and shape continuity for pH treatment (striated line/hollow dot = pH 8.1, solid line/solid dot= pH 7.6). Dots represent a gill tissue sample from an individual crab, whereas larger circles encompass the general area where all gels of a particular treatment group are plotted. Principal components 1 and 2 (PC1 and PC2) and the percentage of the selected data (significant proteins) they explain are shown.

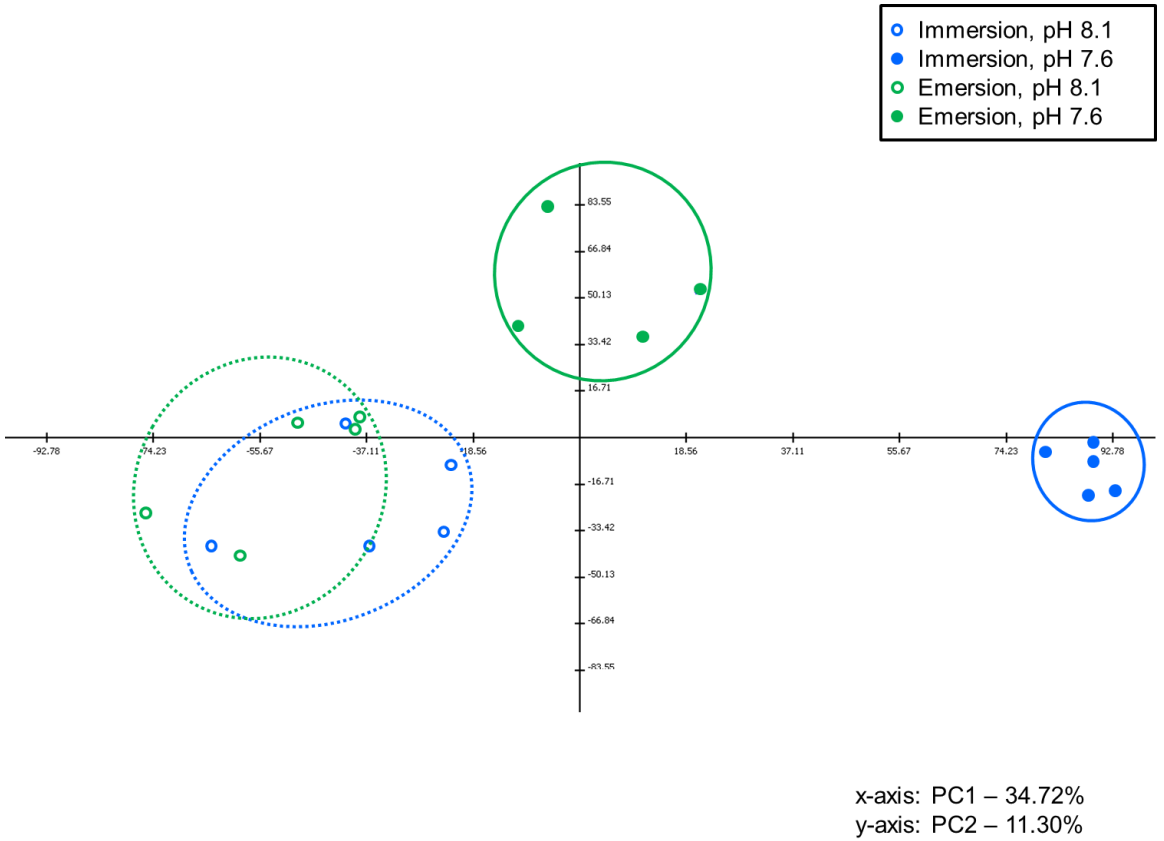

Figure 20B. Principal component analysis (PCA) of all proteins that changed in abundance in response to pH variation. Analysis is based on a 2-way ANOVA, $p \leq 0.05$, 1000 permutations. Each treatment is represented by color for tidal regime (blue = constant immersion, green = 6 h emersion) and shape continuity for pH treatment (striated line/hollow dot = pH 8.1, solid line/solid dot= pH 7.6). Dots represent a gill tissue sample from an individual crab, whereas larger circles encompass the general area where all gels of a particular treatment group are plotted. Principal components 1 and 2 (PC1 and PC2) and the percentage of the selected data (significant proteins) they explain are shown.

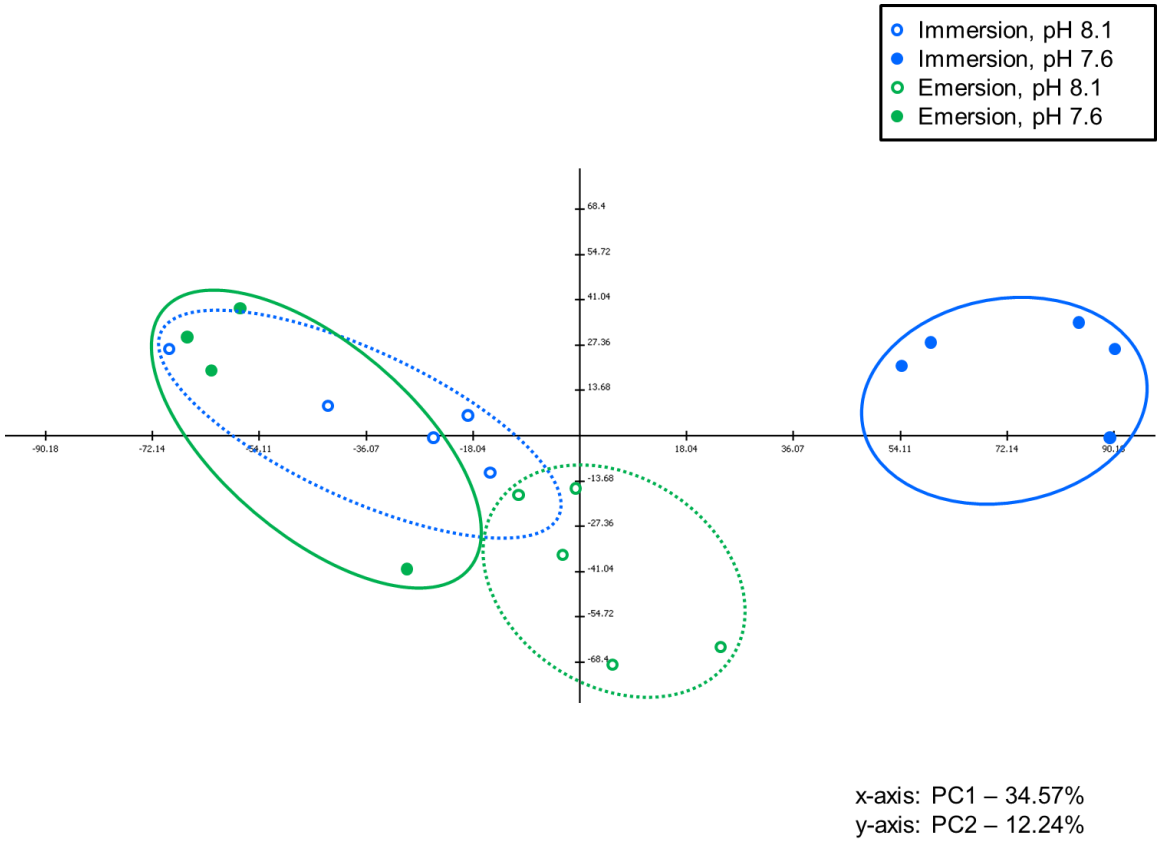

Figure 20C. Principal component analysis (PCA) of all proteins that changed in abundance in response to an interaction of tidal and pH variation. Analysis is based on a 2-way ANOVA, $p \leq 0.05$, 1000 permutations. Each treatment is represented by color for tidal regime (blue = constant immersion, green = 6 h emersion) and shape continuity for pH treatment (striated line/hollow dot = pH 8.1, solid line/solid dot= pH 7.6). Dots represent a gill tissue sample from an individual crab, whereas larger circles encompass the general area where all gels of a particular treatment group are plotted. Principal components 1 and 2 (PC1 and PC2) and the percentage of the selected data (significant proteins) they explain are shown.

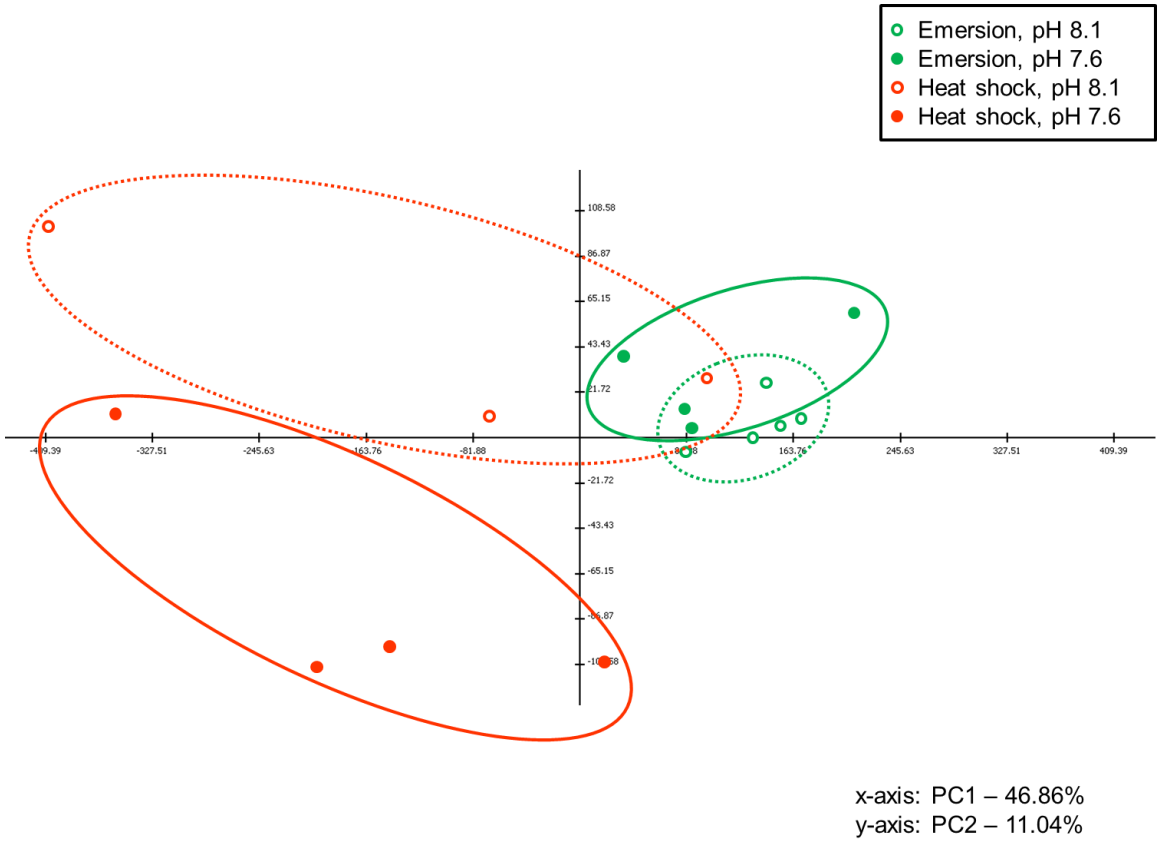

Figure 21A. Principal component analysis (PCA) of all proteins that changed in abundance in response to temperature variation. Analysis is based on a 2-way ANOVA, $p \leq 0.05$, 1000 permutations. Each treatment is represented by color for tidal regime (blue = constant immersion, green = 6 h emersion) and shape continuity for pH treatment (striated line/hollow dot = pH 8.1, solid line/solid dot= pH 7.6). Dots represent a gill tissue sample from an individual crab, whereas larger circles encompass the general area where all gels of a particular treatment group are plotted. Principal components 1 and 2 (PC1 and PC2) and the percentage of the selected data (significant proteins) they explain are shown.

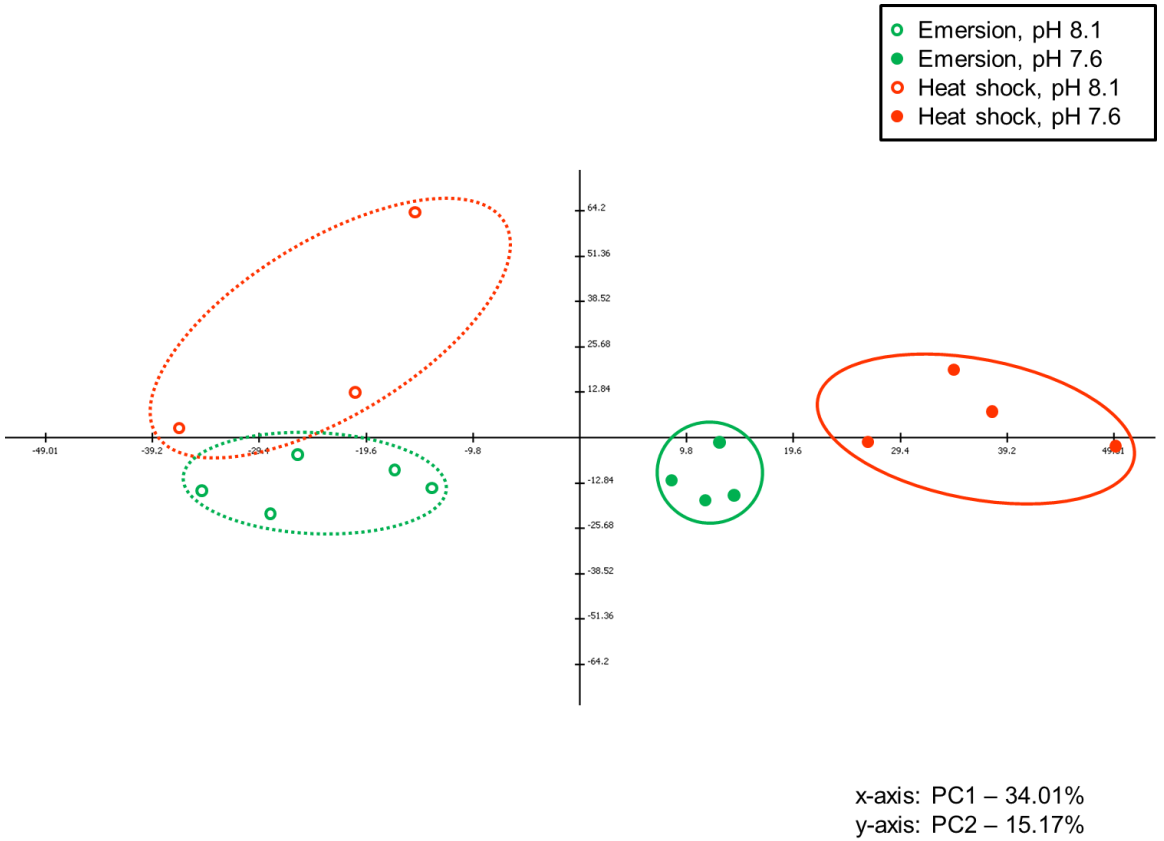

Figure 21B. Principal component analysis (PCA) of all proteins that changed in abundance in response to pH variation. Analysis is based on a 2-way ANOVA, $p \leq 0.05$, 1000 permutations. Each treatment is represented by color for tidal regime (blue = constant immersion, green = 6 h emersion) and shape continuity for pH treatment (striated line/hollow dot = pH 8.1, solid line/solid dot= pH 7.6). Dots represent a gill tissue sample from an individual crab, whereas larger circles encompass the general area where all gels of a particular treatment group are plotted. Principal components 1 and 2 (PC1 and PC2) and the percentage of the selected data (significant proteins) they explain are shown.

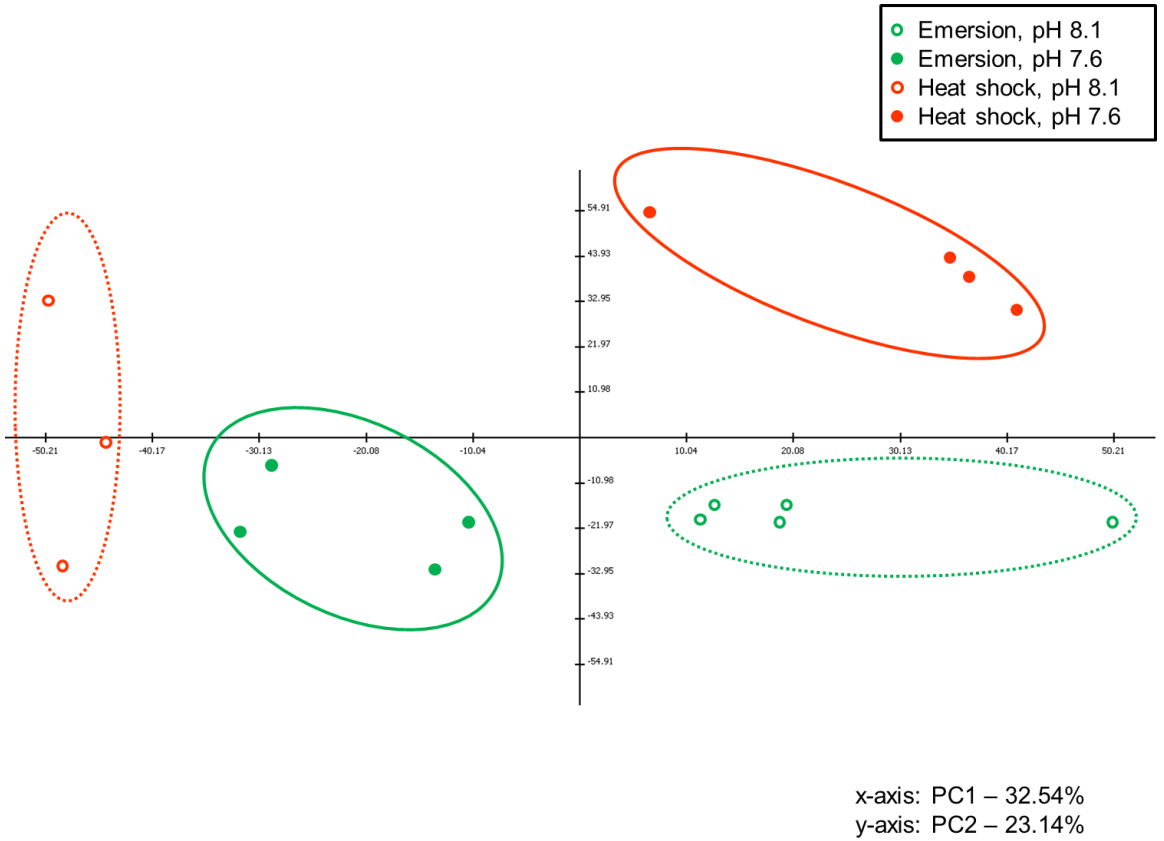

Figure 21C. Principal component analysis (PCA) of all proteins that changed in abundance in response to an interaction of temperature and pH variation. Analysis is based on a 2-way ANOVA, $p \leq 0.05$, 1000 permutations. Each treatment is represented by color for tidal regime (blue = constant immersion, green = 6 h emersion) and shape continuity for pH treatment (striated line/hollow dot = pH 8.1, solid line/solid dot= pH 7.6). Dots represent a gill tissue sample from an individual crab, whereas larger circles encompass the general area where all gels of a particular treatment group are plotted. Principal components 1 and 2 (PC1 and PC2) and the percentage of the selected data (significant proteins) they explain are shown.

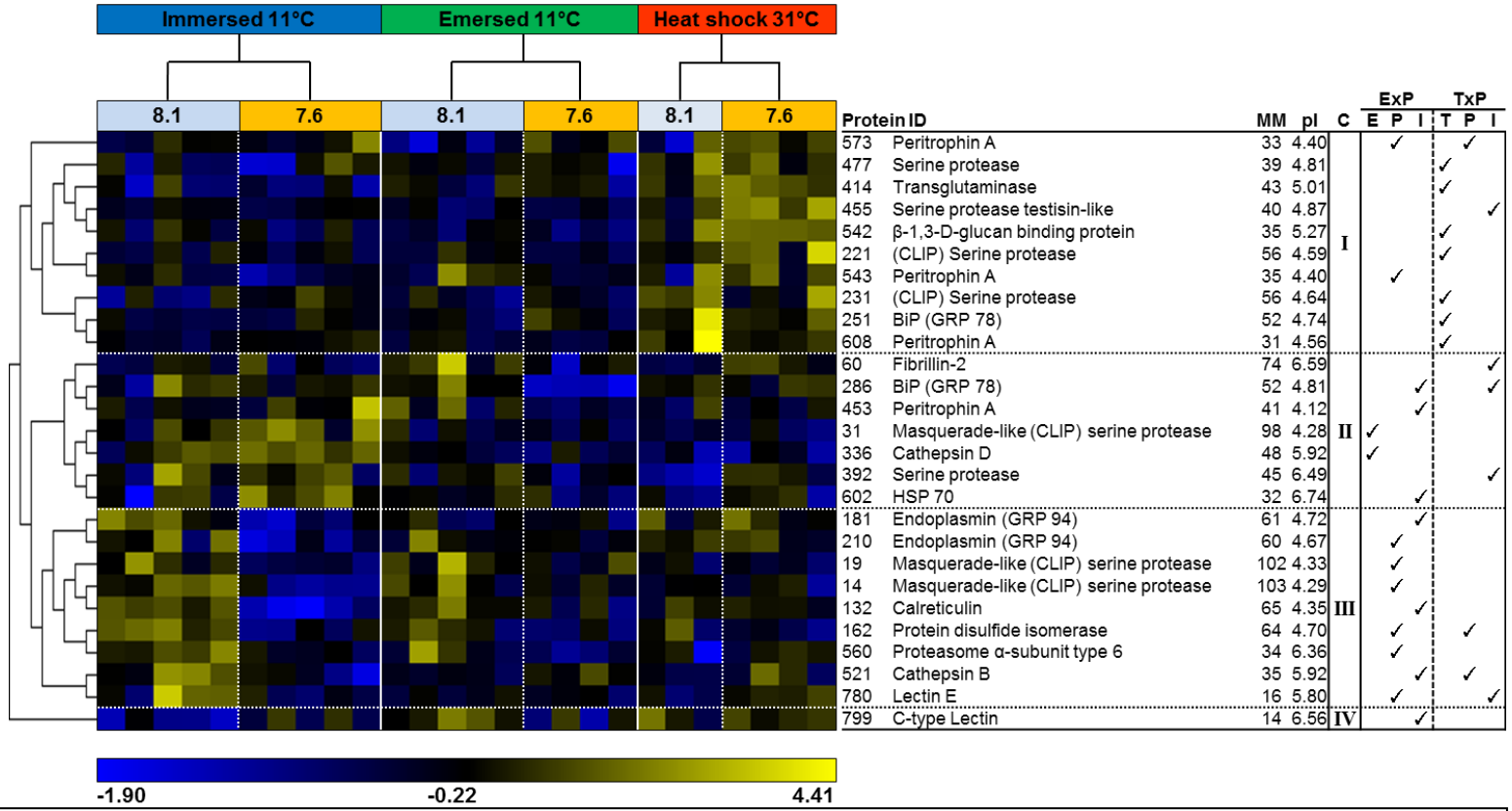

Protein ID		MM	pI	C	ExP E	ExP P	ExP I	TxP T	TxP P	TxP I
573	Peritrophin A	33	4.40	I		✓			✓	
477	Serine protease	39	4.81					✓		
414	Transglutaminase	43	5.01					✓		
455	Serine protease testisin-like	40	4.87							✓
542	β-1,3-D-glucan binding protein	35	5.27					✓		
221	(CLIP) Serine protease	56	4.59					✓		
543	Peritrophin A	35	4.40			✓				
231	(CLIP) Serine protease	56	4.64					✓		
251	BiP (GRP 78)	52	4.74					✓		
608	Peritrophin A	31	4.56					✓		
60	Fibrillin-2	74	6.59	II						✓
286	BiP (GRP 78)	52	4.81				✓			✓
453	Peritrophin A	41	4.12				✓			
31	Masquerade-like (CLIP) serine protease	98	4.28		✓					
336	Cathepsin D	48	5.92		✓					
392	Serine protease	45	6.49							✓
602	HSP 70	32	6.74				✓			
181	Endoplasmin (GRP 94)	61	4.72	III			✓			
210	Endoplasmin (GRP 94)	60	4.67			✓				
19	Masquerade-like (CLIP) serine protease	102	4.33			✓				
14	Masquerade-like (CLIP) serine protease	103	4.29			✓				
132	Calreticulin	65	4.35				✓			
162	Protein disulfide isomerase	64	4.70			✓			✓	
560	Proteasome α-subunit type 6	34	6.36			✓				
521	Cathepsin B	35	5.92				✓		✓	
780	Lectin E	16	5.80			✓				✓
799	C-type Lectin	14	6.56	IV			✓			

Figure 22. Hierarchical clustering of changes in abundance of proteins involved in immunity and protein homeostasis. Pearson's correlation, in response to acclimation to pH (constant pH 8.1 or 6 h nocturnal stress at pH 7.6), tidal regime (constant immersion or afternoon 6 h emersion), and heat shock (constant 11°C or heat shock up to 31°C coinciding with emersion). Blue coloring represents a lower than average protein abundance (standardized values, normalized volumes), whereas yellow represents greater than average protein abundance. Each column represents an individual crab's gill tissue sample, grouped by treatment (N=3-5 for each treatment). The rows represent the standardized abundances of proteins, organized by clusters of similar abundance changes (C), that are identified to the right and whose molecular mass (MM) and isoelectric point (pI) is listed. Significances for tidal regime (emersion; E), pH (P), or interaction (I) effect are ticked based on a two-way permutation ANOVA (tidal regime x pH, or ExP; P≤0.05), and significances for temperature (T), pH (P), or interaction (I) are ticked based on a separate two-way permutation ANOVA (temperature stress x pH, or TxP; P≤0.05).

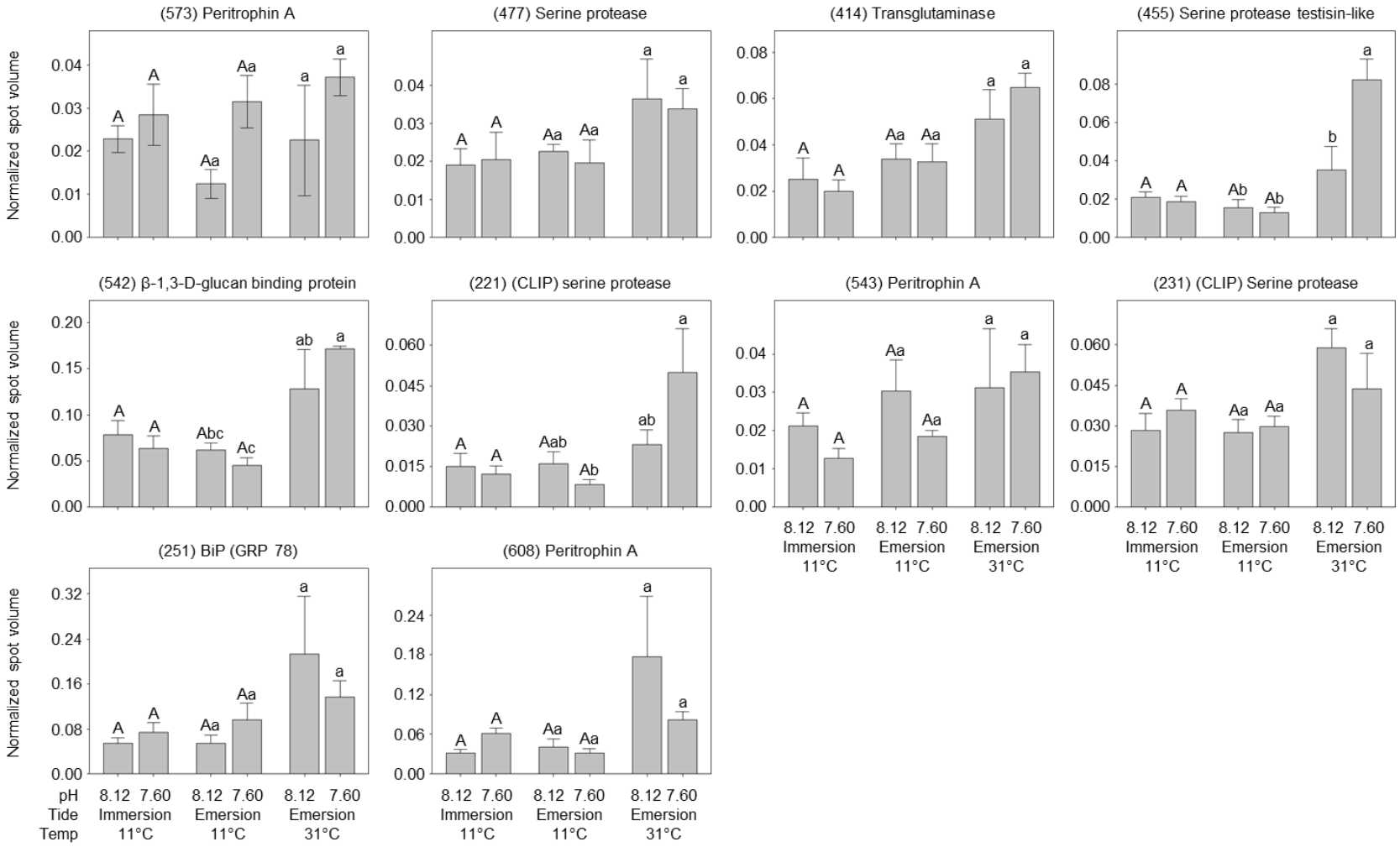

Figure 23A. Expression profiles (including means and +1 SEM) of molecular chaperones and proteolytic enzymes (Cluster I). Spot volumes were obtained by normalizing against the volume of all proteins on the proteome. Treatments with significance in protein abundance are marked with a different letter (based on Tukey's post-hoc analysis; upper case = within ExP, lower case = within TxP).

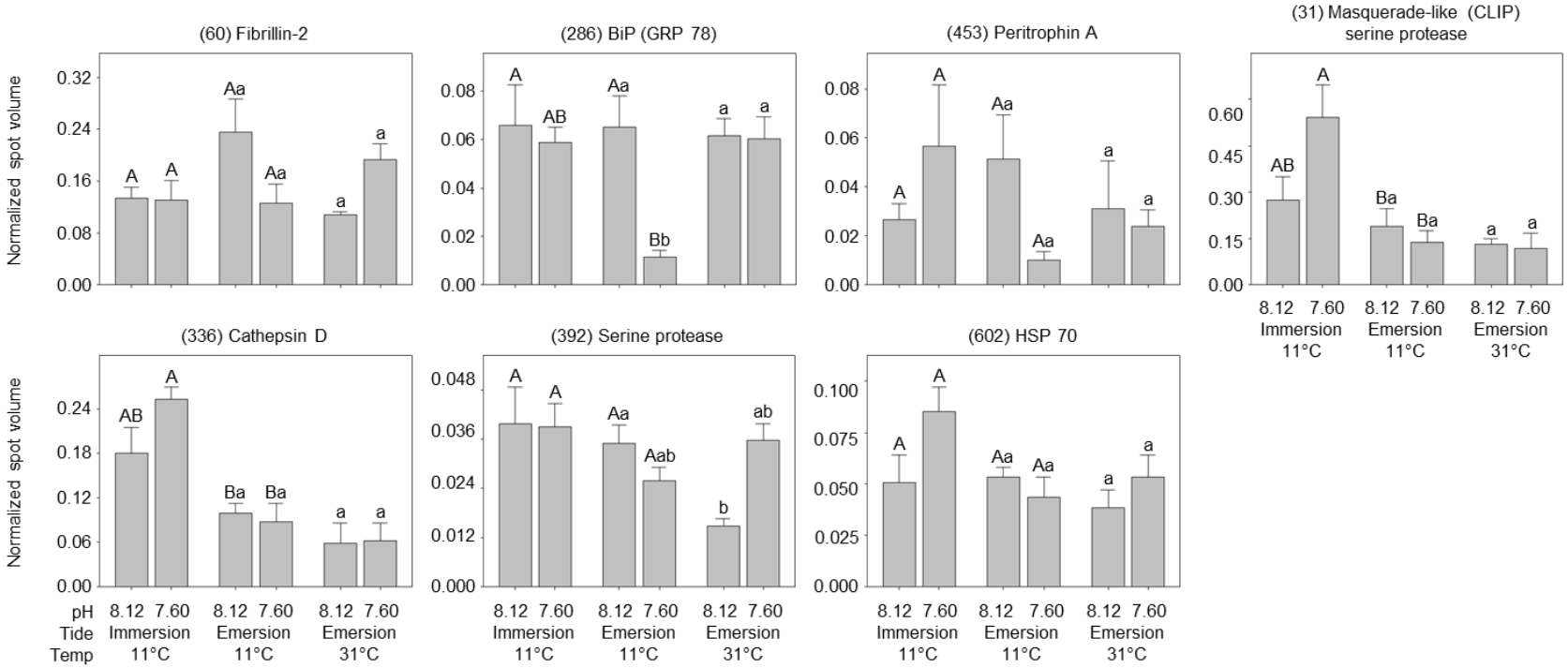

Figure 23B. Expression profiles (including means and +1 SEM) of molecular chaperones and proteolytic enzymes (Cluster II). Spot volumes were obtained by normalizing against the volume of all proteins on the proteome. Treatments with significance in protein abundance are marked with a different letter (based on Tukey's post-hoc analysis; upper case = within ExP, lower case = within TxP).

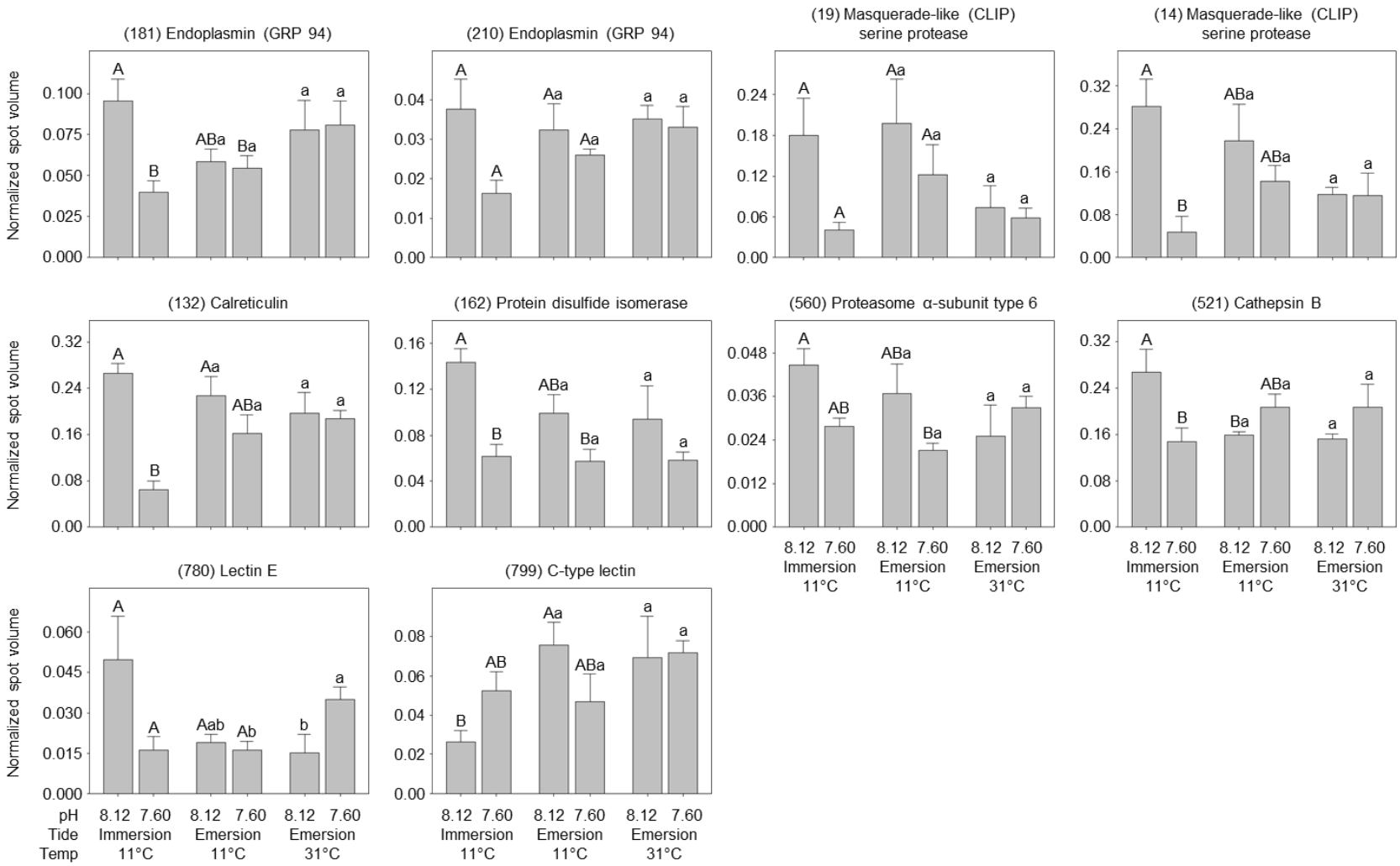

Figure 23C. Expression profiles (including means and +1 SEM) of molecular chaperones and proteolytic enzymes (Cluster III). Spot volumes were obtained by normalizing against the volume of all proteins on the proteome. Treatments with significance in protein abundance are marked with a different letter (based on Tukey's post-hoc analysis; upper case = within ExP, lower case = within TxP).

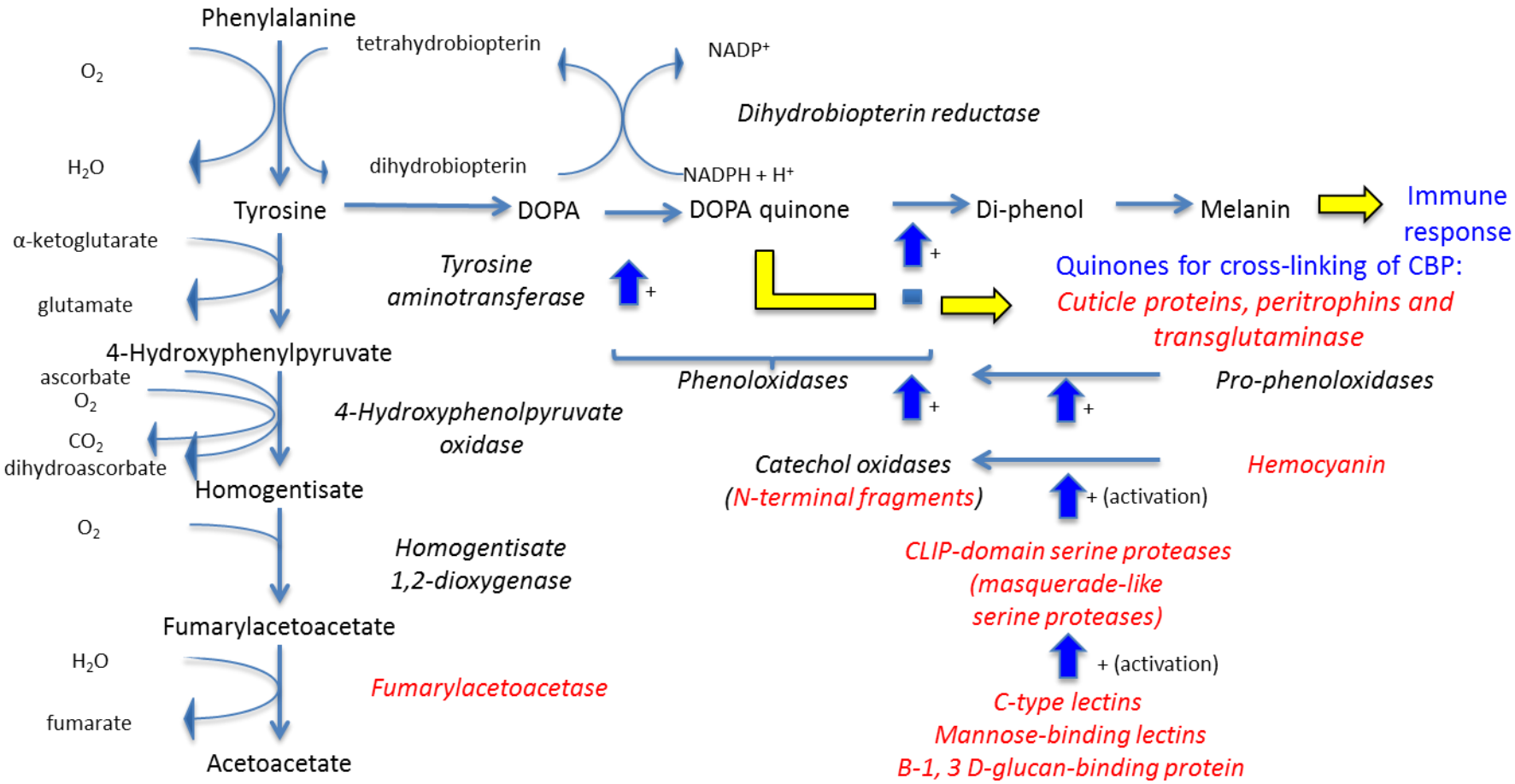

Figure 24. Schematic illustrating hypothetical pathways involved in prophenoloxidase activation, tyrosine metabolism, and downstream cuticle sclerotization. Red text indicates proteins that were identified in this study.

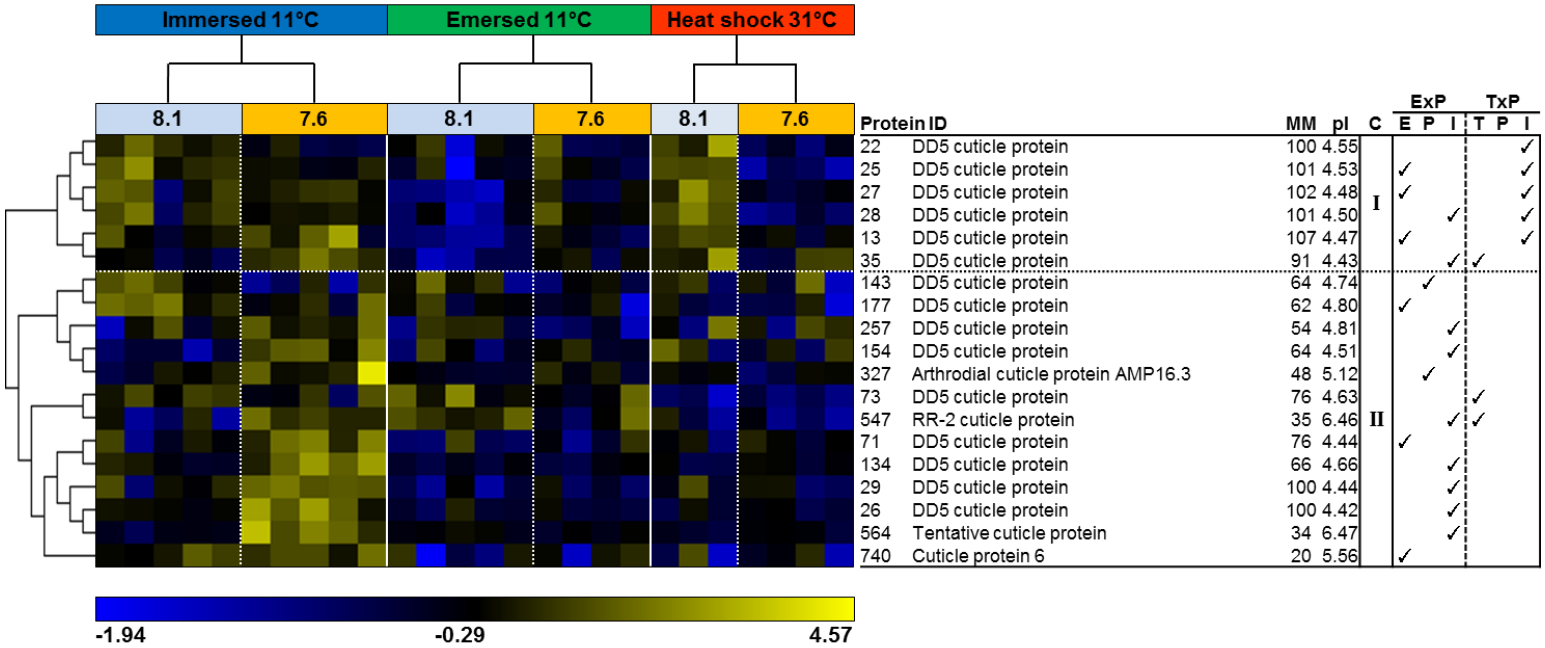

	Protein ID	MM	pI	C	ExP E	ExP P	ExP I	TxP T	TxP P	TxP I
22	DD5 cuticle protein	100	4.55							✓
25	DD5 cuticle protein	101	4.53		✓					✓
27	DD5 cuticle protein	102	4.48	I	✓					✓
28	DD5 cuticle protein	101	4.50				✓			✓
13	DD5 cuticle protein	107	4.47		✓					✓
35	DD5 cuticle protein	91	4.43				✓	✓		
143	DD5 cuticle protein	64	4.74			✓				
177	DD5 cuticle protein	62	4.80		✓					
257	DD5 cuticle protein	54	4.81				✓			
154	DD5 cuticle protein	64	4.51				✓			
327	Arthrodial cuticle protein AMP16.3	48	5.12			✓				
73	DD5 cuticle protein	76	4.63					✓		
547	RR-2 cuticle protein	35	6.46	II			✓	✓		
71	DD5 cuticle protein	76	4.44		✓					
134	DD5 cuticle protein	66	4.66				✓			
29	DD5 cuticle protein	100	4.44				✓			
26	DD5 cuticle protein	100	4.42				✓			
564	Tentative cuticle protein	34	6.47				✓			
740	Cuticle protein 6	20	5.56		✓					

Figure 25. Hierarchical clustering of changes in abundance of cuticle proteins. Pearson's correlation, in response to acclimation to pH (constant pH 8.1 or 6 h nocturnal stress at pH 7.6), tidal regime (constant immersion or afternoon 6 h emersion), and heat shock (constant 11°C or heat shock up to 31°C coinciding with emersion). Blue coloring represents a lower than average protein abundance (standardized values, normalized volumes), whereas yellow represents greater than average protein abundance. Each column represents an individual crab's gill tissue sample, grouped by treatment (N=3-5 for each treatment). The rows represent the standardized abundances of proteins, organized by clusters of similar abundance changes (C), that are identified to the right and whose molecular mass (MM) and isoelectric point (pI) is listed. Significances for tidal regime (emersion; E), pH (P), or interaction (I) effect are ticked based on a two-way permutation ANOVA (tidal regime x pH, or ExP; P≤0.05), and significances for temperature (T), pH (P), or interaction (I) are ticked based on a separate two-way permutation ANOVA (temperature stress x pH, or TxP; P≤0.05). Figure is continued below.

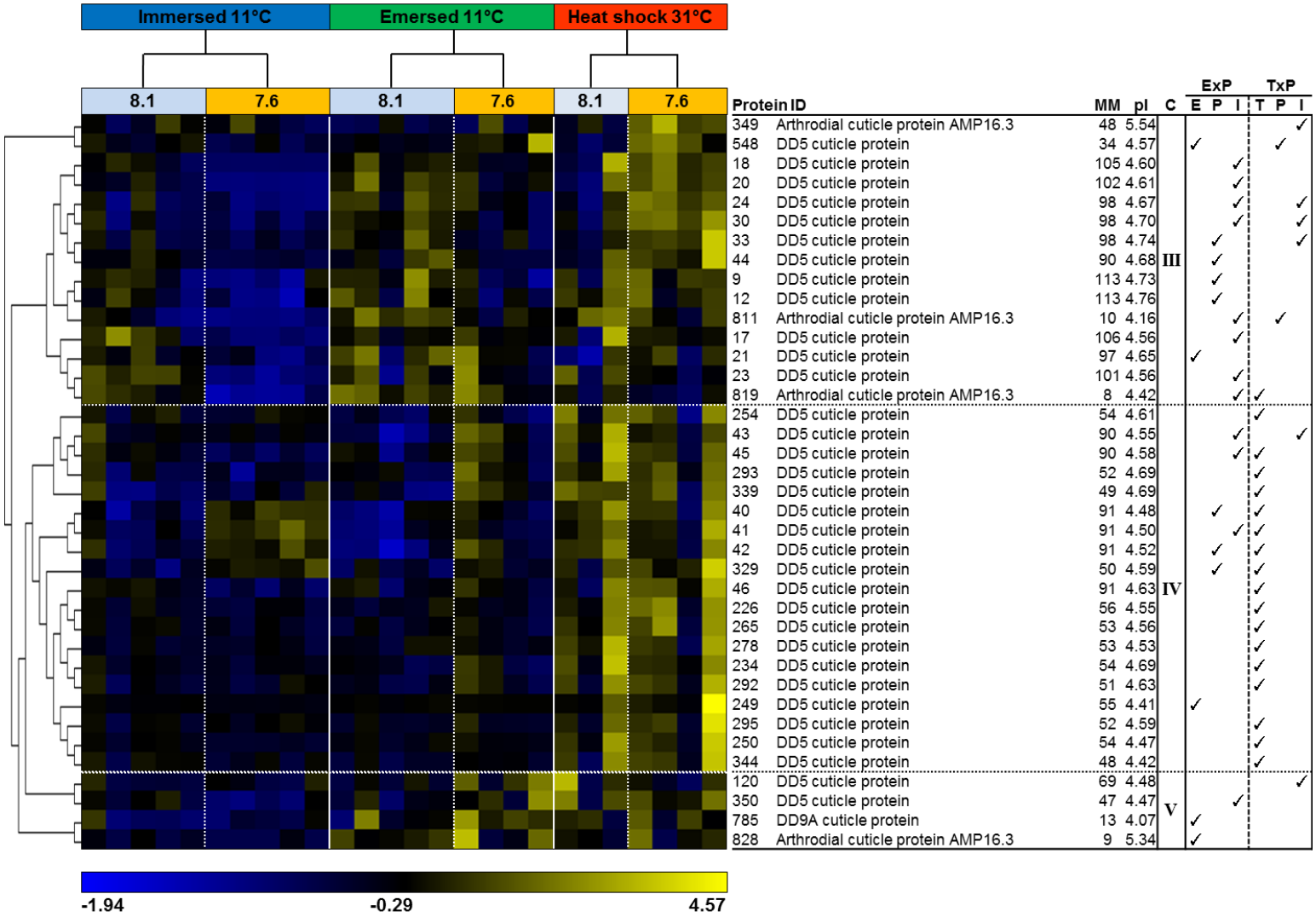

	Protein ID	MM	pI	C	ExP E	ExP P	ExP I	TxP T	TxP P	TxP I
349	Arthrodial cuticle protein AMP16.3	48	5.54							✓
548	DD5 cuticle protein	34	4.57		✓				✓	
18	DD5 cuticle protein	105	4.60				✓			
20	DD5 cuticle protein	102	4.61				✓			
24	DD5 cuticle protein	98	4.67				✓			✓
30	DD5 cuticle protein	98	4.70				✓			✓
33	DD5 cuticle protein	98	4.74			✓				✓
44	DD5 cuticle protein	90	4.68	III		✓				
9	DD5 cuticle protein	113	4.73			✓				
12	DD5 cuticle protein	113	4.76			✓				
811	Arthrodial cuticle protein AMP16.3	10	4.16				✓		✓	
17	DD5 cuticle protein	106	4.56				✓			
21	DD5 cuticle protein	97	4.65		✓					
23	DD5 cuticle protein	101	4.56				✓			
819	Arthrodial cuticle protein AMP16.3	8	4.42				✓	✓		
254	DD5 cuticle protein	54	4.61					✓		
43	DD5 cuticle protein	90	4.55				✓			✓
45	DD5 cuticle protein	90	4.58				✓	✓		
293	DD5 cuticle protein	52	4.69					✓		
339	DD5 cuticle protein	49	4.69					✓		
40	DD5 cuticle protein	91	4.48			✓		✓		
41	DD5 cuticle protein	91	4.50				✓	✓		
42	DD5 cuticle protein	91	4.52			✓		✓		
329	DD5 cuticle protein	50	4.59			✓		✓		
46	DD5 cuticle protein	91	4.63	IV				✓		
226	DD5 cuticle protein	56	4.55					✓		
265	DD5 cuticle protein	53	4.56					✓		
278	DD5 cuticle protein	53	4.53					✓		
234	DD5 cuticle protein	54	4.69					✓		
292	DD5 cuticle protein	51	4.63					✓		
249	DD5 cuticle protein	55	4.41		✓					
295	DD5 cuticle protein	52	4.59					✓		
250	DD5 cuticle protein	54	4.47					✓		
344	DD5 cuticle protein	48	4.42					✓		
120	DD5 cuticle protein	69	4.48							✓
350	DD5 cuticle protein	47	4.47	V			✓			
785	DD9A cuticle protein	13	4.07		✓					
828	Arthrodial cuticle protein AMP16.3	9	5.34		✓					

Figure 25 continued.

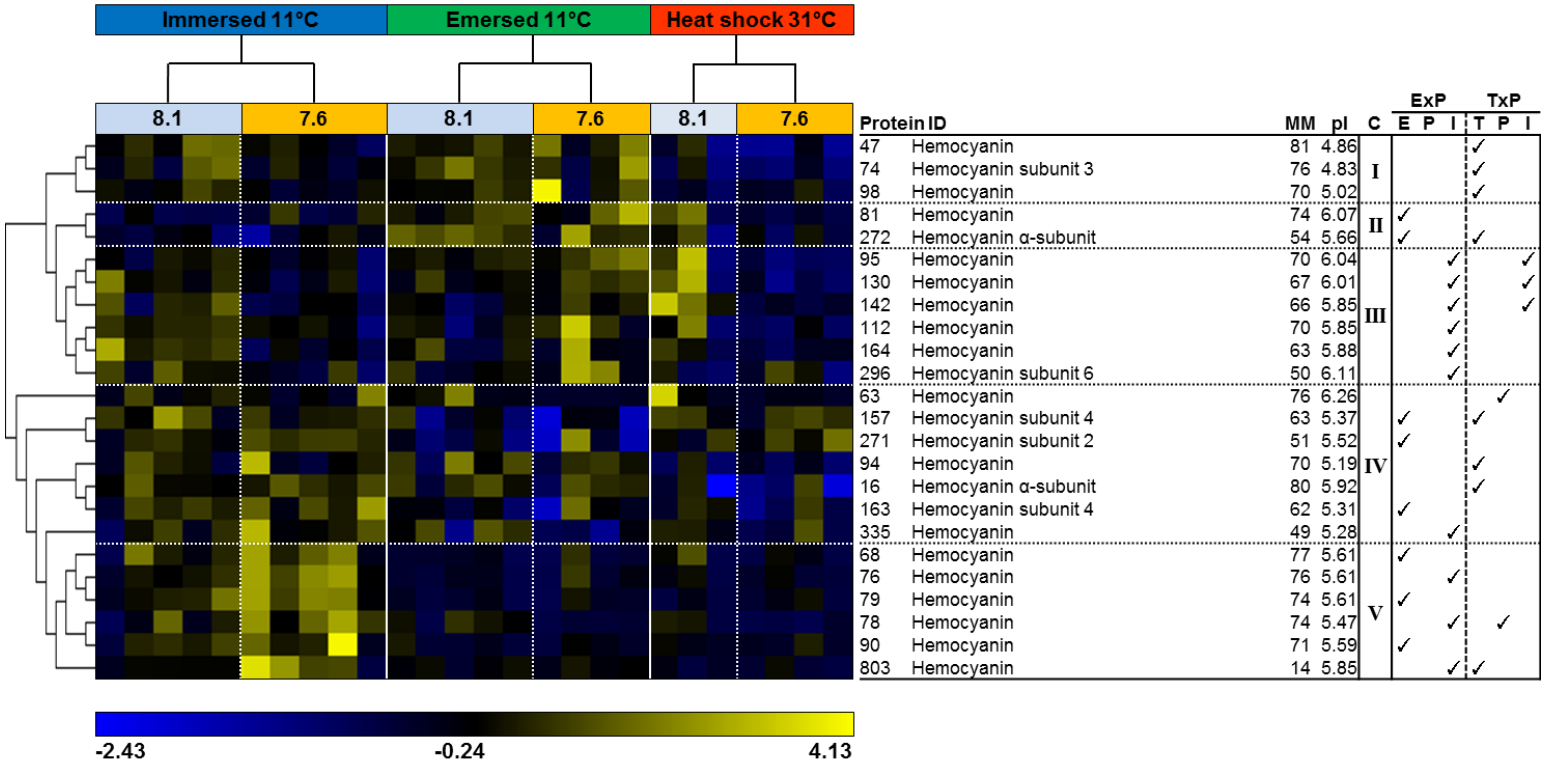

Protein ID		MM	pI	C	ExP E	ExP P	ExP I	TxP T	TxP P	TxP I
47	Hemocyanin	81	4.86	I				✓		
74	Hemocyanin subunit 3	76	4.83					✓		
98	Hemocyanin	70	5.02					✓		
81	Hemocyanin	74	6.07	II	✓					
272	Hemocyanin α-subunit	54	5.66		✓			✓		
95	Hemocyanin	70	6.04	III		✓				✓
130	Hemocyanin	67	6.01			✓				✓
142	Hemocyanin	66	5.85			✓				✓
112	Hemocyanin	70	5.85			✓				
164	Hemocyanin	63	5.88			✓				
296	Hemocyanin subunit 6	50	6.11			✓				
63	Hemocyanin	76	6.26	IV					✓	
157	Hemocyanin subunit 4	63	5.37		✓			✓		
271	Hemocyanin subunit 2	51	5.52		✓					
94	Hemocyanin	70	5.19					✓		
16	Hemocyanin α-subunit	80	5.92					✓		
163	Hemocyanin subunit 4	62	5.31		✓					
335	Hemocyanin	49	5.28			✓				
68	Hemocyanin	77	5.61	V	✓					
76	Hemocyanin	76	5.61			✓				
79	Hemocyanin	74	5.61		✓					
78	Hemocyanin	74	5.47			✓			✓	
90	Hemocyanin	71	5.59		✓					
803	Hemocyanin	14	5.85			✓		✓		

Figure 26. Hierarchical clustering of changes in abundance of hemocyanins. Pearson's correlation, in response to acclimation to pH (constant pH 8.1 or 6 h nocturnal stress at pH 7.6), tidal regime (constant immersion or afternoon 6 h emersion), and heat shock (constant 11°C or heat shock up to 31°C coinciding with emersion). Blue coloring represents a lower than average protein abundance (standardized values, normalized volumes), whereas yellow represents greater than average protein abundance. Each column represents an individual crab's gill tissue sample, grouped by treatment (N=3-5 for each treatment). The rows represent the standardized abundances of proteins, organized by clusters of similar abundance changes (C), that are identified to the right and whose molecular mass (MM) and isoelectric point (pI) is listed. Significances for tidal regime (emersion; E), pH (P), or interaction (I) effect are ticked based on a two-way permutation ANOVA (tidal regime x pH, or ExP; P≤0.05), and significances for temperature (T), pH (P), or interaction (I) are ticked based on a separate two-way permutation ANOVA (temperature stress x pH, or TxP; P≤0.05). Figure is continued below.

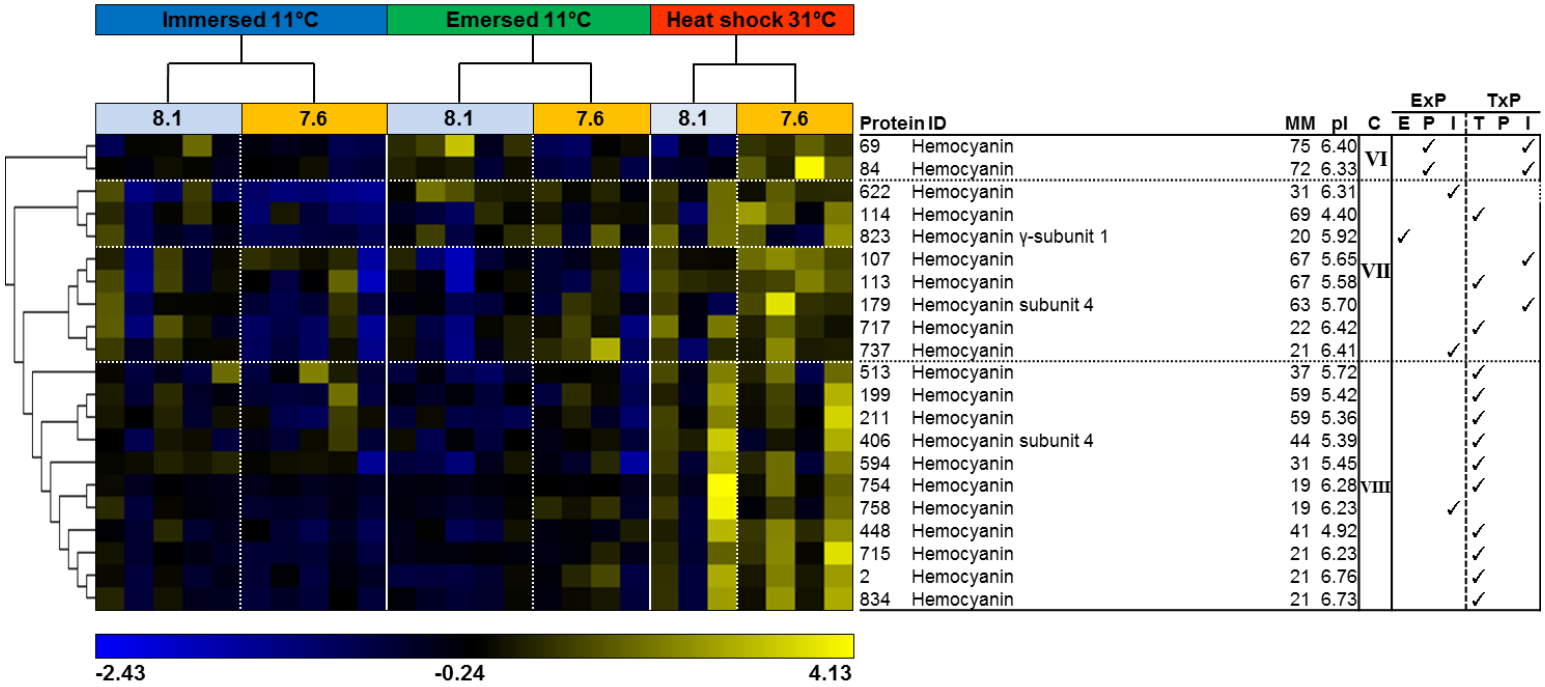

Protein ID		MM	pI	C	ExP E	ExP P	ExP I	TxP T	TxP P	TxP I
69	Hemocyanin	75	6.40	VI		✓				✓
84	Hemocyanin	72	6.33			✓				✓
622	Hemocyanin	31	6.31	VII			✓			
114	Hemocyanin	69	4.40					✓		
823	Hemocyanin γ-subunit 1	20	5.92		✓					
107	Hemocyanin	67	5.65							✓
113	Hemocyanin	67	5.58					✓		
179	Hemocyanin subunit 4	63	5.70							✓
717	Hemocyanin	22	6.42					✓		
737	Hemocyanin	21	6.41				✓			
513	Hemocyanin	37	5.72	VIII				✓		
199	Hemocyanin	59	5.42					✓		
211	Hemocyanin	59	5.36					✓		
406	Hemocyanin subunit 4	44	5.39					✓		
594	Hemocyanin	31	5.45					✓		
754	Hemocyanin	19	6.28					✓		
758	Hemocyanin	19	6.23				✓			
448	Hemocyanin	41	4.92					✓		
715	Hemocyanin	21	6.23					✓		
2	Hemocyanin	21	6.76					✓		
834	Hemocyanin	21	6.73					✓		

Figure 26 continued.

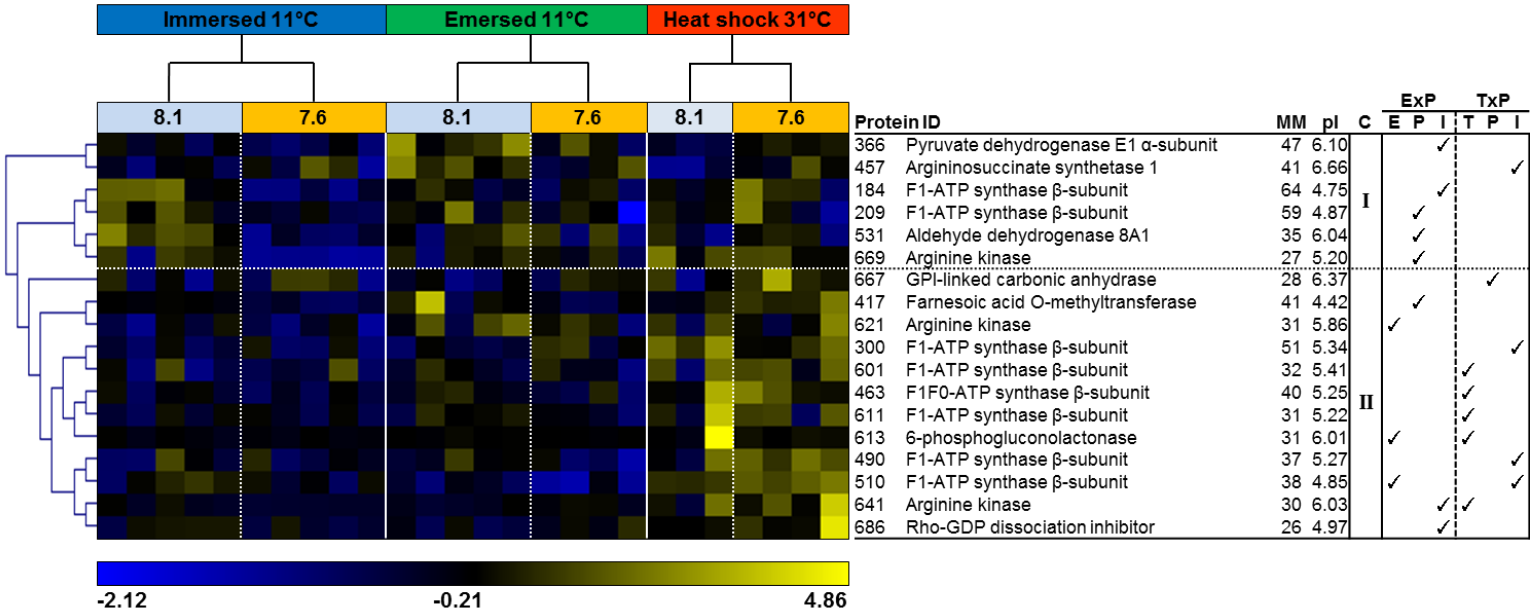

	Protein ID	MM	pI	C	ExP E	ExP P	ExP I	TxP T	TxP P	TxP I
366	Pyruvate dehydrogenase E1 α-subunit	47	6.10				✓			
457	Argininosuccinate synthetase 1	41	6.66							✓
184	F1-ATP synthase β-subunit	64	4.75	I			✓			
209	F1-ATP synthase β-subunit	59	4.87	I		✓				
531	Aldehyde dehydrogenase 8A1	35	6.04	I		✓				
669	Arginine kinase	27	5.20	I		✓				
667	GPI-linked carbonic anhydrase	28	6.37						✓	
417	Farnesoic acid O-methyltransferase	41	4.42			✓				
621	Arginine kinase	31	5.86		✓					
300	F1-ATP synthase β-subunit	51	5.34							✓
601	F1-ATP synthase β-subunit	32	5.41					✓		
463	F1F0-ATP synthase β-subunit	40	5.25	II				✓		
611	F1-ATP synthase β-subunit	31	5.22	II				✓		
613	6-phosphogluconolactonase	31	6.01	II	✓			✓		
490	F1-ATP synthase β-subunit	37	5.27	II						✓
510	F1-ATP synthase β-subunit	38	4.85	II	✓					✓
641	Arginine kinase	30	6.03	II			✓	✓		
686	Rho-GDP dissociation inhibitor	26	4.97	II			✓			

Figure 27. Hierarchical clustering of changes in abundance of proteins involved in energy and nitrogen metabolism. Pearson's correlation, in response to acclimation to pH (constant pH 8.1 or 6 h nocturnal stress at pH 7.6), tidal regime (constant immersion or afternoon 6 h emersion), and heat shock (constant 11°C or heat shock up to 31°C coinciding with emersion). Blue coloring represents a lower than average protein abundance (standardized values, normalized volumes), whereas yellow represents greater than average protein abundance. Each column represents an individual crab's gill tissue sample, grouped by treatment (N=3-5 for each treatment). The rows represent the standardized abundances of proteins, organized by clusters of similar abundance changes (C), that are identified to the right and whose molecular mass (MM) and isoelectric point (pI) is listed. Significances for tidal regime (emersion; E), pH (P), or interaction (I) effect are ticked based on a two-way permutation ANOVA (tidal regime x pH, or ExP; P≤0.05), and significances for temperature (T), pH (P), or interaction (I) are ticked based on a separate two-way permutation ANOVA (temperature stress x pH, or TxP; P≤0.05). Figure is continued below.

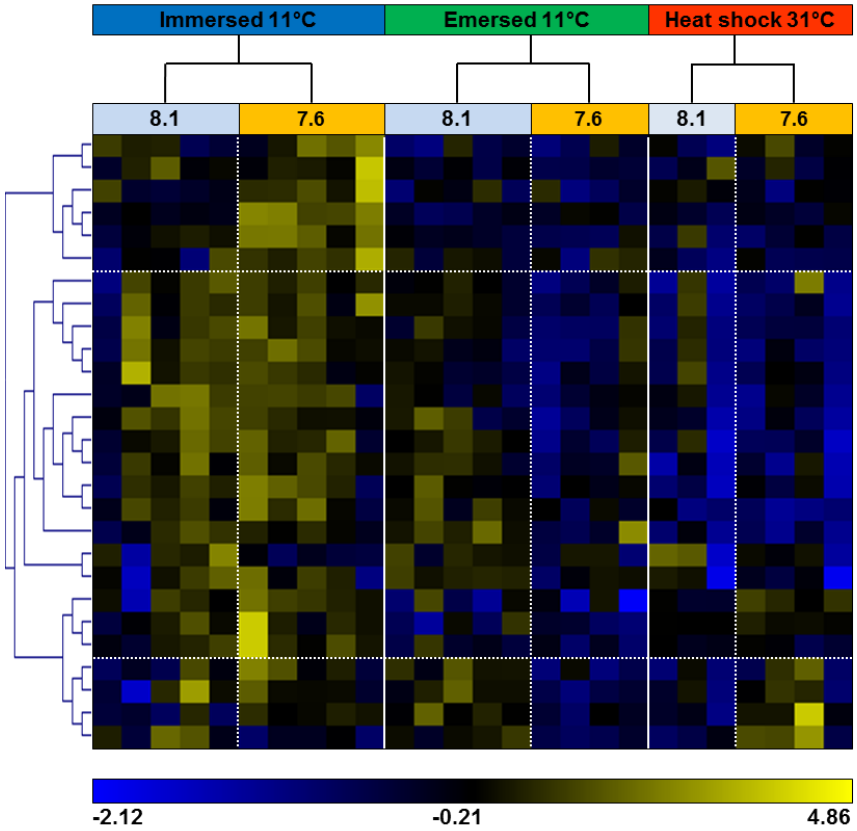

	Protein ID	MM	pI	C	ExP E	ExP P	ExP I	TxP T	TxP P	TxP I
137	Aldehyde dehydrogenase 8A1	65	4.63	III	✓					
444	Neurogenic notch-like	41	4.18		✓					
436	Farnesoic acid O-methyltransferase	41	4.57		✓					
405	Na^+/K^+ ATPase β2-subunit	44	5.81				✓			
458	Argininosuccinate synthetase 1	38	6.67				✓			
695	Peroxiredoxin	26	5.50					✓		
131	NADP-dependent malic enzyme	66	6.40	IV	✓					
155	F1-ATP synthase β-subunit	62	5.20		✓					
158	Aldehyde dehydrogenase 8A1	63	6.47		✓					
214	Enolase	56	6.82		✓					
328	Glyceraldehyde-3-phosphate dehydrogenase	49	6.82		✓					
245	Enolase	56	6.76		✓					
268	Fumarylacetoacetase	54	6.83				✓			
258	Citrate synthase	54	6.43		✓					
337	Glyceraldehyde-3-phosphate dehydrogenase	49	6.64					✓		
264	Catalase	53	6.51					✓		
506	Dihydrolipoyl dehydrogenase	37	6.44					✓		
522	ATP synthase α-subunit	36	6.68					✓		
557	Arginine kinase	34	6.41			✓				
561	Arginine kinase	34	6.64					✓		
514	NADP-dependent malic enzyme	36	6.33		✓					
358	V-type H^+ ATPase subunit A	47	5.79		✓					
568	Dihydrolipoyl dehydrogenase	35	5.81		✓					
198	Glutamate dehydrogenase	61	6.79	V			✓			✓
569	Glyceraldehyde-3-phosphate dehydrogenase	34	6.74							✓
380	Pyruvate dehydrogenase E1 α-subunit	45	6.38				✓			✓
700	Malate dehydrogenase	25	6.52			✓				✓

Figure 27 continued.

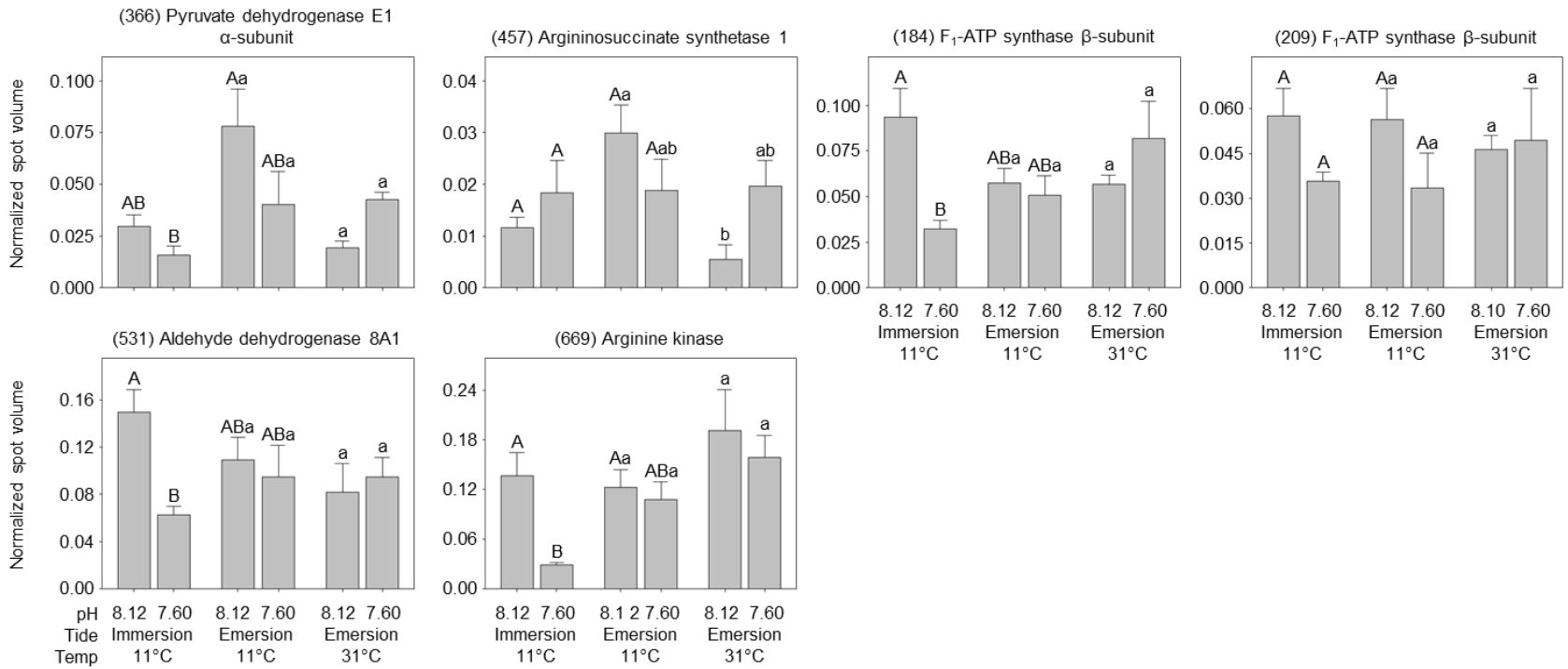

Figure 28A. Expression profiles (including means and +1 SEM) of energy and nitrogen metabolism proteins (Cluster I). Spot volumes were obtained by normalizing against the volume of all proteins on the proteome. Treatments with significance in protein abundance are marked with a different letter (based on Tukey's post-hoc analysis; upper case = within ExP, lower case = within TxP).

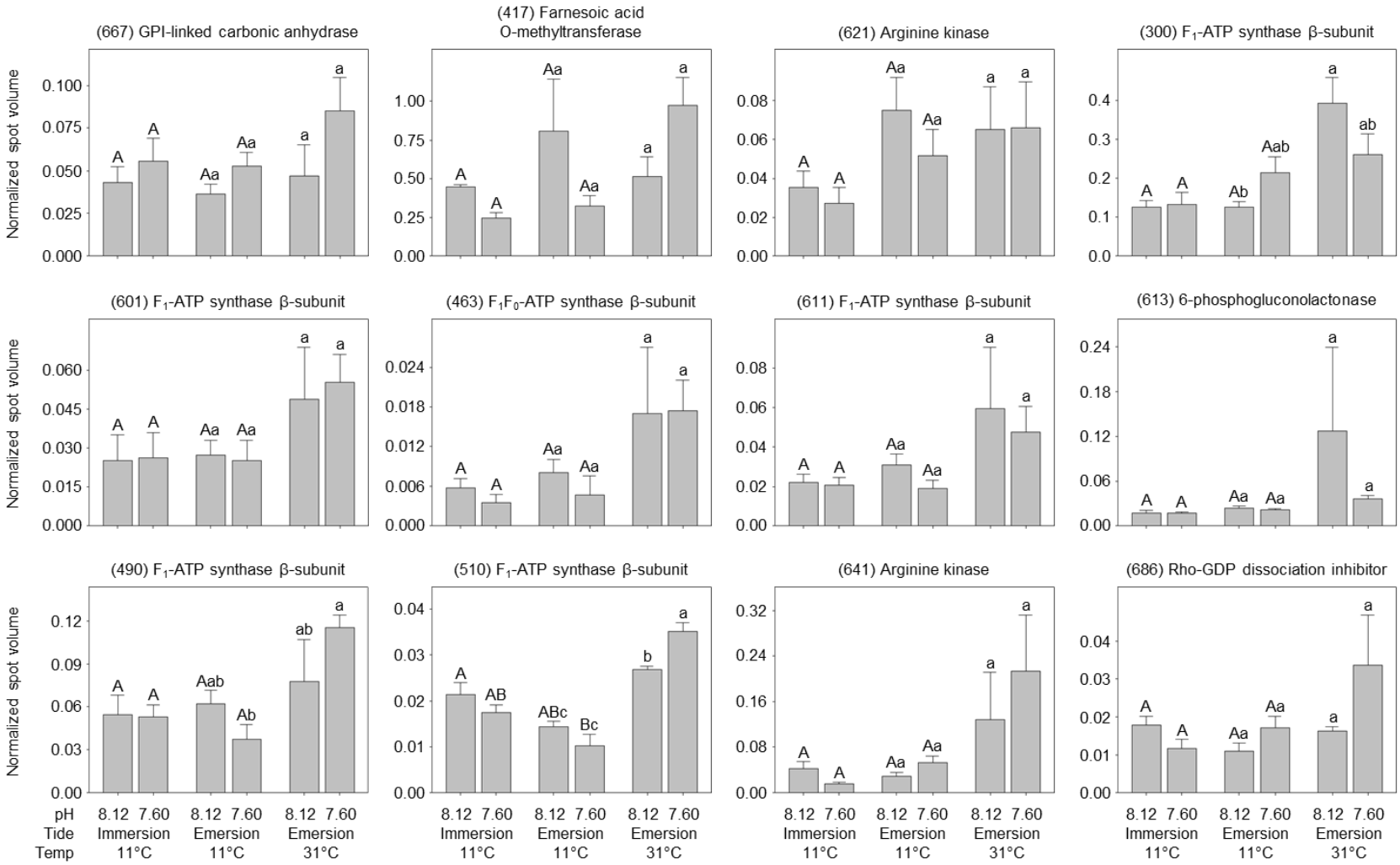

Figure 28B. Expression profiles (including means and +1 SEM) of energy and nitrogen metabolism proteins (Cluster II). Spot volumes were obtained by normalizing against the volume of all proteins on the proteome. Treatments with significance in protein abundance are marked with a different letter (based on Tukey's post-hoc analysis; upper case = within ExP, lower case = within TxP).

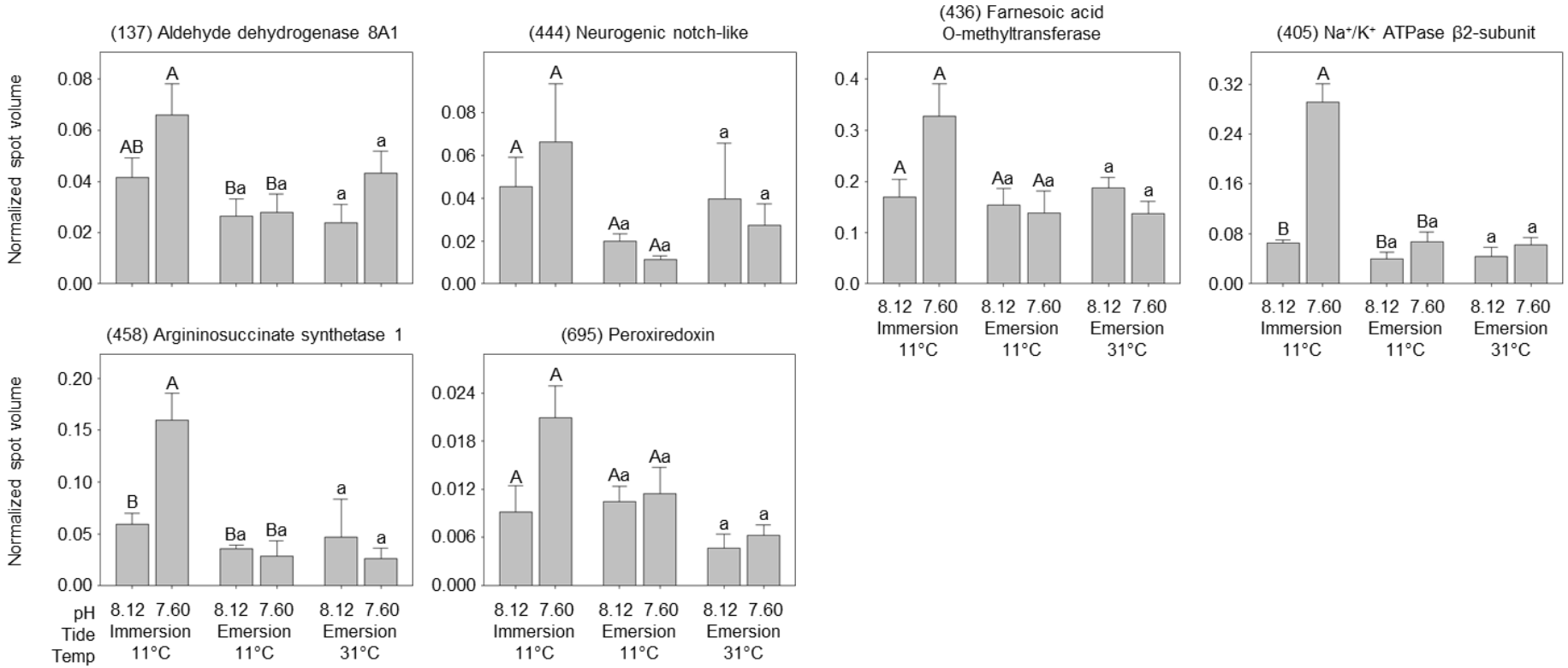

Figure 28C. Expression profiles (including means and +1 SEM) of energy and nitrogen metabolism proteins (Cluster III). Spot volumes were obtained by normalizing against the volume of all proteins on the proteome. Treatments with significance in protein abundance are marked with a different letter (based on Tukey's post-hoc analysis; upper case = within ExP, lower case = within TxP).

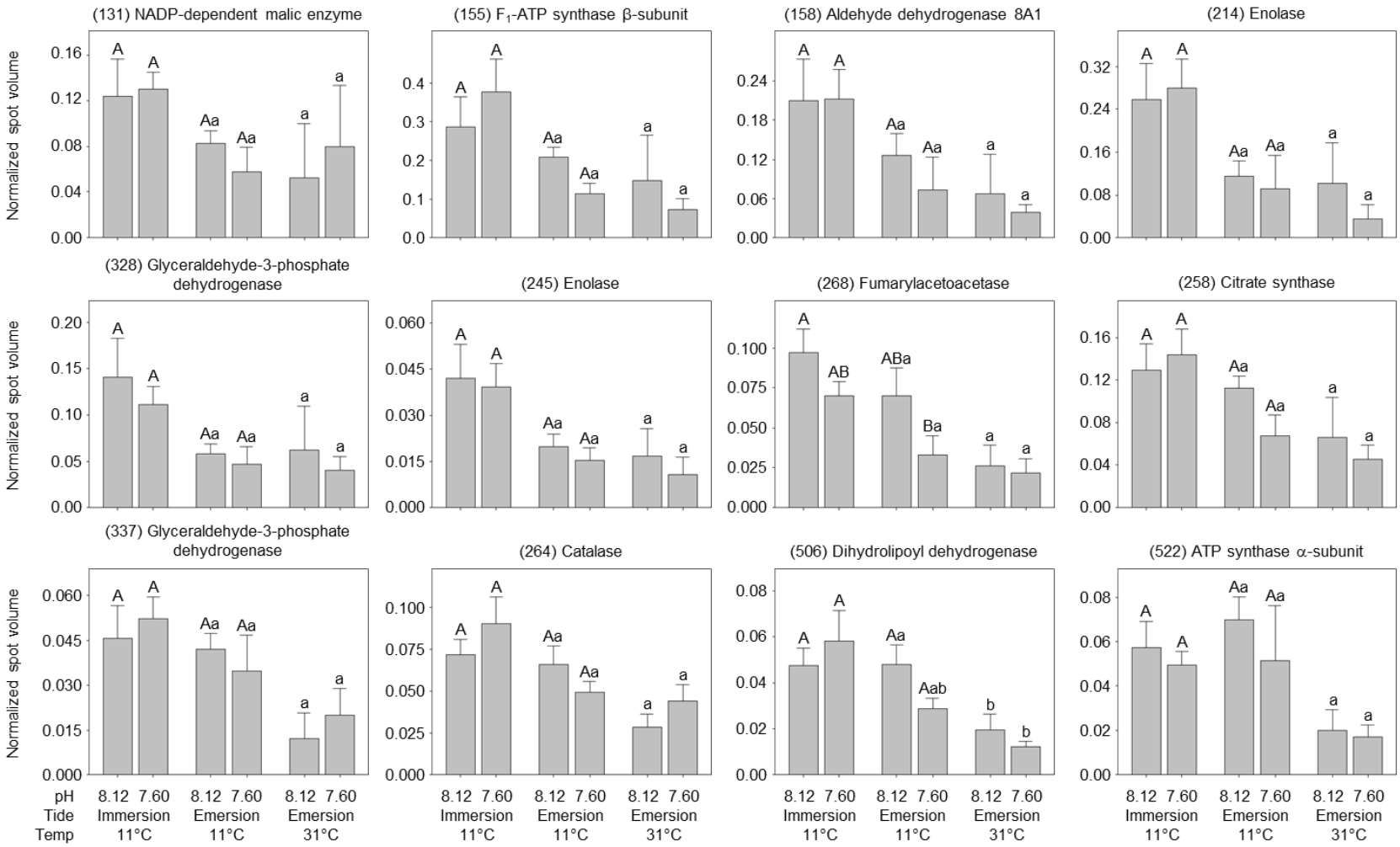

Figure 28D. Expression profiles (including means and +1 SEM) of energy and nitrogen metabolism proteins (Cluster IV). Spot volumes were obtained by normalizing against the volume of all proteins on the proteome. Treatments with significance in protein abundance are marked with a different letter (based on Tukey's post-hoc analysis; upper case = within ExP, lower case = within TxP). Figure is continued below.

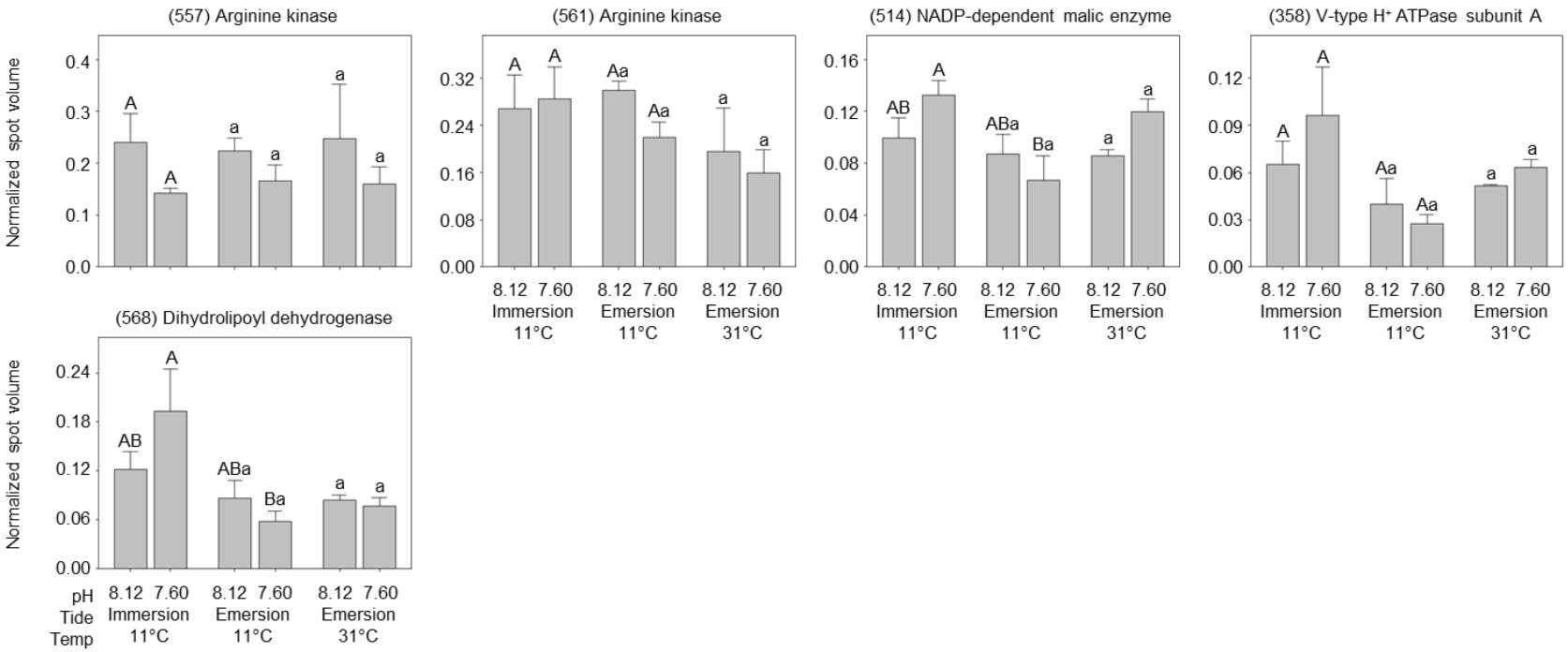

Figure 28D continued.

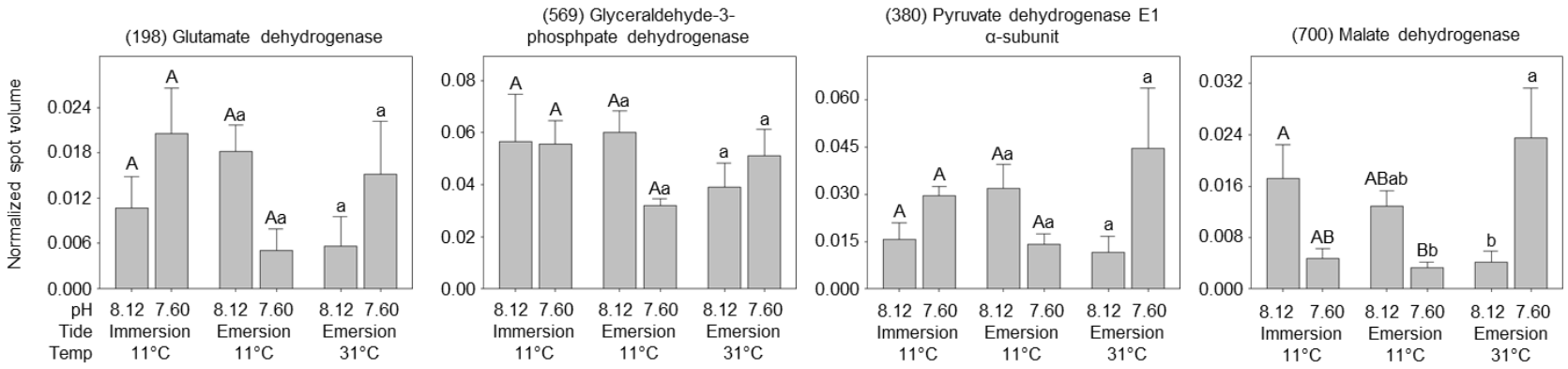

Figure 28E. Expression profiles (including means and +1 SEM) of energy and nitrogen metabolism proteins (Cluster V). Spot volumes were obtained by normalizing against the volume of all proteins on the proteome. Treatments with significance in protein abundance are marked with a different letter (based on Tukey's post-hoc analysis; upper case = within ExP, lower case = within TxP).

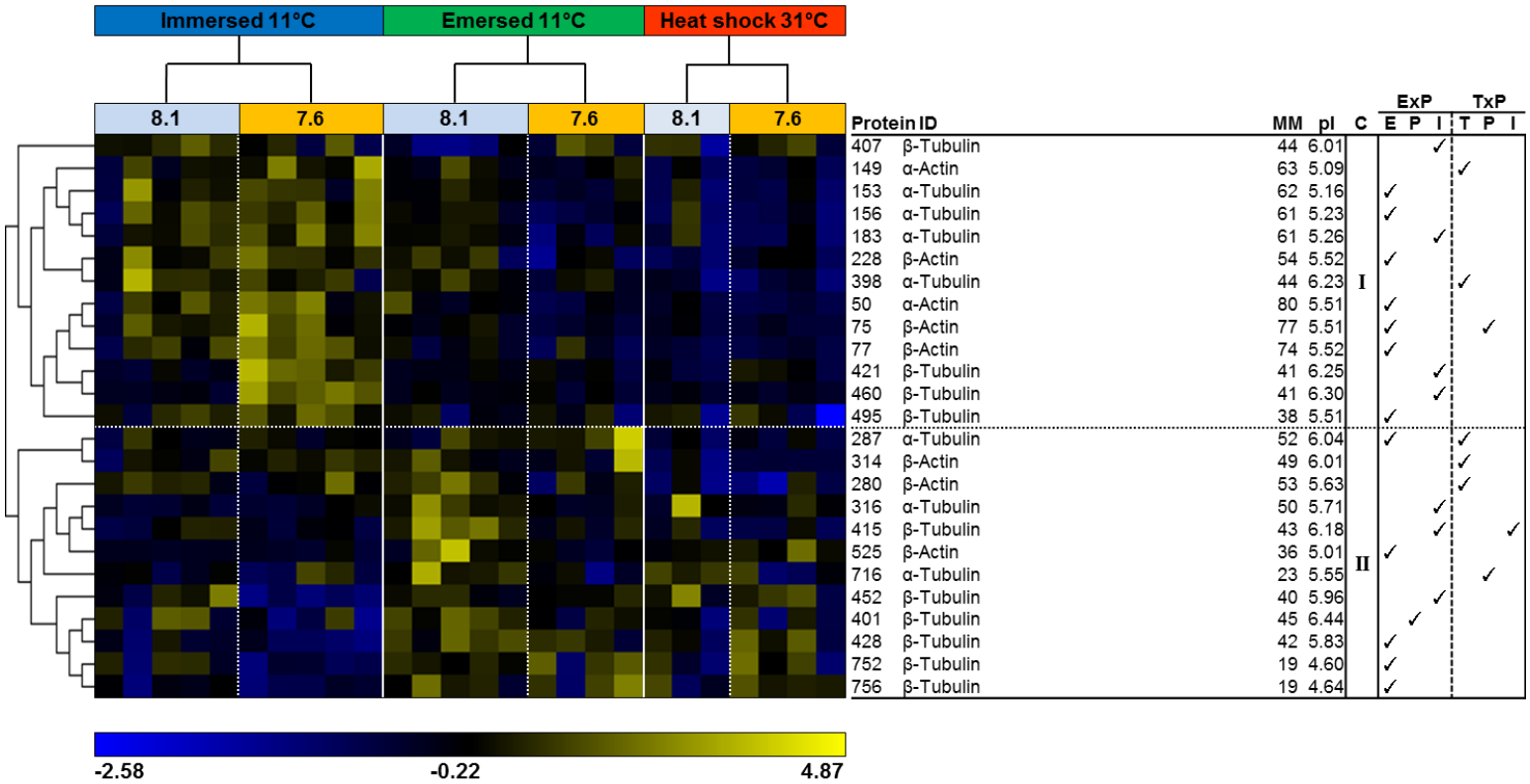

Protein ID		MM	pI	C	ExP E	ExP P	ExP I	TxP T	TxP P	TxP I
407	β-Tubulin	44	6.01				✓			
149	α-Actin	63	5.09					✓		
153	α-Tubulin	62	5.16		✓					
156	α-Tubulin	61	5.23		✓					
183	α-Tubulin	61	5.26				✓			
228	β-Actin	54	5.52		✓					
398	α-Tubulin	44	6.23	I				✓		
50	α-Actin	80	5.51		✓					
75	β-Actin	77	5.51		✓				✓	
77	β-Actin	74	5.52		✓					
421	β-Tubulin	41	6.25				✓			
460	β-Tubulin	41	6.30				✓			
495	β-Tubulin	38	5.51		✓					
287	α-Tubulin	52	6.04		✓			✓		
314	β-Actin	49	6.01					✓		
280	β-Actin	53	5.63					✓		
316	α-Tubulin	50	5.71				✓			
415	β-Tubulin	43	6.18				✓			✓
525	β-Actin	36	5.01	II	✓					
716	α-Tubulin	23	5.55						✓	
452	β-Tubulin	40	5.96				✓			
401	β-Tubulin	45	6.44			✓				
428	β-Tubulin	42	5.83		✓					
752	β-Tubulin	19	4.60		✓					
756	β-Tubulin	19	4.64		✓					

Figure 29. Hierarchical clustering of changes in abundance of cytoskeletal proteins. Pearson's correlation, in response to acclimation to pH (constant pH 8.1 or 6 h nocturnal stress at pH 7.6), tidal regime (constant immersion or afternoon 6 h emersion), and heat shock (constant 11°C or heat shock up to 31°C coinciding with emersion). Blue coloring represents a lower than average protein abundance (standardized values, normalized volumes), whereas yellow represents greater than average protein abundance. Each column represents an individual crab's gill tissue sample, grouped by treatment (N=3-5 for each treatment). The rows represent the standardized abundances of proteins, organized by clusters of similar abundance changes (C), that are identified to the right and whose molecular mass (MM) and isoelectric point (pI) is listed. Significances for tidal regime (emersion; E), pH (P), or interaction (I) effect are ticked based on a two-way permutation ANOVA (tidal regime x pH, or ExP; P≤0.05), and significances for temperature (T), pH (P), or interaction (I) are ticked based on a separate two-way permutation ANOVA (temperature stress x pH, or TxP; P≤0.05). Figure is continued below.

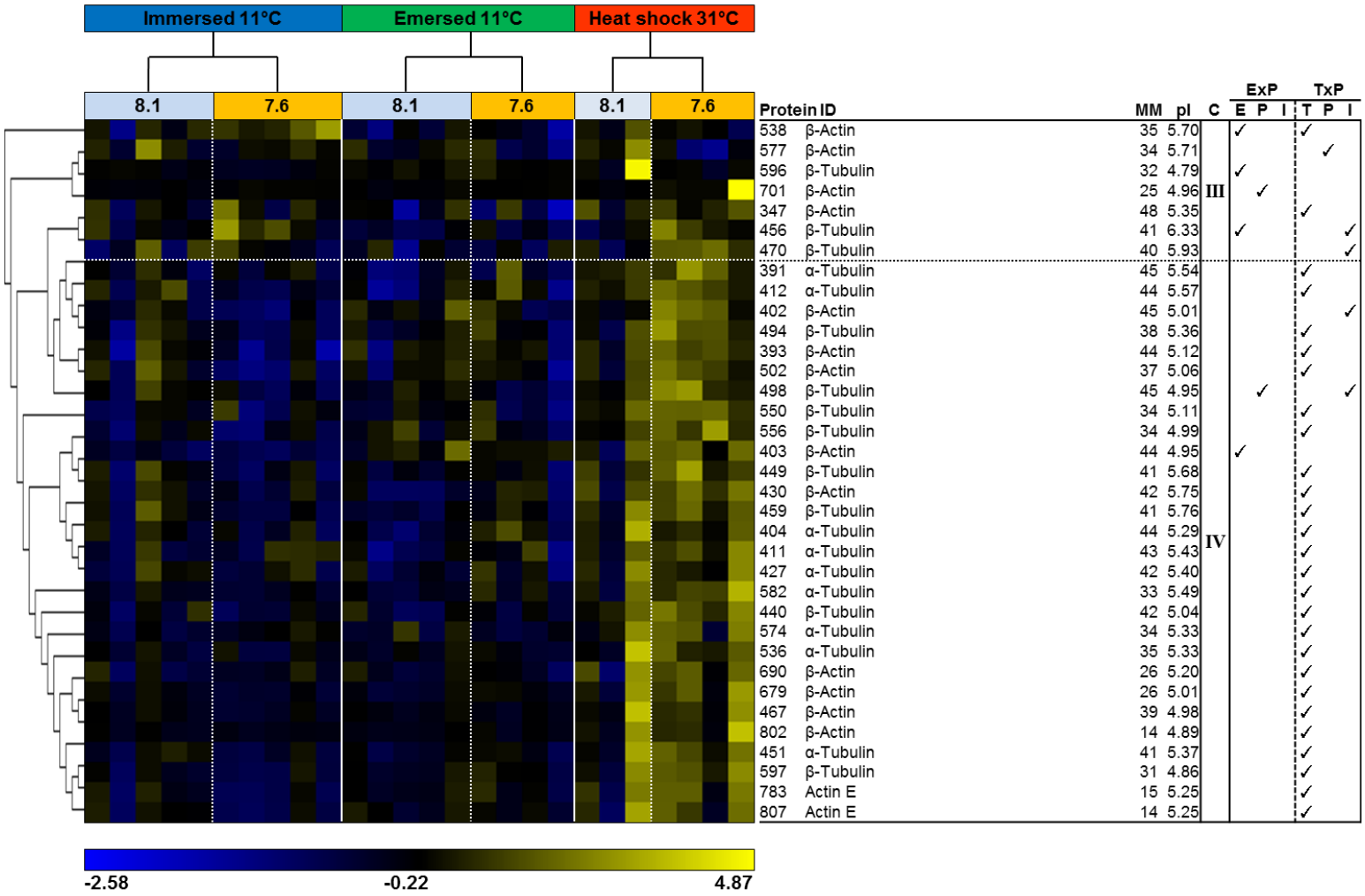

	Protein ID	MM	pI	C	ExP E	ExP P	ExP I	TxP T	TxP P	TxP I
538	β-Actin	35	5.70		✓			✓		
577	β-Actin	34	5.71						✓	
596	β-Tubulin	32	4.79		✓					
701	β-Actin	25	4.96	III		✓				
347	β-Actin	48	5.35					✓		
456	β-Tubulin	41	6.33		✓					✓
470	β-Tubulin	40	5.93							✓
391	α-Tubulin	45	5.54					✓		
412	α-Tubulin	44	5.57					✓		
402	β-Actin	45	5.01							✓
494	β-Tubulin	38	5.36					✓		
393	β-Actin	44	5.12					✓		
502	β-Actin	37	5.06					✓		
498	β-Tubulin	45	4.95			✓				✓
550	β-Tubulin	34	5.11					✓		
556	β-Tubulin	34	4.99					✓		
403	β-Actin	44	4.95		✓					
449	β-Tubulin	41	5.68					✓		
430	β-Actin	42	5.75					✓		
459	β-Tubulin	41	5.76					✓		
404	α-Tubulin	44	5.29					✓		
411	α-Tubulin	43	5.43	IV				✓		
427	α-Tubulin	42	5.40					✓		
582	α-Tubulin	33	5.49					✓		
440	β-Tubulin	42	5.04					✓		
574	α-Tubulin	34	5.33					✓		
536	α-Tubulin	35	5.33					✓		
690	β-Actin	26	5.20					✓		
679	β-Actin	26	5.01					✓		
467	β-Actin	39	4.98					✓		
802	β-Actin	14	4.89					✓		
451	α-Tubulin	41	5.37					✓		
597	β-Tubulin	31	4.86					✓		
783	Actin E	15	5.25					✓		
807	Actin E	14	5.25					✓		

Figure 29 continued.